University of Bath

UNIVERSITY OF
BATH

PHD

Power transformer fault diagnosis based on wavelet transform and artificial neural network

Mao, Peilin

Award date:
2000

Awarding institution:
University of Bath

[Link to publication](#)

POWER TRANSFORMER FAULT DIAGNOSIS BASED ON WAVELET TRANSFORM AND ARTIFICIAL NEURAL NETWORK

Submitted by Peilin Mao
for the degree of PhD
of the University of Bath

2000

COPYRIGHT

Peilin Mao

17/5/2000

UMI Number: U601866

UMI

Dissertation Publishing

UMI U601866

ProQuest

Acknowledgements

I would like to thank Prof. R.K. Aggarwal for his most valuable supervision as well as the enlightening comments and tireless support during the whole course of this research and the preparation of this thesis. Working with him has been an experience to witness his humbleness, patience and perfection in the practice of electrical engineering. I am indebted to him for all the help and advice that I have received.

My sincere thanks to all the academic and technical staff of the school of electrical engineering and all the friends both in UK and China for their help and support.

I also wish to express my deepest and most sincere gratitude to my parents and my entire family for their continuous and enduring love and support, both morally and financially that enabled me to pursue my academic objective.

Finally, I gratefully acknowledge the receipt of a generous scholarship from the University of Bath, without whose financial support this research would not have been possible.

Abstract

Power transformers form a vital link between power generation, transmission and electricity distribution to consumers. In order to ensure high quality and reliability of electricity, accurate classification of the transient phenomena in power transformers is crucial. In this respect, conventional techniques have difficulties due to increased complexity of modern power systems coupled with new power transformer designs.

This thesis describes the research and development of new fault diagnosis classification techniques for power transformers based on the Wavelet Transform (WT) and Artificial Neural Network (ANN). An integral modelling approach that integrates the model of the power transformer with the associated CT model for the purposes of simulating the transient phenomena in power transformer systems is firstly described; this is followed by presentation of electromagnetic simulation studies in power transformers under internal/external faults and inrush currents in two different power transformer systems.

To develop new alternative protection techniques for power transformers, a traditional ANN based approach is firstly investigated and developed; and in particular, its advantages and disadvantages are examined and discussed. Based on these studies, a new feature extraction technique to analyse and identify the most significant features within the power transformer transient phenomena is proposed by using the WT. On the basis of latter, two new approaches for power transformer fault diagnosis particularly for discrimination between internal faults and inrush currents/external faults are proposed. The first technique, which is a WT-based direct decision making approach, clearly shows that the proposed technique can more accurately discriminate between an internal fault and an inrush current, in comparison to that based on the traditional ANN; in particular, the technique is robust to different power transformer systems. In order to further improve the accuracy of power transformer fault diagnosis, an integrated approach combining WT with ANN is proposed as an alternative to the previous technique. The results presented indicate that the proposed two approaches researched

and developed in this work are much better suited in overcoming some of the limitations/disadvantages of the traditional ANN based approach.

Contents

Chapter 1 Introduction

Chapter 2 An Overview of Developments in Protection for Discrimination between Internal Faults and Inrush Currents

Chapter 3 Mathematical Models of a Power Transformer and Instrument Current Transformer

Chapter 4 Electromagnetic Simulation Study of Power Transformer Faults

Chapter 5 Electromagnetic Simulation Study of Power Transformer Inrush Currents

Chapter 6 Traditional ANN-Based Technique for Power Transformer Fault Diagnosis

Chapter 7 Electromagnetic Transient Analysis of Power Transformers Using Wavelet Transform

Chapter 8 Power Transformer Fault Diagnosis By Direct Decision Making Approach Based on Wavelet Transform

Chapter 9 Power Transformer Fault Diagnosis Based on Combined WT and ANN

Chapter 10 Conclusions and Future Work

Index to Figures

Index to Tables

List of Symbols

A	Ampere
kV	Kilo Volts
kVA	Kilo Volt Amperes
MVA	Mega Volt Amperes
MW	Mega Watts
Hz	Hertz
kHz	Kilo-hertz
AC	Alternating Current
DC	Direct Current
LV	Low Voltage
HV	High Voltage
EHV	Extra High Voltage
EMTP	Electro-Magnetic Transients Program
CT	Current Transformer
A/D	Analogue/Digital Converter
ULTC	Under Load Tap Changer
AI	Artificial Intelligent
ANNs	Artificial Neural Networks
MFN	Multilayer Feedforward Network
RMS	Root Mean Square
WT	Wavelet Transform
CWT	Continuous Wavelet Transformer
DWT	Discrete Wavelet Transformer
FT	Fourier Transformer
STFT	Short Time Fourier Transformer
DFT	Discrete Fourier Transformer
CAD	Computer Aided Design
[R]	Resistance matrix

[L]	Inductance matrix
I_{ap}, I_{bp}, I_{cp}	a, b and c three-phase current on LV side of power transformer
I_{as}, I_{bs}, I_{cs}	a, b and c three-phase current on HV side of power transformer
I_{ad}, I_{bd}, I_{cd}	a, b and c three-phase differential current through CT secondary side
I_{am}, I_{bm}, I_{cm}	a, b and c three-phase magnetising current in magnetic branch
ϕ_a, ϕ_b, ϕ_c	a, b and c three-phase transient flux
$I_{a-detail\,1,max}$	Maximum peak value of a-phase wavelet at detail 1 in the first window
$I_{b-detail\,1,max}$	Maximum peak value of b-phase wavelet at detail 1 in the first window
$I_{c-detail\,1,max}$	Maximum peak value of c-phase wavelet at detail 1 in the first window
$I^k_{a-detail\,1,max}$	Maximum peak value of a-phase wavelet at detail 1 in the kth window
$I^k_{b-detail\,1,max}$	Maximum peak value of b-phase wavelet at detail 1 in the kth window
$I^k_{c-detail\,1,max}$	Maximum peak value of c-phase wavelet at detail 1 in the kth window
$I_{a-ratio}$	Ratio of $I^k_{a-detail\,1,max}$ with respect to $I_{a-detail\,1,max}$
$I_{b-ratio}$	Ratio of $I^k_{b-detail\,1,max}$ with respect to $I_{b-detail\,1,max}$
$I_{c-ratio}$	Ratio of $I^k_{c-detail\,1,max}$ with respect to $I_{c-detail\,1,max}$
$P_{a-detail}$	Spectral energy of wavelet signals in a phase
$P_{b-detail}$	Spectral energy of wavelet signals in b phase
$P_{c-detail}$	Spectral energy of wavelet signals in c phase

Chapter 1

Introduction

1.1 Power Transformers and Their Protections

Power transformers are essential and important elements of electrical power systems; in particular, they form a vital link between power generation and transmission lines and/or between transmission lines and loads. However, they do suffer from many types of transient disturbances, including internal faults, inrush currents, external faults and over-excitation. Among these transient disturbances, internal faults must be quickly and accurately detected and the appropriate action must be taken to isolate the faulty transformer from the rest of the power system, so as to minimise the damage and expedite repairs to damaged equipment, thereby keeping both outage times and maintenance costs down. The importance of the latter has increased significantly due to the privatisation and deregulation of the electricity supply industry world-wide.

Many transformers, ranging from small single-phase units to extremely large, three-phase units associated with generators and transmission lines, are in use in power-supply networks around the world. All transformers need to be protected. The inherent characteristics of power transformers introduce a number of unique problems that are not present in the protection of transmission lines, generators, motors, or other power system apparatus. In general, a transformer may be protected by fuses, overcurrent relaying, differential relays, pressure relays, and can be monitored for incipient problems with the help of winding temperature

measurements, and chemical analysis of the gas above the insulating oil. Which of these protective devices will be used in a given condition depends upon the size, location, voltage and connection of the power transformers.

It has been reported in reference [1] that a transformer with capacity of less than 2500 kVA is usually protected by fuses. With ratings between 2500 and 5000 kVA, the transformer may be protected with fuses, but instantaneous and time-delay overcurrent relays may be more desirable from the standpoint of sensitivity. Between 5000 and 10000 kVA an induction disc overcurrent relay connected in a differential configuration is usually applied. Above 10 MVA, harmonic restraint, percentage differential relay is recommended. Temperature and pressure relays are also usually applied with this size transformer to monitor incipient problems with the help of winding temperature measurements, and chemical analysis of the gas above the insulating oil.

In addition to the size of the transformer, the decision regarding the specific protection application to the power transformer is significantly affected by consideration of the importance of the transformer within the power network. If the transformer is an integral part of the bulk power system, it will probably require more sophisticated relays in terms of design. If it is a distribution substation step-down transformer, a single differential relay and overcurrent backup will usually suffice. If the transformer is near a generation source, the high X/R ratio of the fault path will require harmonic restraint relays to accommodate the higher magnetic inrush currents.

Moreover, the higher voltages demand the more sophisticated and costly protective devices, due to the harmful effect of a delayed fault clearance on the system performance, and the high cost of transformer repair; also the winding connection of a three phase transformer, whether delta or star, will make a difference to the protection scheme chosen.

In the application of each protection scheme, the protective relaying should ensure that if a power transformer experiences a fault, it is necessary to take the transformer out of service as soon as possible so that damage, frequency and duration of unwanted outages are minimised. Accordingly, there is a high demand imposed on power transformer protective relays; this includes the requirements of dependability associated with no missing operations, security associated with no false tripping, and operating speed associated with a short fault clearing time.

1.2 Existing Problems and Difficulties in Power Transformer Differential Protection

Protection of large power transformers is one of the most challenging problems in the power system relaying area, because of the complexity of the operating conditions of power transformers. Table 1.1 [2] summarises a number of problems that can cause difficulties related to protective relaying of power transformers.

Table 1.1 Problems related to protective relaying of power transformers

Disturbance	Measurement	Security*	Dependability*	Speed*
Inrush	Accurate estimation of the second and fifth harmonics takes around one cycle. Off-nominal frequencies create extra measuring errors in harmonic ratio estimation.	In modern power transformers, due to magnetic properties of the core, the second harmonic during inrush and the fifth harmonic during over-excitation may be very low, jeopardising relay security.	Presence of higher harmonics does not necessarily indicate an inrush. Harmonics may block a relay during severe internal faults due to saturation of CTs.	Usually takes one full cycle to reject magnetising inrush and stationary over-excitation hypotheses if an internal fault is not severe enough to be tripped by the unrestrained element.
Over-Excitation			The third harmonic may be present in internal fault currents due to saturation of CTs and rotor asymmetry of generators and/or power electronic devices.	
External Faults	Measured currents display an enormous rate of change and are often distorted significantly.	External fault current, when combined with ratio mismatch, may generate a false differential signal. CTs, when saturated during external faults, may produce an extra differential signal.	All means of preventing false trippings during external faults reduce the dependability of relay.	Means of restraining the relay from tripping during external faults may limit the speed of relay operation.
Internal Faults		An internal fault current may be as low as a few percent of the rated value. Attempts to cover such faults jeopardise relay security.	The internal fault current may be as low as a few percent of rated value. Security demands under inrush, over-excitation, and external faults limit relay dependability.	Means of restraining the relay from tripping during inrush, over-excitation, and external faults limit the speed of relay operation.

*Note: Dependability – no missing operation; Security – no false tripping; Speed – short fault clearing time.

With reference to Table 1.1, these difficulties are related to the problems of

□ Inrush

When the power transformer is energised on the primary side with the secondary open-circuited, a transient magnetising inrush current may flow. This inrush current, which appears as an internal fault to the differential relays, may be as high as 8-30 times of the rated current, thereby causing a false operation [3]. A significant amount of harmonics are present in the magnetising inrush current. Of all the harmonic components, the second harmonic is the most prominent.

□ Over-Excitation

Overexcitation of a transformer may result in thermal damage to cores due to excessively high flux in the magnetic circuits. A transformer may be subject to over-excitation or overvoltage condition during load rejection and certain other operation conditions. During overexcitation, the transformer flux remains symmetric, but goes into saturation for equal periods in the positive and the negative half periods of the waveform. There is no second harmonic present in this waveform, but the fifth harmonic is almost as strong as the fundamental frequency component.

□ External Faults

Here external faults are defined as those that are outside the differential protection zone of the power transformer.

□ Internal Faults

Here internal faults are defined as those that are inside the differential protection zone of the power transformer.

Among these problems, distinguishing between internal faults and inrush currents has long been recognised as one of the challenging problems in the power transformer protection [4-9]. Although a conventional transformer protection based

on current differential principles offers a means of detecting internal faults of a power transformer, when the transformer is energised, a large magnetising inrush current flow in the transformer windings, sometimes results in 8-30 times of the rated current and therefore can cause mal-operation of the relay. This is not a fault condition, and therefore does not necessitate the operation of protection, on the contrary the protection relay must remain stable during the inrush transient.

One of the earliest ideas to cope with the magnetising inrush current problem was to de-sensitise the differential relay when the transformer was energised; the less sensitive relay had a higher setting value to block the inrush current, thus avoiding a false trip during the inrush current. However, de-sensitising the differential relay is a poor practice, as it may cause no operation during an internal fault.

The differential relay with voltage supervision to block the relay operation for inrush condition is another method that has been introduced. It may be expected that during inrush conditions, the transformer voltage would be close to normal, while during faults, the voltage would be much less. Thus, an undervoltage relay may be used to supervise the differential relay. However, this type of voltage supervision is not preferred, as the undervoltage relay tends to be slow, and consequently the entire protection becomes slower. More importantly, this type of protection requires a voltage source for the transformer relay, which is an added expense, and may not be justifiable in many cases.

The method currently in use on large power transformers is based upon using the harmonic characterisation of the inrush current. Since a magnetising inrush current generally contains a large second harmonic component in comparison to an internal fault, transformer protection systems are designed to restrain this inrush transient phenomenon by monitoring the large second harmonic [10,11]. However, the second harmonic component may also be generated during internal faults in a power transformer. This may be due to CT saturation or the presence of a parallel capacitor or due to the distributed shunt capacitance in a long EHV transmission line to which

the transformer may be connected [5]. In certain cases, the magnitude of the second harmonic in an internal fault can be close to or greater than that present in the magnetising inrush current. Moreover, the second harmonic components in the magnetising inrush currents tend to be relatively small in modern large power transformers because of improvements in the power transformer core material [12]. Consequently, the commonly employed conventional differential protection technique, based on the second harmonic restraint, will thus have difficulty in distinguishing between an internal fault and an inrush current thereby threatening transformer stability. Alternative, improved protection techniques for accurately and efficiently discriminating between internal faults and inrush currents have thus to be found.

1.3 Objectives of the Project

This research project will focus on the investigation and development of new protection schemes for the discrimination between internal faults and inrush currents/external faults in power transformers. The main objectives of this thesis are:

❑ To establish an accurate modelling approach to simulate various faults and magnetising inrush currents under various power transformer system conditions using the well known Electro-Magnetic Transients Program (EMTP). The effects of CTs on a power transformer protection are taken into account, so that the approach can be used to simulate the situation close to real-life in a power transformer system.

❑ To study a traditional ANN-based technique for the purposes of investigating its performance and limitations for power transformer fault diagnosis particularly for distinguishing between internal faults and inrush currents/external faults, and improving on the performances through new alternative approaches.

❑ To study and develop a new signal feature extraction methodology for the purposes of extracting more distinct features between internal faults and inrush currents. The time-frequency characteristics of faults and inrush currents are investigated through the Wavelet Transform (WT) technique, in order to extract the most significant distinguishing features from each transient signal for the purposes of developing novel protective techniques in power transformer system.

❑ To develop a new WT-based direct decision making approach for distinguishing internal faults from inrush currents/external faults. The approach is extensively tested for a whole variety of practically encountered system and fault conditions. The generalisation of the technique is tested using different power transformer systems.

❑ To further improve the accuracy for distinguishing internal faults from inrush currents/external faults, a novel approach using combined WT and ANN is researched and developed.

❑ Finally, a comparison amongst proposed techniques developed herein and the traditional ANN-based technique is presented, in order to ascertain the effectiveness and advantages of the proposed techniques herein.

1.4 Scope of the Thesis

Chapter 2

A literature search of current existing fault diagnosis classification techniques for power transformers was carried out. Some of the techniques are described in this chapter; their advantages and disadvantages are discussed.

Chapter 3

An accurate mathematical modelling approach for accurately modelling a power transformer for the purposes of simulating its transient phenomena and designing and evaluating a new protective relay is presented in this chapter. Based on the basic model of the power transformer, which is provided in EMTP, the model developed herein is a significantly modified form of the basis model, thereby the resulted model can be used for not only simulating internal terminal faults, but also internal winding faults. In addition, the inrush current modelling is implemented by adding equivalently non-linear element into the basic model. The effects of CTs on differential currents in a power transformer system are taken into account to generate accurate and realistic transient disturbance data.

Chapter 4

Fault transients in a power transformer system are extensively simulated and analysed by using the mathematical modelling approach described in Chapter 3; this includes a number of fault transient events simulated in two different power transformer systems, namely System 1 and System 2; System 1 is a three-phase and two-winding *750MVA, 27kV/420kV, Dy11-connected, five-leg core type* power transformer in a double-end-fed power system network; and System 2 is a three-phase and two-winding *35MVA, 11kV/132kV, Yy0-connected, three-leg core type* power transformer in a single-end-fed power system network. The simulated cases include (i) terminal three-phase, phase-to-phase and two-phase-to-earth as well as single-phase-to-earth faults; (ii) winding turn-to-turn and turn-to-earth faults. Furthermore, internal and external faults both with CT saturation are also modelled, and the typical fault transient waveforms are illustrated.

Chapter 5

As an adjunct to the simulation of the fault transients in Chapter 4, an extensive simulation and analysis of inrush current transients in a power transformer system are carried out based on the mathematical modelling approach described in Chapter 3. Here again, magnetising inrush currents under various transient conditions in both System 1 and System 2 are simulated. In particular, effects of the core remnant flux level in the power transformer and switch-on angle when energising a transformer on inrush currents are taken into consideration.

Chapter 6

The work presented in this chapter is based on applying a traditional ANN approach to distinguish internal faults from inrush currents/external faults. It is in essence a necessary precursor to improving on the performance through novel approaches described later in this thesis. The performance of this technique is investigated throughout and its limitations are discussed.

Chapter 7

In order to develop novel protective techniques for distinguishing internal faults from magnetising inrush currents/external faults, WT technique is used to extract the best distinguishing features between internal faults and inrush currents. In this chapter, a given faulted current signal or inrush current signal is decomposed using the WT; this involves representation of a signal into a series of wavelet components, each of which is a time-domain signal that covers a specific frequency band. Studied results presented show that particular wavelet components could be used as the features to distinguish the internal faults from the inrush currents/external faults.

Chapter 8

In this chapter, a new WT-based direct decision making logic approach is proposed. In the approach, the signal features are extracted using the WT and then quantified. A decision making logic for distinguishing an internal fault from an inrush current/external fault is made based on predefined logic criteria in conjunction with the counting regime. To demonstrate the effectiveness of the proposed technique, especially for application to different power transformer systems, two different power transformer systems, namely System 1 and System 2, are considered.

Chapter 9

In order to investigate the possibility of further improvement of the accuracy for distinguishing internal faults from inrush currents/external faults, over that developed using the WT-based direct decision making logic approach proposed in Chapter 8, an alternative approach to the classification of the transient phenomena in power transformers using the combined WT and ANN is developed. In this approach, WT is firstly applied to decompose the differential current signals into a series of detailed wavelet components. The spectral energies of the selected wavelet components are calculated and then fed into the ANN. The decision for discriminating internal faults from magnetising inrush currents/external faults is then made in terms of the ANN outputs in conjunction with the counting regime. Case studies indicated that the combined WT and ANN approach is able to give a very high accuracy in the classification rate of the transients and is robust to different power transformer systems.

Finally, a comparison, between the traditional ANN-based technique and the two proposed techniques herein (WT-based and combined WT and ANN-based), is also presented in this Chapter.

Chapter 10

Conclusions are drawn and future work in digital relaying for power transformers are discussed in this Chapter.

Chapter 2

An Overview of Developments in Protection
for Discrimination between
Internal Faults and Inrush Currents

2.1 Introduction

Any power transformer protective scheme has to take into account the effect of magnetising inrush currents in order to prevent mal-operation of the relays under the magnetising inrush current conditions. Accurately discriminating internal faults from magnetising inrush currents has long been recognised as one of challenging problems to power transformer protection researchers/engineers. This chapter reviews the developments that have taken place in techniques for discrimination between internal faults and inrush currents in the power transformer protection. It begins with introducing the basic principle of the current differential schemes; and after describing the phenomenon of inrush currents, discusses the conventional differential protection approach, based on 2nd harmonic restraint. However, the conventional differential protection approach shows certain problems and limitations. A number of protection techniques have been proposed to cope with the problems and limitations [5-9, 15-19, 69-73], some are described in this chapter, and their advantages and disadvantages are discussed.

2.2 Conventional Transformer Differential Protection Approach

2.2.1 Basic Principle of Current Differential Schemes

The current differential schemes have been used to protect power transformers since the early years of this century. They are now applied to all large power transformers. Its basic principle is that the currents at both terminals of the protected transformer are compared by means of computing and monitoring a differential (or unbalanced) current. In theory, the non-zero value of the differential signal indicates an internal fault. Figure 2.1 illustrates the principle of the differential relay.
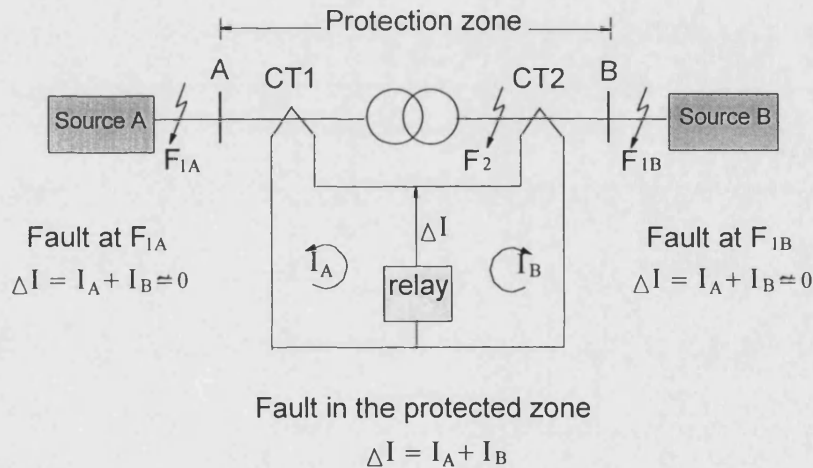
Figure 2.1 Principle of current differential scheme

In Figure 2.1, points F_{1A} and F_{1B} represent external faults on the power transformer system and their differential currents are:

$$\Delta I = I_A + I_B \cong 0 \qquad (2.1)$$

It is apparent from the above that the differential relay does not operate.

Point F_2 represents an internal fault on the power transformer system and its differential current is presented by:

$$\Delta I = I_A + I_B \neq 0 \qquad\qquad (2.2)$$

The differential relay thus operates for this fault condition.

However, in practice, the following important issues must be considered in order to avoid mal-operation of the relay [3,11,13,14].

- It may not be possible to obtain the required CT ratios on the primary and the secondary sides, which are required to satisfy the condition $N_1 n_1 = N_2 n_2$; CTs have to be selected with standard ratios. This leads to ratio mismatch thereby causing a small differential current to flow during normal conditions.

- The transformation errors of the two CTs on the high voltage (HV) and low voltage (LV) side may differ from each other, thus leading to a small differential current when there is normal load flow, or an external fault.

- If the power transformer is equipped with a tap changer, it will introduce a main transformer ratio change when the taps are changed, thus creating an unbalanced current when there is normal load flow, or an external fault.

The above three effects cause a differential current to flow in the relay under normal load flows and external faults. The relay design must therefore accommodate these small levels of differential currents without causing a trip.

Since each of these effects leads to a differential current which is proportional to the actual current flowing in the transformer primary and secondary windings, in practice, a percentage differential relay provides a solution to this problem. In the

percentage differential relay, the detection of the internal fault is based on a percentage differential characteristic; the differential current must exceed a fixed percentage of the 'through' current in the transformer. The through current is defined as the average of the primary and the secondary currents:

$$i_r = \frac{i_A + i_B}{2} \qquad\qquad (2.3)$$

where the current i_r is known as the restraint or bias current, and the relay operates when

$$i_d = i_A - i_B \geq k \cdot i_r \qquad\qquad (2.4)$$

where k is the slope of the percentage differential characteristic. The factor k is generally expressed as a percent value: typically 10%, 20%, or 40%. Clearly, a relay with a slope of 10% is far more sensitive than a relay with a slope of 40%.

Figure 2.2 shows a practical percentage differential characteristic. The relay slope determines the trip zone. The three sources (i.e. ULTC error caused by Under Load Tap Changer, CT error between LV and HV sides and Ratio mismatch in CTs) in differential current during normal transformer operation are shown, as is the margin of safety used in arriving at the slope. The relay has a small pickup current setting I_{pickup}: i.e. the relay does not operate unless the differential current is above this pickup value. The pickup setting is usually set very low: typical values are ¼ ampere secondary [1].
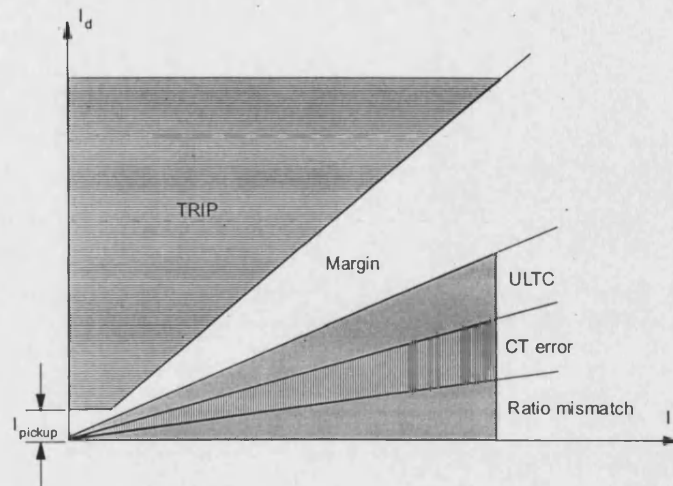
Figure 2.2 Percentage differential relay characteristic

The percentage differential relay assumes that there are relatively small values of differential currents flowing in the relay during normal load flow conditions, or during an external fault. However, under an inrush current condition (this gives rise to a large differential current), the percentage differential relay will mal-operate, unless some special precautions are taken.

2.2.2 Phenomenon of Inrush Currents in Power Transformers

When a power transformer is energised on the primary side with the secondary open-circuited, a transient magnetising inrush current may flow in the primary side of the power transformer, and may be as high as 8-30 times of the rated current because of the extreme saturation of the transformer iron-core. In a mathematical form, the transient magnetising inrush current can be described as follows:

Consider for simplicity a single-phase transformer protected by a differential relay, (shown in Figure 2.3), and the transformer is energised by a sinusoidal voltage

$u = U_m \sin(\omega t + \alpha)$, where α represents the switch-on angle on the voltage waveform.
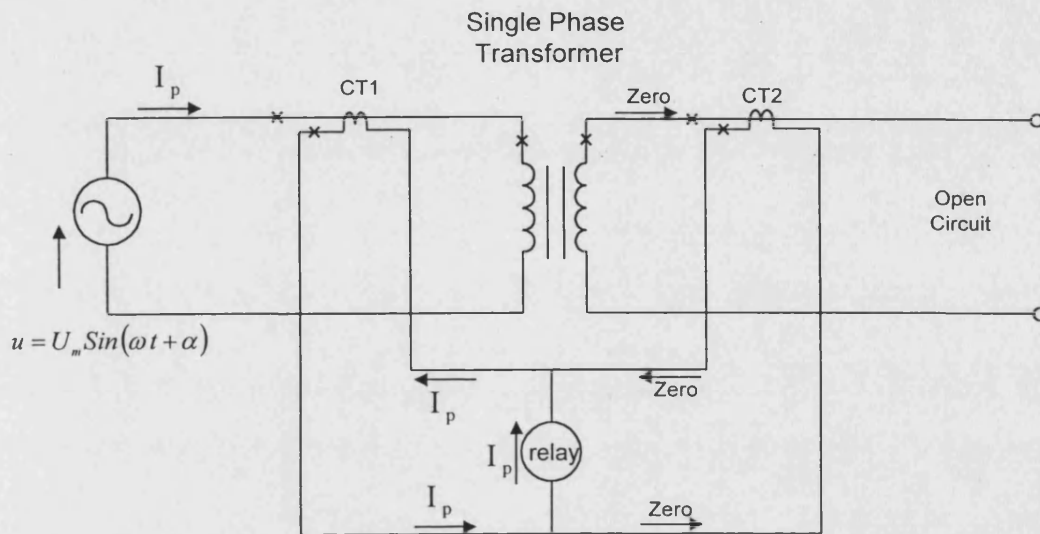
Figure 2.3 Mal-operation due to magnetising inrush current

Faraday's law of induction gives the following relationship for any transformer excited by a sinusoidal voltage:

$$u = N \frac{d\phi}{dt} \tag{2.5}$$

For simplicity, assume the turn of the primary winding of the power transformer is $N = 1$, thus

$$\frac{d\phi}{dt} = U_m \sin(\omega t + \alpha) \tag{2.6}$$

where, ϕ is the flux of the transformer core.

Integrating equation (2.6) from time 0 to t gives the following relationship:

$$\phi = -\frac{U_m}{\omega}\cos(\omega t + \alpha) + \frac{U_m}{\omega}\cos\alpha + \phi_r \qquad (2.7)$$

or $\qquad\qquad \phi = -\phi_m\cos(\omega t + \alpha) + \phi_m\cos\alpha + \phi_r \qquad\qquad (2.8)$

When the transformer is energised by a sinusoidal voltage at the instant of the voltage passes through its zero value, i.e. $\alpha = 0^0$, $\cos\alpha = 1$, the transformer core flux ϕ will have a maximum value, thus, from equation 2.8, we get:

$$\phi = -\phi_m\cos\omega t + \phi_m + \phi_r \qquad (2.9)$$

In equation (2.9), $(-\phi_m\cos\omega t)$ is the steady-state flux; $(-\phi_m\cos\omega t + \phi_m)$ is the transient flux without remnant flux at the switching instant; $(-\phi_m\cos\omega t + \phi_m + \phi_r)$ is the transient flux with remnant flux ϕ_r at the switching instant.

The relationship between the power transformer core flux and magnetising current is determined by core magnetising curve. Figure 2.4 shows a nonlinear (ϕ vs i) curve of the transformer core. In Figure 2.4, i_{m1} represents the magnetising current corresponding to the steady state flux (rated flux). In general, i_{m1} is about 5% the rated current. However, this current can be significantly large under the extreme saturation of the transformer iron-core. It can be seen from equation (2.8) or (2.9) that the maximum flux in a transformer primary winding can reach to two times the steady state flux if the transformer is energised at near voltage zero ($\alpha = 0^0$) without a remnant flux. Because of non-linear characteristics of the transformer core, this doubling of the flux will lead to extreme saturation thereby causing the magnetising inrush current to flow and this may reach several times the rated current as evident

from i_{m2} shown in Figure2.4. Furthermore, if there is, say, 80% remnant flux of the rated flux in the transformer core, instead of it being zero, the peak value of the flux will be about 2.8 times the steady state flux, and it will in turn lead to a further increase in the inrush current, as evident from i_{m3} shown in Figure 2.4.
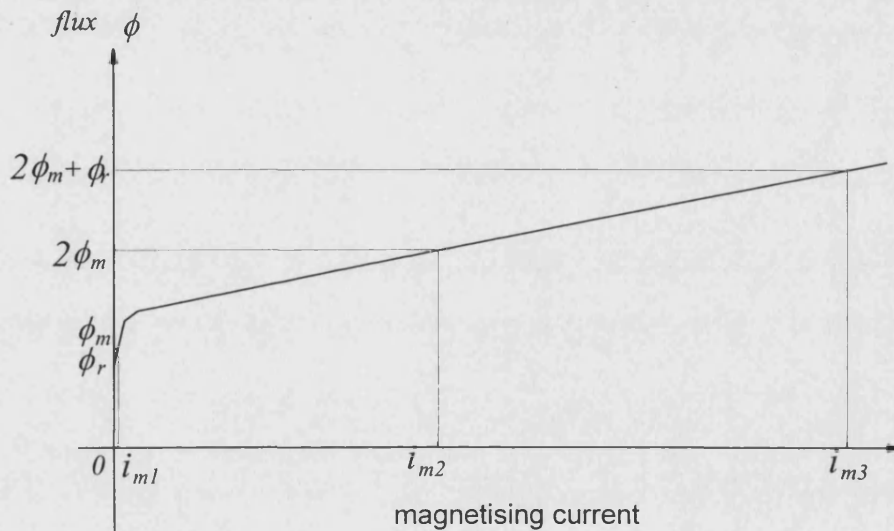
Figure 2.4 Nonlinear (ϕ vs i) curve of the transformer core

The foregoing discussion clearly indicates the reasons as to why the inrush current is generated in a power transformer.

2.2.3 Conventional Differential Protection Approach

The magnetising inrush current phenomenon (described in 2.2.2) produces currents in the primary winding of the transformer, while there are no currents in the secondary side. This results in a differential current and it apparently is not distinguishable from an internal fault current. The normal percentage differential relay is not, therefore, effective.

A detailed analysis has shown that the magnetising inrush current has a DC offset and numerous harmonics. Fourier analysis gives the following DC and harmonic contents in comparison to the fundamental component in a typical magnetising inrush current [10]:

- DC=55%
- Fundamental = 100%
- 2nd harmonic = 63%
- 3rd harmonic = 27%
- 4th harmonic = 5%
- 5th harmonic = 4%
- 6th harmonic = 3.7%
- 7th harmonic = 2.4%

From the foregoing, it can be seen that there is a large second harmonic component in the magnetising inrush current. While normal internal fault currents do not contain second or other even harmonics [11].

A third harmonic is also present in the inrush current with comparable proportion to the second harmonic. However, as a sustained third harmonic component is quite likely to be produced by CT saturation under heavy internal fault conditions, this means that this component cannot, therefore, be regarded as a reliable source of bias [11].

The magnitudes of all other higher harmonics present in the inrush current are too small to be worth considering. Therefore, conventional transformer protection systems are designed to restrain this inrush current by monitoring the ratio between second harmonic and fundamental. Typically such relays will restrain when the second harmonic component exceeds 20% of the fundamental component [11]. Figure 2.5 presents a simplified flowchart of the logic of a conventional digital differential relay for power transformers.
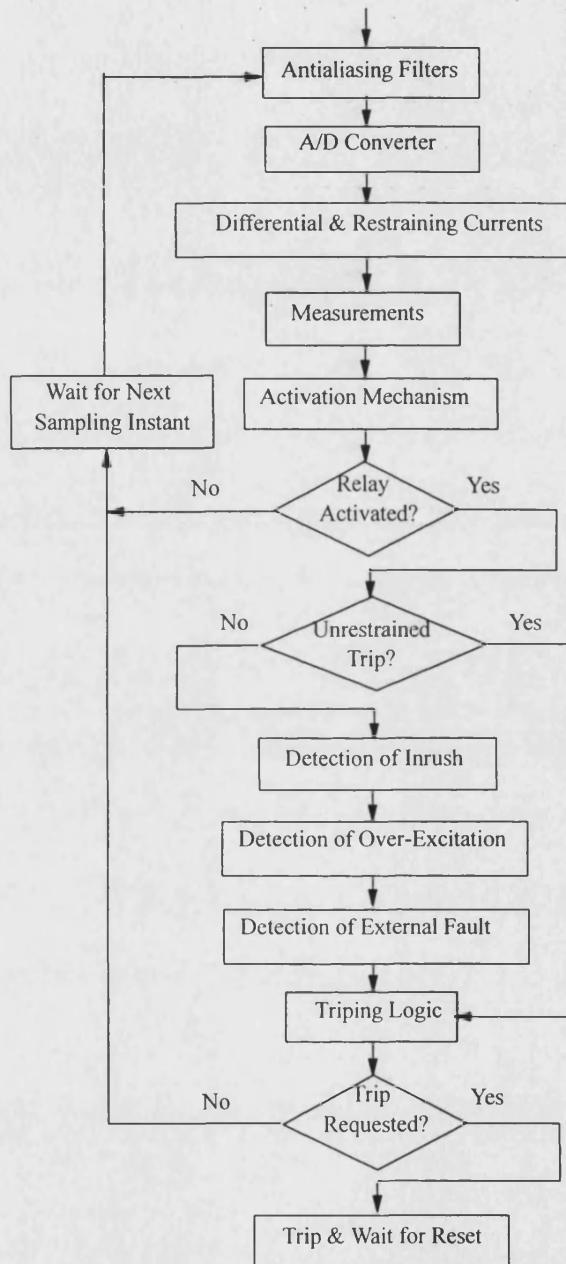
Figure 2.5 Logic for a conventional digital differential relay for power transformers

In Figure 2.5, the second harmonic is used to prevent false tripping during magnetising inrush current conditions; the fifth harmonic is commonly used to restrain the differential relay during stationary over-excitation conditions, because the percentage of fifth harmonic in the transformer magnetising current increases significantly when the transformer is subjected to an over-excitation condition [2]; while the biased percentage characteristic is used to prevent false tripping during external faults.

However, the conventional differential protection approach shows certain limitations; it may not be able to deal with the problems highlighted in Table 1.1 in Chapter 1. In order to satisfactorily deal with these problems, a number of protection techniques have been proposed. Some are described as follows.

2.3 Differential Power Approach

One of the researched protective schemes to deal with the foregoing difficulties for the power transformer protection is differential power method [6]; the method uses differential active power to discriminate between internal faults and inrush currents, instead of using the differential currents.

It is assumed in differential power method that, in the normal operation state of a power transformer, the sum of power flowing into the transformer is very small, because both the copper and core loss are less than 1% of the transformer capacity. When considering instantaneous power, it flows in and out according to the magnetic energy stored in windings. However, the average power or active power is almost negligible. When a power transformer is energised, a large magnetising current flows during the iron core saturation, instantaneous power is also large, but the average power is still small though iron and copper loss as well as eddy current loss may be increased slightly. On the other hand, when a transformer has an internal fault, large power is consumed by the arcing discharge, the average power will be very large;

therefore, if a threshold of average power flowing into the transformer is set, faults can be detected in terms of the changes of average power.

The basic discrimination algorithm of this method can be described as follows. For simplification, only a two-winding transformer is explained here.

The average power is calculated by the following equation:

$$W(t) = \frac{1}{T} \int_{t-T}^{t} (V_1 I_1 + V_2 I_2 - R_1 I_1^2 - R_2 I_2^2) dt \qquad (2.10)$$

where V_1, I_1, V_2, I_2 are instantaneous voltage and current at the primary and secondary winding terminal, $R_1 I_1^2$, $R_2 I_2^2$ are copper loss at the primary and secondary side of a power transformer. W(t) signifies the average power flowing into transformer during one period T (=20 ms in 50Hz system frequency). The average power is very small under an inrush current condition; but will be very large for an internal fault as large amounts of power are consumed. If W (t) exceeds a predefined threshold (a threshold of 0.3 is used in the paper), the relay issues a trip signal.

However, the approach reported in [6] cannot deal successfully with a condition involving CT saturation. In practice, the CT saturation cannot be avoided under certain system and fault conditions and therefore must be considered in the power transformer protection.

2.4 Multisetting Overcurrent Principle

The multisetting overcurrent principle [2] classifies the differential current level into four classes, namely A, B, C, D, and three thresholds Δ_1, Δ_2 and Δ_3 associated with the differential current level are set. Figure 2.6 presents amplitudes of the differential currents under the load, over-excitation, external fault, magnetising inrush, and internal fault conditions.
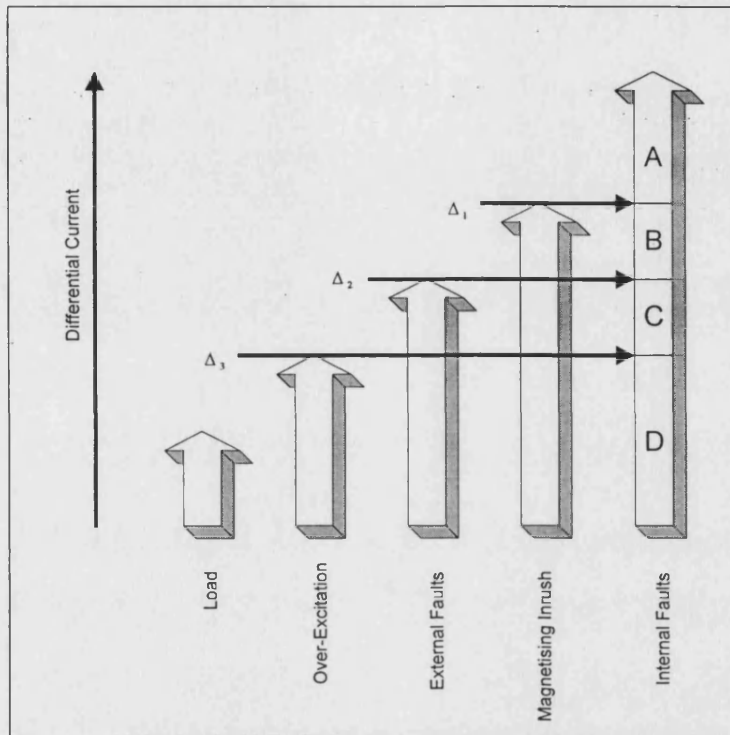
Figure 2.6 Multisetting overcurrent principle

In Figure 2.6, if the amplitude of the current is higher than the highest possible non-internal fault, then the relay trips without further analysis (unrestrained tripping). Thus, internal faults of class A are detected by the unrestrained overcurrent element working with the first threshold Δ_1, while all other faults of class B through D must wait to be detected by the restrained element. The internal faults of class B are detected by the restrained overcurrent element working with the second threshold Δ_2 if the inrush current has been eliminated by the other relaying principle, such as the second harmonic restraint; whereas the external fault and over-excitation condition may not be checked since they are ruled out by the overcurrent element working with the second threshold Δ_2. Similar reasoning applies to the faults of classes C and D. This approach enables reduction of the operating time.

Apparently, for such an approach, there are no recommended criteria for setting various internal parameters of a relay; and in particular, there is no definite approach on how to co-ordinate relay parameters for different current settings. These problems thus need to be investigated further.

2.5 Inrush Current Detector

Another way to avoid the mal-operation of a power transformer protection due to the magnetising inrush current phenomena is to use the inrush current detector [15].

Curve (a) & (b) Transformer inrush
Curve (c)   Fault current
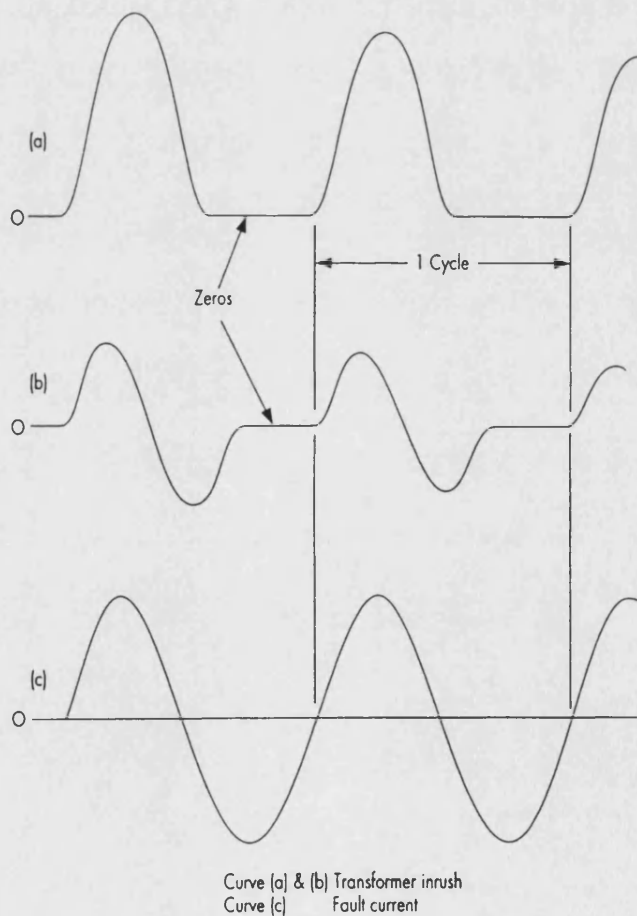
Figure 2.7 Typical internal fault and inrush current waveforms

The operation principle of the inrush current detector is based upon an unique feature of inrush current waveforms, in which zero current periods or zero gaps exist in each cycle. During load or fault conditions, there are no zero gaps in the current waveform (shown in Figure 2.7). Therefore, the detector will detect these zero gaps in the inrush current waveform and initiate an output signal to block the tripping of the relay.

However, under certain condition (such as CT saturation) the gaps may be non-existent; thus, the effectiveness of the inrush current detector becomes questionable.

2.6 Fuzzy Logic Based Approach

In the process of decision making in a power transformer differential relay, there is often a measure of uncertainty. As discussed previously, the differential current may, for example, be caused by other reasons rather than internal faults; this has led to the development of the relay by using several criteria based on " a fuzzy set approach" to improve the reliability of the power transformer protection. In references [16,17], criteria signals (such as amplitude, harmonic contents, etc.) and thresholds associated with the criteria signals were fuzzified and represented by fuzzy numbers. The fuzzy signals (i.e., the fuzzified criteria signals) were then compared with fuzzy settings. Several relaying criteria were used in parallel; the tripping decision was thus made based on the results of the multi-criteria aggregation. The case studies were carried out on a 5.86MW, 140/10.52kV three-phase two winding power transformer.

However, here again for such an approach, there are no recommended criteria for setting various internal threshold parameters of a relay.

2.7 ANN Based Approach

ANNs have the attribute of self-learning and self-organisation of knowledge; furthermore, they can provide the pattern recognition and are proposed by many researchers for implementation of power transformer relaying [7,8,18,19]. In references [7,18], ANN-based schemes for protection of a one-phase power transformer have been initially investigated; while applications of the ANN for a three-phase power transformer protection have been reported in references [8,19]. However, the ANNs in these studies are specific to particular transformer systems, and would have to be retrained again for other systems.

The commonly applied approaches in many ANN-based techniques to power transformer protection assume:

- The ANN is fed by all currents either in the phase or differential-restraining co-ordinates. The data information in a sliding window, consisting of recent and a few historical samples of the signals, is fed into the ANN.

- Output from the ANN encodes the tripping decision.

- Training patterns exposed to the ANN usually cover inrush conditions, internal faults and external faults.

- Additional pre-processing and post-processing may be applied.

However, as the network size increases, the training time becomes longer. This is a critical limitation in the application of ANNs. As the convergence of ANNs can be significantly influenced by the feature of training data, more effort is still required to develop sophisticated techniques for preparation of training data that can result in fast learning performance. In order to do this, a better and more effective feature extraction technique needs to be developed. Moreover, there is no definite way of

choosing the optimum architecture, and there is no clear physical meaning of the ANN parameters, such as weights and biases. All the above issues need to be further studied.

2.8 Summary

The developments that have taken place in power transformer protective techniques for distinguishing internal faults from inrush currents are reviewed. These techniques include the power differential approach; multisetting overcurrent principle; inrush current detector based on the waveform gap identification; fuzzy logic based approach and ANN based approach. The issues and limitations regarding the practical application of each developed technique are also briefly discussed in this chapter.

Chapter 3

Mathematical Models of a Power Transformer

and Instrument Current Transformer

3.1 Introduction

An accurate digital simulation of a power transformer system provides a good supplementary tool to new relay design and relay performance evaluation. This chapter describes a technique for accurately modelling a power transformer for the purposes of simulating its transient phenomena under both fault and magnetising inrush current conditions using EMTP software. This chapter also presents a model of a current transformer (CT), which is used for providing correct operating currents to a protective relay system; in the latter case, the effect of CT saturation on the protective devices has been taken into consideration.

3.2 Mathematical Models of Power Transformers

Realistic modelling of power transformers under various conditions, in particular transient, is never an easy task. The widely-used EMTP provides several possibilities for simulating the main characteristics of a power transformer [20-23]. This involves several subprograms such as XFORMER, TRELEG and BCTRAN. XFORMER can be used for single-phase transformers. BCTRAN are used for single- or three-phase transformers. TRELEG has been replaced by BCTRAN because of ill-conditioning problems in the TRELEG. However, all these programs do not have the ability to

model winding faults, and do not have an ability of integrally modelling and simulating a power transformer differential protection system. Therefore, as mentioned before, it is vitally important to be able to accurately model the fault transient phenomena in a transformer, for example, for the purposes of designing a protection technique. It was against this background that the technique presented herein was developed, and is somewhat based on that in references [20-24].

3.2.1 Modelling of Power Transformers

A power transformer model is built up based on the mutual coupling concept. With this approach, any multi-winding transformer consisting of n coupled coils can be electrically modelled in terms of the terminal voltage V_i, and current i_i, as well as total flux linkage λ_i, of the ith coil as follows [25,26]:

$$V_i = R_i\,i_i + \frac{d\lambda_i}{dt} \tag{3.1}$$

where $i=1,2,3,...,n$. Such a transformer can be represented schematically as shown in Figure 3.1.
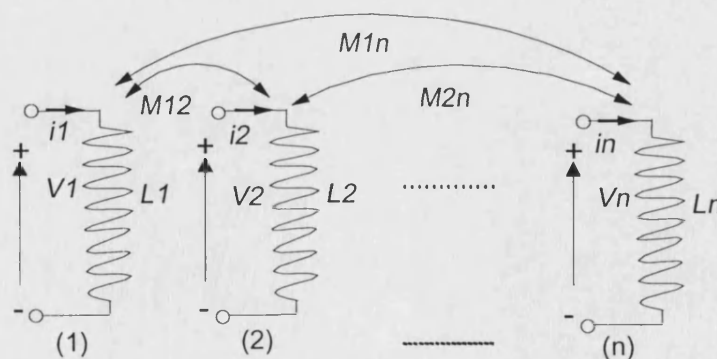
Figure 3.1 A schematic representation of *n*-winding transformer

When magnetic saturation is taken into consideration, λ_i become a non-linear function of the n-winding currents, that is:

$$\lambda_i = \lambda_i(i_1, i_2, \cdots, i_n) \tag{3.2}$$

Thus, for the ith coil, equation (3.1) can be expanded using the chain rule as follows:

$$V_i = R_i\, i_i + \frac{\partial \lambda_i}{\partial i_1}\frac{di_1}{dt} + \frac{\partial \lambda_i}{\partial i_2}\frac{di_2}{dt} + \cdots + \frac{\partial \lambda_i}{\partial i_n}\frac{di_n}{dt} \tag{3.3}$$

The partial derivatives of the flux linkage λ_i with respect to a winding current i_k $(k=1, 2, ..., n)$, are self inductances L_i and mutual inductances M_{ik}, given as:

$$L_i = \frac{\partial \lambda_i}{\partial i_i} \tag{3.4}$$

$$M_{ik} = \frac{\partial \lambda_i}{\partial i_k} \quad (i \neq k) \tag{3.5}$$

Thus, if the power transformer is a three-phase two-winding comprising of six windings, then the mathematical models for such a transformer can be represented by the following matrix relationship:

$$[V] = [R][i] + [L]\left[\frac{di}{dt}\right] \tag{3.6}$$

or

$$\left[\frac{di}{dt}\right] = [L]^{-1}[V] - [L]^{-1}[R][i] \tag{3.7}$$

where

$$[R] = \begin{bmatrix} R_1 & 0 & 0 & 0 & 0 & 0 \\ 0 & R_2 & 0 & 0 & 0 & 0 \\ 0 & 0 & R_3 & 0 & 0 & 0 \\ 0 & 0 & 0 & R_4 & 0 & 0 \\ 0 & 0 & 0 & 0 & R_5 & 0 \\ 0 & 0 & 0 & 0 & 0 & R_6 \end{bmatrix}$$

(3.8)

$$[L] = \begin{bmatrix} L_1 & M_{12} & M_{13} & M_{14} & M_{15} & M_{16} \\ M_{21} & L_2 & M_{23} & M_{24} & M_{25} & M_{26} \\ M_{31} & M_{32} & L_3 & M_{34} & M_{35} & M_{36} \\ M_{41} & M_{42} & M_{43} & L_4 & M_{45} & M_{46} \\ M_{51} & M_{52} & M_{53} & M_{54} & L_5 & M_{56} \\ M_{61} & M_{62} & M_{63} & M_{64} & M_{65} & L_6 \end{bmatrix}$$

(3.9)

$$[V] = [V_1, V_2, V_3, V_4, V_5, V_6]^T$$

(3.10)

$$[i] = [i_1, i_2, i_3, i_4, i_5, i_6]^T$$

(3.11)

$$\left[\frac{di}{dt} \right] = \left[\frac{di_1}{dt} \quad \frac{di_2}{dt} \quad \frac{di_3}{dt} \quad \frac{di_4}{dt} \quad \frac{di_5}{dt} \quad \frac{di_6}{dt} \right]^T$$

(3.12)

and (V_1, V_2 . . . V_6) are the terminal voltages on the primary and secondary windings respectively; (i_1, i_2 . . . i_6) are the currents on the primary and secondary windings respectively; (R_1, R_2 . . . R_6) are the resistances on the primary and secondary windings respectively; (L_1, L_2 . . . L_6) are the self-inductances on the primary and secondary windings respectively; M_{ij} are the mutual-indutances between windings i and j respectively $(i=1,2,...,6; j=1,2,...,6; i \neq j)$.

The foregoing transformer model is then embedded into the basic transmission network model using the EMTP software.

3.2.2 Modelling of Internal Winding Faults

The principle used to model a fault between a coil turn and earth or between turn and turn hinges upon dividing the faulted coil, as shown in Figures 3.2 (a) and (b).

(a)   (b)
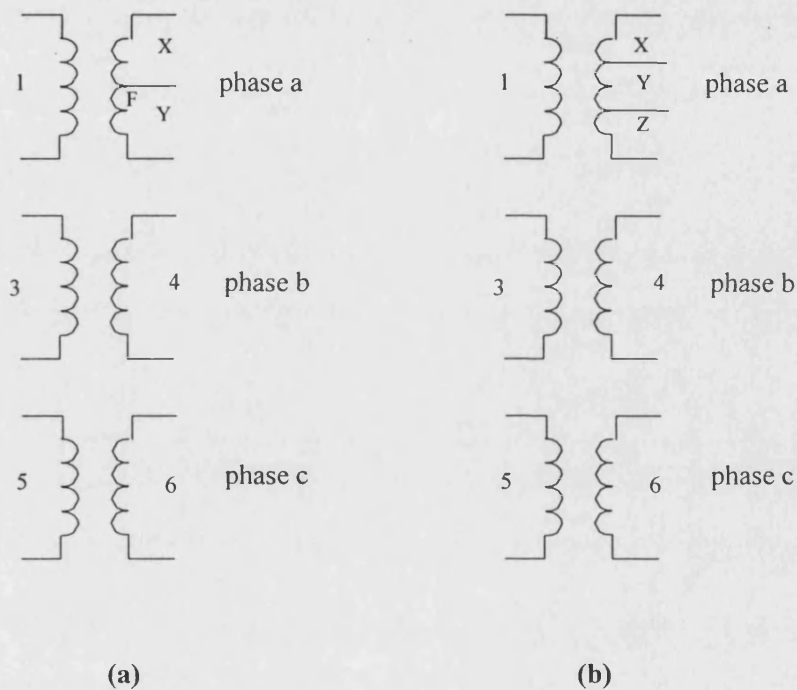
Figure 3.2 Internal winding fault modelling
(a) turn-to-earth fault (b) turn-to-turn fault

When the power transformer winding has no fault, matrices $[R]$ and $[L]$ for a three-phase two-winding transformer are of order 6 as given in equation (3.8) and equation (3.9) respectively. When a turn-to-earth fault occurs on the a-phase winding on high voltage (HV) side as shown in Figure 3.2 (a), the transformer can be described by two *7x7* matrices $[R]_{7x7}$ and $[L]_{7x7}$ respectively. They are described by:

$$[R]_{7x7} = \begin{bmatrix} R_1 & 0 & 0 & 0 & 0 & 0 & 0 \\ 0 & R_X & 0 & 0 & 0 & 0 & 0 \\ 0 & 0 & R_Y & 0 & 0 & 0 & 0 \\ 0 & 0 & 0 & R_3 & 0 & 0 & 0 \\ 0 & 0 & 0 & 0 & R_4 & 0 & 0 \\ 0 & 0 & 0 & 0 & 0 & R_5 & 0 \\ 0 & 0 & 0 & 0 & 0 & 0 & R_6 \end{bmatrix} \qquad (3.13)$$

$$[L]_{7x7} = \begin{bmatrix} L_1 & M_{1X} & M_{1Y} & M_{13} & M_{14} & M_{15} & M_{16} \\ M_{X1} & L_X & M_{XY} & M_{X3} & M_{X4} & M_{X5} & M_{X6} \\ M_{Y1} & M_{YX} & L_Y & M_{Y3} & M_{Y4} & M_{Y5} & M_{Y6} \\ M_{31} & M_{3X} & M_{3Y} & L_3 & M_{34} & M_{35} & M_{36} \\ M_{41} & M_{4X} & M_{4Y} & M_{43} & L_4 & M_{45} & M_{46} \\ M_{51} & M_{5X} & M_{5Y} & M_{53} & M_{54} & L_5 & M_{56} \\ M_{61} & M_{6X} & M_{6Y} & M_{63} & M_{64} & M_{65} & L_6 \end{bmatrix} \qquad (3.14)$$

The position of the fault point is expressed by n_X and n_Y where:

n_X = number of turns of 'sub-coil' x

n_Y = number of turns of 'sub-coil' y

and the additional elements in the matrix $[R]_{7x7}$ in equation (3.13) are defined by:

$$R_X = \frac{n_X}{n_2} R_2 \; ; \qquad R_Y = \frac{n_Y}{n_2} R_2 \qquad (3.15)$$

where R_2 is given by the original 6×6 matrix $[R]$ given in equation (3.8). The additional elements in the matrix $[L]_{7x7}$ in equation (3.14) are given by:

$$L_X = \frac{L_2}{(1/K^2) + (2\sqrt{1 - \sigma_{XY}} / K) + 1} \qquad (3.16)$$

$$L_Y = \frac{L_2}{K^2 + 2K\sqrt{1-\sigma_{XY}} + 1} \tag{3.17}$$

$$M_{XY} = \frac{L_2\sqrt{1-\sigma_{XY}}}{K + 1/K + 2\sqrt{1-\sigma_{XY}}} \tag{3.18}$$

$$M_{Xi} = (K/(K+1))M_{2i} \; ; \tag{3.19}$$

$$M_{Yi} = (1/(1+K))M_{2i} \tag{3.20}$$

$$K = \frac{n_X}{n_Y} \tag{3.21}$$

where K is the voltage ratio between sub-coils x and y; σ_{XY} is a leakage factor. In reference [24], a very simple method is proposed to evaluate the leakage factor (herein, σ_{XY}=0.016); L_2 and M_{2i} are given by the original 6×6 matrices given by equation (3.9).

As described above, for a turn-to-turn fault on the a-phase winding on HV side as shown in Figure 3.2 (b), the dimensions of the aforementioned [R] and [L] matrices are increased to 8×8. They are described as follows:

$$[R] = \begin{bmatrix} R_1 & 0 & 0 & 0 & 0 & 0 & 0 & 0 \\ 0 & R_X & 0 & 0 & 0 & 0 & 0 & 0 \\ 0 & 0 & R_Y & 0 & 0 & 0 & 0 & 0 \\ 0 & 0 & 0 & R_Z & 0 & 0 & 0 & 0 \\ 0 & 0 & 0 & 0 & R_3 & 0 & 0 & 0 \\ 0 & 0 & 0 & 0 & 0 & R_4 & 0 & 0 \\ 0 & 0 & 0 & 0 & 0 & 0 & R_5 & 0 \\ 0 & 0 & 0 & 0 & 0 & 0 & 0 & R_6 \end{bmatrix} \tag{3.22}$$

$$[L] = \begin{bmatrix} L_1 & M_{1X} & M_{1Y} & M_{1Z} & M_{13} & M_{14} & M_{15} & M_{16} \\ M_{X1} & L_X & M_{XY} & M_{XZ} & M_{X3} & M_{X4} & M_{X5} & M_{X6} \\ M_{Y1} & M_{YX} & L_Y & M_{YZ} & M_{Y3} & M_{Y4} & M_{Y5} & M_{Y6} \\ M_{Z1} & M_{ZX} & M_{ZY} & L_Z & M_{Z3} & M_{Z4} & M_{Z5} & M_{Z6} \\ M_{31} & M_{3X} & M_{3Y} & M_{3Z} & L_3 & M_{34} & M_{35} & M_{36} \\ M_{41} & M_{4X} & M_{4Y} & M_{4Z} & M_{43} & L_4 & M_{45} & M_{46} \\ M_{51} & M_{5X} & M_{5Y} & M_{5Z} & M_{53} & M_{54} & L_5 & M_{56} \\ M_{61} & M_{6X} & M_{6Y} & M_{6Z} & M_{63} & M_{64} & M_{65} & L_6 \end{bmatrix}$$
(3.23)

where,

n_X = number of turns of 'sub-coil' x

n_Y = number of turns of 'sub-coil' y

n_Z = number of turns of 'sub-coil' z

$$R_X = \frac{n_X}{n_2} R_2$$
(3.24)

$$R_Y = \frac{n_Y}{n_2} R_2$$
(3.25)

$$R_z = \frac{n_Z}{n_2} R_2$$
(3.26)

$$L_X = \left(\frac{n_X}{n_2}\right)^2$$
(3.27)

$$L_Y = \left(\frac{n_Y}{n_2}\right)^2$$
(3.28)

$$L_Z = \left(\frac{n_Z}{n_2}\right)^2$$
(3.29)

$$M_{XY} = \left(\frac{n_X n_Y}{n_2^2}\right)$$
(3.30)

$$M_{XZ} = \left(\frac{n_X n_Z}{n_2^2} \right) \tag{3.31}$$

$$M_{YZ} = \left(\frac{n_Y n_Z}{n_2^2} \right) \tag{3.32}$$

$$K = \frac{n_X}{n_Y} \quad ; \qquad K' = \frac{n_X}{n_Z} \tag{3.33}$$

$$M_{Xi} = \frac{M_{2i}}{1 + \dfrac{1}{K} + \dfrac{1}{K'}} \tag{3.34}$$

$$M_{Yi} = \frac{M_{2i}}{1 + K + \dfrac{K}{K'}} \tag{3.35}$$

$$M_{Zi} = \frac{M_{2i}}{1 + K' + \dfrac{K'}{K}} \tag{3.36}$$

and R_2 and M_{2i} are given by the original *6×6* matrices presented by equations (3.8) and (3.9) respectively.

Thus in summary, the basic steps involved for simulating the internal winding fault are as follows:

Step 1: use the BCTRAN routine to obtain original linear matrices $[R]$ and $[L]$ of the power transformer, under healthy conditions (as shown in equations (3.8) and (3.9));

Step 2: modify the above matrices $[R]$ and $[L]$ according to the internal winding fault type and obtain the new internal winding fault matrices, $[R]_{7x7}$ and $[L]_{7x7}$ for a turn-to-earth fault; or $[R]_{8x8}$ and $[L]_{8x8}$ for a turn-to-turn fault;

Step 3: simulate the internal winding fault using the modified internal winding fault matrices $[R]_{7x7}$ and $[L]_{7x7}$ or $[R]_{8x8}$ and $[L]_{8x8}$ via the EMTP software.

3.2.3 Modelling of Inrush Currents

An accurate modelling of inrush currents is an important prerequisite for digital protection of power transformers, a number of studies on the area have been carried out [27-32]. In Chapter 2, the phenomenon of inrush currents in power transformers has been described, it is thus apparent from the foregoing that modelling inrush current must take into account the core saturation of a power transformer.

As mentioned in section 3.2.1 of this Chapter, λ_i is a non-linear function of the n-winding currents, it is related to the non-linearity of the power transformer core, which in turn is dictated by the non-linear magnetising curve of the core. This problem of simulating this non-linearity is overcome herein by adding equivalently non-linear element ($\phi - i$ curve) to the matrix [L] shown in equation (3.9).

3.3 Mathematical Models of Current Transformers

A CT is an integral part of any power system, essentially for measurement and protection. The purpose of measuring CT is to measure the system parameters under normal conditions, not exceeding maximum expected full load current, whereas the protective CT has to correctly reproduce fault current so that the protective relays operate satisfactorily. In modern HV and EHV power systems more and more emphasis is placed on the ability of CTs to provide correct operating current to protective relay systems [33-38]. In this study, CT models are intended for the protective relay transient performance analysis, and this includes studying the effects of CT saturation on relays. CT models developed herein are essentially based on those outlined in reference [39]. This model comprises of an equivalent circuit built around an ideal transformer as shown in Figure 3.3. The magnetising branch is represented as a non-linear inductor, and it is represented by a λ-i hysteresis loop.
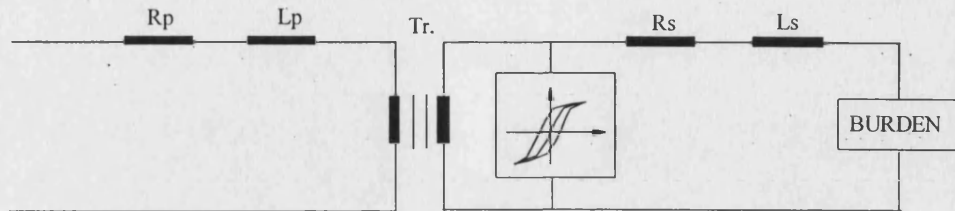
Figure 3.3 EMTP-based CT model

In Figure 3.3, Rp represents primary winding resistance; Lp represents primary winding leakage inductance; Rs represents secondary winding resistance; Ls represents secondary winding leakage inductance; Tr represents an ideal transformer.

3.4 Summary

A modelling approach for accurately modelling a power transformer for the purposes of simulating its transient phenomena and designing and evaluating a new protective relay is presented in this chapter. Based on the basic model of the power transformer, which is provided in EMTP, the model developed herein is a significantly modified form of the basis model, thereby the resulted model can be used for not only simulating internal terminal faults, but also internal winding faults. In additional, the inrush current modelling is implemented by adding equivalently non-linear element into the basic model. Furthermore, CT modelling is also presented; this includes consideration of CT saturation essentially for the purposes of studying the effect of CT saturation on relay performance outlined in a later section.

Chapter 4

Electromagnetic Simulation Study of
Power Transformer Faults

4.1 Introduction

Based on the models described in Chapter 3, transient phenomena of a power transformer system under internal and external faults with/without CT saturation were simulated in two different power transformer systems, namely System 1 and System 2 (as described later in this chapter), using EMTP software. The purpose of the simulation is to generate accurate and realistic fault data, essentially to develop alternative techniques for satisfactorily protecting a power transformer under a whole variety of practically encountered faults, concomitant with its ability to distinguish internal faults from magnetising inrush currents.

4.2 Winding Connections in Power Transformer Systems

The variation of winding connections in the power transformer will influence the transient performances of faults and inrush currents, and this in turn will make a difference to the protection scheme chosen; it is therefore important to consider the various winding connections in power transformer systems [10,11,13]. Unlike a three-phase generator, where the input and output currents are in phase as well as equal in magnitude under normal steady state operation, in a transformer, these

currents are different. Four types of winding connections of power transformer systems with the corresponding phasor diagrams are shown in Figures 4.1 to 4.4.
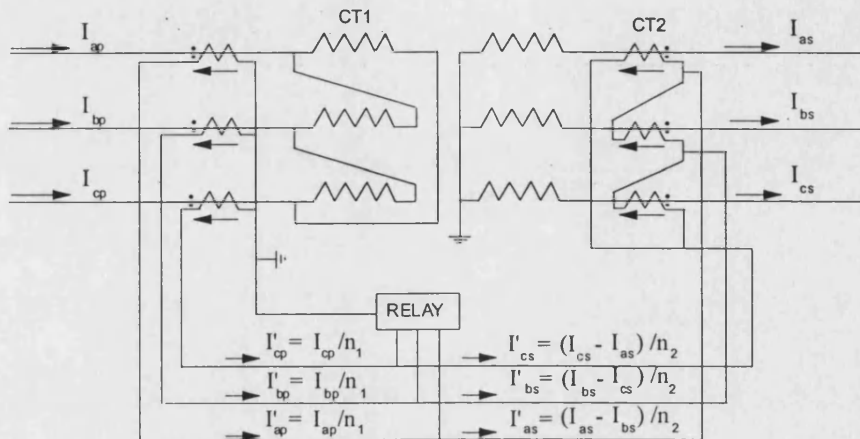
(a) Connections of Dy1 transformer system
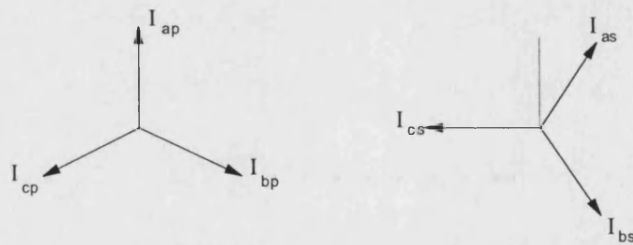
(b) Current phasor diagrams on CT primary side
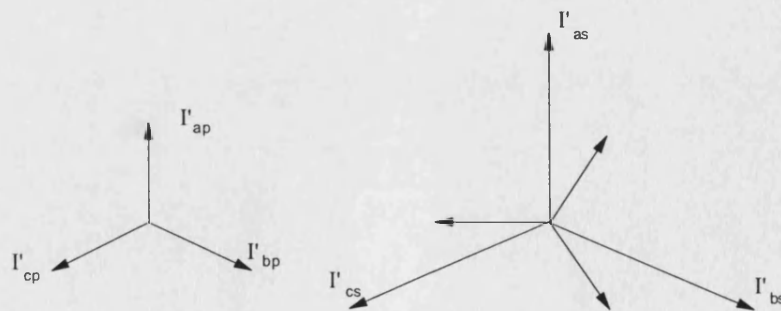
(c) Current phasor diagrams on CT secondary side

Figure 4.1 Winding connections of Dy1 transformer system and phasor diagrams
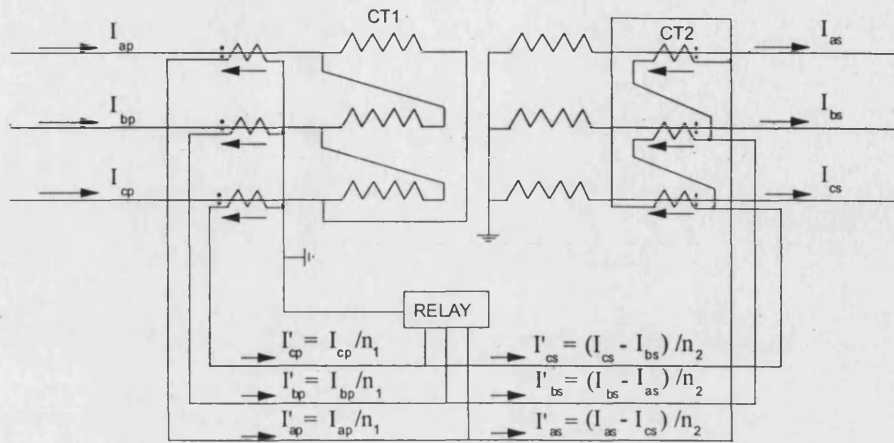
(a) Connections of Dy11 transformer system
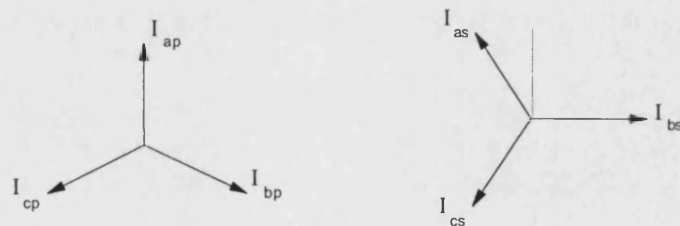
(b) Current phasor diagrams on CT primary side
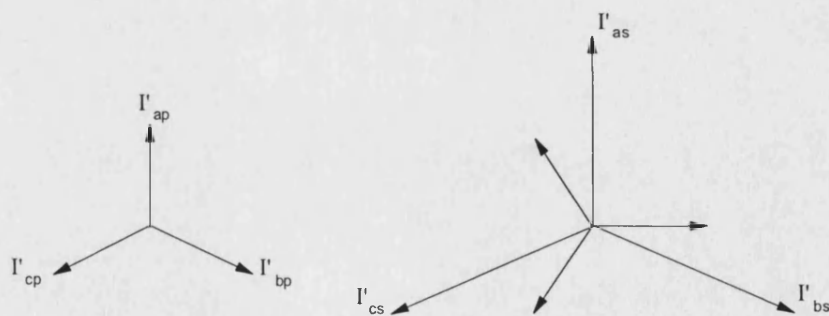
(c) Current phasor diagrams on CT secondary side

Figure 4.2 Winding connections of Dy11 transformer system and phasor diagrams
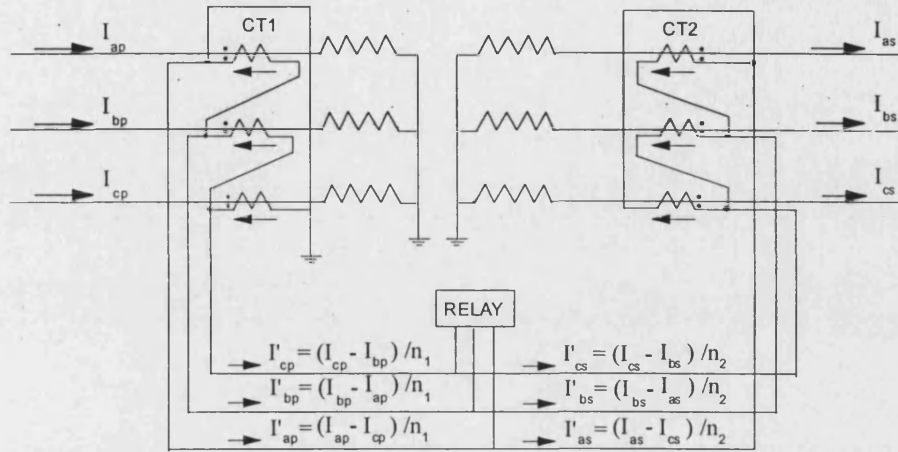
(a) Connections of Yy0 transformer system

$$I'_{cp} = (I_{cp} - I_{bp})/n_1 \qquad I'_{cs} = (I_{cs} - I_{bs})/n_2$$
$$I'_{bp} = (I_{bp} - I_{ap})/n_1 \qquad I'_{bs} = (I_{bs} - I_{as})/n_2$$
$$I'_{ap} = (I_{ap} - I_{cp})/n_1 \qquad I'_{as} = (I_{as} - I_{cs})/n_2$$
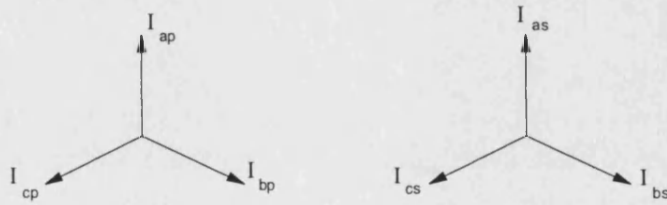
(b) Current phasor diagrams on CT primary side
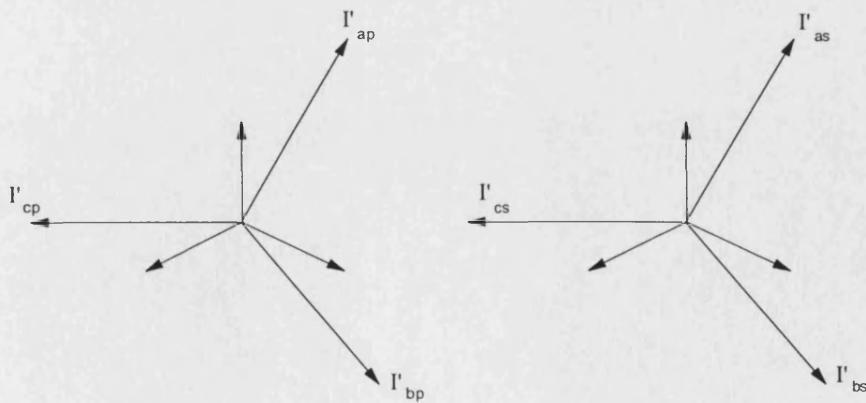
(c) Current phasor diagrams on CT secondary side

Figure 4.3 Windings connections of Yy0 transformer system and phasor diagrams
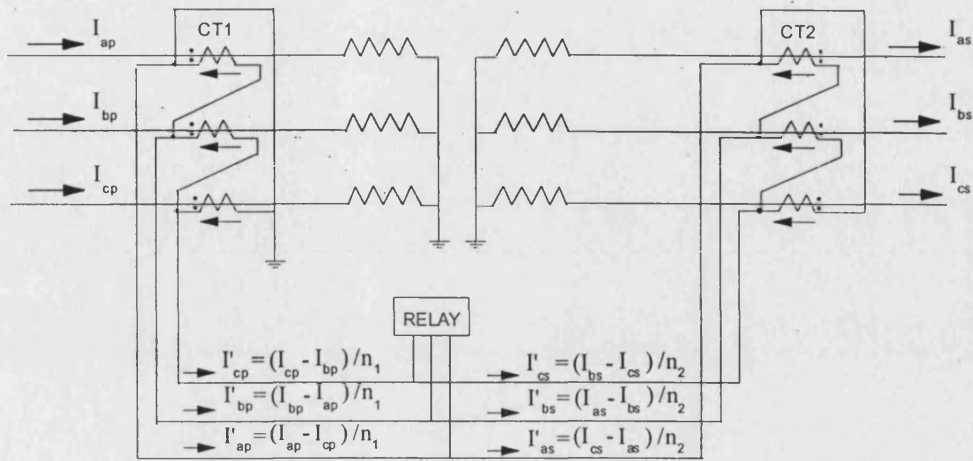
(a) Connections of Yy6 transformer system
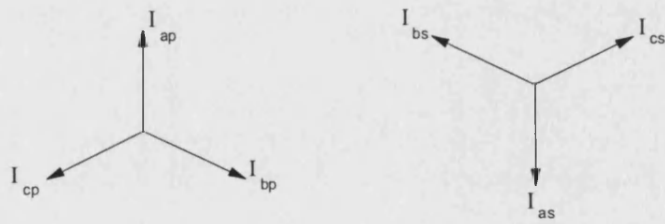
(b) Current phasor diagrams on CT primary side
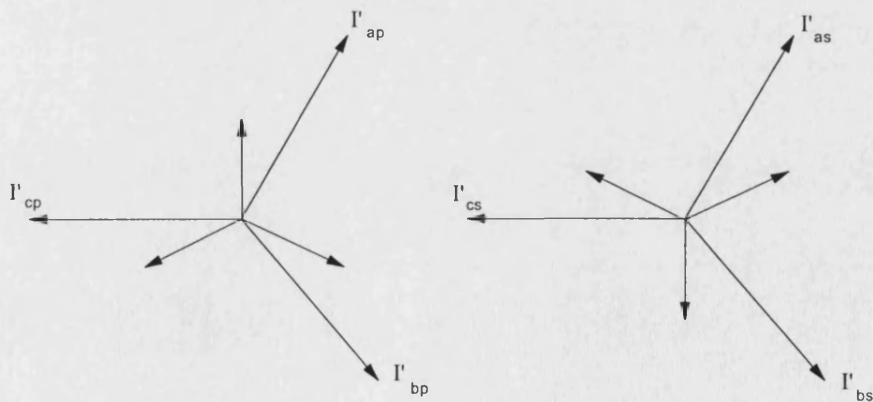
(c) Current phasor diagrams on CT secondary side

Figure 4.4 Winding connections of Yy6 transformer system and phasor diagrams

As a general rule, the CTs on the star side of transformers must be connected in delta, and the CTs on the delta side must be connected in star. This is for (1) compensating phase-angle shift; (2) blocking the zero sequence current from the differential circuit under external ground faults. Moreover, the CT turns ratio (n_1 corresponds to CT1, n_2 corresponds to CT2) should also be properly chosen for amplitude balance so to ensure that the relay does not operate on normal load flow or for an external fault.

4.3 Simulated Power Transformer Systems

As mentioned before, to generate accurate and realistic fault data, essentially to develop alternative techniques for satisfactorily protecting a power transformer under a whole variety of practically encountered faults, concomitant with its ability to distinguish internal faults from magnetising inrush currents, two different power transformer systems are selected as the studied systems in this research work. It is expected that simulation results will be employed to explore new protection techniques that can be able to be used for different power transformer systems.

4.3.1 System 1: A Double-End-Fed Power Transformer System

System 1 consists of a *750MVA, 27/420kV* power transformer connected between a *25kV* source at the sending end and a *400kV* transmission line connected to an infinite bus power system at the receiving end. The simulated power transformer system for case studies is shown in Figure 4.5.
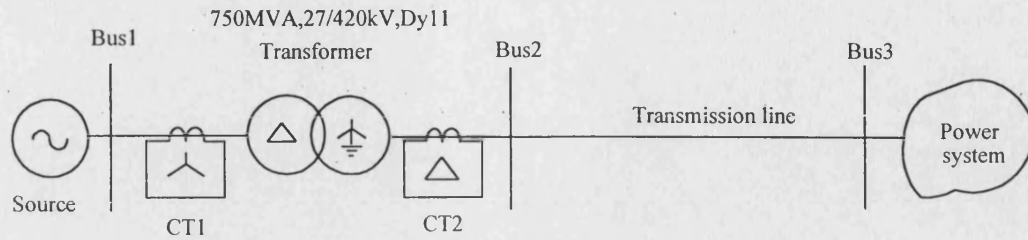
Figure 4.5 A double-end-fed power transformer system

4.3.2 System 2: A Single-End-Fed Power Transformer System

System 2 consists of a *35MVA, 11/132kV* power transformer connected between an *11kV* source and an *132 kV* transmission line. Figure 4.6 shows the simulated power transformer system for case studies.
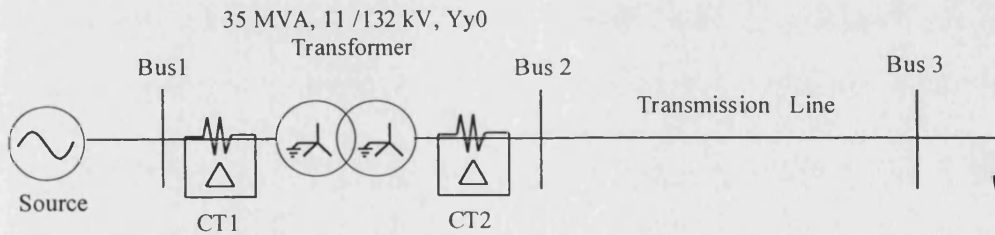
Figure 4.6 A single-end-fed power transformer system

4.3.3 Simulated Fault Types

In order to generate accurate and realistic fault data, for the purposes of developing alternative techniques for satisfactorily protecting a power transformer under a whole variety of practically encountered faults, various power transformer fault transients have been simulated in System 1 and System 2, and some typical fault cases are summarised in Table 4.1.

Table 4.1 List of simulated fault cases

Simulated Case	Type
Internal terminal phase-to-phase faults	Three-phase short circuit fault on LV/ HV sides a-b two phase short circuit on LV/ HV sides a-c two phase short circuit on LV/ HV sides b-c two phase short circuit on LV/ HV sides
Internal terminal phase-to-earth faults	Three-phase-to-earth fault on LV/ HV sides a-b two phase to earth on LV/ HV sides a-c two phase to earth on LV/ HV sides b-c two phase to earth on LV/ HV sides a-phase to earth on LV/ HV sides b-phase to earth on LV/ HV sides c-phase to earth on LV/ HV sides
Internal winding turn-to-turn faults	a-phase 5% turn-to-turn, at mid-point of winding on LV/ HV sides b-phase 5% turn-to-turn, at mid-point of winding on LV/ HV sides c-phase 5% turn-to-turn, at mid-point of winding on LV/ HV sides a-phase 15% turn-to-turn, at mid-point of winding on LV/ HV sides b-phase 15% turn-to-turn, at mid-point of winding on LV/ HV sides c-phase 15% turn-to-turn, at mid-point of winding on LV/ HV sides
Internal winding turn-to-earth faults	a-phase-to-earth at mid-point of winding on LV/ HV sides b-phase-to-earth at mid-point of winding on LV/ HV sides c-phase-to-earth at mid-point of winding on LV/ HV sides a-phase-to-earth at 70% of winding from neutral point on LV/ HV sides b-phase-to-earth at 70% of winding from neutral point on LV/ HV sides c-phase-to-earth at 70% of winding from neutral point on LV/ HV sides
External faults	External faults with CT saturation

4.4 Electromagnetic Simulation Studies of Power Transformer Faults in System 1

An extensive simulation of power transformer faults is firstly carried out on System 1. The some typical fault studies in System 1 are depicted in Figure 4.7.
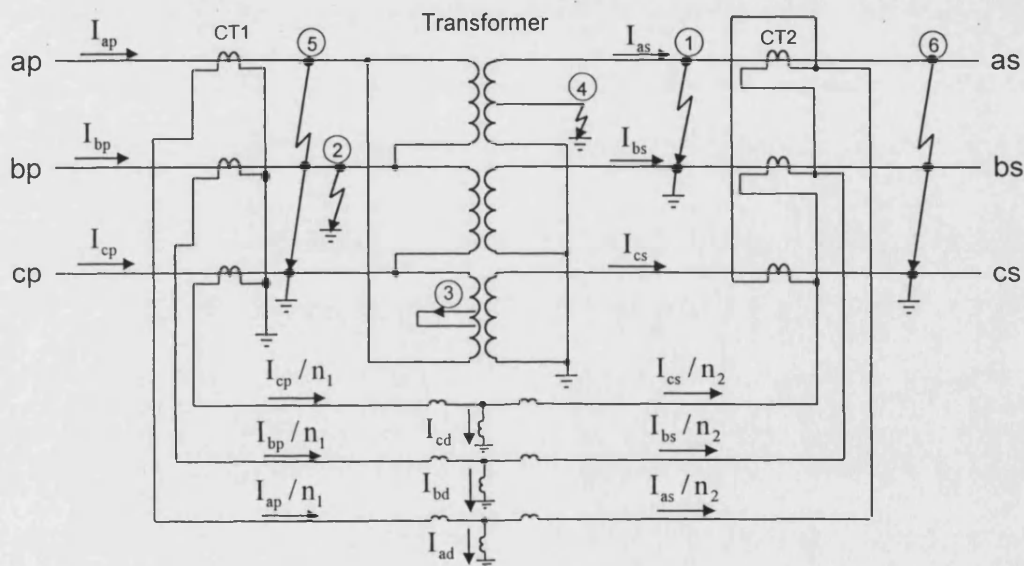
Figure 4.7 Simulation of typical faults in System 1

where, ① stands for a-b two-phase-to-earth terminal fault on high voltage (HV) side; ② stands for b-phase-to-earth terminal fault on low voltage (LV) side; ③ stands for c-phase 5% turn-to-turn winding fault at mid-point of winding on LV side; ④ stands for a-phase turn-to earth winding fault at mid-point of winding on HV side; ⑤ stands for an internal three-phase short circuit on LV side; ⑥ stands for an external three-phase short circuit on HV side. Hereafter, the nomenclature of subscripts is that *ap, bp, cp* refer to a, b and c three phases on primary side of the power transformer (LV side), *as, bs, cs* refer to a, b and c three phases on secondary side of the power transformer (HV side), *ad, bd, cd* refer to a, b and c three-phase differential signals through the CT secondary sides.

The simulation results, which correspond to the faults typified in Figure 4.7, will be given in the following sections.

4.4.1 Simulation of Internal Faults without CT Saturation

Internal fault simulation studies of power transformers without CT saturation are firstly carried out, and some typical results are presented and analysed respectively.

4.4.1.1 Terminal Two-Phase-to-Earth Faults

First of all considering an a-b two-phase earth fault on the high voltage side of the transformer (Figure 4.7 ①), it is apparent from Figure 4.8 (a) and (b) that there is more high frequency (HF) distortion on the current waveforms on the high voltage (HV) side compared to that experienced on the low voltage (LV) side. This would be somewhat expected by virtue of the fact that the magnitudes of currents are significantly higher on LV side and are predominantly power frequency which completely swamp over any high frequency distortion. In contrast, the magnitudes of the power frequency currents on HV side are relatively much smaller. Moreover, the HV side is directly connected to the transmission line and the travelling wave effect generated on the transmission line also has some bearing on the distortion observed on HV side.
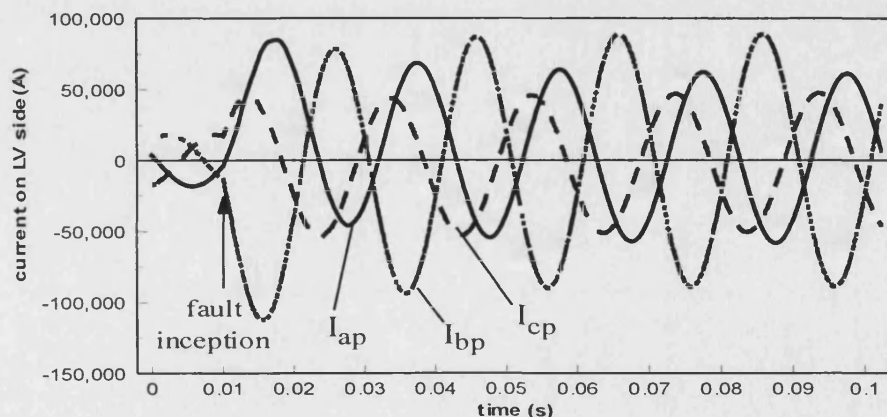
(a) currents on LV side
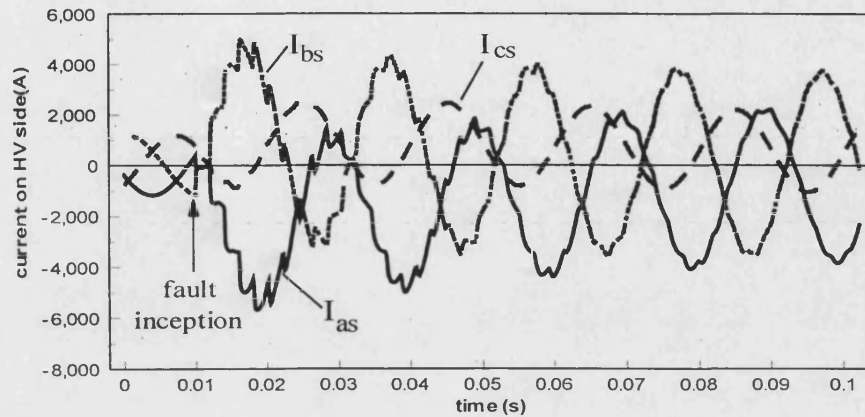
(b) currents on HV side
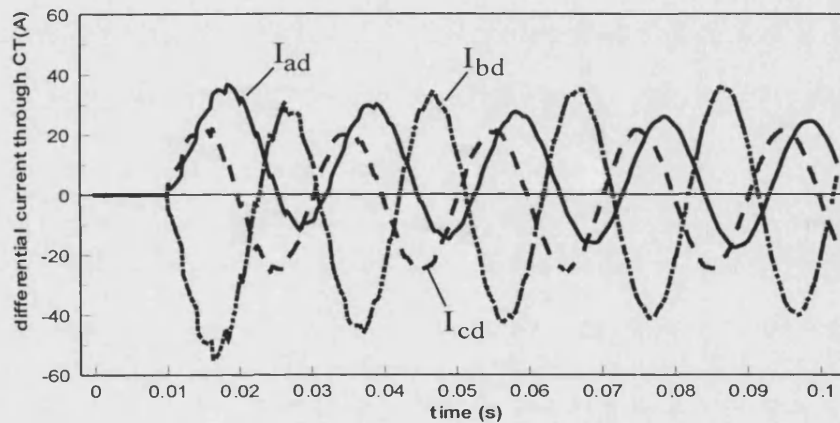
(c) differential currents through CT secondary side

Figure 4.8 Current waveforms of an a-b two-phase-to-earth fault on HV side

4.4.1.2 Terminal Single-Phase-to-Earth Fault

Fault transient phenomenon similar to the foregoing (particularly in terms of waveform distortion) is observed for a b-phase-to-earth fault on LV side of the transformer (Figure 4.7 ②). Here of course, the a and c phase currents on LV shown in Figure 4.9 (a) are very small compared to the faulted b-phase and this is also the case when observing the differential currents through the CT secondary as shown in Figure 4.9 (c).
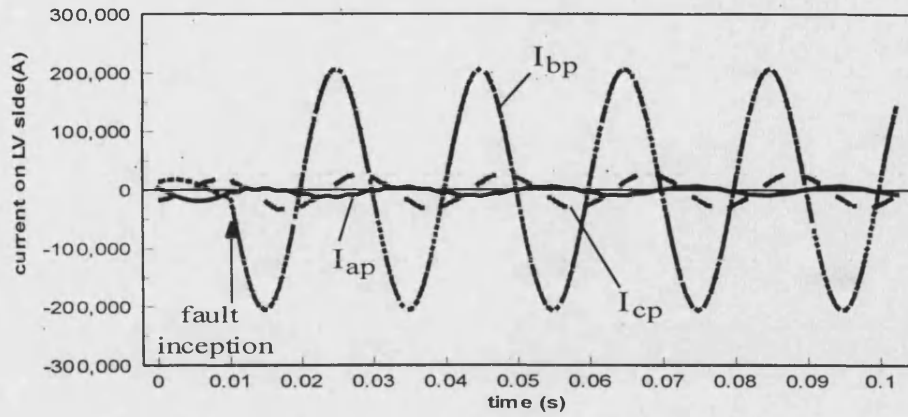
(a) currents on LV side
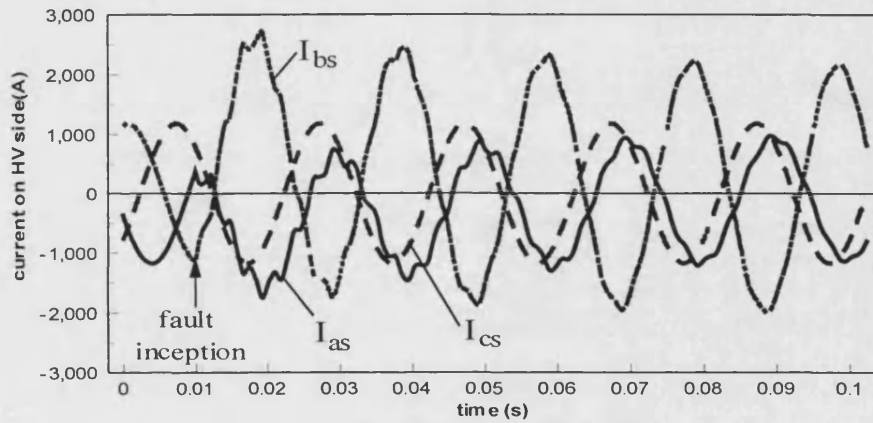
(b) currents on HV side
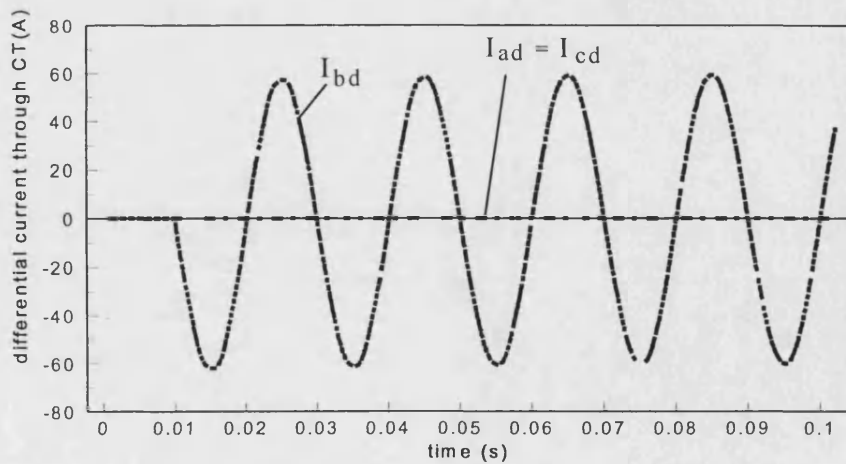
(c) differential currents through CT secondary side

Figure 4.9 Current waveforms of a b-phase to earth fault on LV side

4.4.1.3 Winding Turn-to-Turn Fault

A c-phase 5% turn-to-turn fault at mid-point of the winding on LV side of the transformer is shown in Figure 4.7 ③. A short circuit of a few turns of the winding will give rise to heavy fault current in the short circuited loop, but the terminal currents both on HV and LV sides are quite small. It is evident from Figure 4.10 (a)-(c) that the currents on either HV side or LV side during the period of the turn-to-turn fault are only slightly different from the normal load current and as a direct consequence of this, the differential currents generated are much smaller compared to those caused by other types of faults.
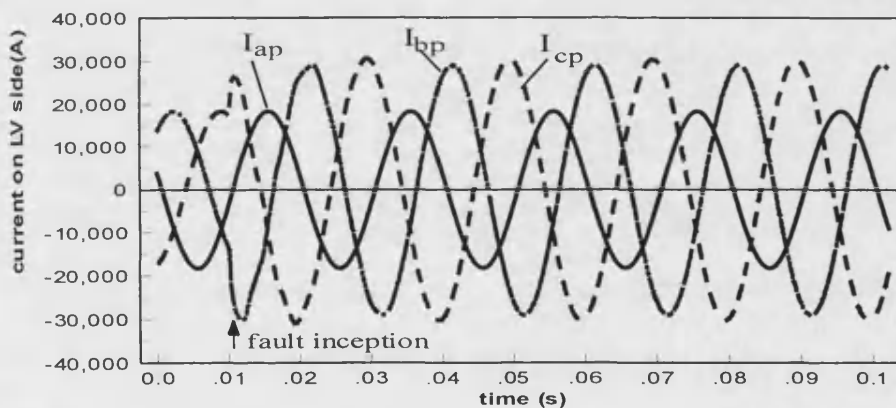
(a) currents on LV side
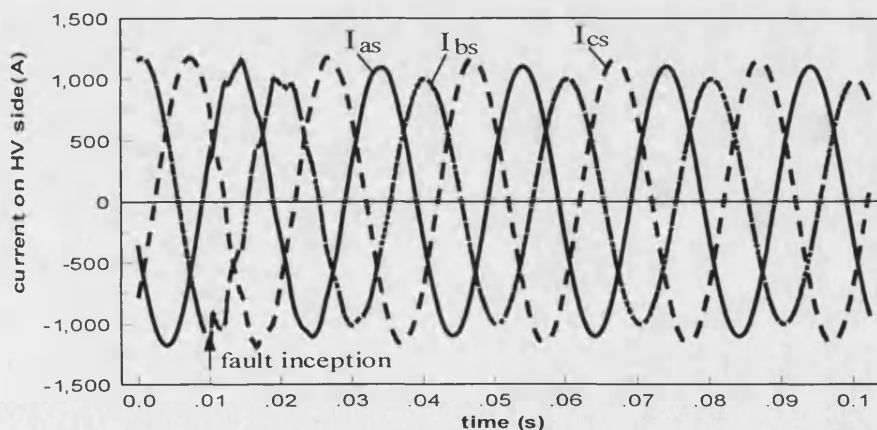
(b) currents on HV side
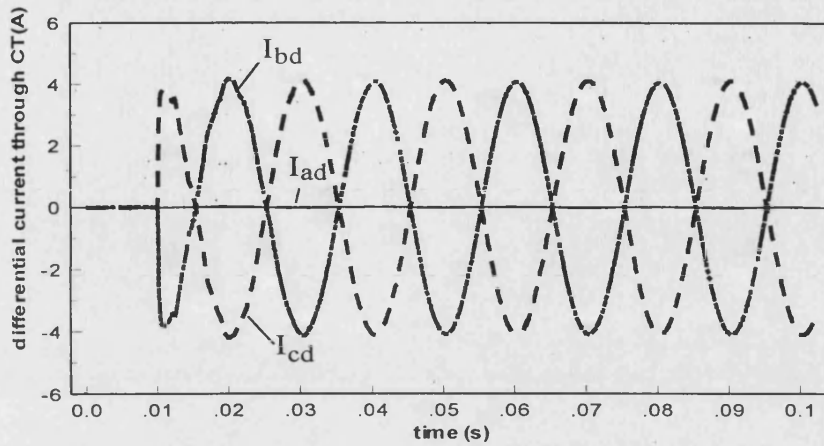
(c) differential currents through CT secondary side

Figure 4.10 Current waveforms of a c-phase 5% turn-to-turn fault at mid-point of winding on LV side

4.4.1.4 Winding Turn-to-Earth Fault

Figure 4.7 ④ shows the transformer currents for an a-phase-to-earth fault at the mid-point of the winding on HV side. Here again, the terminal currents are little different from the normal load currents. From Figure 4.11 (c), it can be seen that the differential currents are again very small.
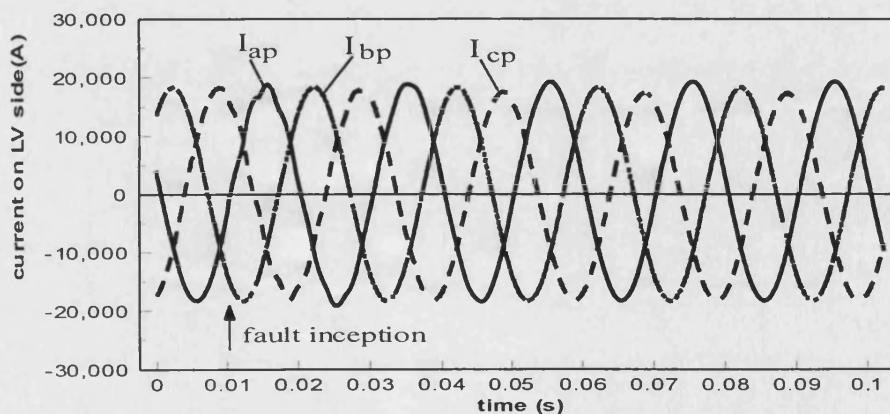
(a) currents on LV side
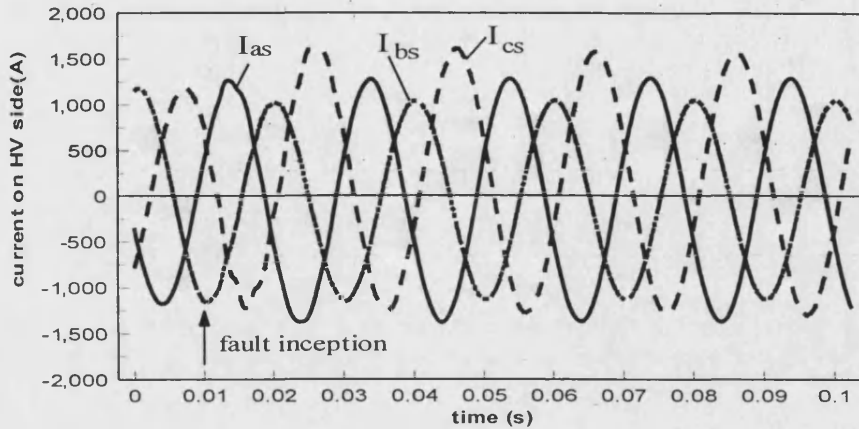
(b) currents on HV side
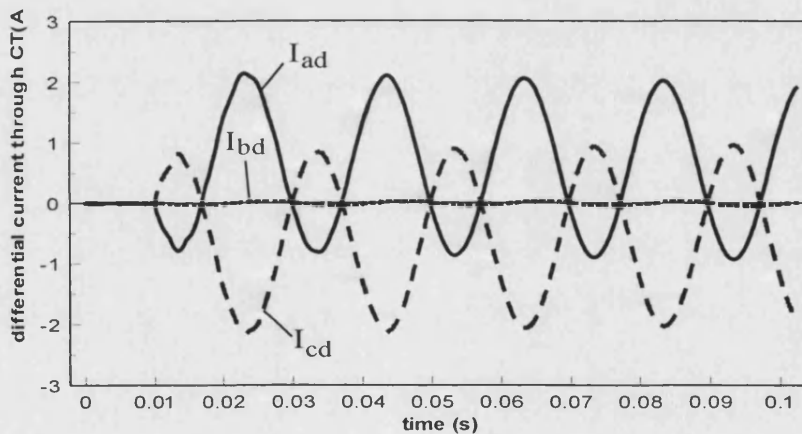
(c) differential currents through CT secondary side

Figure 4.11 Current waveforms of an a-phase turn-to-earth fault at mid-point of winding on HV side

It is thus apparent from the foregoing that there is a wide variation both in the magnitude and distortion in the fault current waveforms, depending upon the type of fault and its location. Importantly, any new protection technique must be capable of dealing with this wide diversity of fault data.

4.4.2 Simulation of Internal Faults with CT Saturation

It is well known that CT saturation can cause a severe distortion in CT secondary currents thereby rendering them to be totally different from the CT primary waveforms. This in turn can lead to a large second harmonic to be generated during internal faults, thereby resulting in the conventional differential protection, based on the second harmonic restraint, to block the operation of the protection under certain internal faults. It is thus vitally important to be able to simulate CT saturation under internal faults; this has been accomplished herein by (i) variation in the fault inception angles, (ii) through different levels of CT remnant flux.

4.4.2.1 Effect of Fault Inception Angle on Fault Current

Since the D.C. component of the fault current is the dominant factor in causing CT saturation and it is influenced by the fault inception angle α, two typical case studies are presented, which involve a three-phase short circuit occurring on LV of the power transformer (shown in Figure 4.7 ⑤) when the fault inception angles are $\alpha=0°$ and $\alpha=90°$, respectively, under a condition that there is an initial remnant flux (50% rated flux) in a, b and c three-phase CT core on LV side respectively, and a zero remnant flux in a, b and c three-phase CT core on HV side respectively. For simplification, only a-phase current result is depicted in Figures 4.12 and 4.13. Note that in these Figures, ① stands for the desired CT secondary current, and ② stands for the actual CT secondary current.
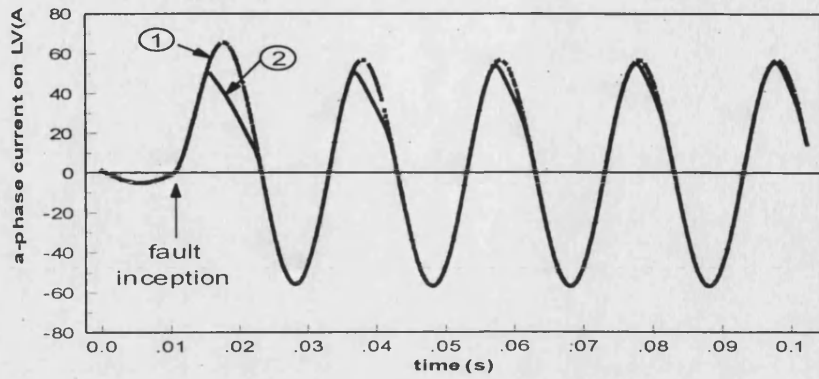
(a) a-phase CT secondary current on LV side
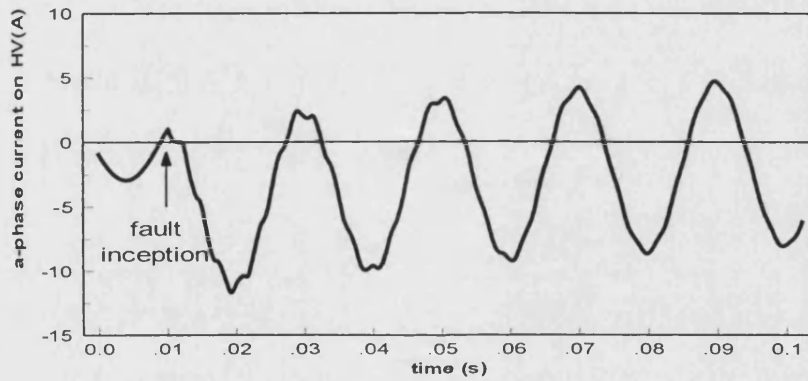
(b) a-phase CT secondary current on HV side
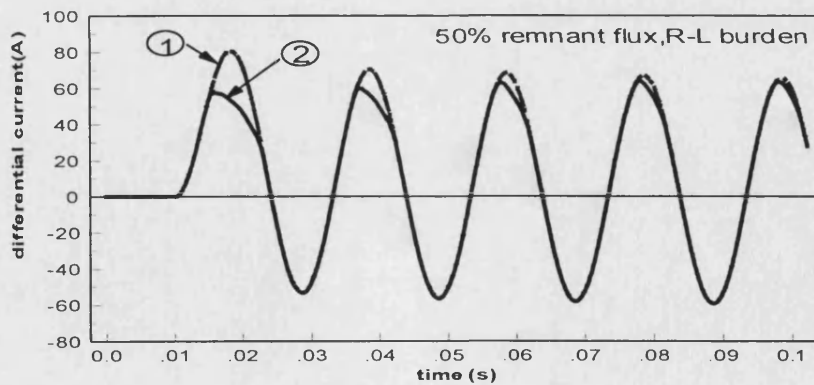
(c) a-phase differential current

Figure 4.12 Current waveforms of an internal three-phase short circuit on LV side under fault inception angle α=0⁰
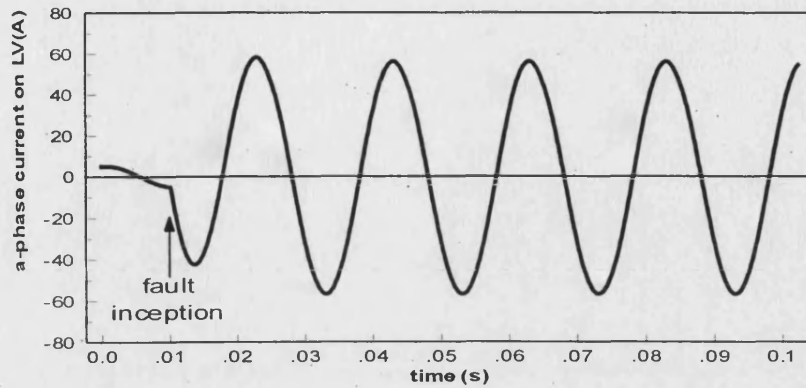
(a) a-phase CT secondary current on LV side
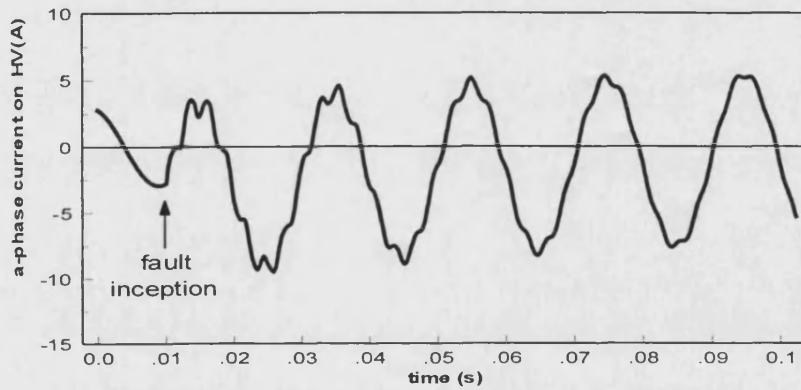
(b) a-phase CT secondary current on HV side
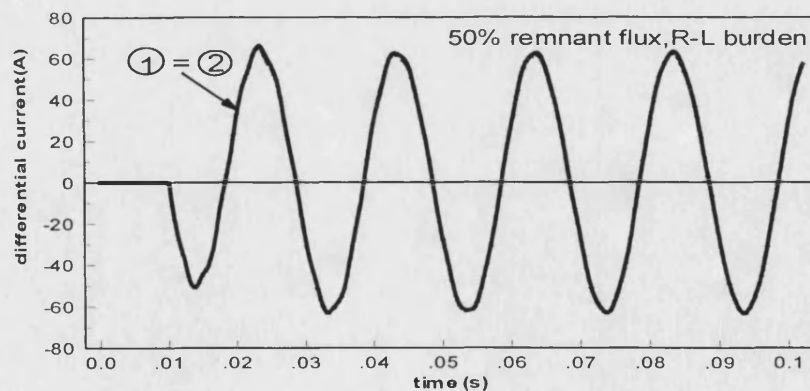
(c) a-phase differential current

Figure 4.13 Current waveforms of an internal three-phase short circuit on LV side under fault inception angle $\alpha=90^0$

From Figure 4.12, which corresponds to fault inception angle $\alpha=0°$, it can be seen that the D.C. component in a-phase current on LV is large in the initial period following a fault, together with the initial remnant flux in a-phase core, and as a consequence, the a-phase CT on LV side saturates, resulting in a marked difference between the CT primary current (referred to secondary) and the CT secondary current shown in Figure 4.12 (a); whereas, the a-phase CT on HV side does not saturate due to the less D.C offset at the fault inception and the zero remnant flux in the CT core, the a-phase current is therefore faithfully reproduced on HV side shown in Figure 4.12 (b); Figure 4.12 (c) shows the a-phase differential current, as expected, a-phase differential current is distorted, as evident from Figure 4.12 (c)

In sharp contrast, when the fault inception angle is $\alpha=90°$, i.e. the maximum voltage point of the a-phase voltage, there is no D.C. offset in a-phase current on LV, even there is the initial remnant flux in the a-phase core, the a-phase current is still faithfully reproduced, as evident from Figure 4.13 (a); similar as foregoing, the a-phase CT on HV side does not saturates due to the less D.C offset at the fault inception and the zero remnant flux in the CT core, the a-phase current on HV is therefore faithfully reproduced shown in Figure 4.13 (b); as therefore expected, a-phase differential current does not distort, as evident from Figure 4.13 (c).

4.4.2.2 Effect of Remnant Flux Level in CT Core on Fault Current

In practice, there are many conditions (such as line auto-reclosure after a transient fault clearance) that may leave a remnant flux in the core of the CT; this can have a significant bearing on the CT secondary current. Comparing Figure 4.12 and Figure 4.14, which are for the same fault inception angle, except that there is a higher remnant flux (70% remnant flux compared to 50%) in the case shown in Figure 4.14, it is apparent that the remnant flux level has a significantly higher influence in the CT secondary current in that there is more severe distortion on the CT secondary current as clearly evident from comparing Figure 4.12 (a), (c) and Figure 4.14 (a), (c).
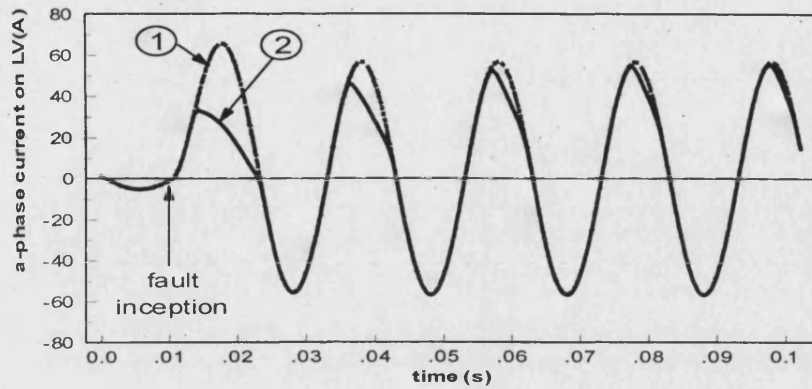
(a) a-phase CT secondary current on LV side
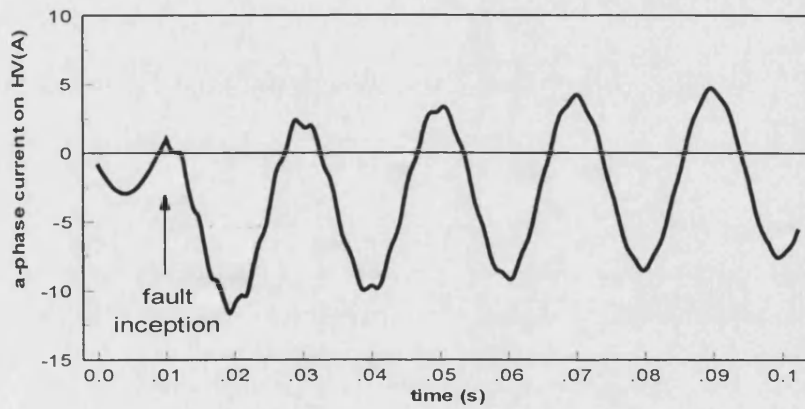
(b) a-phase CT secondary current on HV side
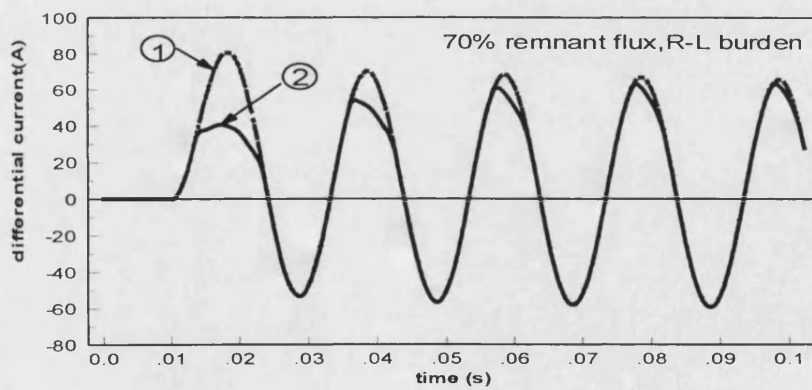
(c) a-phase differential current

Figure 4.14 Current waveforms of an internal three-phase short circuit on LV side under 70% remnant flux

4.4.3 Simulation of External Faults with CT Saturation

A differential relay is designed to restraint under normal load flows and for external faults. However, external short circuits can in fact result in very large differential currents, if the CT saturates. It is thus crucial to be able to ascertain CT saturation effects on the measure currents under external faults. Figure 4.15 shows the simulated waveforms for an external three-phase short circuit, which occurs on Bus 2 (shown in Figure 4.7 ⑥) under a condition that there is an initial remnant flux (50% rated flux) in a, b and c three-phase CT cores on LV side, and a zero remnant flux in a, b and c three-phase CT cores on HV side. From Figure 4.15 (a), it can be seen that, as expected, there is some distortion in the a-phase CT secondary current on LV side. The CT secondary current waveforms on the high voltage side are, on the other hand, distortion free as shown by Figure. 4.15 (b). This imbalance (due to distortion on the low voltage side) manifests itself into generating a significant differential current as evident from Figure 4.15 (c), and this can lead to relay instability in the conventional current differential protection.
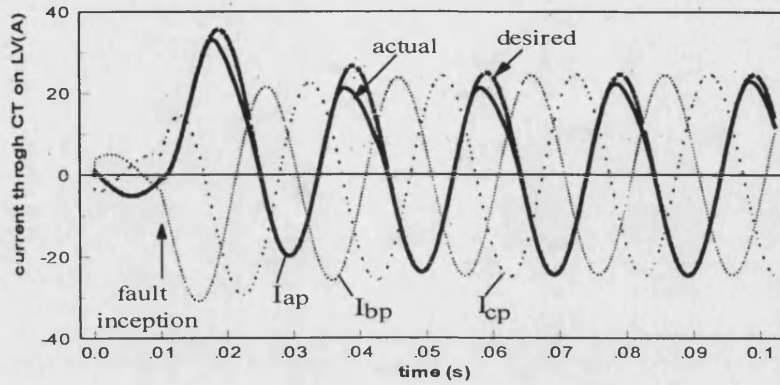
(a) CT secondary currents on LV side
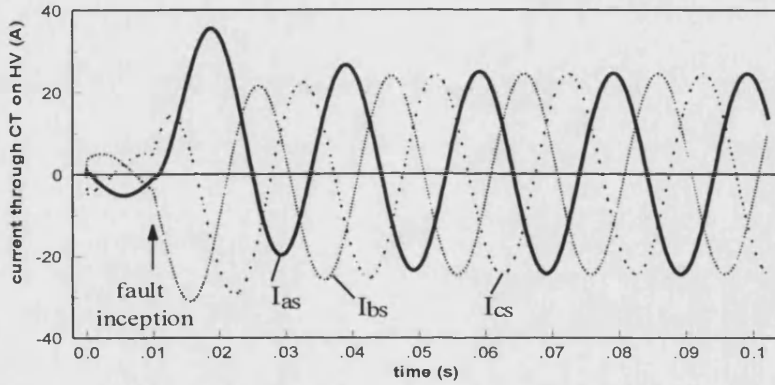
(b) CT secondary currents on HV side
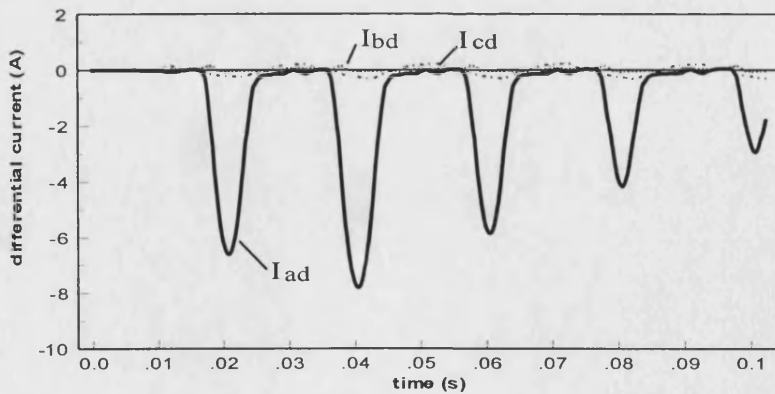
(c) differential currents

Figure 4.15 Current waveforms of an external three-phase short circuit on HV side with CT saturation

Generally, the degree of CT saturation relies on the DC components in the primary current and the CT parameters. Figure 4.16 therefore shows the effects on the a-phase differential current with the different levels of initial CT remnant flux for the same fault condition as the case shown in Figure 4.15. From Figure 4.16 it is apparent that as the initial CT remnant flux progressively increases from 0% to 35%, 50%, 60% rated flux, the magnitude of differential current also gradually increases and under certain conditions can exceed the setting level of the differential current protection thereby resulting in mal-operation of the power transformer protection.
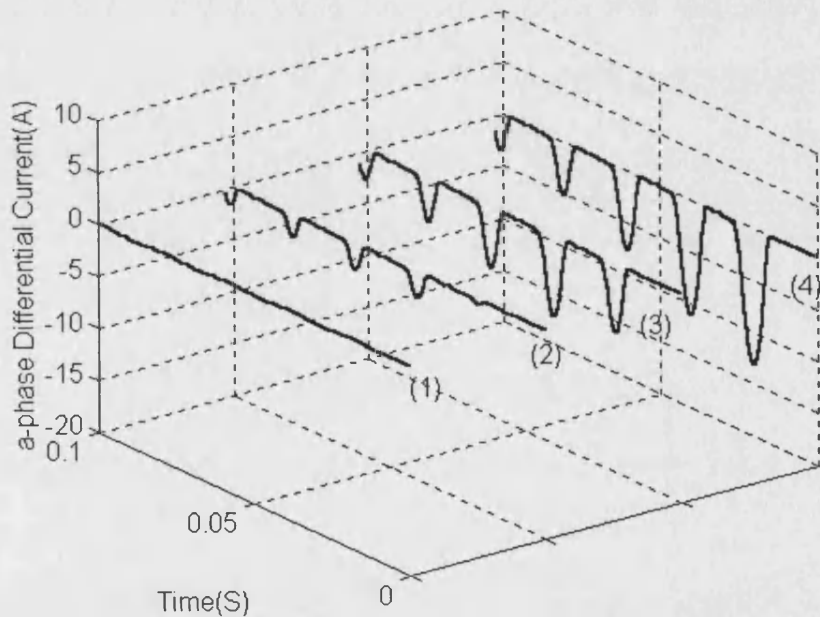
Figure 4.16 Differential currents with respect to different remnant flux levels in CTs under an external fault condition (1) no remnant flux; (2) 35% rated flux of remnant flux; (3) 50% rated flux of remnant flux;(4) 60% rated flux of remnant flux

4.5 Electromagnetic Simulation Studies of Power Transformer Faults in System 2

Similar to the case studies carried out on System 1, the fault transient phenomena are also studied on System 2 shown in Figure 4.6. Some typical fault studies in System 2 are depicted in Figure 4.17.
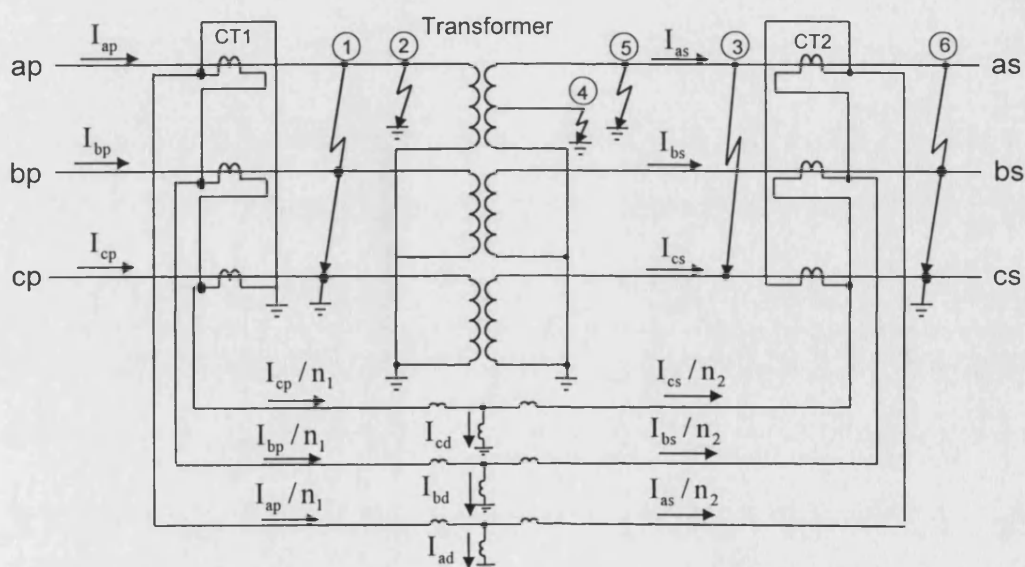
Figure 4.17 Simulation of typical faults in System 2

where, ① stands for an internal three-phase-to-earth short circuit on LV side; ② stands for an internal a-phase-to-earth terminal fault on LV side; ③ stands for an internal a-c two-phase short circuit on HV side; ④ stands for an internal a-phase turn-to-earth winding fault at mid-point of the winding on HV side; ⑤ stands for an internal a-phase-to-earth fault on HV side; ⑥ stands for an external three-phase short circuit on HV side.

The simulation results, which correspond to the faults typified in Figure 4.17, will be given in the following sections. For simplicity, only differential current waveforms of each case study are presented hereafter.

4.5.1 Simulation of Internal Faults without CT Saturation

Figure 4.18 presents a typical simulation result for a three-phase-to-earth short circuit on LV side of the power transformer (Figure 4.17①). It can be seen from Figure 4.18 that the differential currents reach to the very high magnitude level due to the severe three-phase short circuit fault, and differential current waveforms observed through the CT secondary side are still normal sinusoidal waveforms without distortion; this is so because CTs do not saturate.
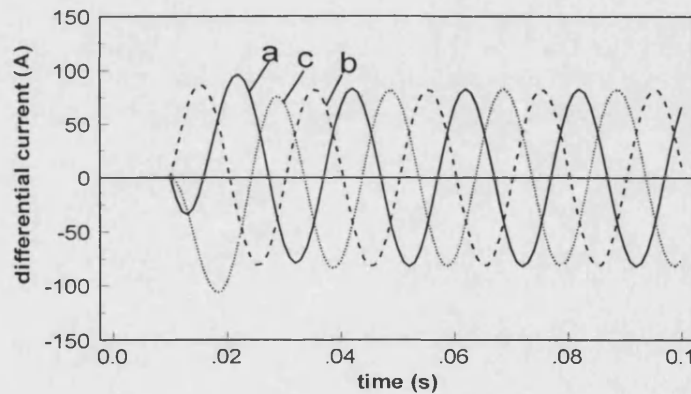
Figure 4.18 Differential current waveforms of a terminal three-phase-to-earth short circuit on LV side

Figure 4.19 presents another typical simulation result for a terminal *a*-phase-to-earth fault on LV side (Figure 4.17②). It is apparent that the differential currents are much smaller under such a single-phase fault than an internal three-phase fault shown in Figure 4.18. It can be also seen that although the fault type is an *a*-phase-to-earth fault, there are significant large differential currents in both a and c phases due to the effect of the protection connection on CTs.
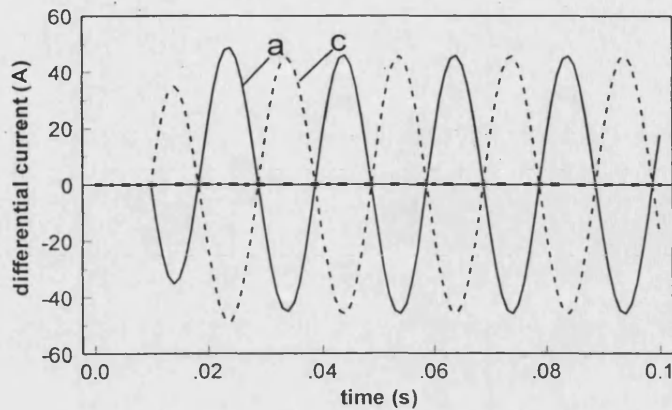
Figure 4.19 Differential current waveforms of a terminal *a*-phase-to-earth fault on LV side

Figures 4.20 and 4.21 respectively present simulation results for (1) a terminal *a-c* two-phase short circuit fault on HV side (Figure 4.17③); and (2) a turn-to-earth fault at mid-point of *a*-phase winding on HV side (Figure 4.17④). It is apparent that the differential currents generated under a turn-to-earth fault (Figure 4.21) are much smaller compared with the terminal internal fault shown in Figure 4.20. Here again, differential current waveforms observed through the CT secondary are normal sinusoidal waveforms without distortion; this is so because CTs do not saturate.
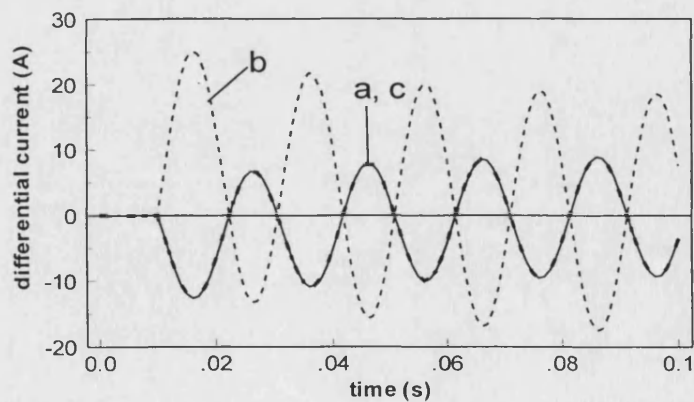
Figure 4.20 Differential current waveforms of a terminal *a-c* two-phase short circuit fault on HV side
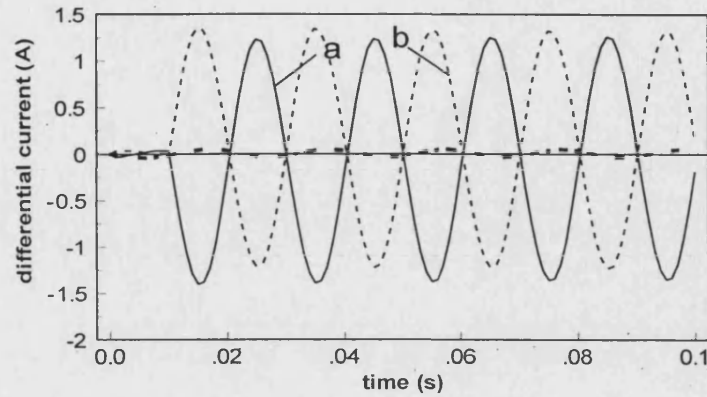
Figure 4.21 Differential current waveforms of a turn-to-earth fault at mid-point of a-phase winding on HV side

4.5.2 Simulation of Internal Faults with CT Saturation

The impacts of the CT saturation on differential currents are also studied on System 2 (shown in Figure 4.6). Similar to the case studies carried on System 1, CT saturation under various fault and system conditions, including the variations in the fault inception angles, remnant flux levels in CTs, and CT secondary burdens, are studied. Some of typical results are presented in the following sections.

4.5.2.1 Effect of Fault Inception Angle on Fault Current

Figure 4.22 presents an *a*-phase differential current waveform for *a*-phase-to-earth fault on HV side (Figure 4.17⑤) when the fault inception angles are $\alpha=0°$ and $\alpha=90°$ respectively, under a conditions that there is 70% rated flux of remnant flux in a-phase CTs on both LV and HV sides. Figure 4.22 (a) presents *a*-phase differential current under the fault inception angle $\alpha=0^0$; and Figure 4.22 (b) presents a-phase differential current under the fault inception angle $\alpha=90^0$.

From Figure 4.22 (a) it can be seen that due to CT saturation, the *a*-phase differential current observed through the CT secondary is distorted. A difference between

distorted/actual secondary currents and prospective secondary currents is clearly illustrated in this figure. It can be seen from Figure 4.22 (b) that although the fault and remnant flux conditions are the same as Figure 4.22 (a), the fault inception angle is changed from $\alpha=0^0$ to $\alpha=90^0$, the *a*-phase differential current observed through the CT secondary is faithfully reproduced as evident form Figure 4.22 (b).
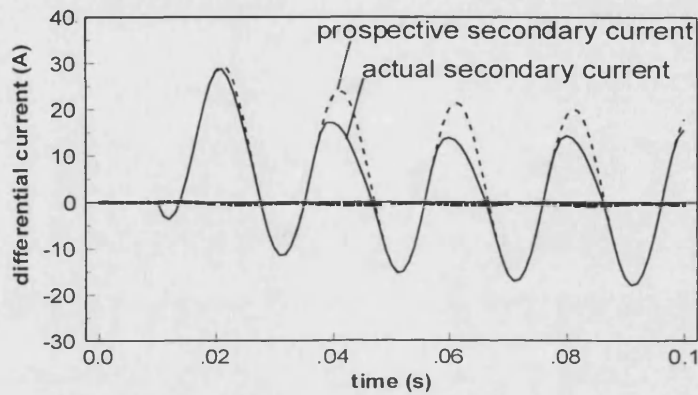
(a) *a*-phase differential current under fault inception angle $\alpha=0^0$
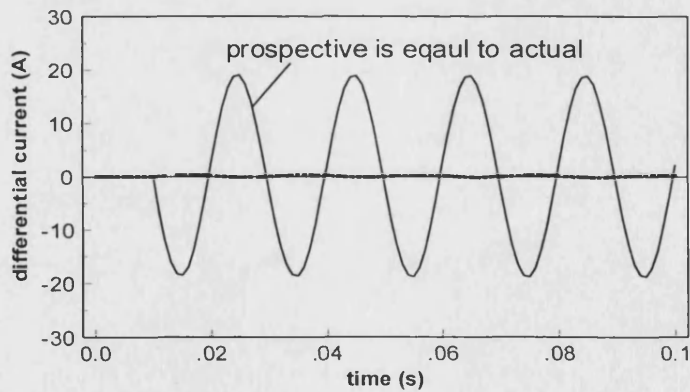
(b) a-phase differential current under fault inception angle $\alpha=90^0$

Figure 4.22 An *a*-phase differential current for an *a*-phase-to-earth fault on HV side with fault inception angles $\alpha=0^0$ and $\alpha=90^0$, respectively

4.5.2.2 Effect of Remnant Flux Level in CT Core on Fault Current

The effects of the remnant flux of CTs on differential currents are also studied on System 2. Figure 4.23 presents an *a*-phase differential current waveform when there are the same fault and system condition as Figure 4.22 (a) except there are no remnant flux on *a*-phase CTs on both LV and HV sides. Comparing Figure 4.22(a) and Figure 4.23, it can be seen that in Figure 4.23, a-phase differential current observed from the CT secondary does not distort, as there is no remnant flux on *a*-phase CT.
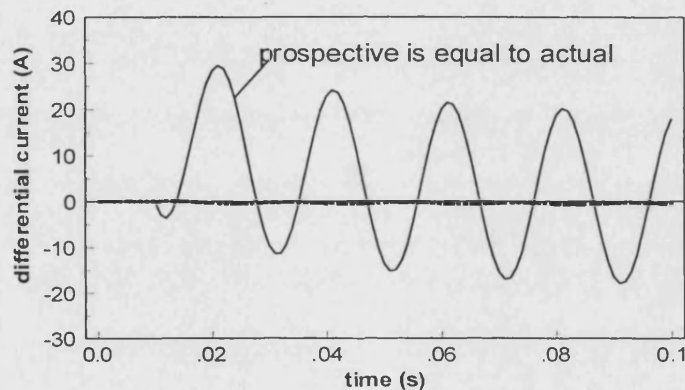
Figure 4.23 An a-phase differential current for an a-phase-to-earth fault on HV side without remnant flux in a-phase CTs on both LV and HV sides

4.5.2.3 Effect of CT Secondary Burden on Fault Current

It is well known that the burden type of CT secondary can affect the CT performance. A purely resistive burden of the CT can cause more severe saturation than a resistive inductive burden or a purely inductive burden. The effects of the CT secondary burden on differential currents are also studied on System 2. Figure 4.24 presents an *a*-phase differential current waveform when there is the same fault and remnant flux conditions as Figure 4.22 (a), but a-phase CTs on both LV and HV sides are with purely resistive burden. Comparing Figure 4.24 and Figure 4.22 (a) it

can be seen that the CT in Figure 4.24 is driven into saturation much earlier, i.e. in the first half cycle compared to Figure 4.22(a). As a consequence, a high distortion in the secondary current of the CT occurs in this case.
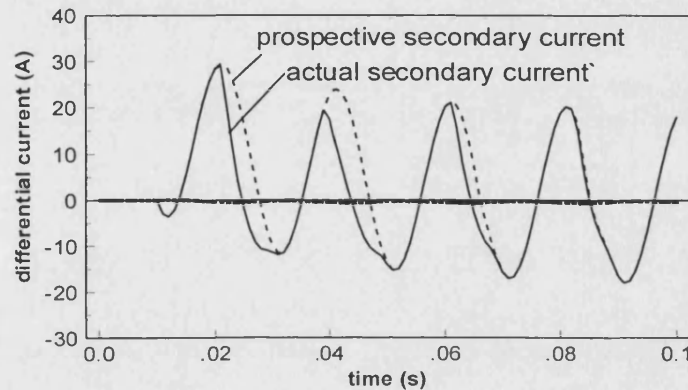
Figure 4.24 An a-phase differential current for an a-phase-to-earth fault on HV side with purely resistive burden in CTs

4.5.3 Simulation of External Faults with CT Saturation

The effect of CT saturation on differential currents under an external fault condition is also studied on System 2. Figures 4.25 and 4.26 respectively present the simulation results for (1) an external three-phase short circuit on HV side (Figure 4.17⑥) with a-phase CT saturation on both LV and HV sides (Figure 4.25), and (2) an external three-phase short circuit on HV side (Figure 4.17⑥) with a-phase CT saturation on LV side only (Figure 4.26). The simulation results indicate that CT saturation will produce significant differential currents under an external fault condition, and this situation may happen with CT saturation on one side (LV or HV) only, or on both LV and HV sides simultaneously.
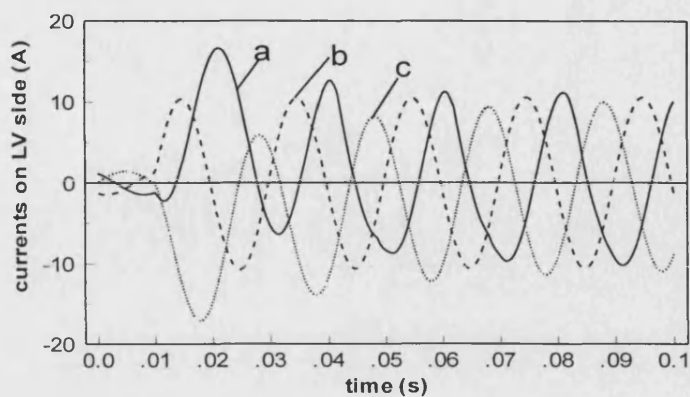
(a) CT secondary currents on LV side
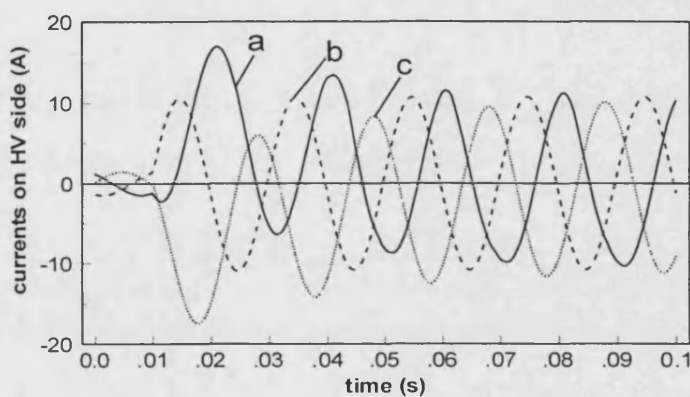
(b) CT secondary currents on HV side
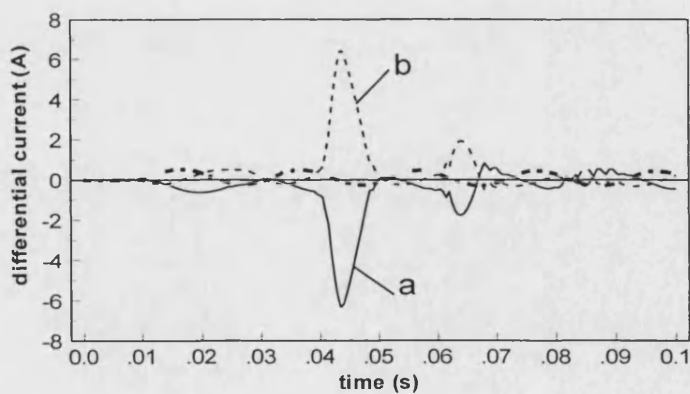
(c)differential currents

Figure 4.25 Current waveforms of an external three-phase short circuit with a-phase CT saturation on both LV and HV sides
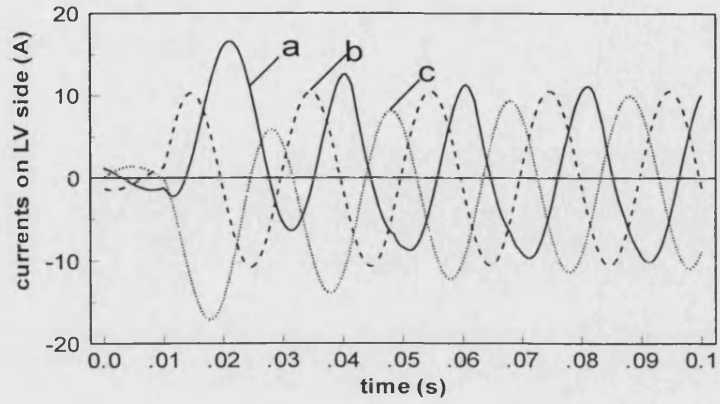
(a) CT secondary currents on LV side
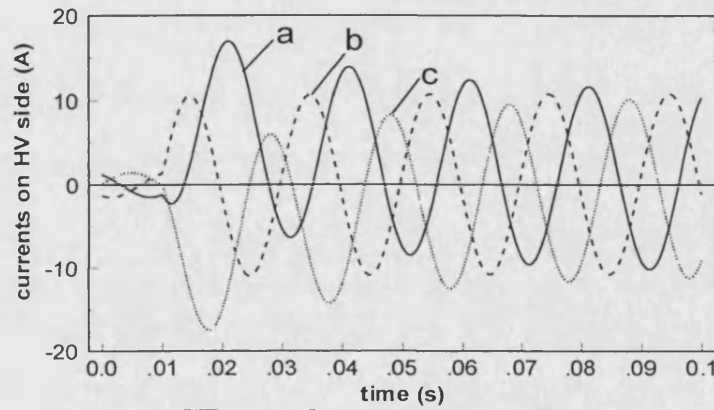
(b) CT secondary currents on HV side
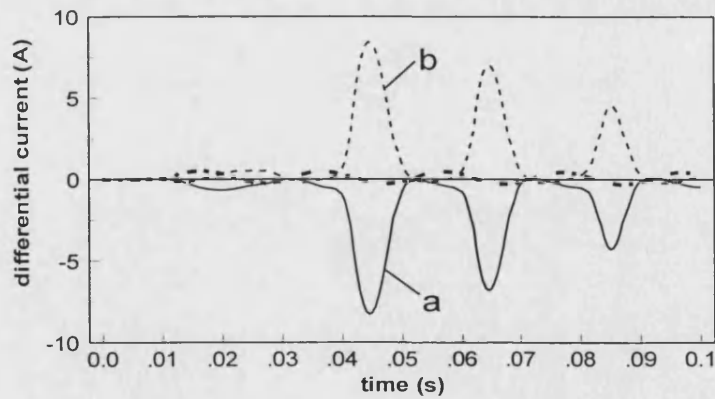
(c) differential currents

Figure 4.26 Current waveforms of an external three-phase short circuit with a-phase CT saturation on LV side only

4.6 Summary

It is vitally important to simulate a power transformer system as accurate as possible in order to develop novel protection techniques. In this chapter, the simulation and analysis of two power transformer systems under a whole variety of practically encountered fault conditions have been implemented based on the developed modelling approach presented in Chapter 3 by using EMTP software; in particular, the effects of CT saturation on differential currents are included in the simulation.

Chapter 5

Electromagnetic Simulation Study of
Power Transformer Inrush Currents

5.1 Introduction

When a power transformer is energised on the primary side with the secondary open-circuited, the current flowing in the primary side is the magnetising current. Normal steady-state magnetising currents of power transformers are about 2-5% (or even less) of the rated current. However, under transient conditions (i.e. a short period following energisation) the maximum initial-magnetising current may be as high as 8-30 times of the rated current. During the transient period, the magnitudes of the inrush current slowly decay to the normal steady-state values. The slow decay time is as a direct consequence of the loop resistance of the power supply circuit being small. The time constant of the inrush current decay varies from about 10 cycles to as long as 1 min in highly inductive circuits [3].

In order to clearly distinguish internal faults from the magnetising inrush currents, an investigation into the magnetising inrush current phenomenon in a power transformer is crucial. Based on the models described in Chapter 3, in this chapter, an extensive digital simulation study of the magnetising inrush phenomenon is presented with reference to the foregoing System 1 and System 2. The effects of the different remnant flux levels in the transformer core, different power supply switch-on angles, coupled with CT saturation on magnetising inrush current transients, have been taken into consideration.

5.2 Types of Magnetising Inrush Currents

In general, a magnetising inrush current can occur under three conditions, which are namely described as (1) initial magnetising inrush current; (2) recovery magnetising inrush current; and (3) sympathetic magnetising inrush current [3].

5.2.1 Initial Magnetising Inrush Current

An initial magnetising inrush current may occur when energising the transformer. This inrush has the possibility of producing the maximum value. It therefore will be considered as the basis for the case studies in this thesis. An extensive digital simulation of magnetising inrush phenomenon carried out on System 1 and System 2 will be given in the following sections.

5.2.2 Recovery Magnetising Inrush Current

After an external fault is cleared, an inrush may occur because the voltage returns to normal as shown in Figure 5.1. This is called the recovery magnetising inrush current. The worst case for the recovery inrush may occur when there is a solid three-phase external fault near the transformer. In such a case, the voltage is firstly reduced to nearly zero on the transformer. However, when the external fault is cleared, the voltage suddenly returns to an essentially normal value. This sudden change in the voltage may produce a magnetising inrush in the transformer. The recovery inrush is always less than the initial inrush because the transformer is only partially energised.
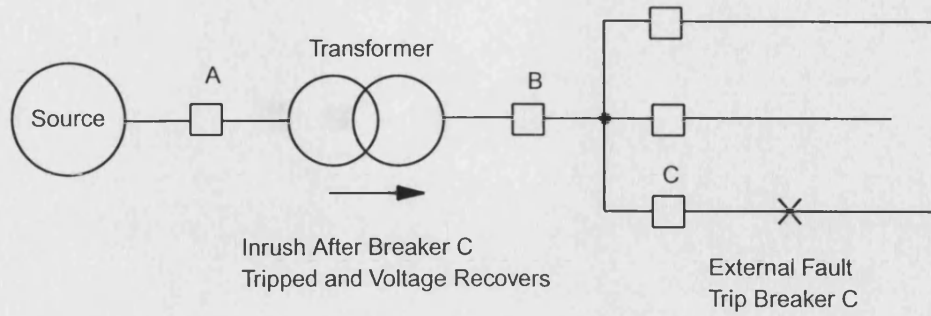
Figure 5.1 Recovery inrush after clearing an external fault

5.2.3 Sympathetic Magnetising Inrush Current

A magnetising inrush current can also occur in an energised transformer when a nearby transformer is energised. This is called sympathetic magnetising inrush current. A common situation may occur when paralleling a second transformer with a transformer already in operation as shown in Figure 5.2. In such a case, the dc component of the inrush current in transformer 2 can also saturate the energised transformer 1, resulting in a sympathetic magnetising inrush in the energised transformer 1. Again, the sympathetic inrush in the transformer 1 will always be less than the initial inrush.
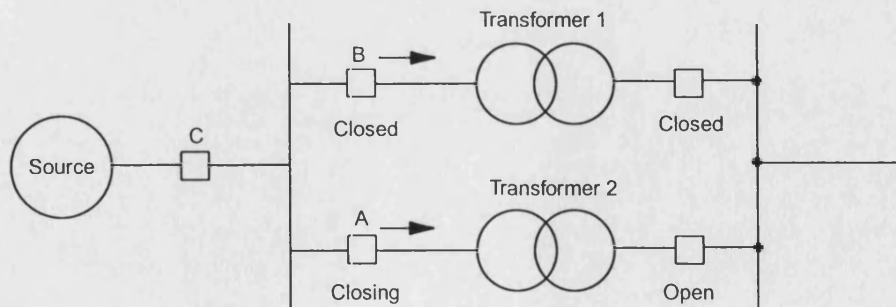
Figure 5.2 Sympathetic inrush when paralleling a second transformer with an
energised transformer

5.3 Power Transformer System Diagrams for Inrush Current Simulation Studies
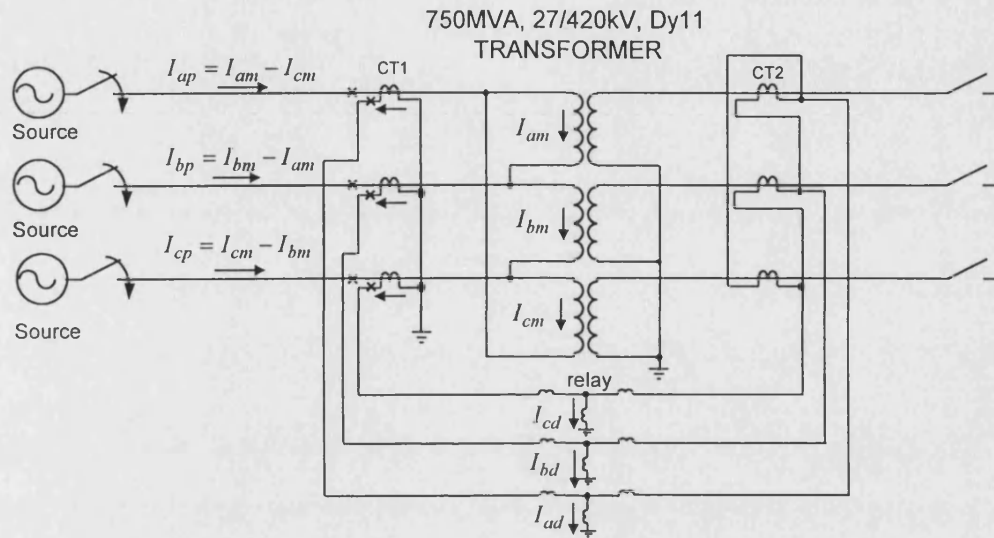
Figure 5.3 Diagram of System 1 for inrush case studies
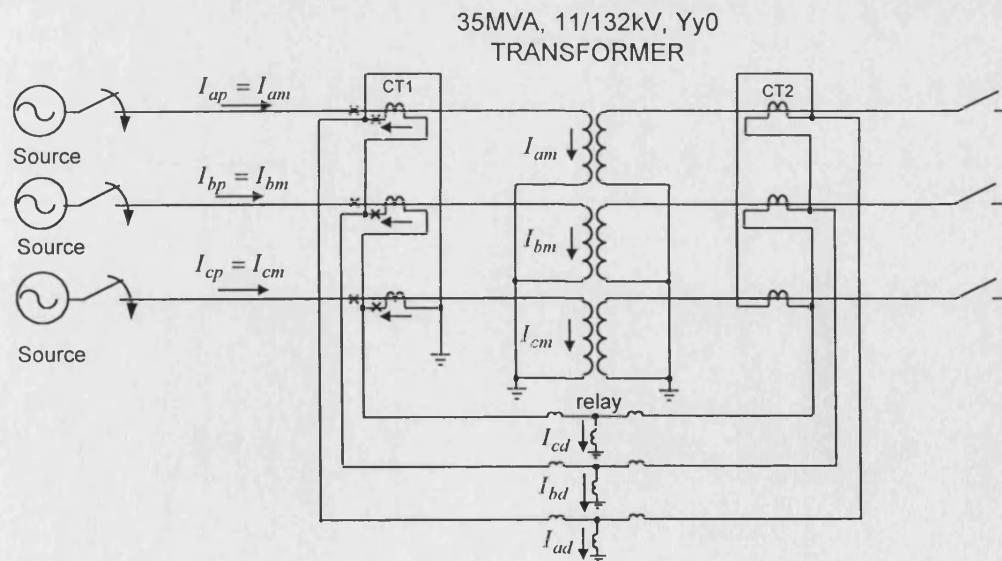
Figure 5.4 Diagram of System 2 for inrush case studies

As mentioned above, the initial magnetising inrush will be investigated in detail in this research work. Figures 5.3 and 5.4 show the diagrams of the two simulated power transformer systems for inrush current studies, where the secondary side of each power transformer is open, and the primary side of each power transformer is energised. The modelling techniques associated with the inrush current phenomenon have already been described in Chapter 3.

5.4 Electromagnetic Simulation Studies of Inrush Currents in System 1

5.4.1 Magnetising Current under Steady-State Condition

Figure 5.5 shows the simulated results of the steady state magnetising current, which will occur when the transformer had been energised at or near maximum positive voltage; or after the transient inrush current has decayed to the steady state magnetising current.
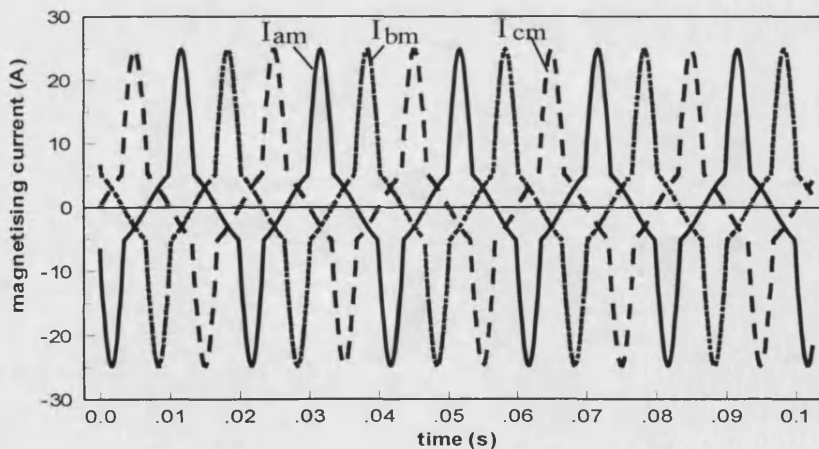
Figure 5.5 Magnetising current under steady-state condition

From Figure 5.5, it can be seen that the magnetising currents I_{am}, I_{bm} and I_{cm}, which correspond to a, b and c three-phase currents in the magnetic branch of the

transformer, are very small compared with the rated current of the power transformer. This is evident from the following calculations.

The rated current is given by:

$$I_{rated} = \frac{750MVA}{\sqrt{3} \times 27kV} = 16(kA),$$

and the magnetising current in steady state shown in Figure 5.5 is:

$$I_{magnetising} = 24 \ (A)$$

Thus, the ratio between the rated current and the steady state magnetising current is:

$$\frac{I_{magnetising}}{I_{rated}} = \frac{24}{16000} \times 100\% = 0.15\%$$

It can be seen that the steady state magnetising current is only 0.15% of rated current in this case study. However, the maximum initial magnetising current may be as high as 8-30 times the rated current under the transient condition, particularly when the transformer is energised. The following sections will give the simulation results of the magnetising inrush current phenomenon under transient conditions.

5.4.2 Magnetising Inrush Current under Transient Conditions

5.4.2.1 Effect of Core Remnant Flux Level on Inrush Current

Detailed analyses presented in Chapter 2 shows that the magnetising inrush currents are produced due to the severe saturation of the transformer core. In a three-phase circuit, inrush currents will always occur in one or two phases and generally all three phases, with the voltages phase angle 120^0 apart. Figure 5.6 (a) shows typical

magnetising inrush current waveforms (I_{am}, I_{bm} and I_{cm}) when a transformer is energised at voltage V_a ($\alpha=0^0$), where α is the switch-on angle. Figure 5.6 (b) shows the corresponding transient fluxes ϕ_a, ϕ_b, and ϕ_c, in which there is no remnant flux in the transformer core.
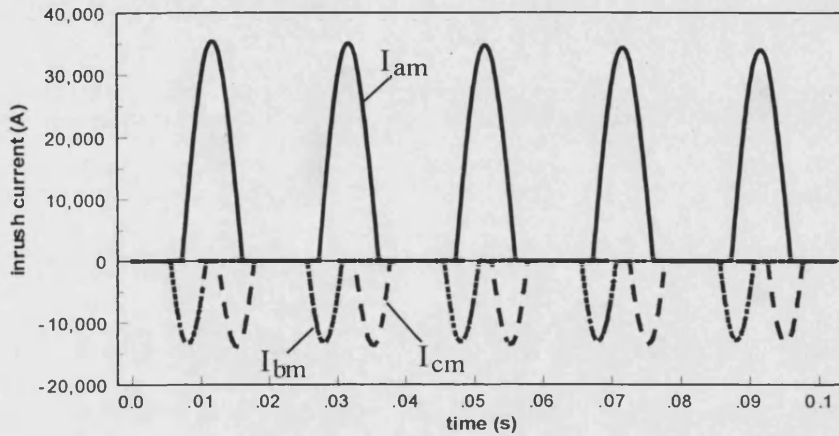
(a) magnetising inrush current
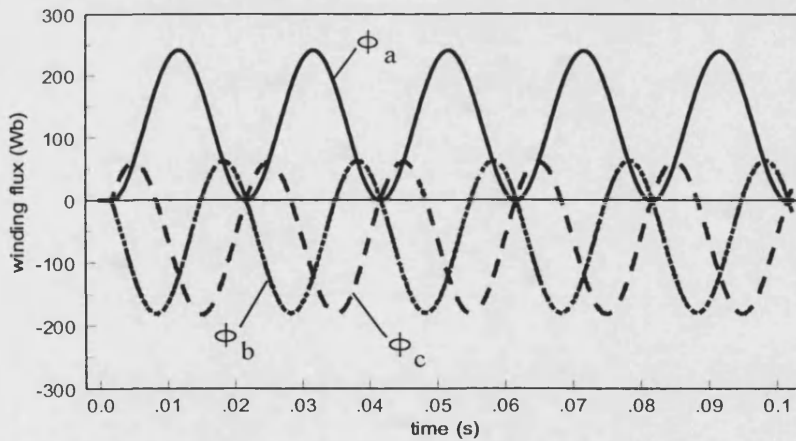
(b) transient flux

Figure 5.6 Simulation of inrush currents without remnant flux in transformer core

From Figure 5.6 (a), it can be seen that the inrush currents occur in all three phases, and the a-phase inrush current is larger than the corresponding b-phase and c-phase inrush currents. This is so because during transient period following energisation, the a-phase flux level doubles the rated flux, the rated flux being 121.45Wb for the

simulated power transformer given in Table A.4.2 in Appendix; the increase in b-phase and c-phase transient fluxes is less compared to the a-phase (evident from Figure 5.6 (b)). This results in a a-phase transformer core to be more severely saturated than the b-phase and c-phase transformer cores. Furthermore, it has also been found that the inrush current decays slowly; this is by virtue of the fact that in this study, the transformer is close to the source, and the resistance of the source-transformer loop is thus very small, resulting in a relatively large decay time constant of the inrush current.

If a transformer has been energised previously, there is a high probability that on de-energisation some remnant flux would have been left in the iron; this flux can be positive or negative, which may either add to or subtract from the total flux upon re-energisation, thereby increasing or decreasing the inrush current.

To demonstrate this scenario, it has been assumed that there are a remnant flux of +72.9Wb (70% rated flux) in a-phase core, -36.5Wb (-35% rated flux) in both b-phase and c-phase, respectively. The magnetising inrush currents with respect to these initial remnant flux conditions are depicted in Figure 5.7 (a); while Figure 5.7 (b) shows the transient flux under these initial remnant flux conditions. As can be seen, the presence of the remnant flux significantly increases the magnitude of the magnetising inrush current. This is evident from a comparison between Figure 5.6 (a) and Figure 5.7 (a); the maximum value of the a-phase magnetising inrush current in Figure 5.6 (a) is 35kA, while the maximum value of a-phase magnetising inrush current in Figure 5.7 (a) is 65kA.
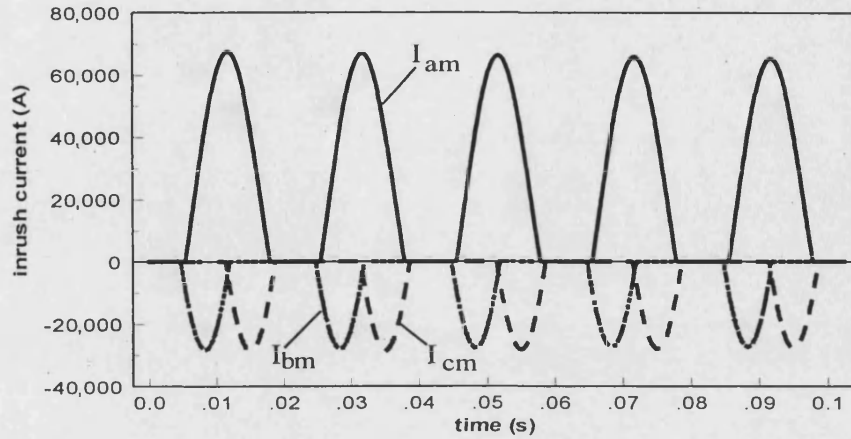
(a) magnetising inrush current
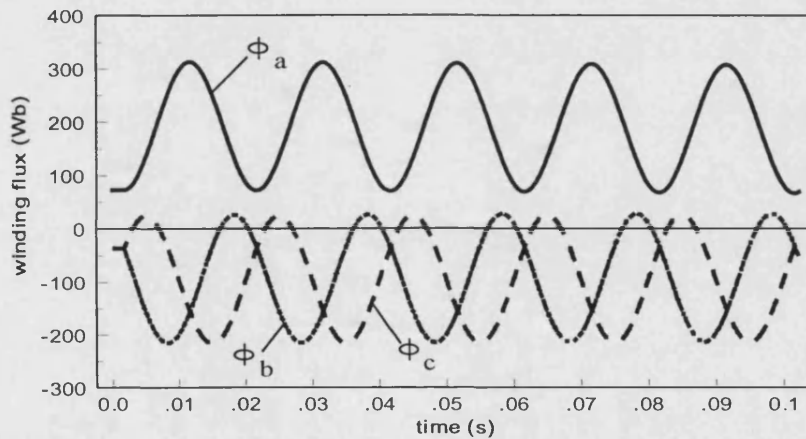
(b) transient flux

Figure 5.7 Simulation of inrush currents with remnant flux in transformer core

5.4.2.2 Effect of Switch-On Angle on Inrush Current

A transformer may not always be energised at voltage $V_a(\alpha=0^0)$, where α is the switch-on angle. Various switch-on angles will result in various peak values of the inrush current. To demonstrate the effects of switch-on angles on the inrush current, the inrush currents are simulated under a different switch-on angle $\alpha=60^0$ as shown in Figure 5.8.
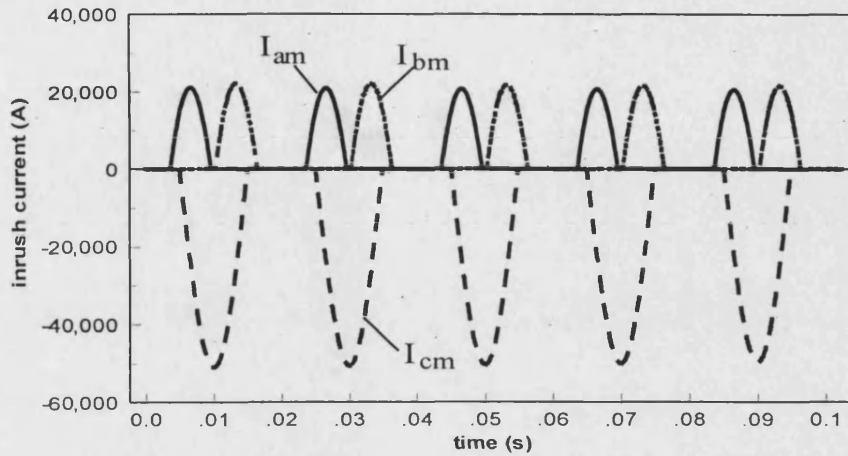
Figure 5.8 Simulation of inrush currents at switch-on angle $\alpha=60^0$

Comparing Figure 5.8 with Figure 5.7 (a), which are with the same initial remnant flux condition except that in Figure 5.7 (a) the power transformer is energised at $V_a(\alpha=0^0)$, it is clearly evident that the a-phase magnetising inrush current at the switch-on angle $\alpha = 0^0$ shown as Figure 5.7 (a) is significantly larger (approximately 5 times rated current) than the magnetising inrush current at the corresponding switch-on angle $\alpha = 60^0$ shown as Figure 5.8 (this is approximately 1.3 times rated current). This result demonstrates the significant effect of the power supply switch-on angle on inrush currents.

To further illustrate the foregoing phenomenon, Figure 5.9 presents the changes in the a-phase inrush current corresponding to switch-on angles $\alpha=30^°$, $90^°$, $150^°$, $210^°$, $300^°$, respectively; this simply displays the marked effect of re-energisation angle on the magnitude of the peak value of the inrush current.
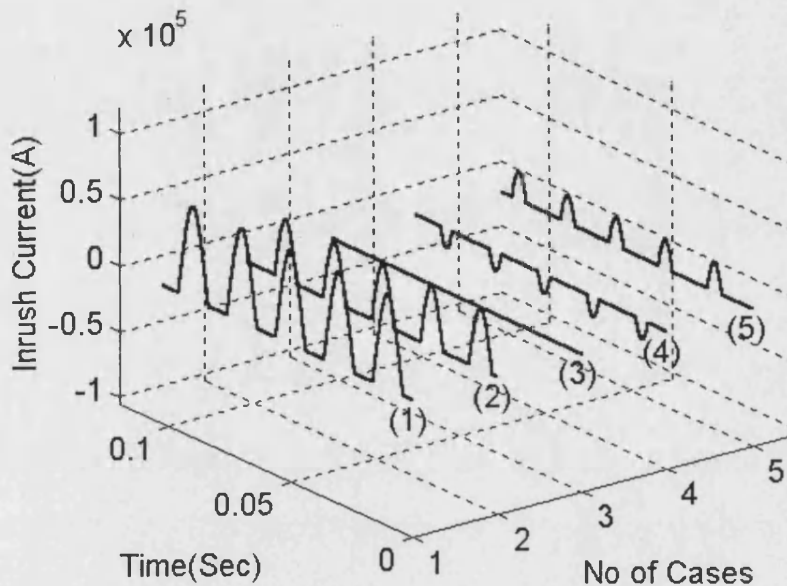
Figure 5.9 A-phase magnetising inrush currents with respect to different switch-on angles α (1) α=30°; (2) α=90°; (3) α=150°; (4) α=210°; (5) α=300°

5.5 Electromagnetic Simulation Studies of Inrush Currents in System 2

Similar to the case studies carried out on System 1, the magnetising inrush current phenomenon is also studied on System 2 shown in Figure 5.4. Some typical simulation results are presented in the following sections.

5.5.1 Effect of Core Remnant Flux Level on Inrush Current

Figures 5.10 (a) and (b) present the results of the magnetising inrush currents for a condition associated with the transformer being energised at voltage $V_a(\alpha=0^0)$, with:

(i) no remnant flux in the transformer core (Figure 5.10 (a)), and (ii) 50% remnant flux in the transformer core (Figure 5.10 (b)). From these figures it can be seen that there are very similar features of the magnetising inrush currents compared with the case study results associated with System 1, as shown in Figure 5.6 (a) and Figure 5.7 (a).
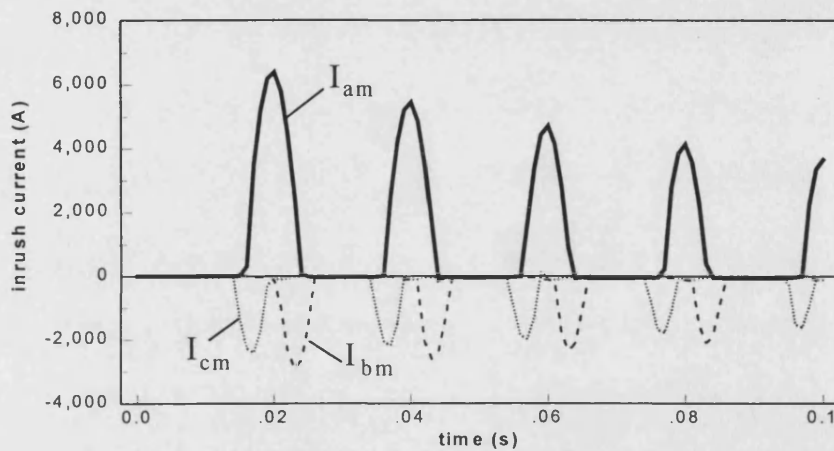
(a) inrush current with no remnant flux
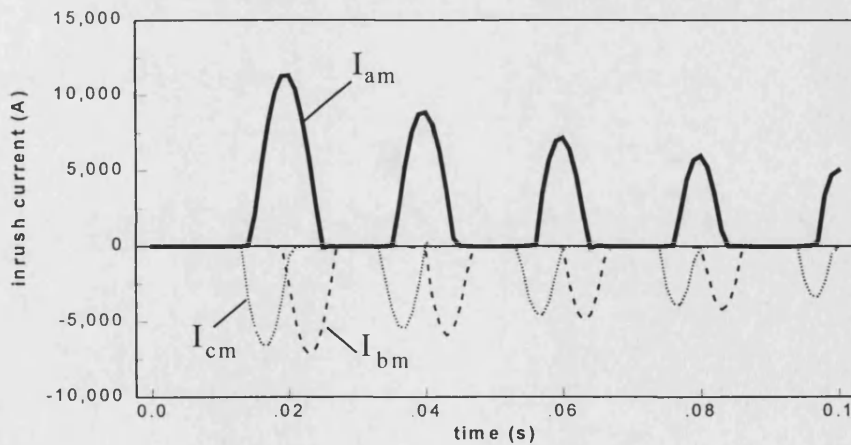
(b) inrush current with 50% remnant flux

Figure 5.10 Inrush currents with different remnant flux in transformer core

5.5.2 Effect of Switch-On Angle on Inrush Current

Figure 5.11 presents the simulation results of the inrush currents under a condition that there is the same initial remnant flux as Figure 5.10(b) except that in Figure 5.11 the power transformer is energised at voltage V_a ($\alpha=240^0$). It is apparent that the a-phase inrush current energised at $\alpha=0^0$ shown in Figure 5.10(b) is larger than the inrush current energised at $\alpha=240^0$, this indicates the significant effect of the switch-on angle on inrush currents.
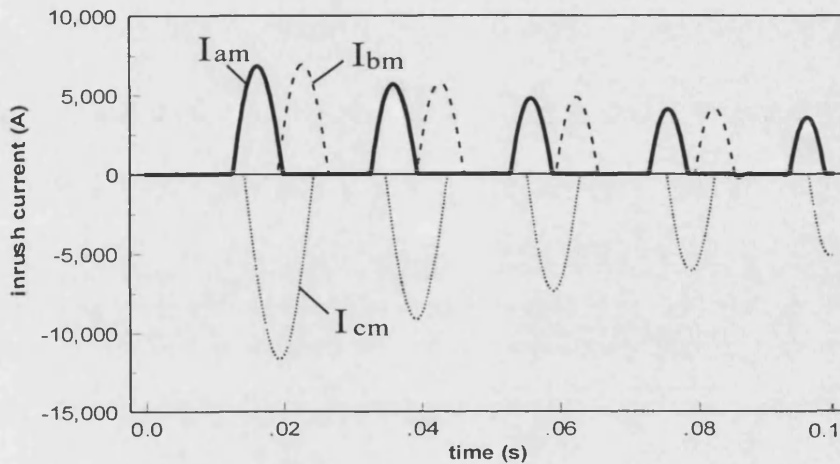
Figure 5.11 Inrush currents when transformer is energised at voltage V_a ($\alpha=240^0$)

5.5.3 Effect of CT Saturation on Inrush Current

Figures 5.12 and 5.13 illustrate the effect of CT saturation on the inrush current waveforms. In these figures, Figure 5.12 shows the result when the a-phase CT on LV side is saturated only; while the Figure 5.13 shows result when both a-phase and b-phase CT on LV side are saturated. From Figure 5.12(b), it can be seen that the a-phase inrush current on CT secondary side is severely distorted due to the a-phase CT saturation; while from Figure 5.13(b), it can be seen that both the a-phase and b-phase inrush currents on CT secondary side are severely distorted due to both a-phase and b-phase CT saturation. An interesting point to note here is that typically,

the inrush current waveform should have a number of gaps where the current magnitude is zero; however, these gaps observed through CT secondary side, are lost due to CT saturation, as apparent from Figures 5.12(b) and 5.13(b). A direct consequence of this effect is that it will make practical protection schemes, which rely on gaps features to distinguish inrush currents from internal faults described in Chapter 2, have a difficulty.
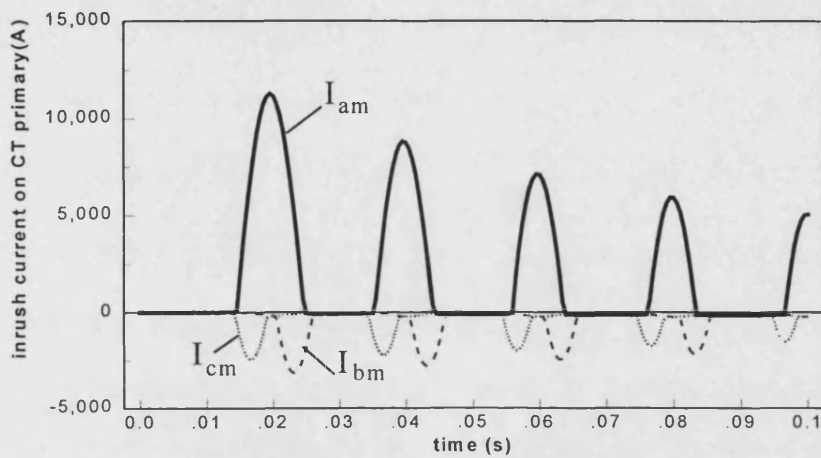
(a) inrush current on CT primary side
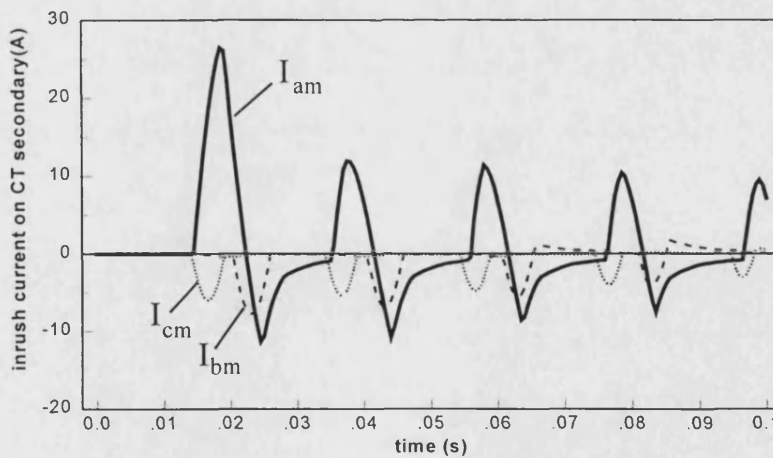
(b) inrush current on CT secondary side

Figure 5.12 Simulation of inrush currents with a-phase CT saturation on LV side
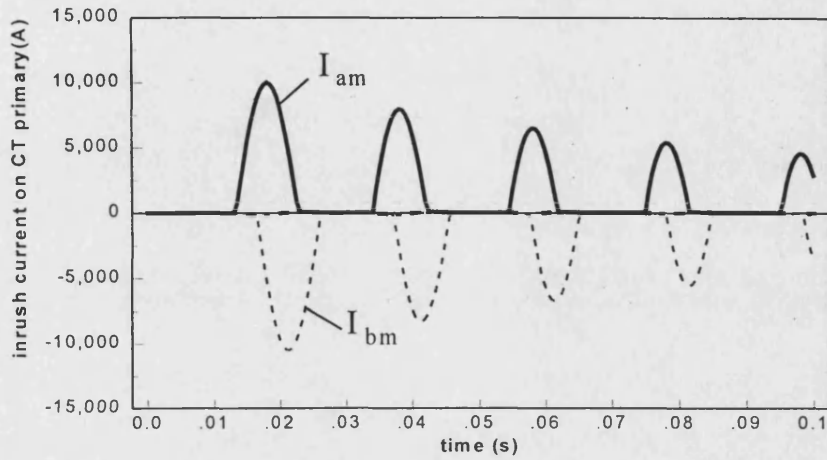
(a) inrush current on CT primary side
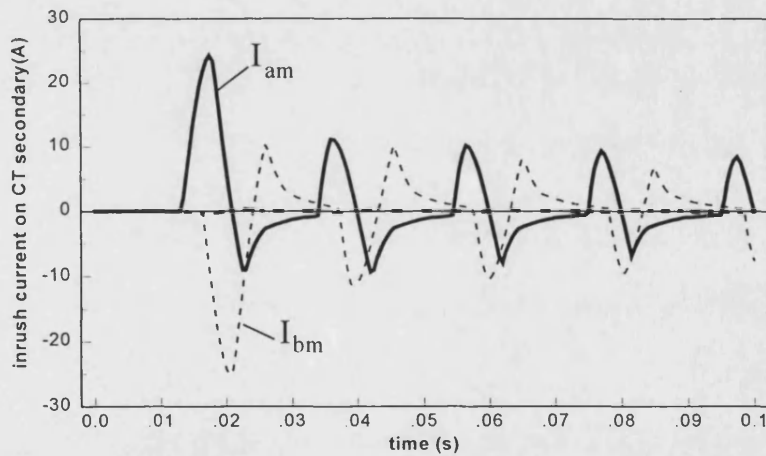
(b) inrush current on CT secondary side

Figure 5.13 Simulation of inrush currents with both a-phase and b-phase CT saturation on LV side

5.6 Summary

In this chapter, an extensive digital simulation study of the magnetising inrush phenomenon has been performed on both System 1 and System 2. It has been found that the factors controlling the duration and magnitude of the magnetising inrush are: (1) size and location of the transformer; (2) resistance of the loop from the source to the transformer; (3) prior history, i.e. remnant flux level, of the transformer; and (4) transformer energisation angle. The simulation results obtained will be used to develop novel protective schemes for power transformer fault diagnosis especially for distinguishing between internal faults and inrush currents, which will be described in the following chapters.

Chapter 6

Traditional ANN-Based Technique for Power Transformer Fault Diagnosis

6.1 Introduction

As discussed previously, there have been a number of techniques researched and developed to distinguish between internal faults and magnetising inrush currents in a power transformer. Some of these are based on conventional methods and a few on AI, and all the techniques developed hitherto have advantages and disadvantages. The work presented in this chapter is based on applying a traditional ANN to solve the aforementioned problem, and is in essence a necessary precursor to improving on the performance through a novel approach described later in this thesis.

6.2 Motivation for Using ANNs for Power System Engineers

An artificial neural network is an intelligent system motivated by research into the human brain. The human brain is the most complex computing device, and its powerful thinking, remembering and problem-solving capabilities have motivated scientists to investigate how a machine can implement the thought and action of human beings.

Modern power systems are required to generate and supply high quality electric energy to consumers. In order to achieve this requirement, computers are applied to

power system operation, planning, monitoring and control; power system application programs for analysing system behaviour are stored in computers. For example, at the planning stage of a power system network, system analysis programs are executed repeatedly; engineers adjust and modify the input data to these programs according to their experience and knowledge about the system until satisfactory plans have been determined. However, the computer programs developed are based on mathematical models and are implemented using languages suitable for numeric computation only. Although methods based on mathematical model have been successful for solving a number of problems in the power system area, there remain a number of problems where methods based on mathematical model lead to less than satisfactory solutions; for example, a model of the relevant part of a system cannot be easily identified, posing difficulty in the system modelling. In this respect, an ANN provides an attractive alternative computation concept to the conventional approach, the latter being based on a programmed instruction sequence and prescribed rules. The main advantages of the ANNs are [40-45]:

□ ANNs are adaptive in nature. They can take data and learn from it. Thus ANNs bridge the gap between individual examples and general relationships. This ability differs from standard software techniques because it does not depend on the programmer's prior knowledge of rules. ANNs can reduce development time by learning underlying relationships even if they are difficult to find and describe. They can also solve problems that lack existing solution.

□ ANNs can generalise: they can handle incomplete data, provide an ability to fault tolerance. Generalisation is useful in practical applications because real world data is noisy.

□ ANNs are non-linear: they can capture complex interaction amongst the input variables in a system. In a linear system, changing a single input produces a proportional change in the output, and the input's effect depends only on its own value. In a non-linear system, the effect depends on the values of other inputs,

and the relationship is a higher-order function. In this respect, systems in the real world are often non-linear.

❑ ANNs are highly parallel: their numerous identical, independent operations can be executed simultaneously.

The advantages of ANNs have encouraged various power system engineers and researchers to apply them to solve various power system problems such as load forecasting, security assessment, fault diagnosis, etc.

6.3 ANN Model

A model of ANN is determined according to network architecture, activation function and learning algorithm. The network architecture specifies the way the neurons are connected. The activation function specifies how the neural network with a given set of weights calculates the output vector y for any input vector x. The learning algorithm specifies how the neural network adapts its weights for all given training vectors x.

6.3.1 Multilayer Feedforward Network

There are many types of ANNs, but the most commonly used is the Multilayer Feedforward Network (MFN) [46-53]. In theory, a three-layer network can form arbitrarily complex shapes, and is capable of separating any classes. A typical layout of such a network is shown in Figure 6.1. It is a three-layer (input, hidden, and output) feedforward ANN, where the subscripts i, j and k refer to any unit in the input layer, hidden layer and output layer, respectively.
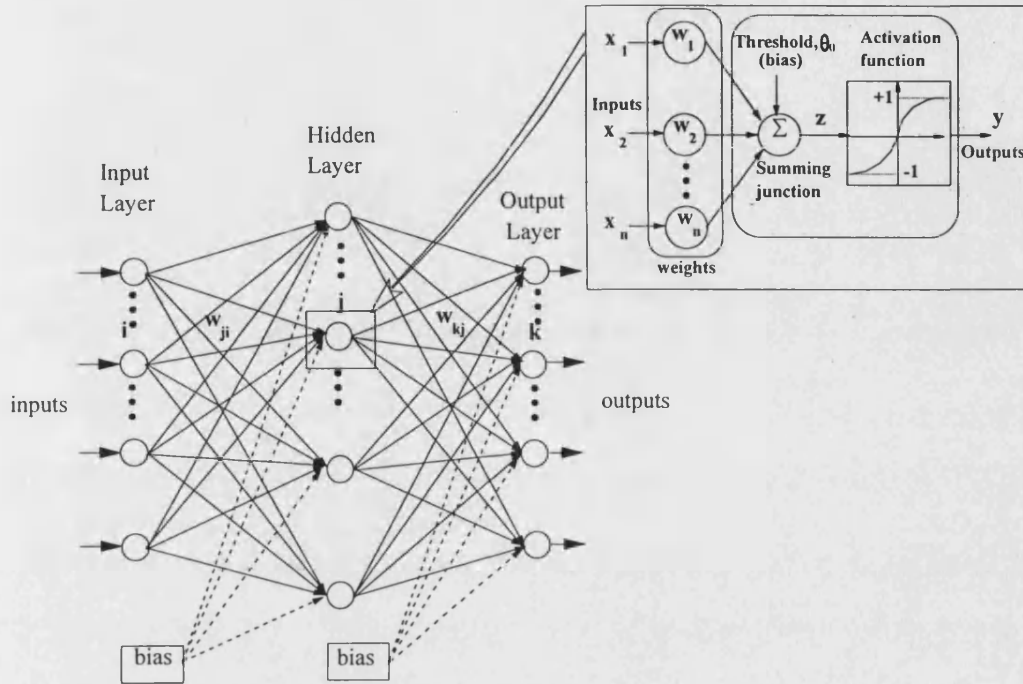
Figure 6.1 A three-layer feedforward ANN

In Figure 6.1, the nodes are the processing units (neurons). Mathematically, the function of a neuron can be modelled as:

$$z = \sum_{i=1}^{n} w_{ji} x_i \qquad (6.1)$$

$$y = f(z) = f\left[\sum_{i=1}^{n} w_{ji} x_i - \theta_0 \right] \qquad (6.2)$$

where, $[x_1, x_2 ...., x_n]$ represents the input signals, $[w_{j1}, w_{j2} ...., w_{jn}]$ is the connection weights from input signals to neuron j in the hidden layer, z is weighted summation of input signals, y is the neuron output, and $f(z)$ is the nonlinear activation function with threshold θ_0 (bias).

6.3.2 Activation Function

The activation function is one of important elements in the neuron model. It defines the output of a neuron in terms of the activity level of its input. There are three basic types of activation functions: Step function, Sigmoid function, and Hyperbolic tangent function; the commonly used sigmoid function is defined by:

$$f(z) = \frac{1}{1 + e^z} \qquad (6.3)$$

and the hyperbolic tangent function is defined by:

$$f(z) = \frac{e^z - e^{-z}}{e^z + e^{-z}} \qquad (6.4)$$

Hyperbolic tangent function is just a bipolar version of the sigmoid function. It should be noted that the sigmoid function is a smooth version of a {0,1} step function, whereas the hyperbolic tangent function is a smooth version of {-1,1} step function. Figure 6.2 shows the characteristics of the sigmoid and the hyperbolic tangent transfer functions.
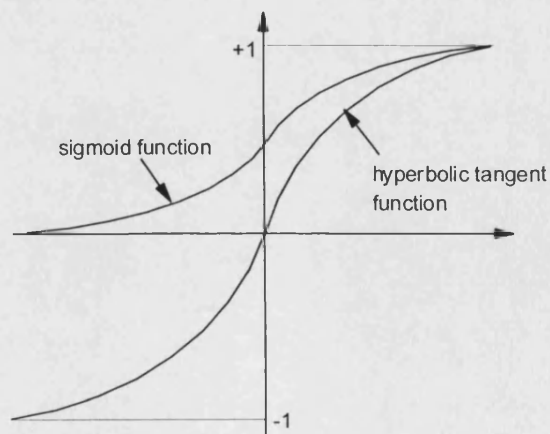
Figure 6.2 Characteristics of Sigmoid and Hyperbolic tangent functions.

6.3.3 Back-Propagation Learning Algorithm

The learning algorithm of MFN is called the 'back-propagation algorithm'. The main objective of the learning algorithm is to minimise the error between the desired and actual outputs through adjusting the weights by back-propagating the error from the output to input layer through the hidden layer. It is based on an iterative gradient algorithm and is outlined below.

Step 1   **Initialise weights and thresholds**

set all weight and node thresholds to small random values.

Step 2   **Present input and desired outputs**

Present a continuously valued input vector space *X* to the input layer neurons, and desired output vector *d*.

Step 3   **Calculate actual output**

Use equation (6.2) to propagate the network input vectors through the hidden layer neurons to the output layer neurons, and calculate actual output.

Step 4   **Adapt weights**

The process of adapting weights is usually called the learning or training process. It starts from the output layer, and works backwards to the input layer. In the training process, the connection weights w_{ji} and w_{kj} between neurons are determined by minimising the following error function:

$$E = \frac{1}{2}\sum_k (t_k - y_k)^2 \tag{6.5}$$

where t_k is the desired output of neuron k;

y_k is the actual output of neuron k.

The weights w_{ij} and w_{kj} are adjusted to minimise the error function E for the set of training patterns by a straightforward application of gradient descent. The whole iteration algorithm to adjust the connection weights can be summarised as follows[43]:

For neuron k in the output layer, the weight w_{kj} is adjusted as follow

$$w_{kj}(t+1) = w_{kj}(t) + \Delta w_{kj}(t) \tag{6.6}$$

$$\Delta w_{kj}(t) = \eta \delta_k y_j + \beta \Delta w_{kj}(t-1) \tag{6.7}$$

$$\delta_k = (t_k - y_k)y_k(1 - y_k) \tag{6.8}$$

where , t is the iteration number;

η is the learning coefficient;

δ_k is the error on the output neuron

β is the momentum.

For neuron j in the hidden layer, the weights w_{ji} can be updated using similar equations, i.e.,

$$w_{ji}(t+1) = w_{ji}(t) + \Delta w_{ji}(t) \tag{6.9}$$

$$\Delta w_{ji}(t) = \eta \delta_j y_i + \beta \Delta w_{ji}(t-1) \tag{6.10}$$

$$\delta_j = y_j(1-y_j)\sum_k \delta_k w_{kj} \qquad\qquad (6.11)$$

Step 5   **Iteration**

Iterate the computation by presenting new epochs of training examples to the network until the free parameters of the network stabilise their value and the average squared error computed over the entire training set is at a minimum or acceptably small value

6.4 ANN Based Scheme

The function and objective of protective relaying to be developed here is to distinguish accurately between internal faults and other conditions (pattern recognition) and, consequently, to issue or block tripping signals (decision making). This brings into focus the application of ANN-based methods (the subject of this section) as an alternative to the existing protection relaying functions.

It is well known that ANNs have the ability to learn the desired inputs/outputs mapping based on training examples, without looking for an exact mathematical model. Once an appropriate ANN has been trained, the interconnections or links of the ANN will contain a representation of non-linearity of desired mapping between inputs and outputs. Figure 6.3 shows an ANN-based relay for the power transformer protection, where the input signals of the ANN are three-phase differential currents, which directly come from the CTs in the power transformer system. A 2nd order Butterworth filter with a cutoff frequency of approximately half sampling frequency of 500Hz is firstly employed to avoid any errors due to signal aliasing. The three-phase differential currents are then passed through an anologue-digital (A/D) converter and fed into the ANN. The decision logic unit issues a trip or block signal depending on the ANN outputs.
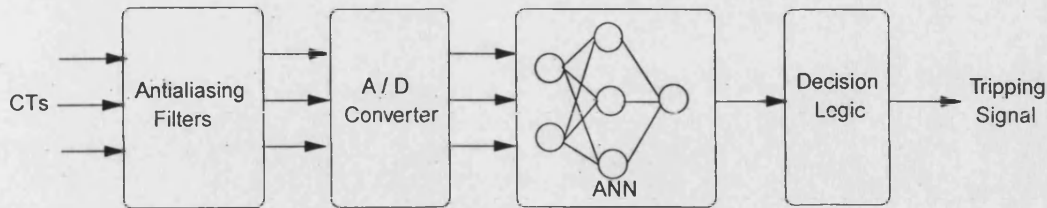
Figure 6.3 Basic configuration of ANN-based relay for power transformer

6.5 ANN Architecture for Power Transformer Fault Diagnosis

The block diagram shown in Figure 6.3 typifies an ANN-based protection scheme. One of the difficult tasks in applying ANN technique to solve a particular protection problem is to chose the right ANN topology in terms of the input vector, the number of hidden layers and the number of neurons in each layers, and finally the number of outputs.

6.5.1 Input Selection

The inputs of an ANN should be representative of the whole of the feature space signifying the relationship between the input/output patterns. In this respect, the two commonly applied approaches of selecting the most significant input features are: (i) a sampled time domain moving window and (ii) features based on frequency decomposition of a time domain window. The approach presented herein is based on the former of the two and was arrived at after an extensive series of studies. Furthermore, in the case of the power transformer fault diagnosis, the chosen input samples are differential currents through CT secondary side, which are readily available in a practical protection system of a power transformer. However, the data window length and sampling rate for the ANN are parameters that are chosen,

depend upon a particular application. In the technique presented herein, the data window length chosen is 1 cycle and therefore, for each input differential current, there are 10 samples at a sampling frequency of 500Hz. Thus, for a three-phase transformer, 30 continuous differential current samples in each window are taken as ANN inputs.

6.5.2 Output Selection

Only two classes of disturbance are relevant in the power transformer fault diagnosis problem described herein, viz. internal faults and other conditions, and the ANN is expected to operate for all types of internal faults but inhibit relay operation under other conditions such as inrush currents and external faults. This means that the ANN operating as a protection relay is required to respond with two distinct values to indicate whether the input signals represent internal faults or other conditions. Thus, there is only one ANN output; a value of 1 signifies an internal fault, and 0 is used to indicate an inrush current or external fault.

6.5.3   Determination of Number of Hidden Layers

Having defined the inputs and outputs, the next task is to determine the best structure of the MFN for the given training data, since the number of hidden layers and the number of hidden neurons directly affect convergence performance during training and its generalisation ability.

As mentioned before, a three-layer network (input layer, one hidden layer, and an output layer) can form arbitrarily complex shapes, and is capable of separating any classes, and is therefore the most commonly used architecture for solving power system applications. Herein also, a three-layer network is chosen.

6.5.4 Determination of Number of Hidden Neurons

Having determined the number of hidden layers, the next task is to ascertain the number of hidden neurons. As is well known, the MFN classification time, i.e., the required time to produce an output from an input, depends on the number of neurons in the network, and so it is vitally important to have the lowest number of neurons but without jeopardising the accuracy of the classification. Through a series of tests and modifications, 6 hidden neurons produced a satisfactory performance. Moreover, it was found that the ANN converged in a shorter time with a simpler structure when the hyperbolic tangent activation function rather than the commonly used sigmoid function, was employed. The near optimal ANN architecture best suited to solving the power transformer fault diagnosis problem is shown in Figure 6.4.
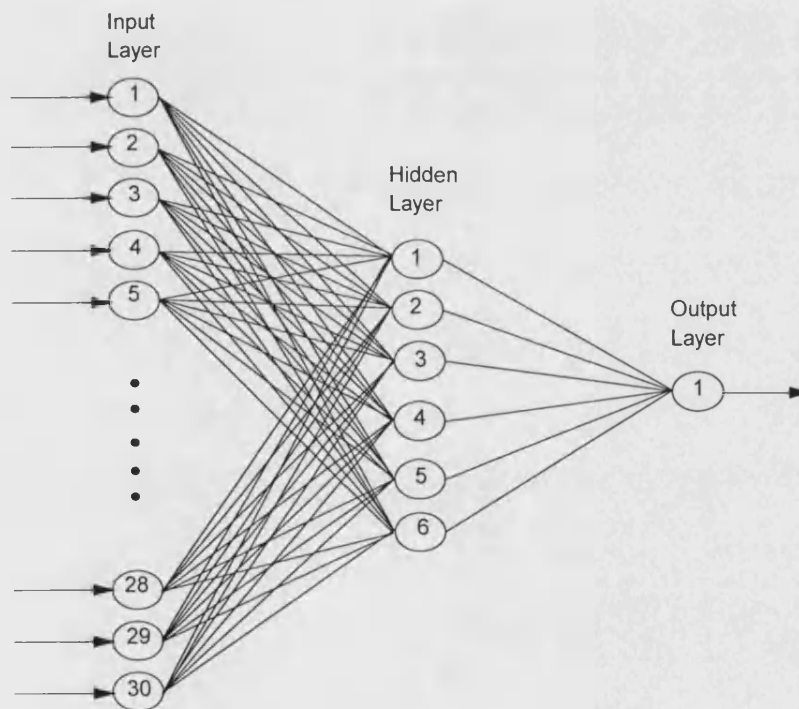
Figure 6.4 ANN architecture for power transformer fault diagnosis

6.6 Generation of Training and Test Data

In order to set up the training/test data for the ANN, the digital simulations were carried out using the EMTP software for two power transformer systems, i.e., System 1 and System 2, which are illustrated in Figures 4.5 and 4.6, respectively, presented in Chapter 4. The simulation results were obtained under a whole variety of practically encountered system and fault conditions, which are described in detail in Chapters 4 and 5 respectively. The distribution of training and test cases for both Systems 1 and 2 are shown in Table 6.1.

With reference to Table 6.1, amongst 245 cases generated from System 1, 145 cases were used to train the ANN and 100 cases were used to test performance of the ANN; there were 120 cases generated from System 2, and these were used to further test the performance of the ANN without retraining it for System 2.

Table 6.1 List of training and testing cases

Simulated systems / Type of case	System 1		System 2 (Test cases)
	Training cases	Test cases	
No-fault situation	3	2	5
Inrush current	36	12	12
External fault	20	10	20
Internal fault	86	76	83
Total cases	145	100	120

6.7 Data Window

The training and test data are a series of differential current samples, and the method of inputting data into the ANN is based on the moving data window concept, as

illustrated in Figure 6.5. A window of 30 samples (representing three phases differential currents) is moved sample by sample covering 120ms (6 cycles) for each differential current for a particular training case during ANN training. Thus, there are 50 patterns associated with each training case.
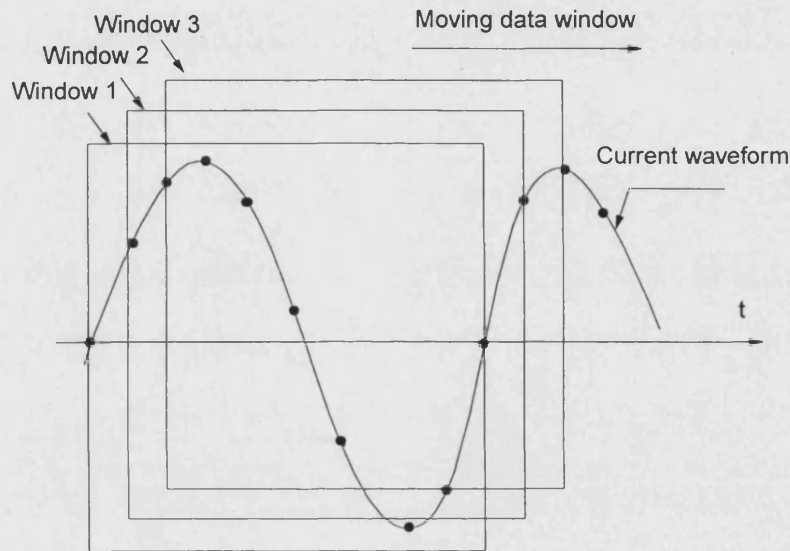
Figure 6.5 Moving data window for ANN input

6.8 ANN Training and Testing

The training and test data are firstly generated from the simulations performed on System 1. Once the ANN has been trained, it is then tested with data that is different from that used for training. Since the quality of generalisation is very important in any ANN application, the trained ANN is further tested with the data that is generated through the simulations of System 2 to test the robustness and generalisation of the trained ANN.

6.8.1 Scaling of Input Data

For an effective training of the ANN, scaling of the input values is required. Scaling refers to the desired range of values required at the input of the ANN. The range into which the values must be scaled are primarily defined by the activation function in the nodes. If the input value to a neuron is larger than the output of the node as defined by the activation function, it will be in a range of the function where the output is almost saturated. This means that the ANN is unable to learn.

A linear scaling which for a variable X in the range of $[X_{min}, X_{max}]$ will assign the value A in the range of $[A_{min}, A_{max}]$ is adopted to linearly scale the inputs to the network. This scaling is suitable for the activation function. Thus the general equation to scale the inputs is given by:

$$A = \left[\frac{A_{max} - A_{min}}{X_{max} - X_{min}} \right] (X - X_{min}) + A_{min} \qquad (6.12)$$

where X_{max} and X_{min} represent the maximum and minimum values of the original input signal, respectively; X represents the original input signal; A represents the scaled input signal; and A_{max} and A_{min} represent the maximum and minimum values of the input signal after scaling. In this work, the chosen values are: $A_{max}=1$, $A_{min}= -1$. Note that the same scaling method must be used for both training and input test data.

6.8.2 ANN Training

The training data consist of 145 cases (7250 patterns), which include (a) no-fault situation (2%); (b) external faults with and without CTs saturation (14%); (c) inrush current cases (24%); (d) internal fault cases (60%). The network was trained by randomly processing the training patterns using the back-propagation learning algorithm. The learning coefficient that controls the rate of convergence and stability, which was described in the formula (6.7), was initially chosen to be 0.5 and was

gradually reduced during the ANN training. The momentum factor that is added to speed up the training and avoid local minima, which was also described in the formula (6.7), was initially chosen to be 0.4 and was gradually reduced as the learning coefficient. The 245 cases (12250 patterns) on System 1 were firstly prepared to evaluate the performance of the ANN. Roughly, 60 % of these cases were used for the ANN training, and the other 40% were used for the subsequent testing. The training cases were then all mixed together and the foregoing training process was repeated until the root mean square (RMS) error between the actual output and the desired output reached an acceptable value of 0.05 (RMS error criteria). The learning performance is shown in Figure 6.6. It can be seen that the ANN reached the requisite RMS of 0.05 in approximately 55,000 learning iterations.
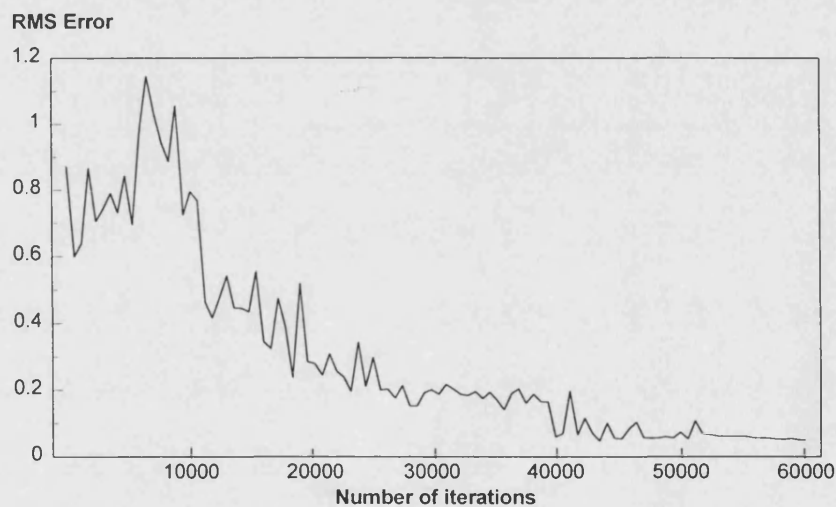
Figure 6.6 Performance of ANN training

It was also found that the convergence performance of the ANN was adversely affected by certain types of inputs during the training process. For example, if the training data included a very low level fault current case, in which the magnitudes of differential currents generated are much smaller compared to those caused by other types of faults, the learning performance of the ANN becomes significantly slower

and less accurate. An example of this is that for a *c*-phase 5% turn-to-turn fault at mid-point of winding on LV side of the transformer; the differential currents generated in this case (approximately 4A through CT secondary side) are much smaller compared to those caused by other types of faults (approximately 100A through CT secondary side for an internal three-phase to earth fault on LV side). Thus, if a low level fault case (even one case) is included in the training set of the ANN, the ANN only manages to reach a value 0.1 of the RMS in approximately 100,000 learning iterations, i.e., both the convergence speed and accuracy of the ANN are impaired due to the impact of this fault case.

6.8.3 Test Results for System 1

In order to test the effectiveness of the ANN, the data used for testing is different and 'unseen' from that used for training as shown in Table 6.1. During the testing, a target tolerance of 0.15 was used; this effectively means that the network produced a response of 0.85 or greater then thus signified internal faults and 0.15 or less for other conditions (i.e. inrush currents, no-fault situations or external faults with and without CT saturation). The relay is expected to assert a trip signal when the ANN output is ≥ 0.85, and block when the ANN output is ≤ 0.15.

Figures 6.7-6.9 typify some of the responses of the ANN under a variety of commonly encountered faults: (i) internal single-phase to earth fault cases as shown in Figure 6.7; (ii) internal two-phase to earth fault cases as shown in Figure 6.8; (iii) internal three-phase short circuit cases as shown in Figure 6.9. It is apparent from the results that the ANN gives the correct classification results by virtue of its output being greater than 0.85; in practice ANN-based relay would issue a trip signal.
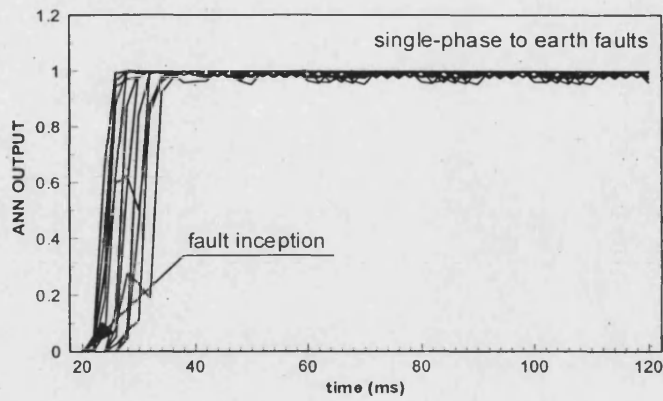
Figure 6.7 ANN outputs for a moving data window for a set of single-phase to earth faults
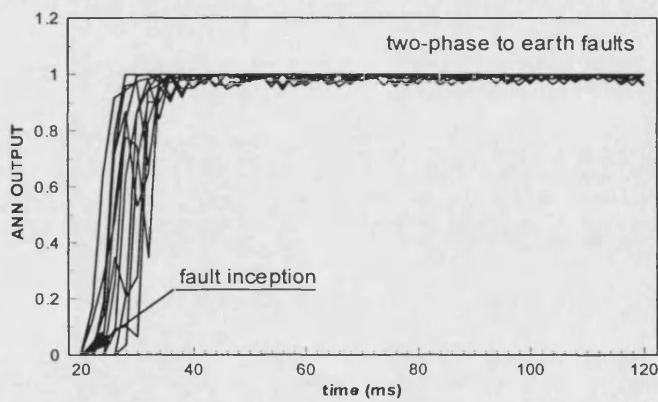
Figure 6.8 ANN outputs for a moving data window for a set of two-phase to earth faults
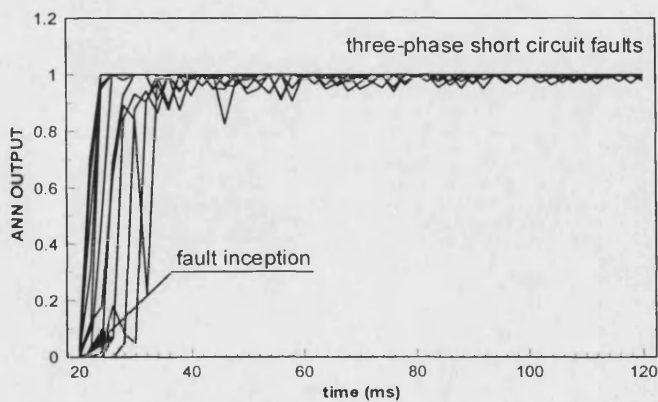
Figure 6.9 ANN outputs for a moving data window for a set of three-phase short circuit faults

Figure 6.10 gives the responses of the ANN to a set of internal faults with CT saturation. It is clearly evident that after the fault inception time, some outputs of the ANN for such cases take much longer time to converge to the requisite output for the correct classification of the faults, in comparison with that associated with internal faults without CT saturation as shown in Figures 6.7-6.9. This is so by virtue of the fact that the signal waveform is more severely distorted in the first two cycles due to CT saturation, which was evident from the simulation results presented in Figure 4.12 in section 4.4.2.1 of Chapter 4. However, the outputs of the ANN become consistently greater than the expected output value 0.85 after two cycles from the fault inception time. Of course in practice, this erratic behaviour of the ANN during the initial period could be easily overcome by incorporating, within the relay algorithm, a decision logic based on a counting regime (as outlined in section 6.8.4). This effectively means that the response speed of the ANN will become slow due to CT saturation.
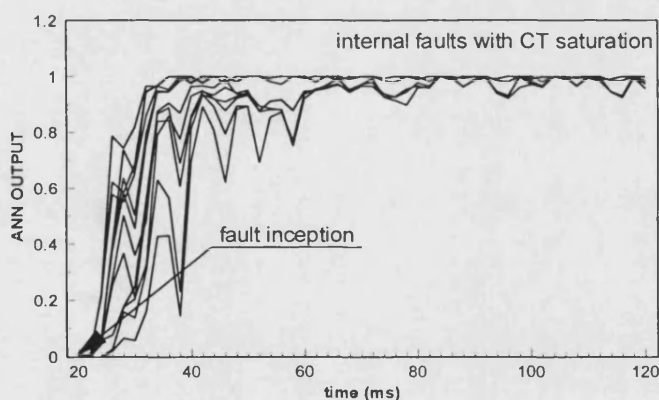
Figure 6.10 ANN outputs for a moving data window for a set of internal faults with CT saturation

As described in section 4.4.3, the power transformer protection is designed to restrain under normal load flows and external faults. A number of typical cases under such conditions were tested for the trained ANN; the results indicated that the

performance of the ANN was satisfactory in view of the fact that the ANN gave the outputs of less than 0.15, the ANN thus correctly inhibiting relay operation. This is so because the differential currents under such conditions are very small, in comparison to those under internal fault conditions, so that there are good separation of classes amongst them.

However, the external faults can in fact result in very large differential currents if CT saturation ensues. It is vitally important to verify if the protection relay under such a condition is stable i.e., still inhibits circuit breaker operation. The effect of external faults with CT saturation under various system conditions on the accuracy attained is thus examined. Figures 6.11 typifies responses of the ANN to a set of external faults with CT saturation. It is clearly evident that the performance of the ANN-based relay is satisfactory.
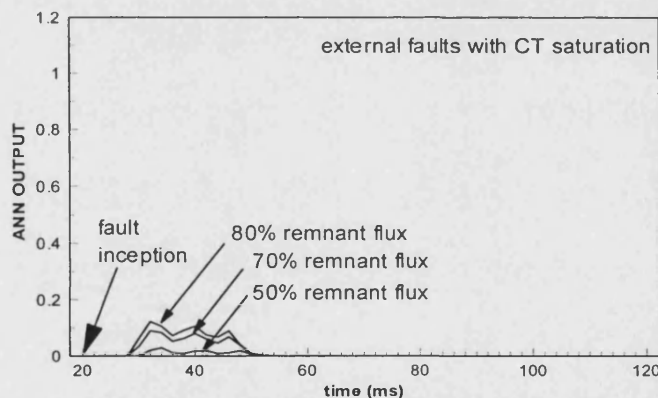
Figure 6.11 ANN outputs for a moving data window for a set of external faults with CT saturation

Figures 6.12 illustrates some typical responses of the ANN to a set of inrush current cases. Here again, it can be seen that the ANN gives the correct classification by virtue of its outputs being less than 0.15.
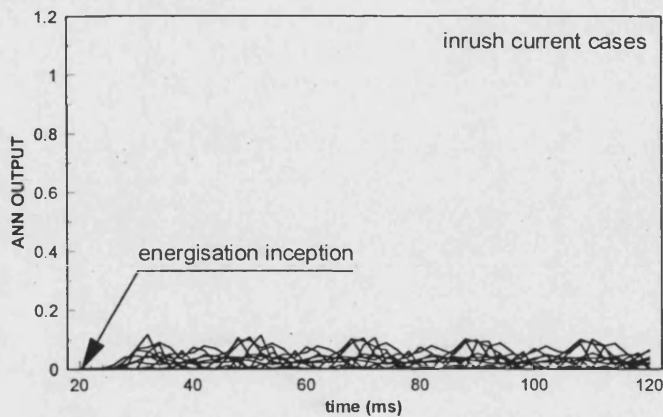
Figure 6.12 ANN outputs for a moving data window for a set of inrush currents

However, as mentioned at the training stage of the ANN, for some low-level internal fault currents, such as turn-to-turn or turn-to-earth faults, the learning rate of the ANN becomes slower and its performance is less accurate. Here again, at the testing stage, the ANN for such cases gives poor classification. Figure 6.13 represents the responses of the ANN to a set of low level internal fault currents. From this figure, it can be seen that although the expected outputs of the ANN should be 0.85 or greater, the ANN gives a value of less than 0.85 in some cases. This is due to the fact that the magnitudes of differential currents for such cases are much smaller than other internal fault cases thereby having a detrimental affect on the ANN performance.
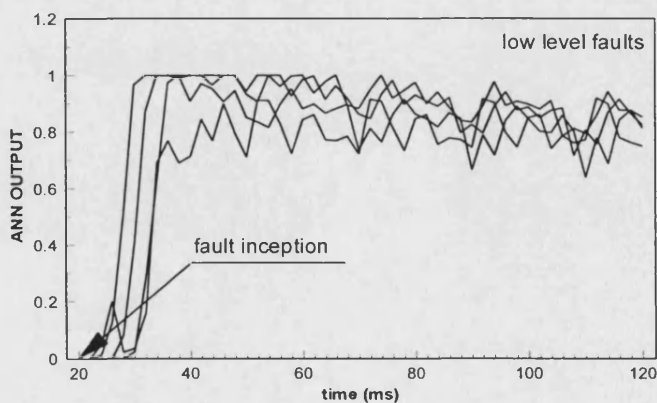
Figure 6.13 ANN outputs for a moving data window for a set of low level faults

6.8.4 Decision Logic Unit

As mentioned before, in order to increase the ANN-based relay security and dependability, a decision logic based on a counting regime is required to confirm the ANN output state; One very effective approach, for example, is that based on a strategy whereby a counter is incremented if the ANN output is ≥ 0.85 and decremented otherwise (without allowing it to go negative); the relay is set to give a trip signal once the counter reaches a certain preset level; with this approach, although the relay response would be slower with the onset of any CT saturation as shown in Figure 6.10, it would nonetheless ensure correct relay response for internal faults with and without CT saturation. Figure 6.14 typifies the decision logic based on a counting regime.
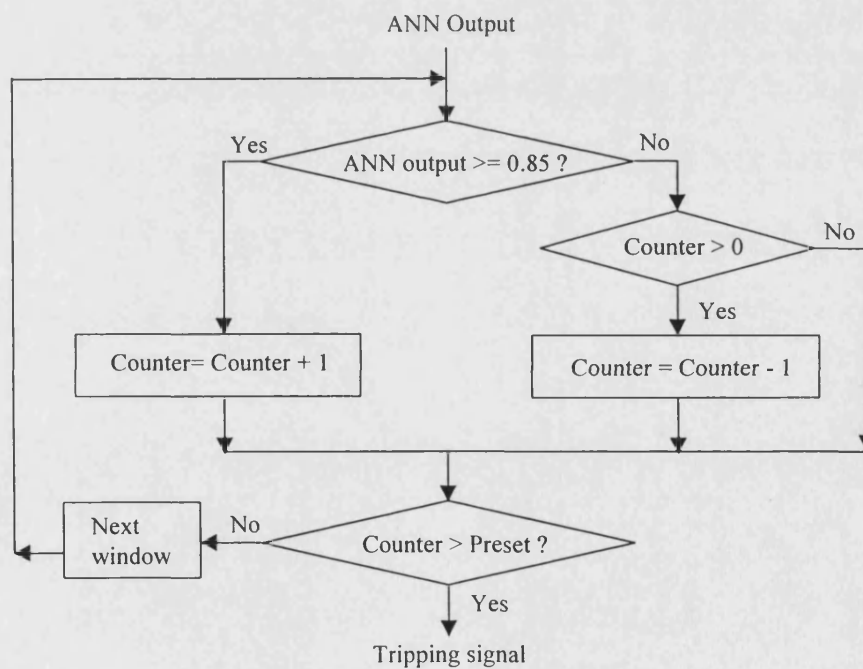
Figure 6.14 Decision logic based on a counting regime

To measure the performance of the trained ANN, two measuring indices are defined as follows:

$$Misclassification\ rate\,(MR) = \frac{N_F}{N_T} \times 100\%$$

(6.13)

and

$$Correct\ classification\ rate\,(CR) = \frac{N_T - N_F}{N_T} \times 100\%$$

(6.14)

where N_T represents the total number of test cases, and N_F represents the total number of misclassified cases during testing. The number of misclassified cases during testing are based on those cases during which the outputs of the ANN are less than 0.85 when internal fault signals are fed into the ANN, or the outputs of the ANN are greater than 0.15 when inrush current or external fault signals are fed into the ANN.

For all the test cases evaluated on System 1, the total results show that when the ANN was tested with System 1, the designed ANN relay was able to distinguish internal faults from inrush currents or external faults with less 5% misclassification rate.

6.8.5 Test Results for System 2

The ANN that was trained and tested for System 1 was also directly tested by data generated from System 2, without actually training the ANN for this system. The results are shown in Figures 6.15-6.19. From these figures, it is clearly evident that without retraining the ANN, there is little robustness in that, although in some cases, the ANN gives correct classification results, but in the majority of cases, the classification is very poor. For example, the outputs of the ANN shown in Figures 6.15-6.18 are expected to be of a value 0.85 or greater when internal fault data are fed into ANN, but unfortunately, this is not the case herein. Likewise although the

outputs of the ANN shown in Figure 6.19 are expected to be at a value 0.15 or less when inrush current data are fed into the ANN, however, as shown in Figure 6.19, in many cases, the ANN will issue an unwanted trip signal due to its output being greater than 0.15 in many cases. It should be mentioned that the previously described trip logic would overcome this problem to a certain extent, but it would be dangerous to rely solely on this logic when employing the ANN-based relay on System 2.
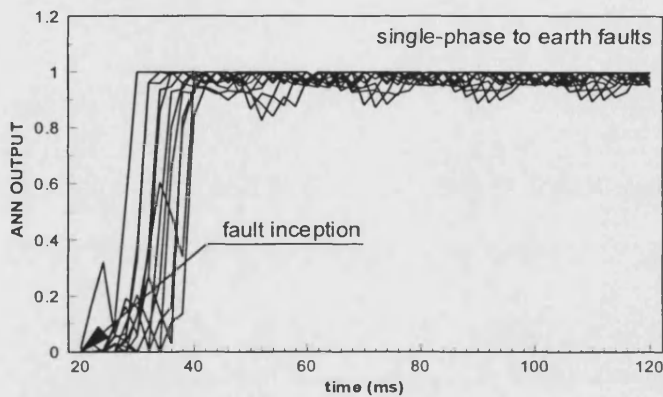
Figure 6.15 ANN outputs for a moving data window for a set of single-phase to earth faults
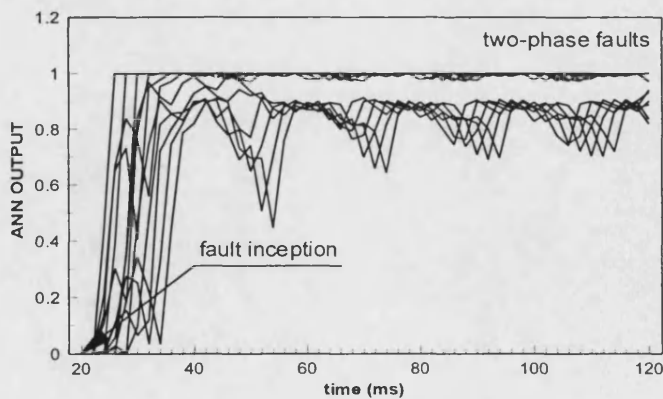
Figure 6.16 ANN outputs for a moving data window for a set of two-phase faults
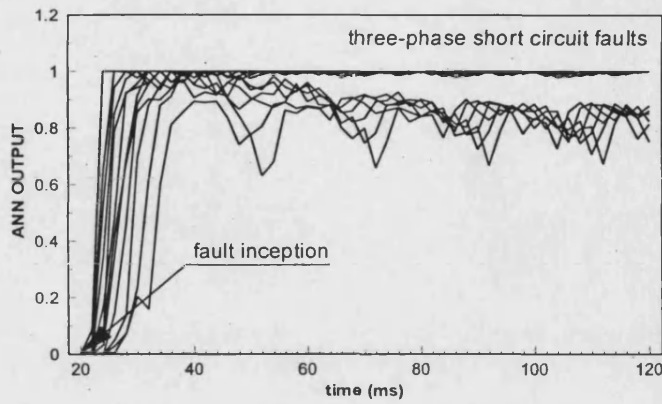
Figure 6.17 ANN outputs for a moving data window for a set of three-phase short circuit faults
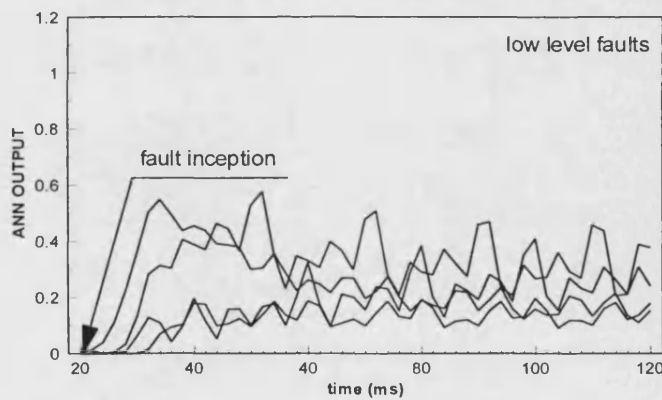
Figure 6.18 ANN outputs for a moving data window for a set of low level faults
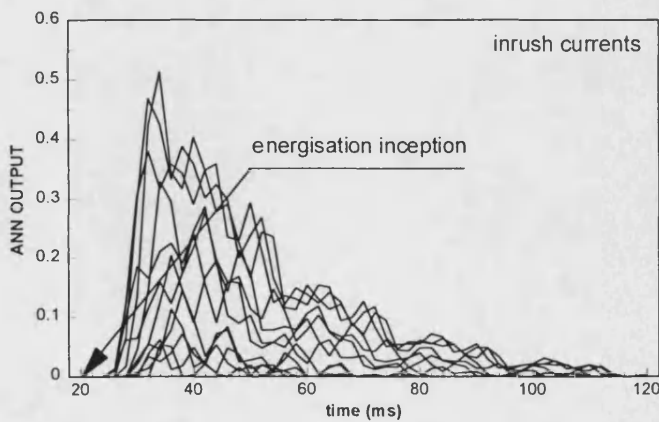
Figure 6.19 ANN outputs for a moving data window for a set of inrush currents

The case studies carried out on System 2 have clearly demonstrated that the ANN trained for System 1 cannot be directly used in another power transformer system at all. Without retraining the ANN for new system data, a very poor classification rate will be produced. This effectively means that once an ANN has been trained and tested to give a satisfactory performance for a particular power transformer system using feature extraction based on the time-domain window approach, its performance is very adversely affected if it is then employed for the fault diagnosis on another transformer system with different specifications, without actually retraining the ANN. An alternative approach of feature extraction methodology and/or alternative fault diagnosis techniques must thus be investigated and developed in order to overcome the problem of robustness.

6.9 Summary

In this Chapter, an ANN model and its advantages to solve the problems are presented. A preliminary investigation of the ANN-based power transformer fault diagnosis technique has been carried out through case studies, in which time-domain signals are directly fed into an ANN to implement the power transformer fault diagnosis. The study has shown that an ANN can be very useful in the field of power transformer fault diagnosis. Case study results have shown that by directly employing time-domain current signals as a signal feature representation, the trained ANN can give a correct classification rate of greater than 95%. However, if the trained ANN is directly used for a different power transformer system without retraining, the ANN-based technique will give a very poor classification rate. Moreover, the training was also tried with two systems together and it was found that the ANN could not converge. This is so because the feature extraction methodology adopted is not representative of a feature space wide enough to cope with a different transformer system. This understanding has led to an investigation and development of a new feature extraction methodology as well as fault diagnosis technique for power transformer protection, the subject of the following Chapters.

Chapter 7

Electromagnetic Transient Analysis of Power Transformers Using Wavelet Transform

7.1 Introduction

An accurate and efficient means to distinguish internal faults from magnetising inrush currents has been the subject of considerable research effort in recent years. In order to achieve this, an effective feature extraction methodology radically different from that described in the previous chapter, is crucial to implement reliable classification. In this chapter, a new method to analyse the power transformer transient phenomena is proposed by using the Wavelet Transform (WT) technique. The WT is a powerful tool in the analysis of the power transformer transient phenomenon because of its ability to extract information from the transient signals simultaneously in both the time and frequency domain, rather than employing the conventional Fourier Transform (FT) which can only give information in the frequency domain.

The potential benefits of applying WT for analysing the power system transients have been well recognised in recent years [54-58]. Several relevant papers have been presented for power system analyses using the WTs [59-65]. These application studies cover the detection and analysis of power system transient signals [59-62] and the transient power quality problem [63-64] as well as the fault detection of power transformers during impulse testing [65], etc.

In this chapter, application of the WT for analysing the fault and magnetising inrush current transient phenomena in power transformers is presented. The proposed method is based on the fact that a given faulted current signal or inrush current signal is firstly decomposed using WT; the signal is thus realised into a series of wavelet components, each of which is a time-domain signal that covers a specific frequency band. These components can then be employed as specific and significant features to effect a fault classification technique.

7.2 Wavelet Transform and Its Implementation

7.2.1 Time-Domain Signals

It is well known that most of the signals in a power system, such as current and voltage signals, are time-domain signals commonly known as a time-amplitude representation of the signal, as shown Figure 7.1 (a). However, this is not always the best representation of the signals. In many cases, the most significant information is hidden in the signals. Therefore mathematical transformations are applied to signals to obtain further information, such as FT, Short-Time Fourier Transform (STFT) as well as WT.

7.2.2 Fourier Transform

FT that realises a signal into constituent sinusoids of different frequencies is the most widely employed transform technique being used in Electrical Engineering. Basically, it is a mathematical technique for transforming a signal from a time domain one to a frequency domain one. To implement a FT on a digital processor with discrete (sampled) and finite-length (time-limited) signals, the Discrete Fourier Transform (DFT) is used.

For many signals, Fourier analysis is extremely useful because the signal's frequency content is very important, and FT gives what frequency components (spectral

components) exist in the signal, as shown in Figure 7.1 (b). However, FT does not indicate when in time these frequency components exist, and this means that time information of the signal is lost. When considering the FT of a signal, it is impossible to ascertain when a particular fault took place, whereas these are very important characteristics for analysing transient signals, such as those present in the faults and inrush currents in a power transformer. Thus, FT is not the best technique to analyse a non-stationary signal.

7.2.3 Short-Time Fourier Transform

In an effort to correct the aforementioned deficiency, a method called the STFT was proposed. The STFT adapts the FT to analyse only a small section of the signal by means of dividing the signal into small segments by small windows, and these segments are then assumed to be stationary. The STFT represents a sort of compromise between the time and frequency-based views of a signal. It provides some information about when in time these frequency components exist as shown in Figure 7.1 (c). However, this method can only give the time-frequency information with limited precision, and that precision is determined by the size of the window. While the STFT's compromise between time and frequency information can be useful, the drawback is that once a particular size for the time window is chosen, that window is the same for all frequencies.

7.2.4 Wavelet Transform

Compared with STFT, WT analysis represents a windowing technique with variable-sized regions. It allows the use of long time intervals if requiring more precise low frequency information and shorter regions if requiring more precise high frequency information. These can be clearly shown in Figure 7.1 (d).
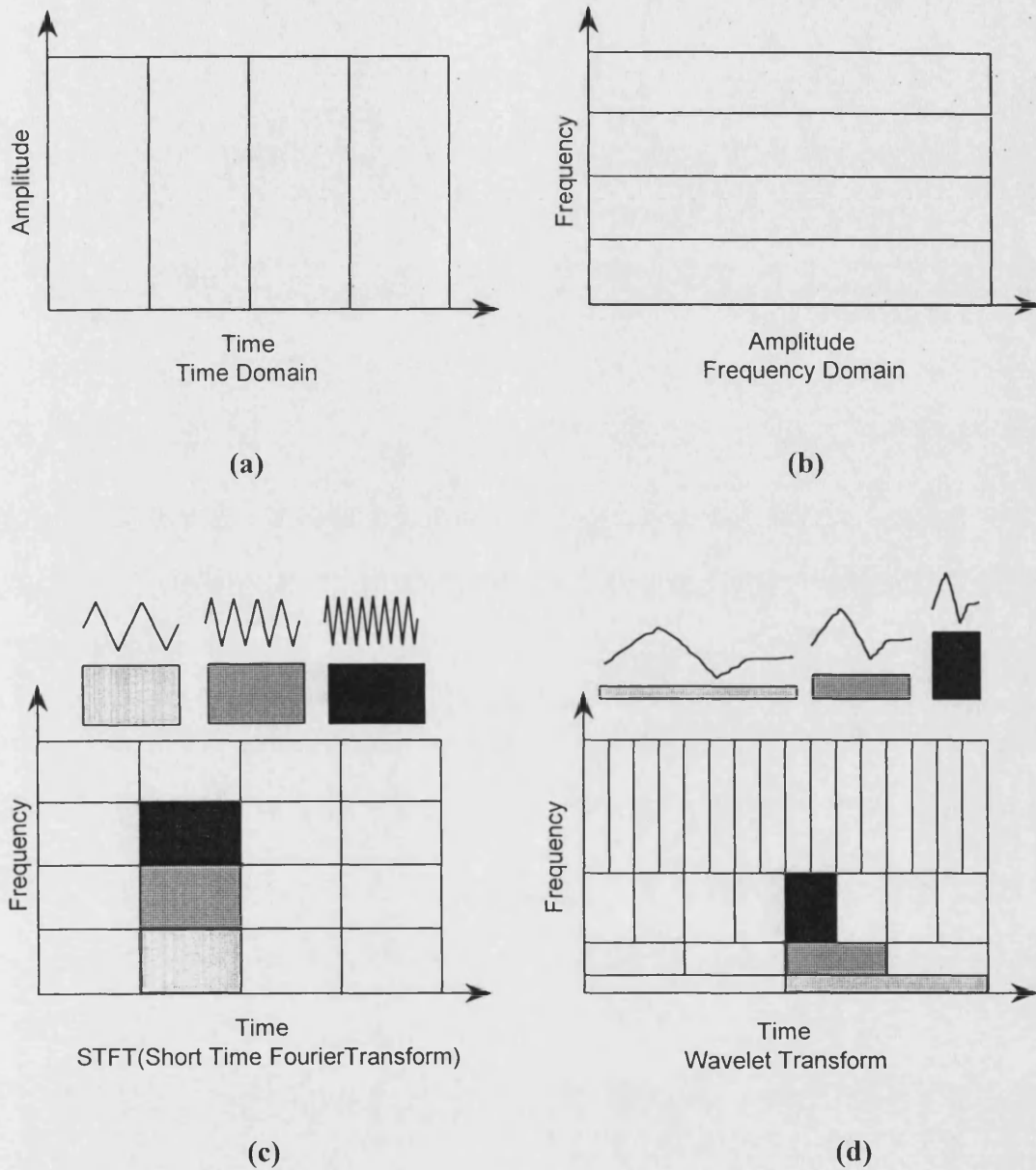
Figure 7.1 Different representations of transient signals

WT provides a multiple resolution of the transient signal both in time and frequency [54,55]. Unlike FT which uses one basis function (sine waves or cosine waves), WT relies on wavelets of a rather wide functional form. The basis wavelet is termed as a

mother wavelet. WT can decompose a given signal into a series of wavelet components, each of which represents a time-domain signal that covers a specific frequency band, and it allows the detection of the time of occurrence of abrupt disturbances, such as detection of fault transients in power transformer systems. Thus the WT is more suitable to the study of the signal, which has low frequency components with discontinuities and sharp spikes.

7.2.5 Continuous Wavelet Transform

Similar to the relationship between a continuous FT and a discrete FT, there is a Continuous Wavelet Transform (CWT) and a Discrete Wavelet Transform (DWT). The CWT is not employed as often as the DWT. The CWT is primarily employed to derive properties; whereas DWT is sufficient for most practical applications (in particular those employing digital technology); the DWT provides enough information and significantly reduces the computation time.

Mathematically, the CWT of a given function x(t), with respect to a mother wavelet g(t), is defined as [54,55]:

$$CWTx(a,b) = \frac{1}{\sqrt{a}} \int_{-\infty}^{+\infty} x(t)g(\frac{t-b}{a})dt \qquad (7.1)$$

where a is a scale parameter, b is a translation parameter, and $g(t)$ is the mother wavelet function. It is apparent from equation (7.1) that through CWT the original one dimensional time-domain signal $x(t)$ is mapped to a new two-dimensional function space across scale a and translation b by the wavelet transform. A wavelet transform coefficient, $CWTx(a,b)$, at a particular scale and translation represents how well the original signal $x(t)$, and scaled and translated mother wavelet match. Thus, the set of all wavelet coefficients, $CWTx(a, b)$, are the wavelet representation of the original signal $x(t)$ with respect to the mother wavelet $g(t)$.

7.2.6 Discrete Wavelet Transform

Since the CWT is computed by changing the scale of the analysis window, shifting the window in time, multiplying by the signal, and integrating over all times, it generates substantial redundant information. Therefore, instead of continuous scale and translation, the mother wavelet may be scaled and translated discretely by making 'a' and 'b' discretised. DWT is given by:

$$DWTx(m,k) = \frac{1}{\sqrt{a_0^m}} \sum_n x(n) g\left(\frac{k - nb_0 a_0^m}{a_0^m} \right) \qquad (7.2)$$

The above equation is generally expressed as DWT of *x(n)*. The *g(n)* is the mother wavelet; a_0^m is the scale parameter; $nb_0 a_0^m$ is the translation parameter. The simplest choice of a_0 and b_0 are $a_0 = 2$ and $b_0 = 1$. The result is geometric scaling i.e. *1, 1/2, 1/4, 1/8, ...*, and translation by *0, n, 2n, ...*. This choice completely removes information redundancy amongst the decomposed signals. With this, the WT is called a dyadic-orthogonal wavelet transform.

7.2.7 Implementation of DWT

By simple rearrangement of the DWT equation (7.2), the following equation can be obtained:

$$DWTx(m,k) = \frac{1}{\sqrt{a_0^m}} \sum_n x(n) g\left(a_0^{-m} k - b_0 n \right) \qquad (7.3)$$

Upon closer observation of this equation, it is noted that it is similar to the equation for digital FIR filters.

$$y[k] = \frac{1}{c}\sum_n x(n)h(k-n) \qquad\qquad (7.4)$$

By comparing equations (7.3) and (7.4), the impulse response of the filter in the DWT equation is $g(a_0^{-m}k - b_0 n)$. By selecting $a_0 = 2$ ($a_0^{-m} = 1, 1/2, 1/4, 1/8, \cdots\cdots$) and $b_0 = 1$, the DWT could be implemented by using a multi-stage filter with the mother wavelet as the low-pass filter and its dual as the high-pass filter, as shown in Figure 7.2. Down-sampling the output of the low-pass filter by a factor of 2 ($\downarrow 2$) would scale the wavelet by a factor of 2 for the next stage, thereby simplifying the process of dilation.
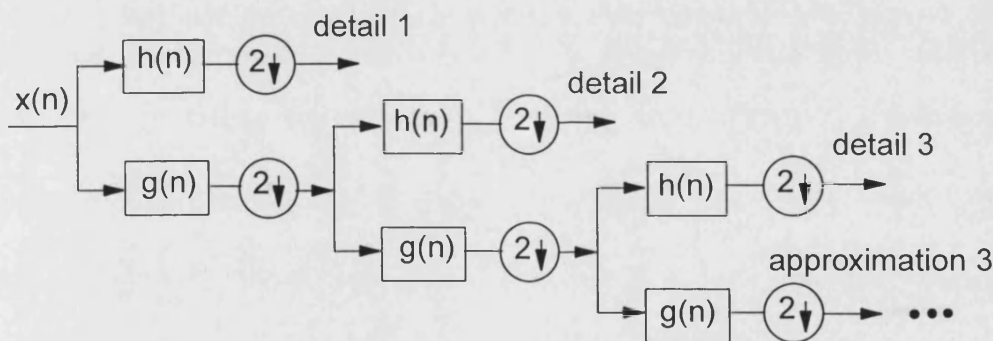
Figure 7.2 Implementation of DWT

Note that in Figure 7.2, x(n) is the original signal, g(n) and h(n) are low-pass and high-pass filters, respectively. At the first stage, an original signal is divided into two halves of the frequency bandwidth, and sent to both high-pass filter and low-pass filter. Then the output of low-pass filter is further cut in half of the frequency bandwidth, and sent to the second stage. The same procedure is performed until the signal is decomposed to a pre-defined certain level. Finally a bunch of signals, which

actually represent the same original signal but all corresponding to different frequency bands can be obtained. The output of the filter bank could be viewed as shown in Figure 7.3, in which the DWT output is represented in a two dimensional grid similar to that of the STFT, but with a very different division in time and frequency. The rectangles shown in Figure 7.3 have equal area to maintain a constant time-bandwidth product.

It is worth pointing out that the frequency band of each detail of the DWT is directly related to the sampling rate of the original signal. Figure 7.3 also presents the time-frequency relationship of DWT.
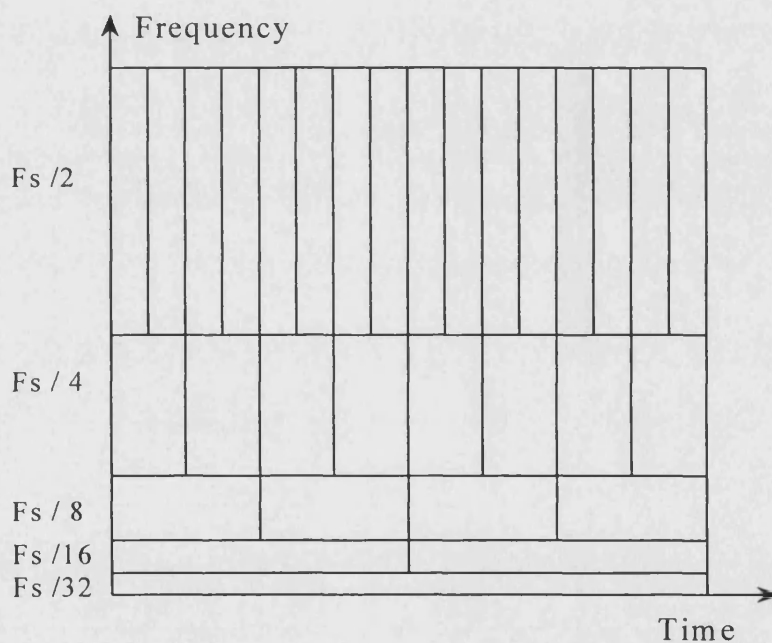
Figure 7.3 Time-frequency relationship of DWT

As indicated in Figure 7.3, if the original signal is being sampled at F_s Hz, the highest frequency that the signal could contain, from Nyquist's theorem, would be $F_s/2$ Hz. This frequency would be seen at the output of the high frequency filter, which is the first detail. Thus the band of frequencies between $F_s/2$ and $F_s/4$ would be

captured in detail 1; similarly, the band of frequencies between Fs/4 and Fs/8 would be captured in detail 2, and so on.

7.2.8 Selection of Mother Wavelet

There are many types of mother wavelets [56,57], such as Harr, Daubichies, Coiflet and Symmlet wavelets. The choice of the mother wavelet plays a significant role in detecting and localising different types of fault transients. In addition to this, the choice also depends on a particular application. In the study of power transformer transients, we are particularly interested in detecting and analysing low amplitude, short duration, fast decaying and oscillating type of high frequency current signals. One of the most popular mother wavelets suitable for a wide range of application used is Daubichies's wavelet. In the work presented herein, D4 wavelet is used, and this is shown in Figure 7.4.
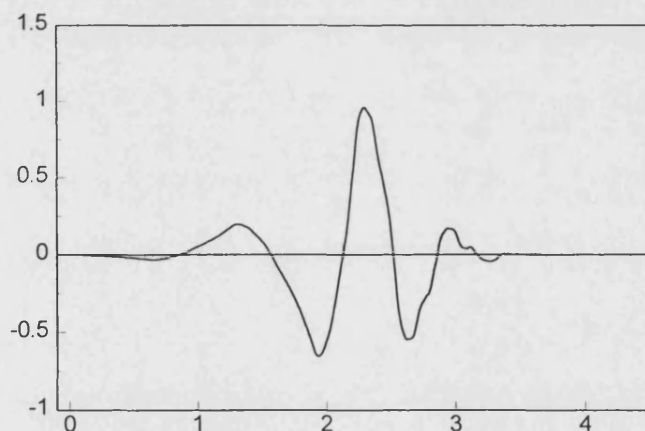
Figure 7.4 D4 mother wavelet

7.3 Wavelet Analysis of Transient Phenomena in System 1

In order to investigate the effectiveness of the WT to detect and analyse the power transformer transients, particularly fault and inrush current transients, various

internal faults and inrush currents are simulated in Systems 1 and 2, and these have been presented in detail in Chapter 4 and Chapter 5 respectively; the corresponding differential current signals are evaluated and realised using the WT technique [57]. As mentioned before, the D4 wavelet is used in DWT in the following studies. For illustrative purposes, some typical DWT analysis results are presented in detail in the following section.

7.3.1 Wavelet Analysis of Inrush Currents

As mentioned in the previous chapters, the magnetising inrush currents may be very large under transient conditions because of the extreme saturation of the iron-core in the power transformer. Figure 7.5(a) shows typical magnetising inrush current waveforms, which correspond to a, b and c three phase differential currents through the CT secondary sides. As can be seen, the current waveforms are distorted quite significantly; gaps appear over the times of the inrush currents. At the edges of the gaps, the current magnitude changes from near zero to a significant value or from a significant value to near zero; this would be expected by virtue of the fact that sudden changes from one state to other different states produce little ripples, which very often are not visible from the fundamental frequency signals as apparent in Figure 7.5 (a). However, this can be discerned and clearly demonstrated by the WT. For brevity, only the DWT of the a-phase differential current is shown herein.

Note that in implementing the DWT, the original inrush current signal has been sampled at 25kHz and passed through a DWT, with the structure of Figure 7.2. The frequency space is divided as indicated in Figure 7.3. Thus, 5-detailed signals that contain a frequency band of 12.5kHz ~ 6.25kHz at detail 1, 6.25kHz ~ 3.125kHz at detail 2, 3.125kHz ~ 1.562kHz at detail 3, 1.562kHz ~ 781Hz at detail 4 and 781Hz ~ 390 Hz at detail 5 as well as one approximate signal in the frequency band 390Hz ~ DC level, are shown in Figure 7.5(b)-(g). From these figures, it can be clearly seen that there are very useful features in the decomposed magnetising inrush current signals. A certain high frequency component can be located better in time than a low

frequency component. In contrast, a low frequency component can be located better in the frequency domain than the high frequency component, and this effectively means that all of the features for a particular signal are obtained. In this study, we are interested in those components that are located better in time, so that, detail 1-3 is considered for the further feature analysis.

It should be mentioned that the technique presented is based on employing the high frequency phenomenon associated with transformer transients. It is therefore necessary to use the high sampling rate of 25 kHz. Furthermore, in practice this high sampling rate should not pose much difficulty in the hardware implementation of the technique in view of the fact that modern digital processors are well equipped to cater for very high sampling rates in excess of 200 kHz.

(a)

(b)

(c)

(d)

(e)

(f)

(g)
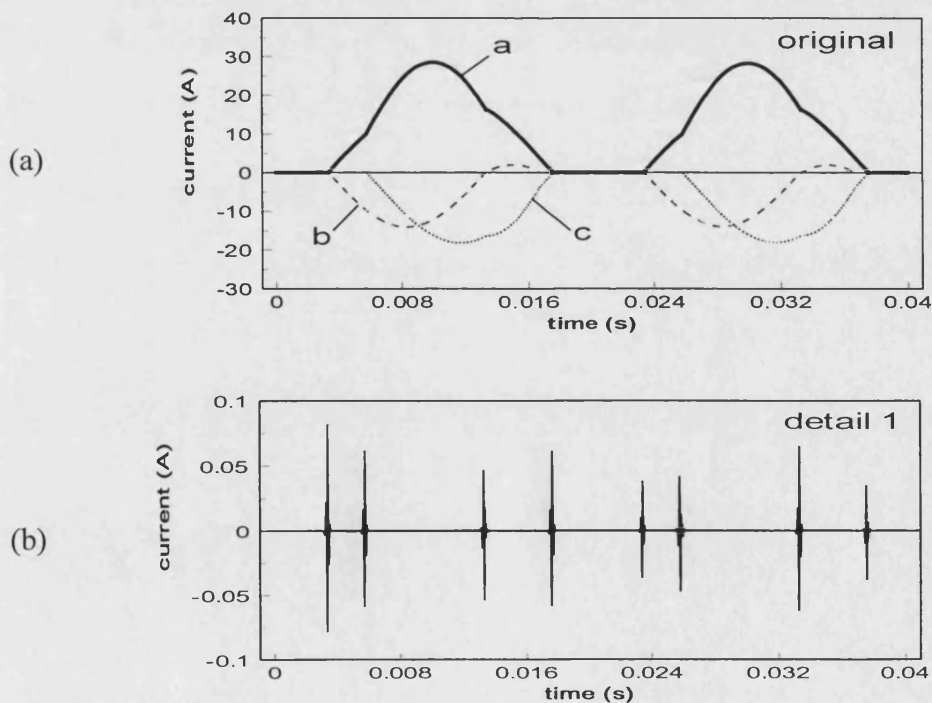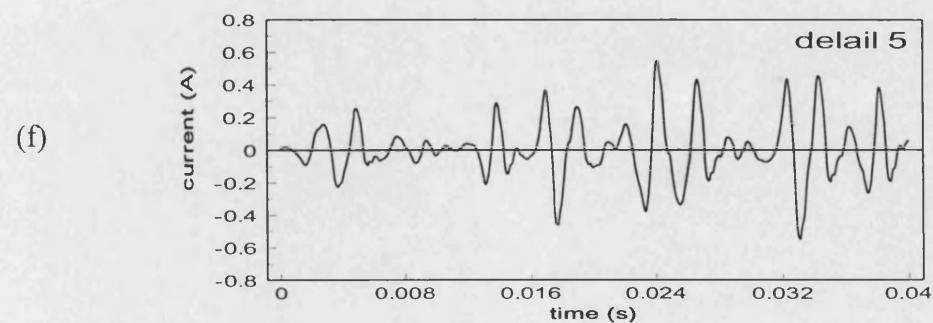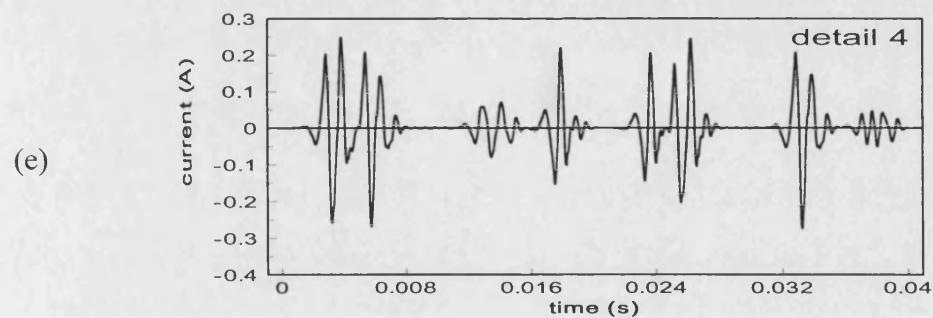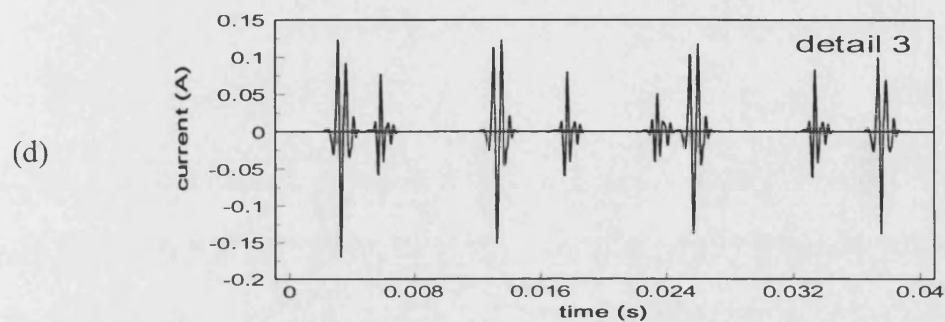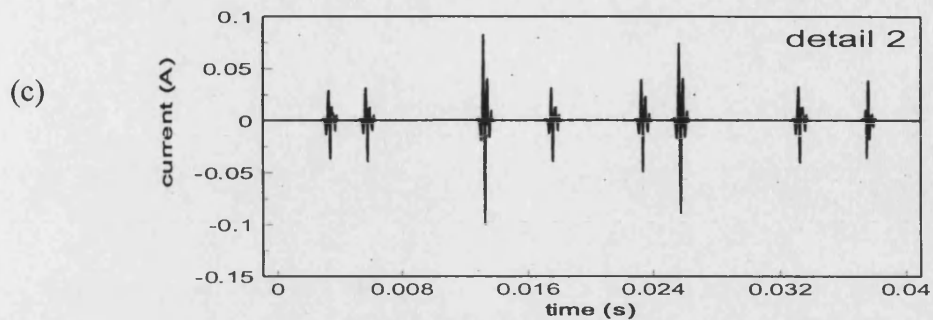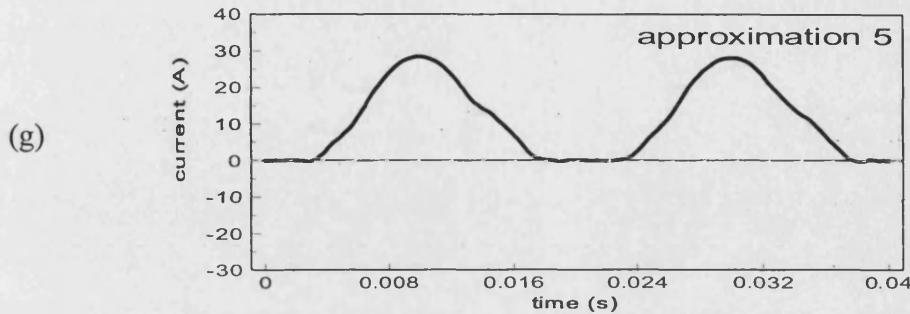
Figure 7.5 5-successive details and an approximation for an inrush current in System 1

From Figures 7.5(b)-(d), which correspond to details 1-3, it can be seen that there are a number of sharp spikes during the shown period of the inrush current transient. From the foregoing analysis, a number of these arise at edges of gaps at which the inrush current suddenly changes from one state to other different states; others are produced because the primary windings of the power transformer are connected as delta, so that the a-phase differential current is in fact the difference between the a-phase magnetising inrush current and c-phase magnetising inrush current. This gives rise to the non-smooth points in the current waveforms, which in turn cause sharp spikes to appear in the DWT of the current waveforms.

7.3.2 Wavelet Analysis of Internal Fault Currents

Figure 7.6(a) shows typical internal fault current waveforms, which correspond to a, b and c three-phase differential currents through the CT secondary sides, under an a-b two-phase earth fault on the high voltage side of the power transformer. It is apparent that there are high frequency distortions in the current waveforms. This is as a direct consequence of the effects of the distributed inductance and capacitance of the transmission line. This can lead to a significant second harmonic in the internal fault, thereby posing difficulty in an accurate discrimination between magnetising inrush and internal fault currents by the conventional protection method.

For brevity, only the DWT of the a-phase differential current is presented here as shown in Figures 7.6(b)-(g). From Figures 7.6(b)-(d), which correspond to the details 1-3 of the DWT, we can see that there are several sharp spikes appearing from the inception time of the internal fault. However, in marked contrast to the inrush current case, these sharp spikes rapidly decay to near zero within one cycle, whereas those sharp spikes under inrush current case suffer from little attenuation during the entire inrush transient period, which can last from about 10 cycles for small transformers to 1 min for large units. It is apparent that this difference can be effectively used as one of the key features to distinguish the internal fault from the inrush current.

(d)

(e)

(f)

(g)
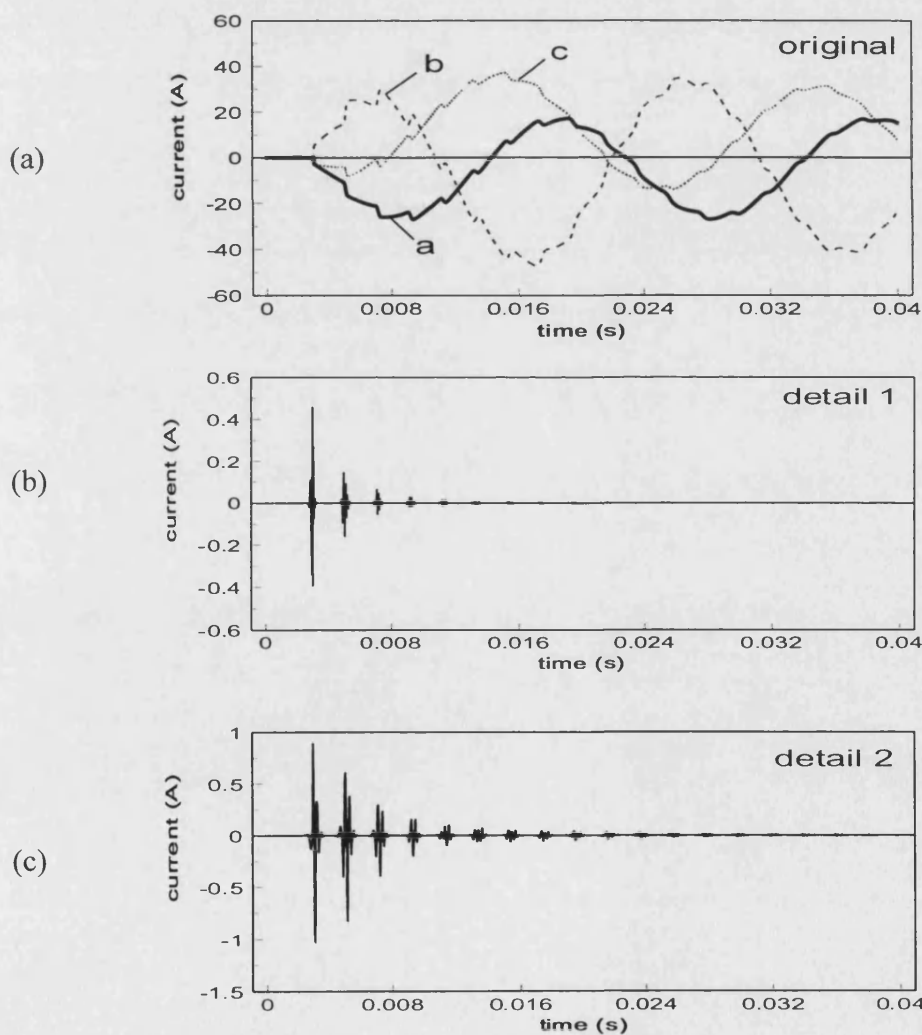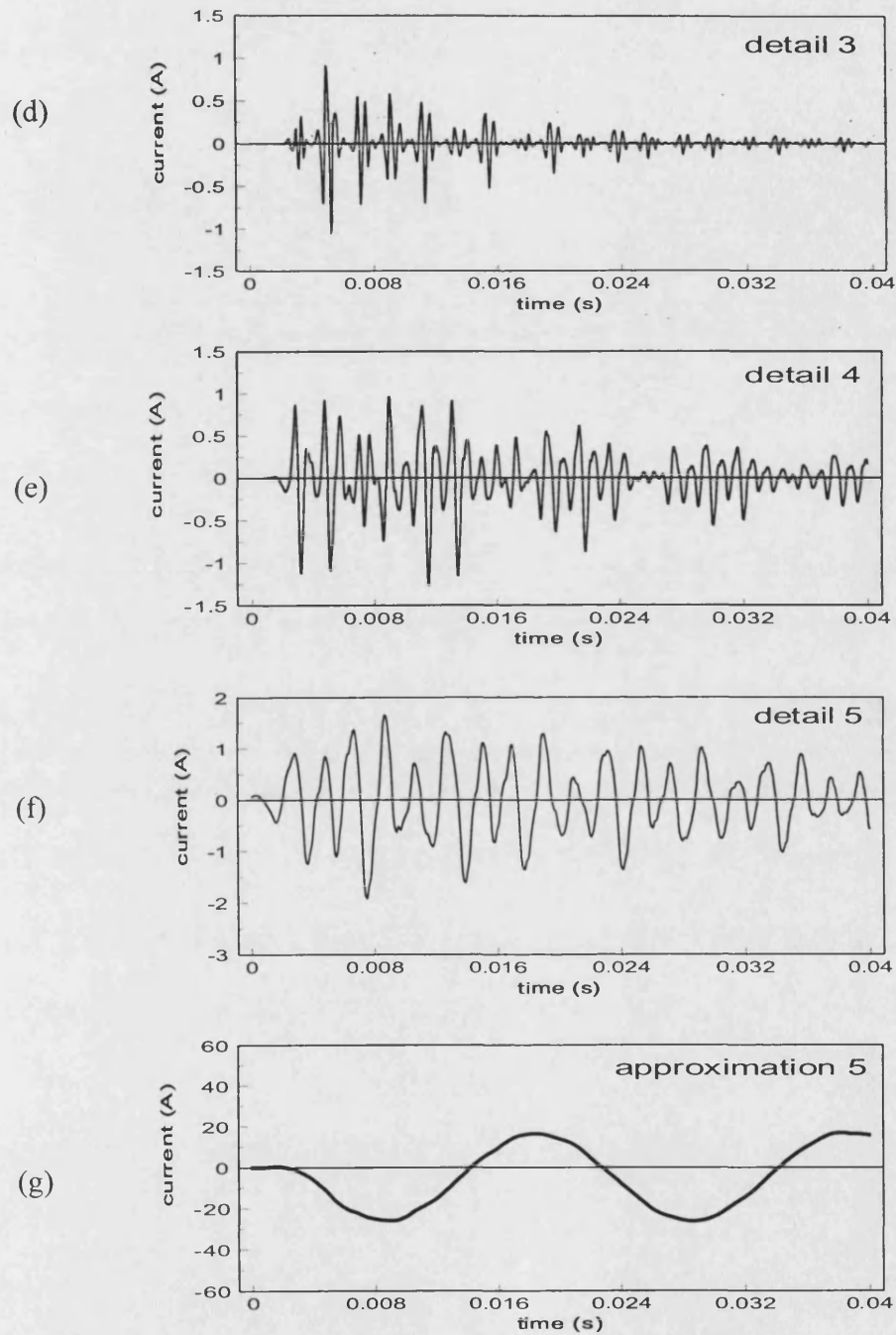
Figure 7.6 5-successive details and an approximation for an ab-phase to earth fault on HV side in System 1

7.3.3 Wavelet Analysis of External Fault Currents with CT Saturation

A power transformer differential current protection is designed to restraint under normal load flows and for external faults. However, external short circuits can in fact result in very large differential currents, if the CTs saturate. It is thus crucial to be able to ascertain CT saturation effects on the measured currents under external faults. The severity of CT saturation is accentuated by the presence of remnant flux in the CT core. Figure 7.7 (a) shows the simulated differential currents through the CT secondary sides under the conditions that an external three-phase short circuit occurs on HV side, and there is an initial remnant flux (65% rated flux) in the a-phase CT core on LV side, and a zero remnant flux in a-phase CT core on HV side. From Figure 7.7(a), it can be seen that, as expected, there is a significant imbalance current appearing in a-phase differential current.

(c)

detail 2

(d)

detail 3

(e)

detail 4

(f)

detail 5

(g)
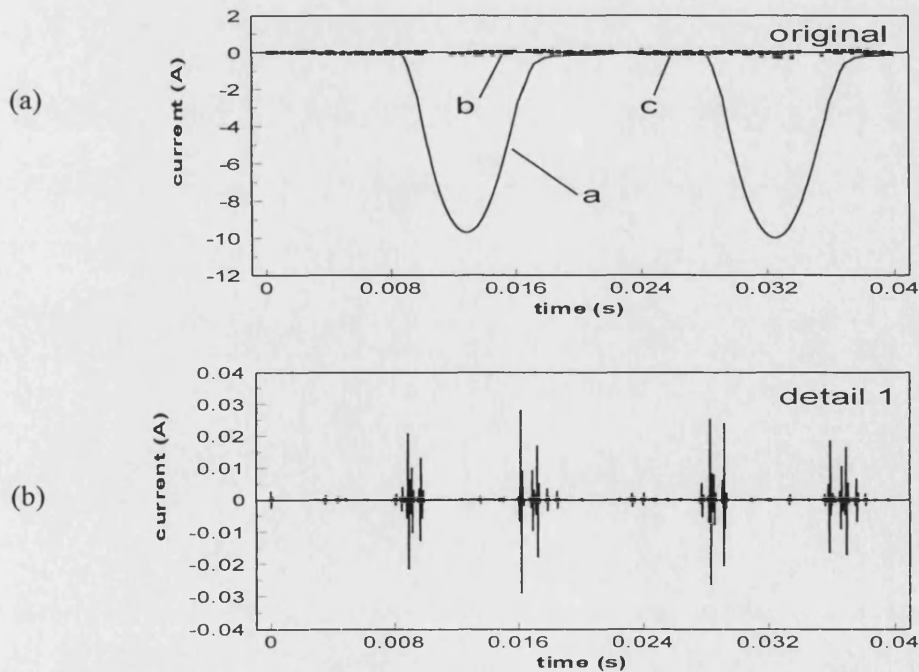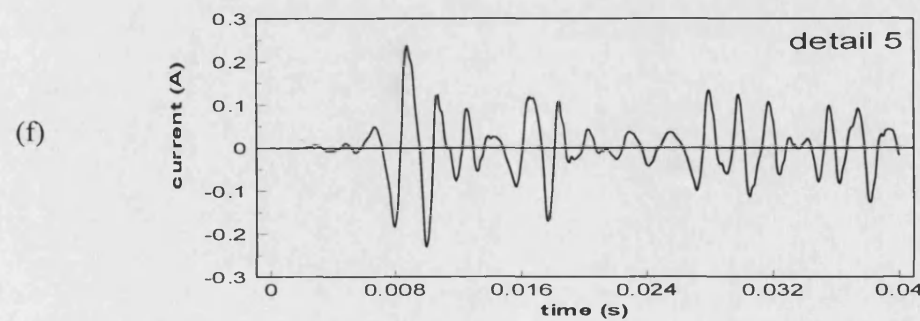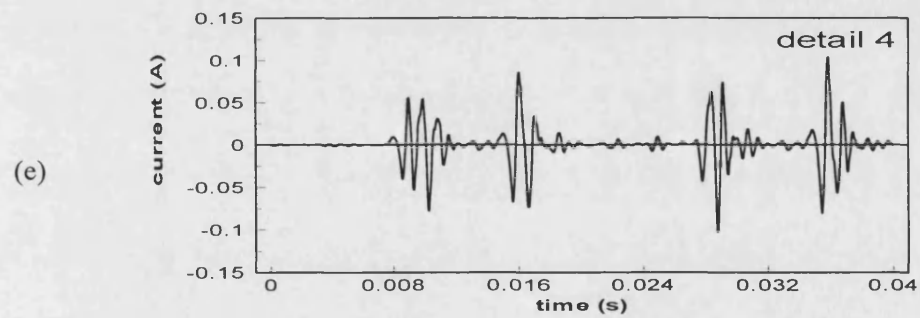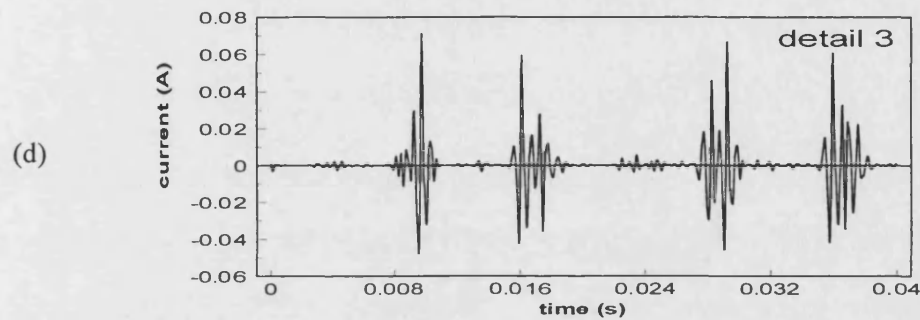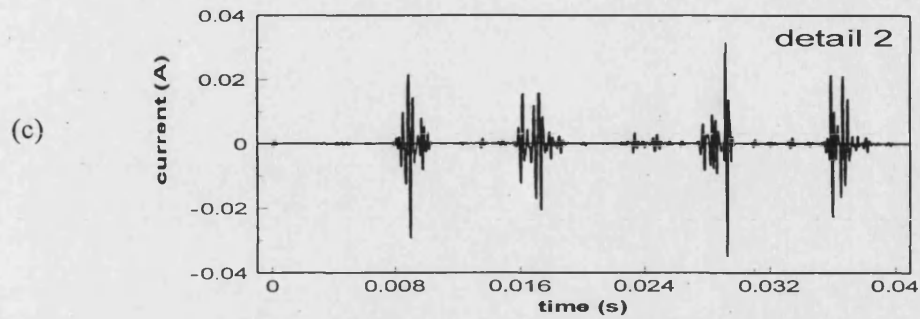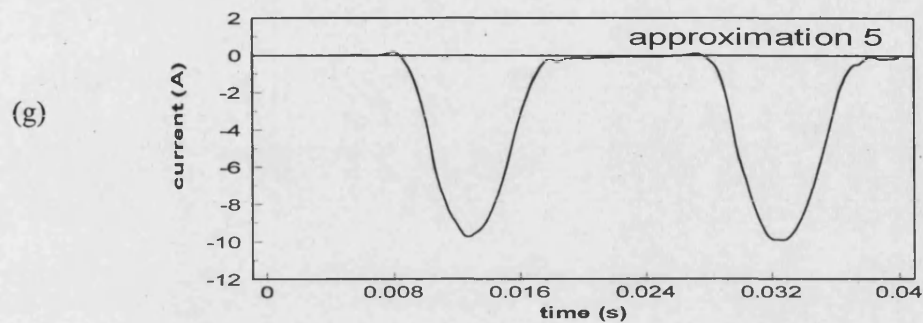
Figure 7.7 5-successive details and an approximation for an external fault under CT saturation condition in System 1

Figures 7.7 (b)-(d) present the DWT results of a-phase differential current given in Figure 7.7 (a). From Figures 7.7(b)-(d), which correspond to the details 1-3 of the DWT, it can be seen that there are several sharp spikes that last during the entire period of the saturation transient, which depends on the D.C component and the remnant flux of CT core. However, unlike the case for the internal fault, these spikes suffer from little attenuation during the saturation transient. Here again, It is the apparent unique features that can be used to distinguish between an internal fault and an external fault under CT saturation.

7.4 Wavelet Analysis of Transient Phenomena in System 2

Similar to the DWT analysis carried out on System 1, the transient phenomena of the magnetising inrush currents and internal fault currents are also studied through DWT analysis as applied to System 2. Some typical results are presented in the following section.

7.4.1 Wavelet Transform of Inrush Currents

Figure 7.8 (a) shows typical magnetising inrush current waveforms for System 2, which correspond to a, b and c three-phase differential currents through the CT secondary sides. Figures 7.8 (b)-(g) present the DWT results of a-phase differential current given in Figure 7.8 (a). From Figures 7.8 (b)-(g), which correspond to the details 1-5 and approximation 5 of the DWT for a-phase differential current, it can be clearly seen that wavelet signals in System 2 have analogous features compared with the wavelet signals presented in Figures 7.5 (b)-(g) in System 1, and they were analysed and described in some detail in section 7.3.1.

(d)

(e)

(f)

(g)
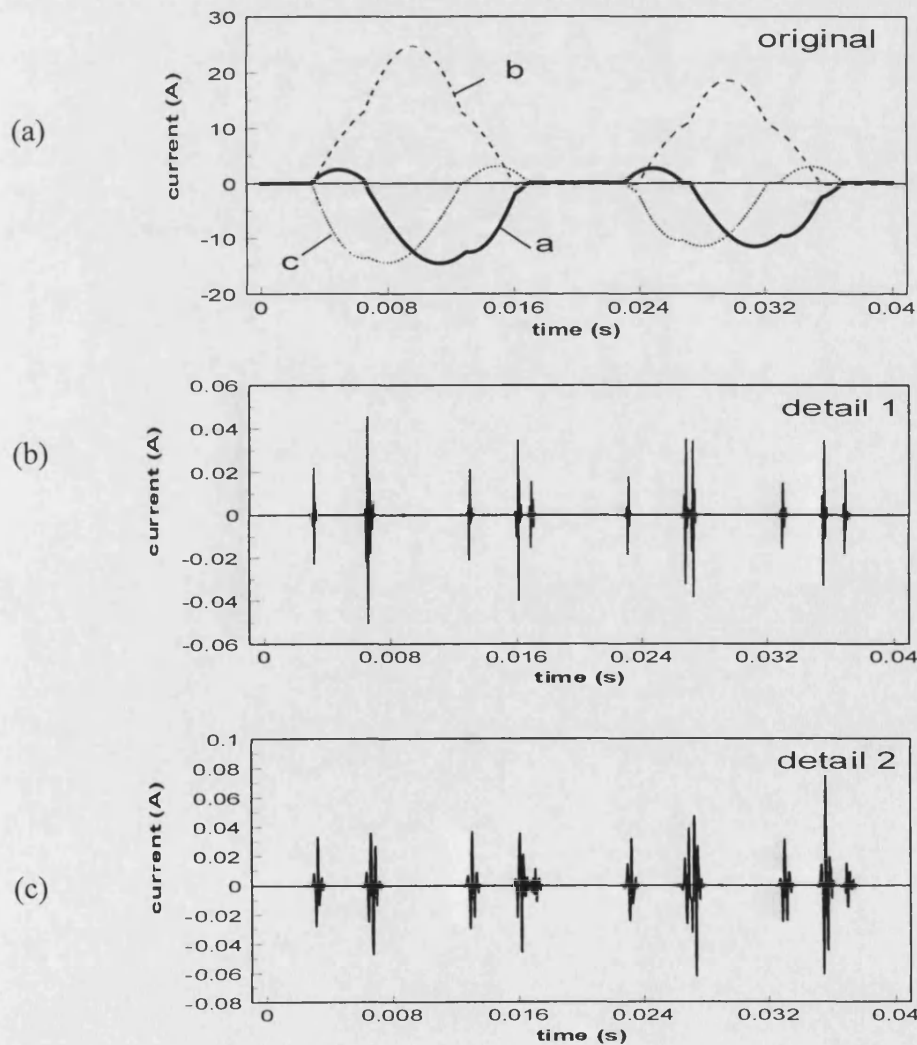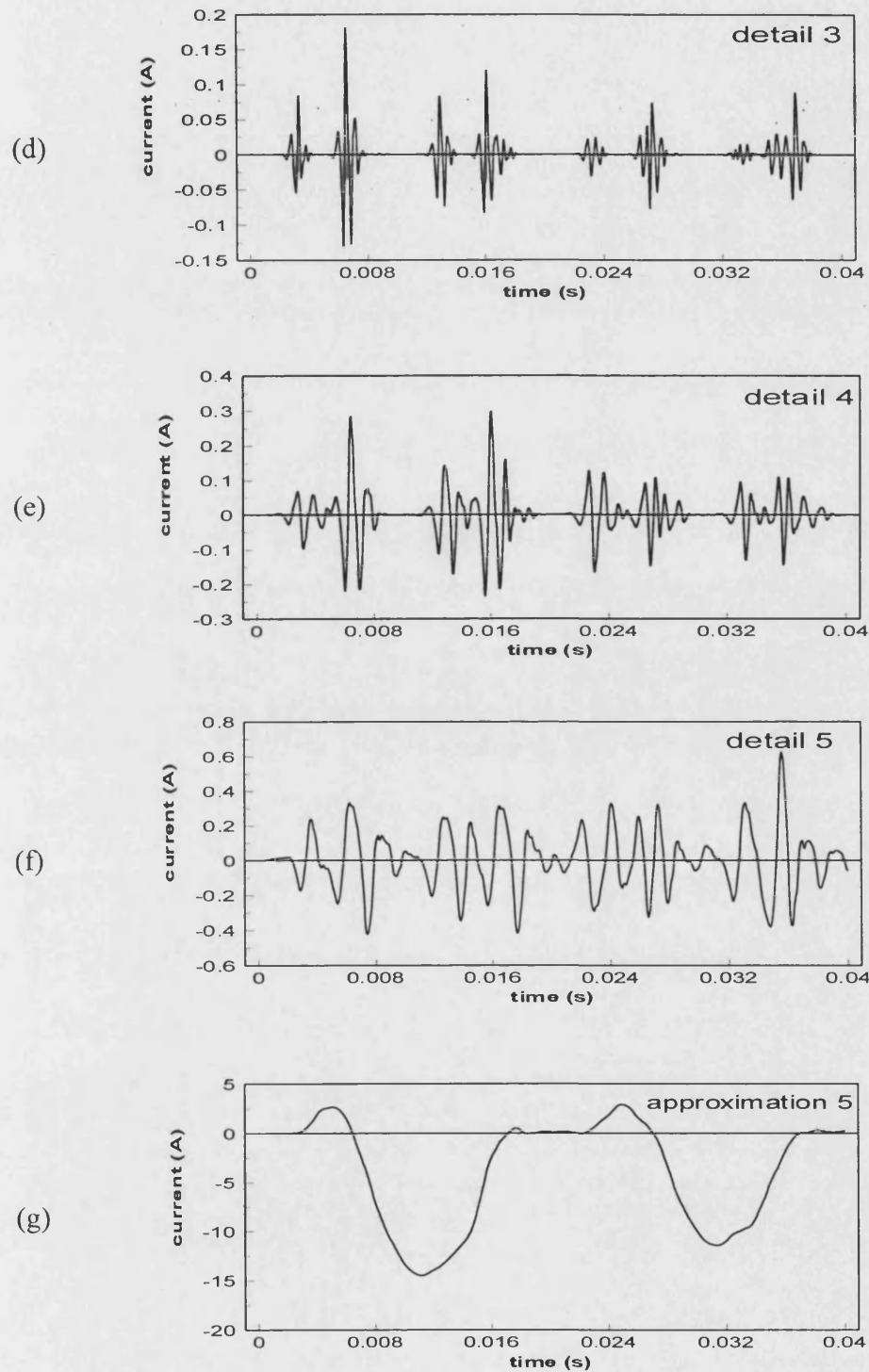
Figure 7.8 5-successive details and an approximation for an inrush current in System 2

7.4.2 Wavelet Transform of Internal Fault Currents

Figure 7.9 (a) shows typical internal fault current waveforms, which correspond to a, b and c three-phase differential currents through the CT secondary sides, under a-b two-phase short-circuit on the high voltage side of the power transformer in System 2; while Figures 7.9 (b)-(g) present the corresponding DWT for a-phase differential current. Here again, there are similar features in DWT results presented in Figures 7.9 (b)-(g), in comparison with those analysed in System 1 presented in section 7.3.2.

(d)

(e)

(f)

(g)
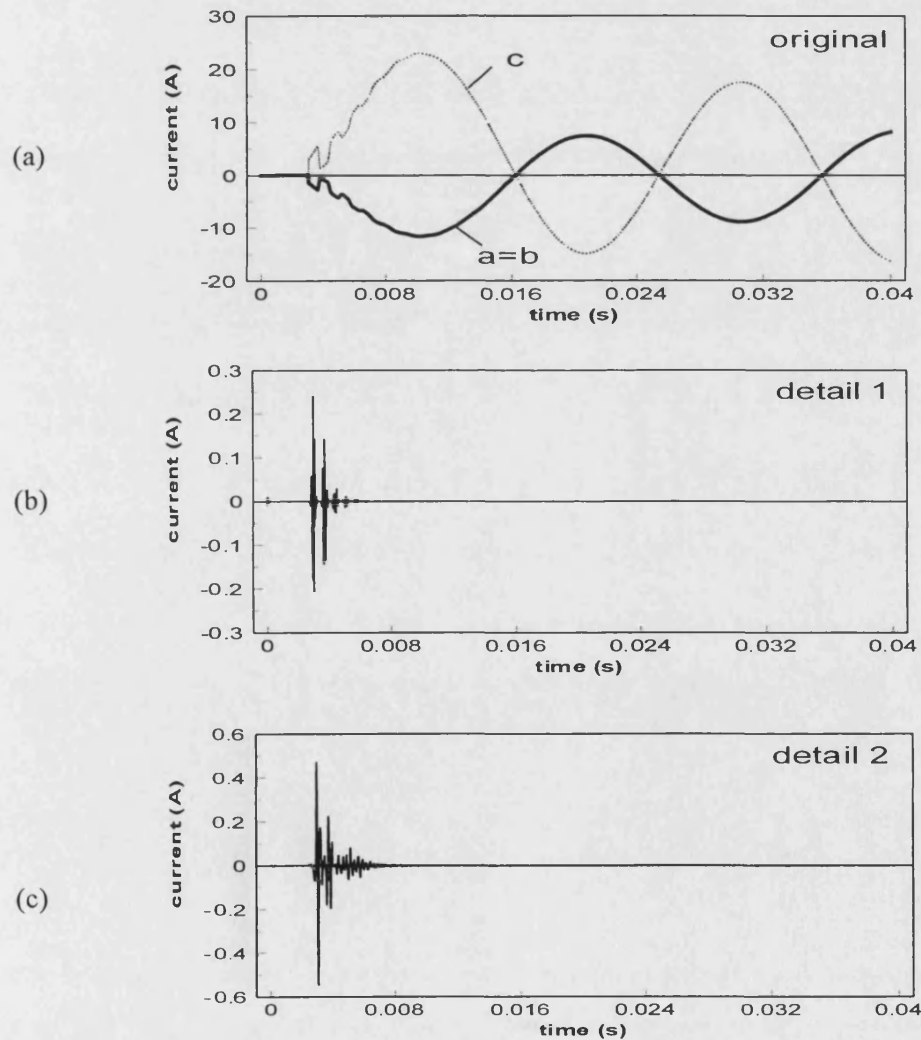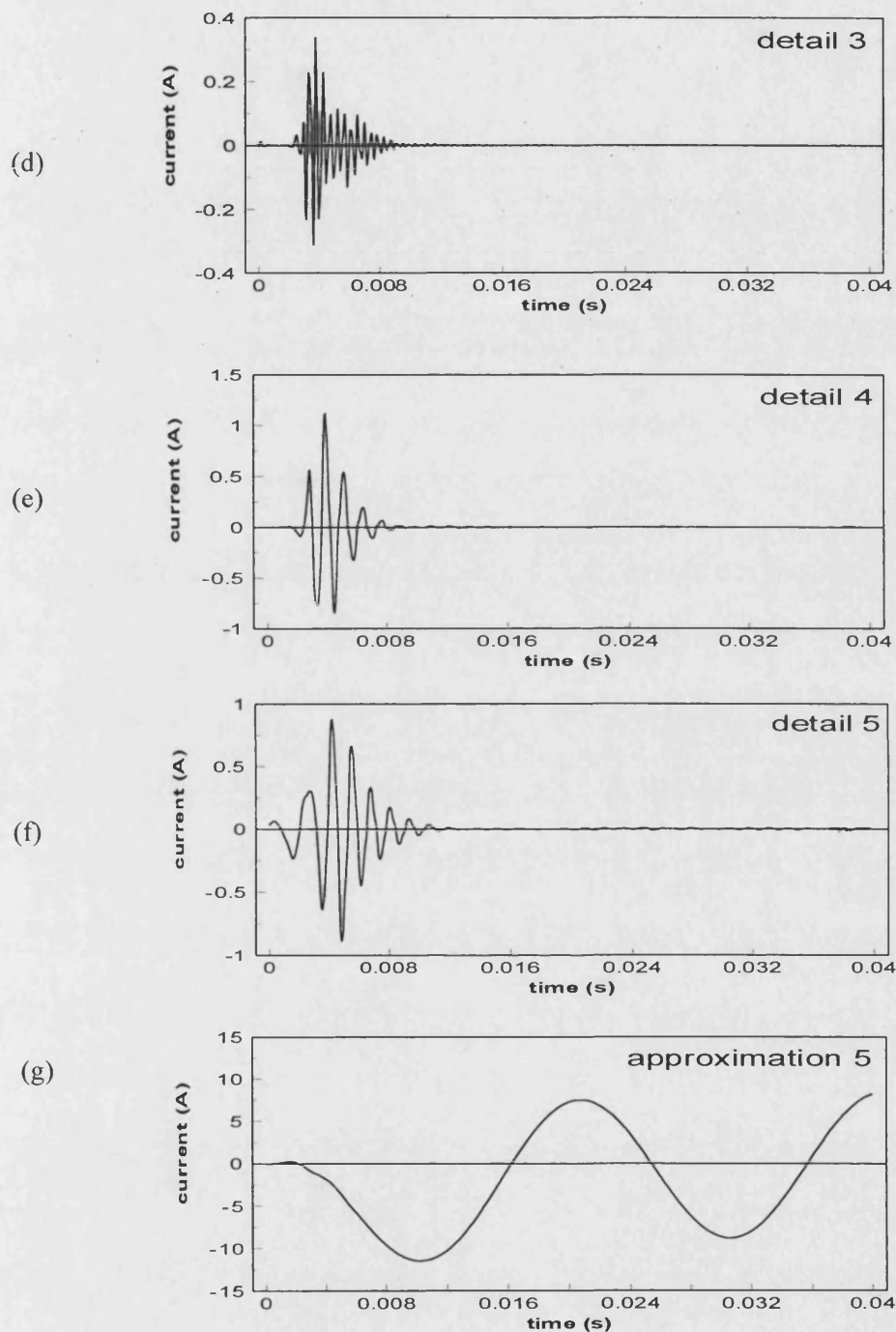
Figure 7.9 5-successive details and an approximation for an ab-phase short circuit on HV side in System 2

7.5 Summary

An effective feature extraction methodology for power transformer fault diagnosis is crucial. In this chapter, a new method to analyse power transformer transient phenomena is proposed by using WT technique. This method offers important advantages over other methods such as the conventional FT due to good time and frequency localisation characteristics. Analysis results presented clearly show that particular wavelet components can be used as the features to distinguish internal faults from inrush currents/external faults. This attribute is now used in the design of novel protection techniques for the power transformer fault diagnosis, as outlined in the next chapter.

Chapter 8

Power Transformer Fault Diagnosis by Direct Decision Making Approach Based on Wavelet Transform

8.1 Introduction

In Chapter 7, a new method to analyse power transformer transient phenomena using the WT is proposed. It has shown that the signal features extracted and represented by WT have a more distinct property than that extracted by FT due to the good time and frequency localisation characteristics of the WT. Based on the developed feature extraction method, this chapter describes a WT-based power transformer fault diagnosis approach, especially for distinguishing internal faults from inrush currents. The approach is based on the analysis of signals described previously in Chapter 7; the selected wavelet components are employed as specific and significant features to effect a fault classification technique.

In the developed approach, the WT technique is firstly applied to decompose the differential current signals into a series of wavelet components; then by processing selected wavelet components, a decision for distinguishing an internal fault from an inrush current is directly made through pre-defined decision making logic criteria.

8.2 WT-Based Direct Decision Making Approach

The WT-based direct decision making approach for power transformer fault diagnosis is shown in Figure 8.1. The technique comprises of an anti-aliasing filter, analogue-digital converter, feature extraction, feature selection, quantification of feature and logic criteria units.
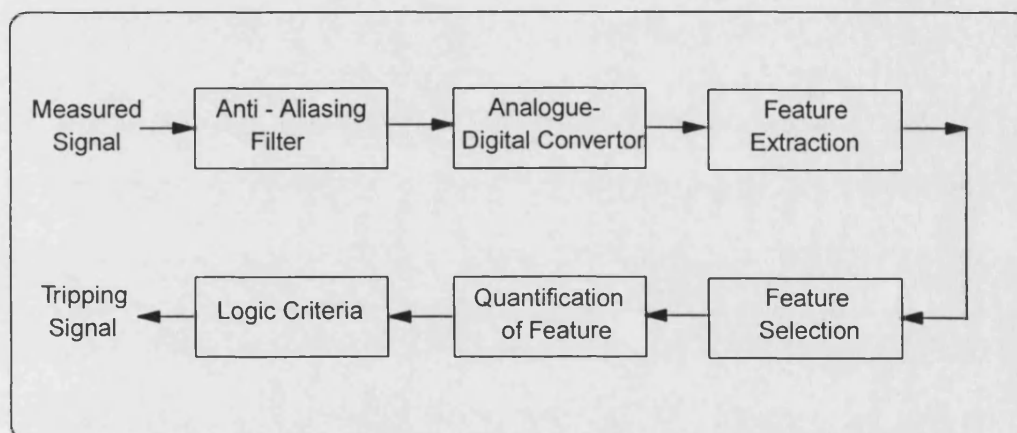
Figure 8.1 WT-based direct decision making approach

8.2.1 Anti-Aliasing Filter and Analogue-Digital Converter

In Figure 8.1, the measured signals from CTs (i.e., three-phase differential current signals) are passed through an anti-aliasing filter, which is a 2nd-order Butterworth filter with a cutoff frequency of approximately half the digital sampling frequency of 25kHz (the same as that used in the DWT implementation described in section 7.3.1), and is used to avoid any errors arising caused by signal aliasing. The signals then are fed into a 12-bit analogue-digital converter [66,67].

8.2.2 Feature Extraction and Feature Selection

The feature extraction is implemented by DWT, the mathematical concepts of which were presented in Chapter 7. The role of feature selection is to retain information that is important for class discrimination and discard that which is irrelevant thereby leading to a classifier with better generalisation properties. As analysed in Chapter 7, wavelet details 1-3 of the differential currents have more distinct features as they are located better in time; thus, any one of these wavelet details 1-3 can be employed as the selected features. In this work, wavelet detail 1 signals of three-phase differential currents are taken as the selected signal features to effect the power transformer fault diagnosis technique, which will be described in the following section.

8.2.3 Quantification of Feature

The decision for discriminating between internal faults and inrush currents is made based on the quantification of the feature, which is presented by a ratio obtained from the selected wavelet components, and is given by the following equations:

$$I_{a-ratio} = \frac{I^k_{a-detail\,1,max}}{I_{a-detail\,1,max}} \qquad (8.1)$$

$$I_{b-ratio} = \frac{I^k_{b-detail\,1,max}}{I_{b-detail\,1,max}} \qquad (8.2)$$

$$I_{c-ratio} = \frac{I^k_{c-detail\,1,max}}{I_{c-detail\,1,max}} \qquad (8.3)$$

where

$I_{a-detail\,1,max}$, $I_{b-detail\,1,max}$, $I_{c-detail\,1,max}$, respectively, represent the maximum peak values of a-phase, b-phase, c-phase wavelet at detail 1 in the first window;

$I^k_{a-detail\,1,max}$, $I^k_{b-detail\,1,max}$, $I^k_{c-detail\,1,max}$, respectively, represent the maximum peak values of a-phase, b-phase, c-phase wavelet at detail 1 in the kth subsequent moving windows after the first window.

Note that $I_{a-ratio}$, $I_{b-ratio}$ and $I_{c-ratio}$, respectively, represent the ratios of the maximum peak value in the kth subsequent moving window (after the first window) with respect to the maximum peak value in the first window. The window length in this work is ½ cycle (10 ms at 50Hz), and the moving window is then moved by ¼ cycle, i.e., the data in the previous ¼ cycles is discarded.

8.2.4 Logic Criteria

Having quantification of the selected feature, the decision for discriminating between internal faults and inrush currents can be made through the pre-defined logic criteria. The logic criteria are defined as follows:

IF *($I_{a-ratio}$ >ε or $I_{b-ratio}$ >ε or $I_{c-ratio}$ >ε)* THEN

it is an inrush current or external fault

OTHERWISE

it is an internal fault.

END

where, ε represents the predefined threshold, and it is determined in terms of the ratio values of the quantified features between internal faults and inrush currents or external faults. After careful testing and examining to all cases studied, in this work, *ε=0.4.*

8.3 Relay Structure

A simplified flow chart of the relay structure for the proposed approach is shown in Figure 8.2, where block (1) signifies that the relay is activated if any one of three-phase differential currents is above a pickup setting level (typical value is ¼ ampere) in terms of the percentage differential characteristic that was previously described in section 2.2.1 of Chapter 2; block (2) implements the DWT to the windowed differential currents; block (3) carries out the calculation of equations (8.1)-(8.3); finally the decision is made by block (4) where the decision logic criteria in conjunction with the counting regime are employed to distinguish internal faults from inrush currents/external fault currents. If an internal fault is detected, the relay will issue a tripping signal; otherwise, the relay will be restrained and go on to the next moving window signal.
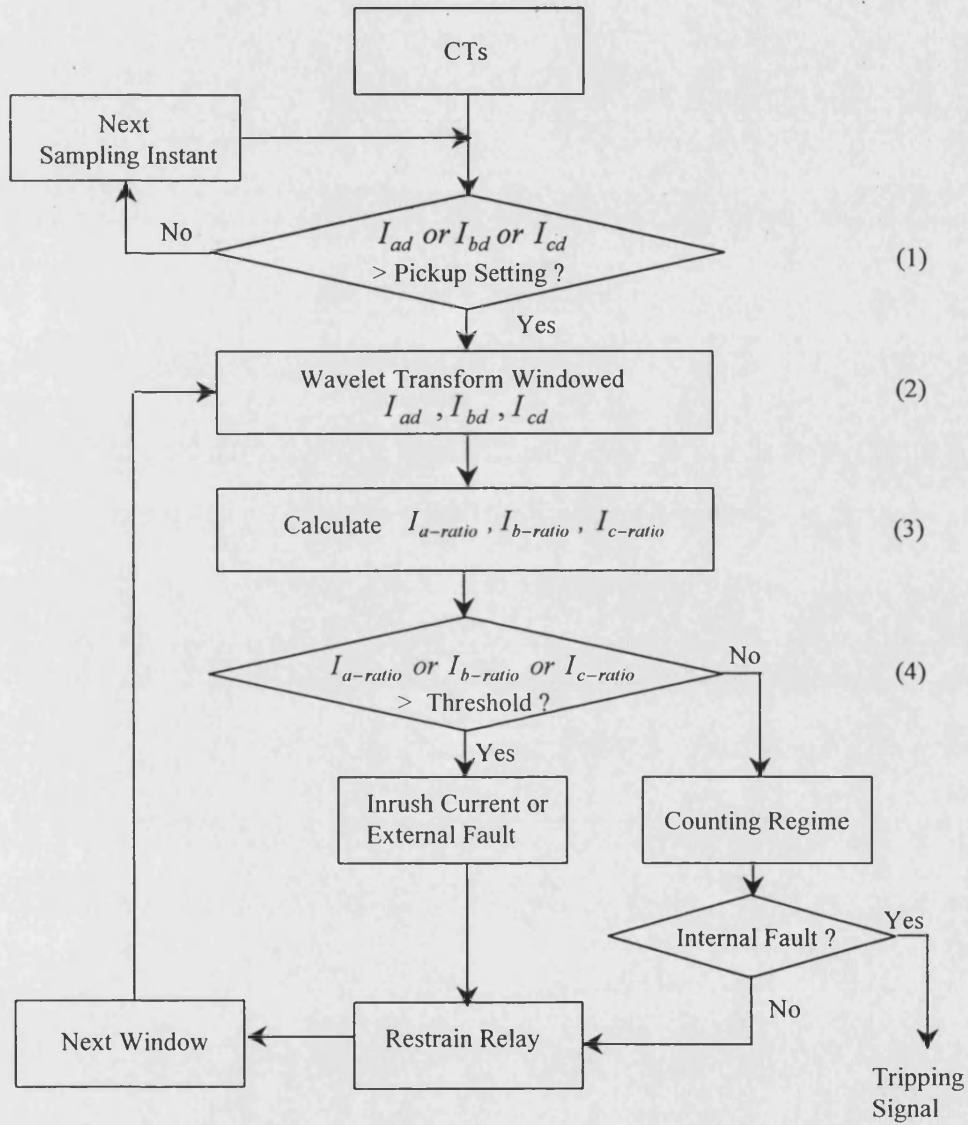
Figure 8.2 Flow chart of relay structure

8.4 Performance of Relay for System 1

In order to demonstrate the effectiveness of the developed approach, the cases studied under a whole variety of practically encountered system and fault conditions described in detail in Chapters 4 and 5, are considered. The distribution of the cases employed herein is the same as that shown in Table 6.1 presented in Chapter 6, in which 245 cases generated from System 1 are used for testing the performance of the relay for System 1.

The test results indicate that the developed approach is able to distinguish between internal faults and inrush currents with a very high classification rate. Importantly, the approach gives correct classification for all low-level internal faults, which posed certain difficulties for the ANN-based approach studied in Chapter 6. This is so by virtue of the good separation of classes provided by the feature extraction methodology, coupled with good selection of logic criteria.

In order to demonstrate the classification process of the relay, Figures 8.3-8.6 typify the response of the relay for the typical cases. Note that in each figure, (a) represents the three-phase differential currents through CT secondary side; (b)-(d) represent corresponding DWTs at detail 1; (e) represents the response of the relay.

Figures 8.3-8.4 present the classification process of the relay for: (i) an inrush current as shown in Figure 8.3; and (ii) an internal fault under ab-phase to earth on HV side as shown in Figure 8.4. From Figures 8.3 (e)-8.4(e), it can be seen that the relay gives the correct classification results by satisfying the criteria (as outlined in section 8.2.4), i.e., giving an output value of greater than 0.4 for the inrush current case, and an output value of less than 0.4 for the internal fault case.
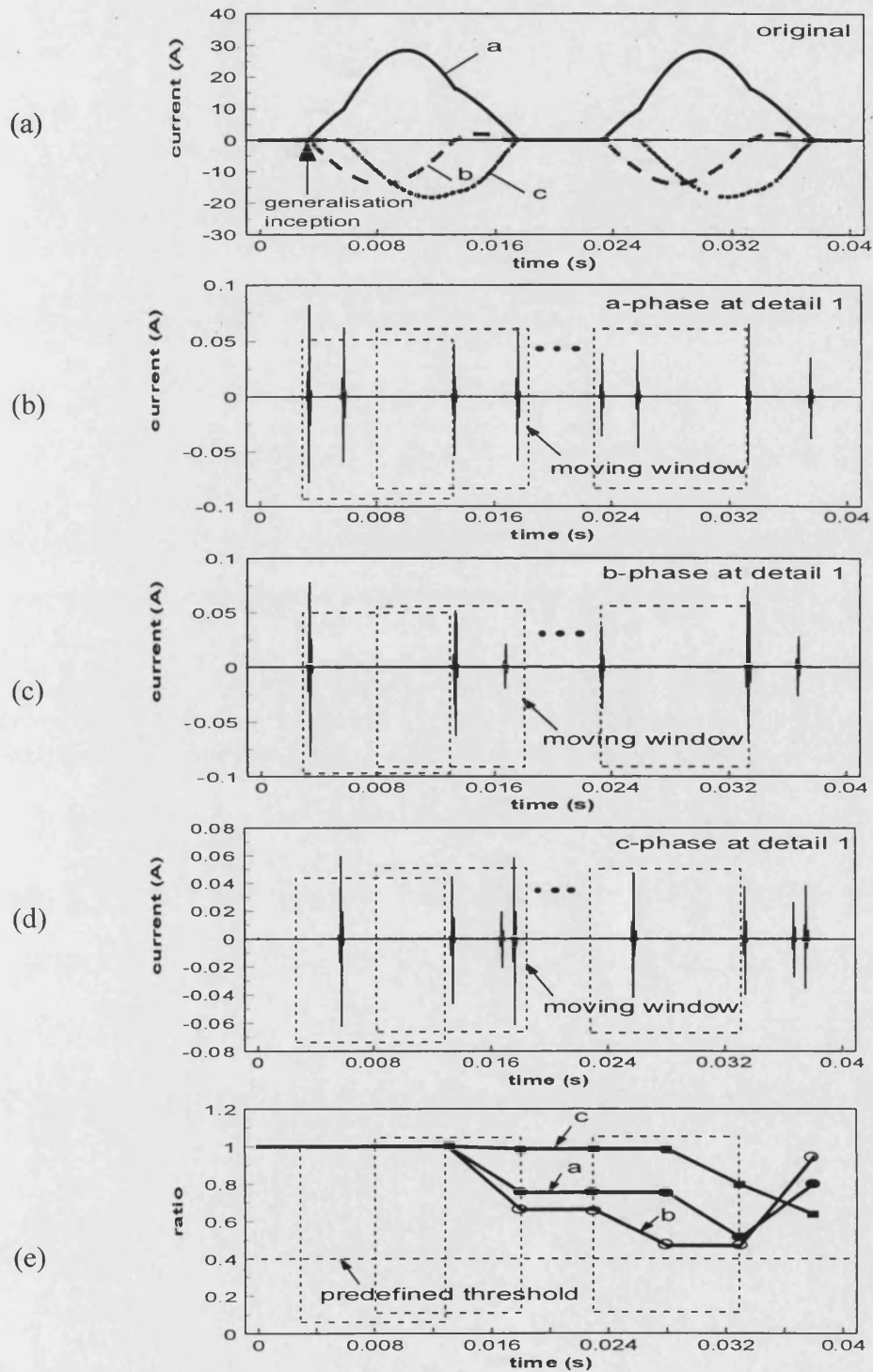
Figure 8.3 Classification process of relay for inrush currents in System 1
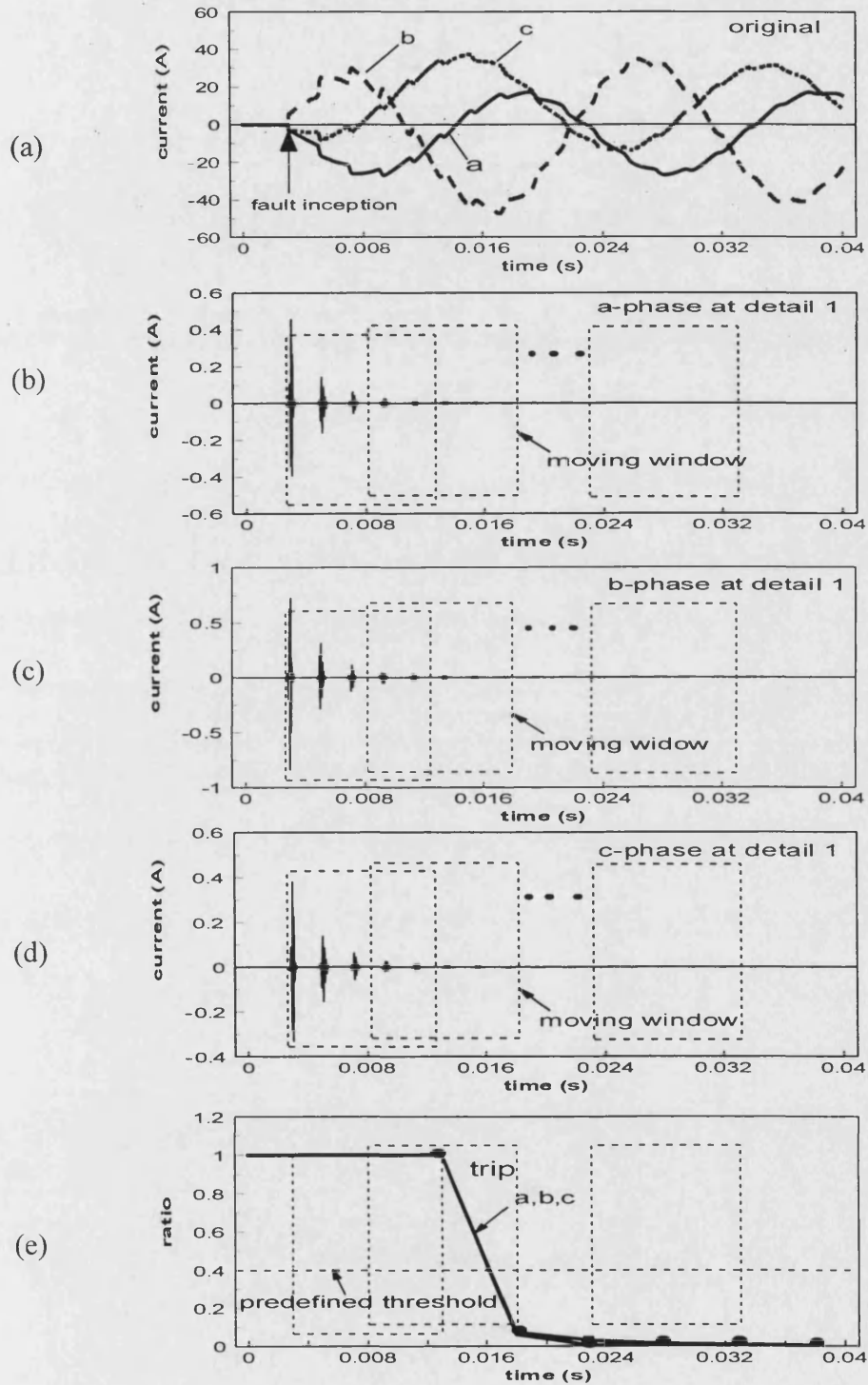
Figure 8.4 Classification process of relay for an ab-phase to earth fault on HV side in System 1

Figure 8.5 demonstrates the classification process of the relay for a low-level internal fault case, i.e., an a-phase 5% turn-to-turn fault at mid-point of winding on LV side, in which the traditional ANN-based approach gave an incorrect classification result. From Figure 8.5 (e), it can clearly see that the relay gives the correct classification result by giving an output value of less than 0.4 for such a low-level fault.

(e)
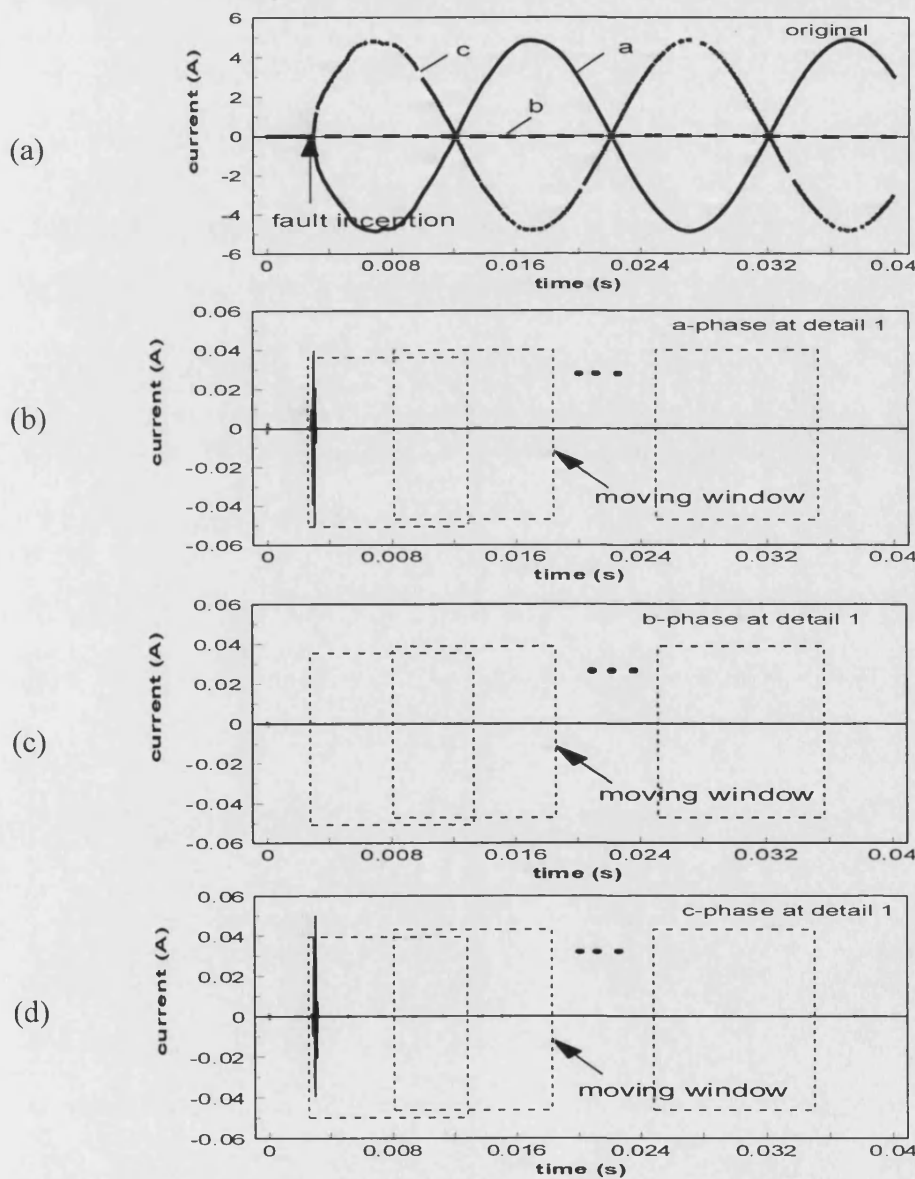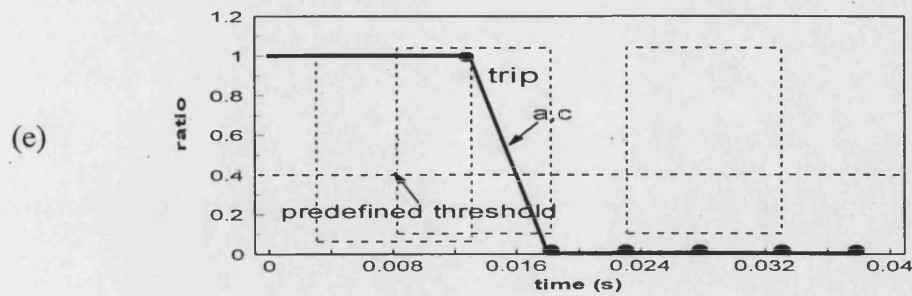
Figure 8.5 Classification process of relay for an a-phase 5% turn-to-turn fault at mid-point of winding on LV side in System 1

Case studies carried out on System 1 indicate that although the WT-based direct decision making approach has demonstrated a much improved performance compared with the traditional ANN-based approach studied in Chapter 6, however, there is still a special case, in which the relay gives an unstable response amongst the total 245 cases studied.

Figure 8.6 illustrates the classification process of the relay for such a case, which is an external three-phase short circuit on HV side together with a-phase CT saturation on LV side. Note that in this special case, there are no b-phase and c-phase DWTs presented here; this is so because only a-phase differential current is greater than the setting level due to a-phase CT saturation, and the decision is thus made only according to the selected *a*-phase wavelet feature.

(a)

(b)

(c)
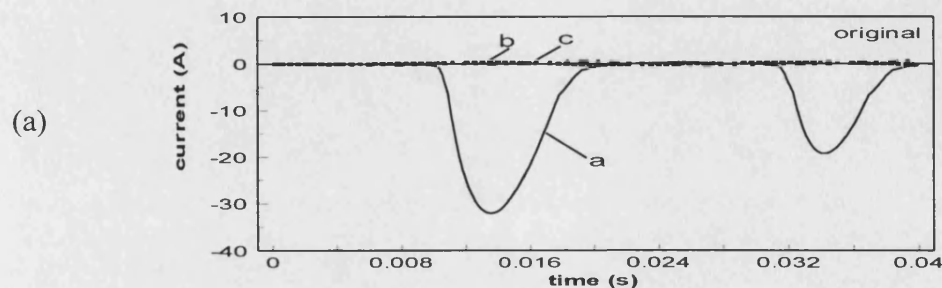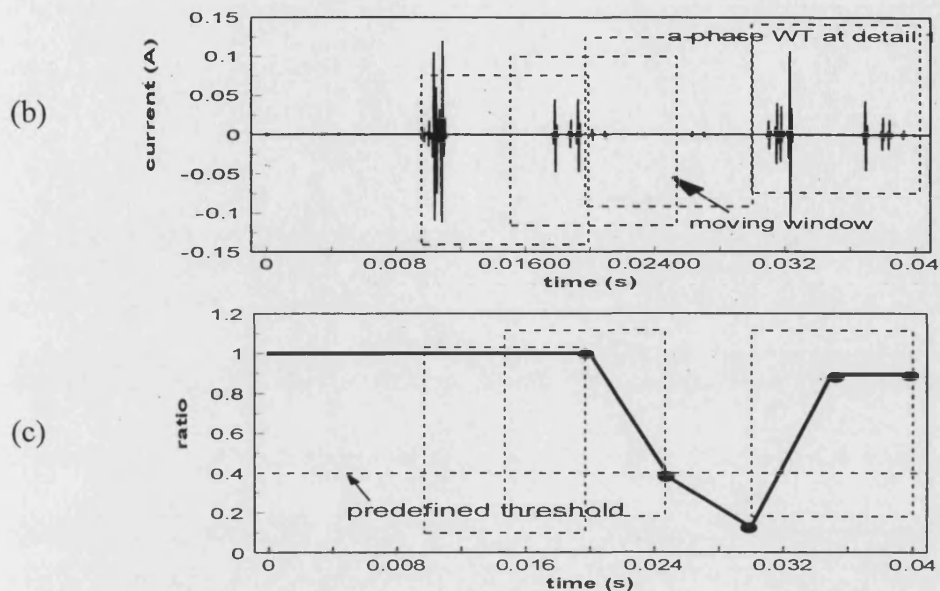
Figure 8.6 Classification process of relay for an external three-phase short circuit on HV side together with an a-phase CT saturation on LV side in System 1

From the above example, it can be seen that for such an external three-phase short circuit fault, the expected output value of the relay should be greater than 0.4, thereby inhibiting the relay from asserting a trip signal for the power transformer. However, as shown in Figure 8.6 (c), the behaviour of the relay is somewhat erratic, i.e., it has a convergence problem in that its output does not consistently stay above the requisite level of 0.4.

The reason for producing such an unstable response is that for this special case, *a*-phase CT saturation leads to an *a*-phase differential current, and thus the a-phase signal becomes the only information for classification. From Figure 8.6 (b), it can be seen that the gap (or the period of the near zero value) between the second and third peak values is much longer under such a case, and this results in the output value of the relay being less than 0.4; the relay thus sees this an internal fault during that time period. It should be mentioned that the counting regime as shown in Figure 8.2 would overcome this problem to a certain extent.

8.5 Performance of Relay for System 2

Similar with the case studies carried out on System 1, the technique developed was also tested on System 2 by using the same pre-defined decision logic criteria and threshold value setting as used for System 1. The objectives of this testing are to examine the robustness and generalisation of the approach, particularly its ability for the application to different power transformer systems. The cases employed for testing herein for System 2 are the same as that shown in Table 6.1 presented in Chapter 6, in which 120 test cases generated from System 2 were employed for assessing the performance of the approach.

For all 120 cases studied, the results clearly indicate that the approach is also very effective in distinguishing between internal faults and inrush currents with a very satisfactory classification result for System 2. This is by virtue of the fact that the feature extraction methodology adopted in the approach is representative of a feature space wide enough to cope with a different transformer system; it therefore overcomes the problem of the robustness, which posed difficulties for the traditional ANN-based approach studied in Chapter 6.

Figure 8.7 and Figure 8.8 demonstrate the classification process of the relay for two typical cases of: (i) an inrush current and (ii) an internal ab-phase short circuit on HV side. Figure 8.7 (a) and Figure 8.8 (a) show three-phase differential currents through CT secondary sides; Figures 8.7 (b), (c) and (d) as well as Figures 8.8 (b), (c), and (d) present corresponding DWTs at detail 1, respectively; Figure 8.7 (e) and Figure 8.8 (e) respectively present the response of the relay. From Figures 8.7 (e) and 8.8 (e) it can clearly see that the relay gives the correct classification results by giving an output value of greater than 0.4 for the inrush current case, and an output value of less than 0.4 for the internal fault case.
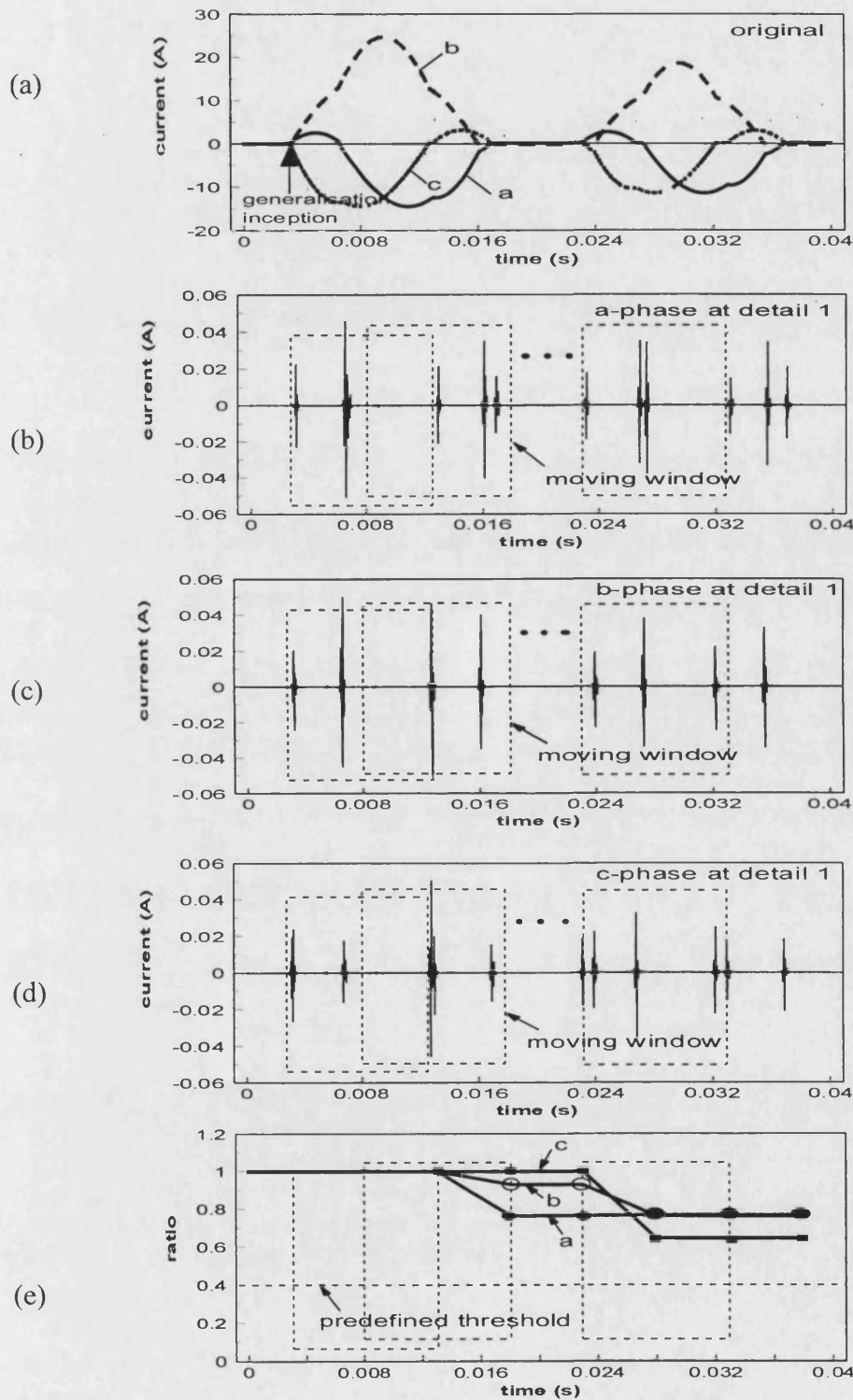
Figure 8.7 Classification process of relay for inrush currents in System 2
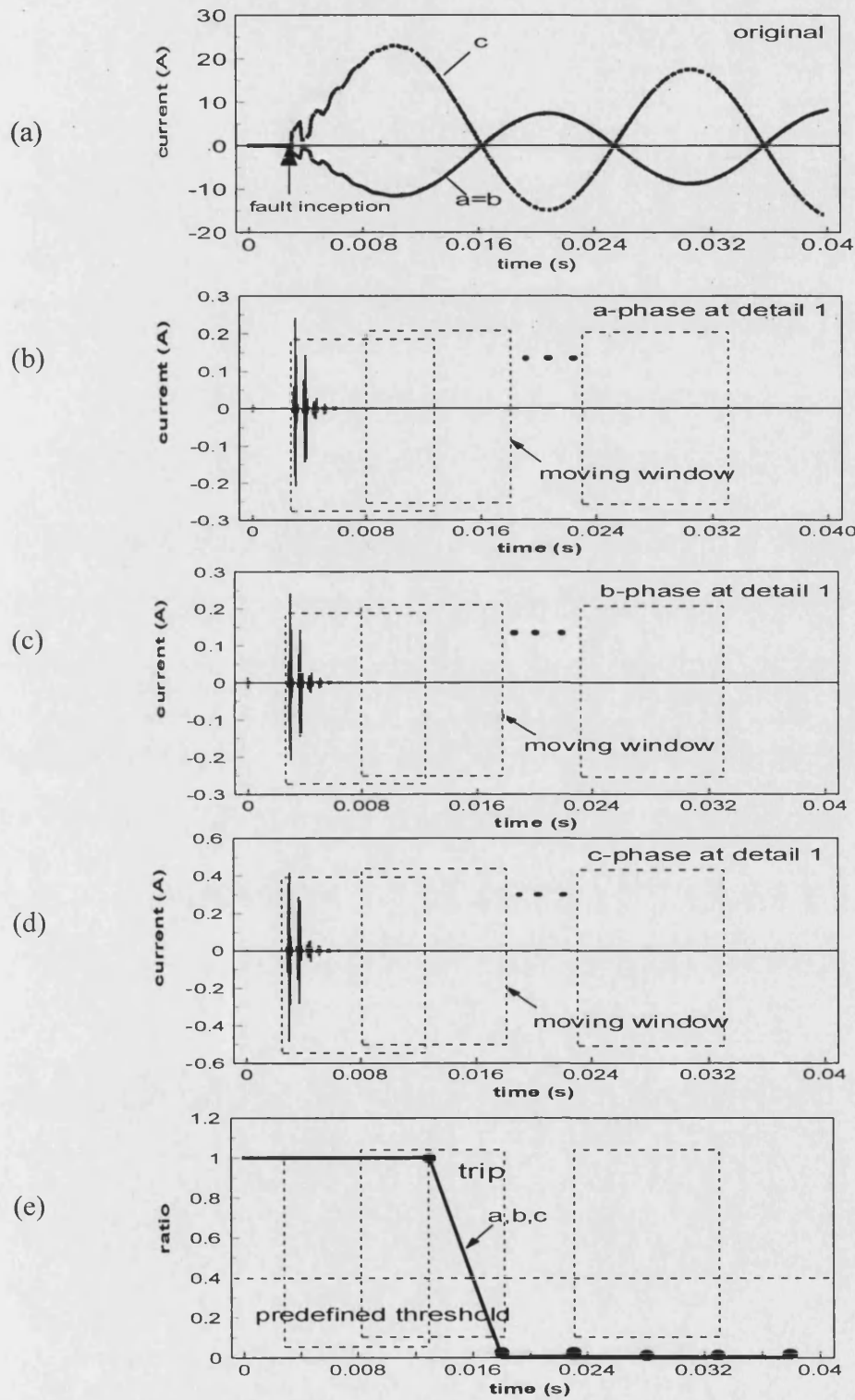
Figure 8.8 Classification process of relay for an ab-phase short circuit on HV

side in System 2

The ability of the approach in dealing with low-level internal fault cases was also examined. Here again, the relay gave the correct classification results for such type of faults.

8.6 Response Evaluation

The overall performance evaluation of the relay for various system and fault cases generated from Systems 1 and 2, has indicated that the misclassification rate of the relay is 1.4% within the tested 365 cases (i.e. correct classification rate $\geq$ 98.6%). This is a significant improvement over the traditional ANN-based approach. More importantly, the results clearly demonstrate the robustness and generalisation of the WT-based technique in its ability to deal satisfactorily with two different power transformer systems (Systems 1 and 2).

8.7 Summary

In this chapter, a WT based direct decision making approach for discrimination between internal faults and inrush currents for power transformer fault diagnosis is proposed. In the technique developed, the WT is firstly applied to decompose the differential current signals (attained through the CTs secondary side) into the wavelet components. Thus, more distinct signal features that respectively represent internal faults and inrush currents are extracted due to the good time and frequency localisation characteristics of the WT. As a consequence, by processing the extracted features, a decision for distinguishing an internal fault from an inrush current or external fault in different power transformer systems can be directly made using the pre-defined decision making logic criteria. The extensive simulation results presented show that the proposed technique can more accurately discriminate between an internal fault and an inrush current; in particular, the technique is able to give correct classification result for low-level fault cases and is robust to different

power transformer systems, as compared to the traditional ANN-based approach presented in Chapter 6.

Chapter 9

Power Transformer Fault Diagnosis
Based on Combined WT and ANN

9.1 Introduction

A traditional ANN-based approach studied in Chapter 6 shows that an ANN overcomes a number of problems/limitations experienced with conventional techniques when applied to power transformer fault diagnosis. However, an ANN trained for a particular power transformer system cannot be directly used in another power transformer system with different specifications, without actually retraining the ANN. In order to overcome the problem of robustness, a WT-based direct decision making approach for power transformer fault diagnosis was proposed in Chapter 8. The extensive simulation results presented show that the WT-based direct decision making approach can more accurately discriminate between an internal fault and an inrush current/external fault; in particular, the approach is robust to different power transformer systems in comparison to the traditional ANN-based approach. However, there were still some problems experienced such as those associated with CT saturation, etc. This chapter brings these two strands together and proposes a novel approach for the power transformer fault diagnosis using combined WT and ANN. The rationale behind this investigation was to ascertain whether some further improvements could be made in accuracy when diagnosing power transformer transient phenomena in comparison to the previous two approaches.

In the combined WT and ANN based approach, the WT is firstly applied to decompose the differential current signals of the power transformer into a series of wavelet components; the spectral energies of the selected wavelet components are then calculated and employed to train an ANN to implement the discrimination between internal faults and inrush currents/external faults.

9.2 The Combined WT and ANN Based Approach

Figure 9.1 shows the block diagram of the combined WT and ANN based approach for a power transformer fault diagnosis. It comprises of an anti-aliasing filter, analogue-digital converter, feature extraction, feature selection, spectral energy calculation and ANN-based decision making units. Herein, the feature extraction, feature selection, spectral energy calculation and ANN-based decision making units will be described in some detail except for the anti-aliasing filter and analogue-digital converter units as they are the same as those described in section 8.2.1 of Chapter 8.
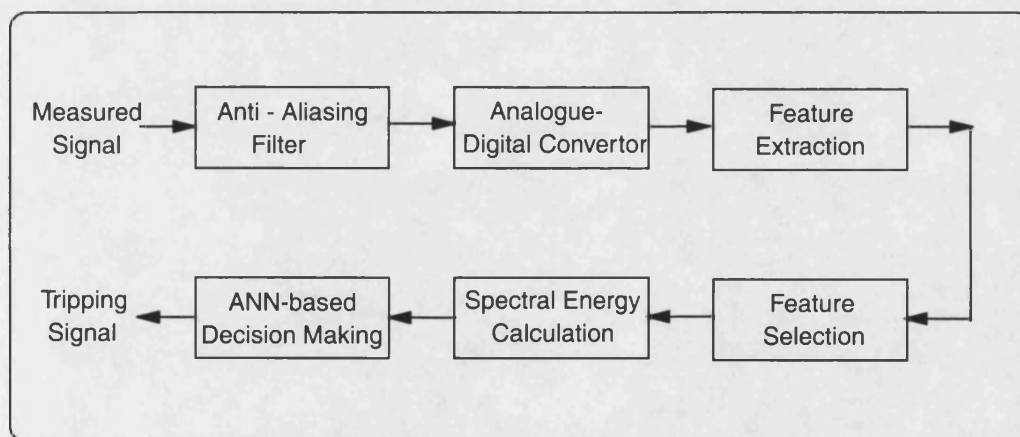
Figure 9.1 Combined WT and ANN based fault diagnosis approach

9.2.1 Feature Extraction and Feature Selection

In Figure 9.1, the feature extraction is implemented by DWT, which was described in Chapter 7. The feature selection is based on the wavelet components of the decomposed differential current signals. As analysed in Chapter 7, wavelet details 1-3 have more distinct features, as they are located better in time. In this work, the wavelet details 1-3 are taken simultaneously as the selected features to increase the accuracy and reliability of fault diagnosis.

9.2.2 Spectral Energy Calculation

The spectral energies of the selected wavelet signals are chosen herein as the ANN inputs (shown in Figure 9.1), rather than directly using the wavelet signals. This was because if the wavelet signals are directly used as the inputs to the ANN, it will result in rather a large number of inputs (i.e., increase the complexity of the ANN architecture) thereby posing difficulty in ANN convergence in terms of the speed and accuracy. The employment of spectral energy components overcomes this drawback; it not only reduces ANN size, but also retains important features of the wavelet signals.

The spectral energies of the wavelet details 1-3 are calculated by the following equations:

$$P_{a-detail,i} = \sum_{k=1}^{n} I_{a-detail,i}^2(k)\Delta t \quad ; \quad (i=1,2,3) \tag{9.1}$$

$$P_{b-detail,i} = \sum_{k=1}^{n} I_{b-detail,i}^2(k)\Delta t \quad ; \quad (i=1,2,3) \tag{9.2}$$

$$P_{c-detail,i} = \sum_{k=1}^{n} I_{c-detail,i}^2(k)\Delta t \quad ; \quad (i=1,2,3) \tag{9.3}$$

where $P_{a-detail,i}, P_{b-detail,i}, P_{c-detail,i}$ respectively represent the spectral energies of wavelet signals in a, b and c phases; $I_{a-detail,i}, I_{b-detail,i}, I_{c-detail,i}$ respectively represent the wavelet signals in a, b and c phases; the subscript *detail,i* represents the wavelet details 1 , 2 and 3 (i=1,2,3); Δt= time step length; n represents the sample number in a window.

9.2.3 ANN-Based Decision Making

With reference to Figure 9.1, the ANN-based decision making unit is used to issue a trip signal under an internal fault condition, and inhibit relay operation for an inrush current or external fault. The inputs fed into the ANN are based on the aforementioned features of spectral energies of the selected wavelet signals.

9.3 Relay Structure

A flow chart of the relay structure for combined WT and ANN based approach is shown in Figure 9.2. The relay is activated if any one of the three-phase differential currents (i.e., I_{ad} or I_{bd} or I_{cd}) exceeds a pickup setting level in terms of the percentage differential characteristic that was previously described in section 2.2.1 of Chapter 2. The DWT is then applied to the windowed differential currents I_{ad}, I_{bd}, I_{cd}. These in turn are used to evaluate the a, b and c three-phase wavelet signals, i.e., $I_{a-detail,1}$, $I_{a-detail,2}$, $I_{a-detail,3}$ at details 1-3 for a phase, $I_{b-detail,1}$, $I_{b-detail,2}$, I_{b-det3} at details 1-3 for b phase and $I_{c-detail,1}$, $I_{c-detail,2}$, $I_{c-detail,3}$ at details 1-3 for c phase. Then, the spectral energies of the wavelet details 1-3 are calculated according to equations (9.1), (9.2) and (9.3) respectively. The resultant spectral energies are then fed into the ANN. The decision for discrimination between an internal fault and an inrush current/external fault is then made in terms of the ANN output in conjunction with the counting regime. If the internal fault is detected, a trip signal will be issued; otherwise, the relay will be restrained.
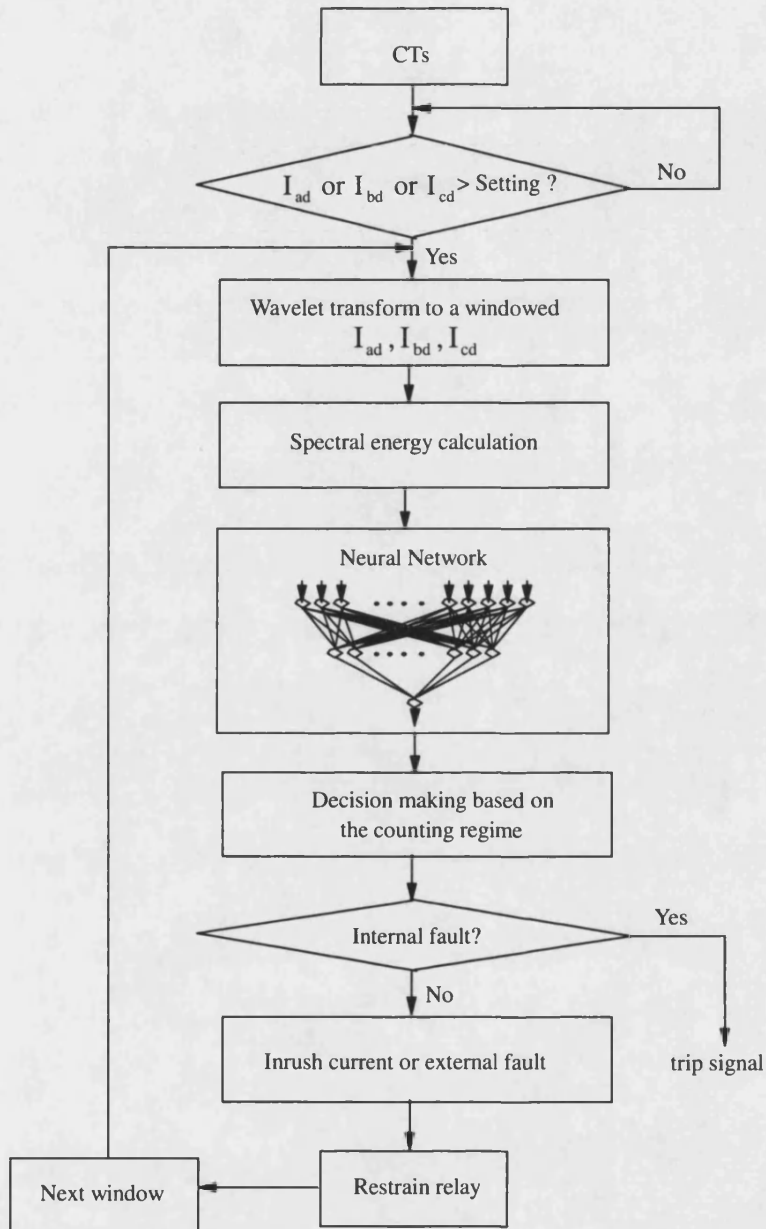
Figure 9.2 Flow chart of combined WT and ANN based approach

9.4 ANN Architecture and Training

The ANN-based decision making unit as shown in Figure 9.1 plays a significant role in the combined WT and ANN based approach for the accurate fault diagnosis of power transformers. The near optimal ANN topology is determined based on input vector, the number of hidden layers and the number of neurons in each layer, and the number of outputs.

9.4.1 ANN Input

As described in section 6.5.1 of Chapter 6, the method of inputting data into the ANN herein is again based on the moving data window concept. The window length is half a cycle (10ms at 50Hz frequency), and the moving window is then moved by ¼ cycle, i.e., the data in the previous ¼ cycles is discarded. Each data window is further divided into 3 equal time periods to calculate the spectral energy, therefore, 9 samples are obtained from details 1-3 for each phase. Thus, there are total 27 samples fed into the ANN for a, b and c three phase signals.

In order to illustrate the spectral energy based input features for the ANN, Figures 9.3 and 9.4 typify two sets of training data for System 1 for the cases of (i) an inrush current, and (ii) an ab-phase to earth fault on HV side. Comparing Figures 9.3 and 9.4, it is clearly evident that there are significant differences in the spectral energy components attained for the two cases. For example, the spectral energy for the inrush current as shown in Figure 9.3 suffers from little attenuation during the period of the inrush current transient. In marked contrast, the spectral energy under the internal fault as shown in Figure 9.4 rapidly decays to near zero following fault inception. It is apparent from the foregoing example that the usage of the spectral energy retains important features of the wavelet signals, and can be effectively used to develop a technique for distinguishing an internal fault from an inrush current/external fault.
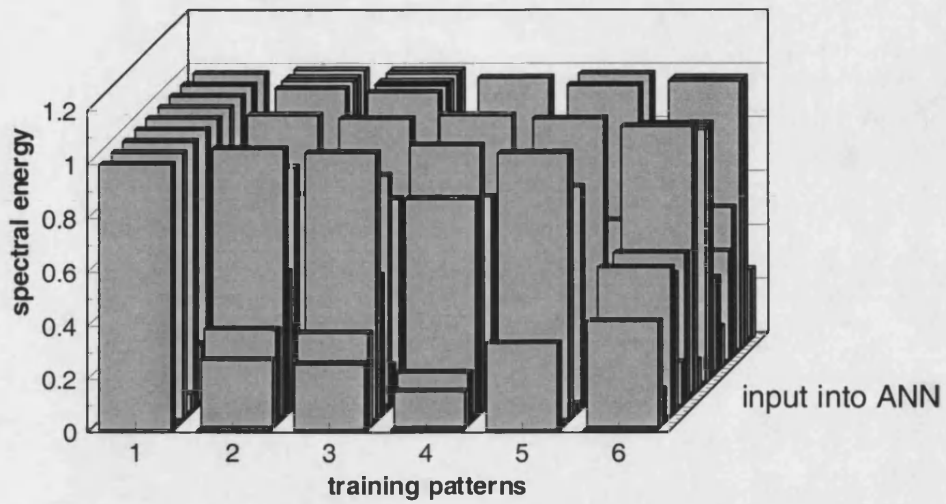
Figure 9.3 A typical training data set for an inrush current for System 1
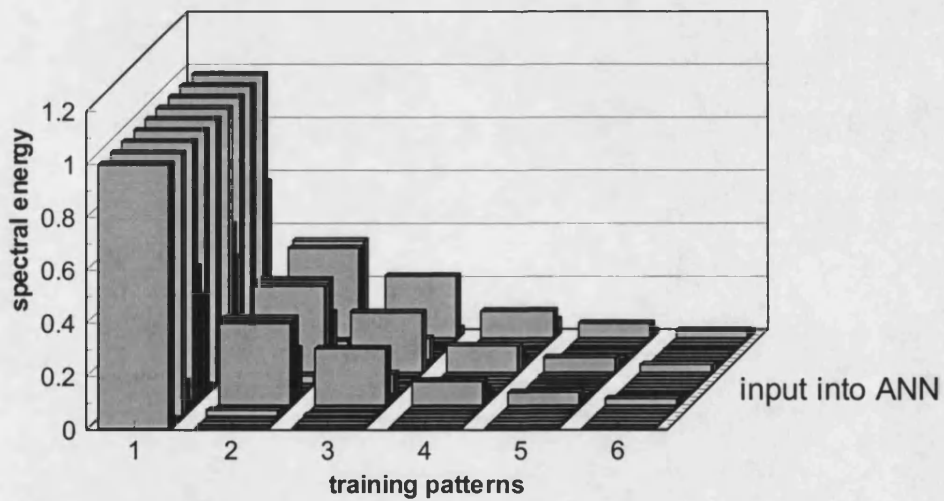
Figure 9.4 A typical training data set for an ab-phase to earth fault on HV side

for System 1

Figures 9.5 typifies a typical training data set for System 1 for a three-phase to earth fault on HV side together with a-phase CT saturation on LV side. Here, it can be seen that the spectral energy gradually decays after fault inception. Although the decay speed under such a case is slightly slower than that presented in Figures 9.4, there is nonetheless a significant difference in the spectral energy components between such an internal fault and an inrush current.
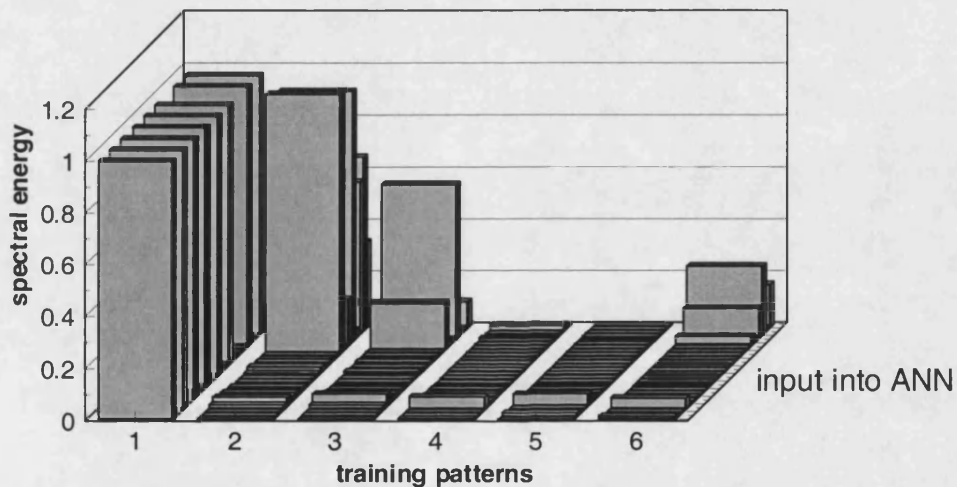
Figure 9.5 A typical training data set for a three-phase to earth fault on HV side together with a-phase CT saturation on LV side for System 1

The features of the ANN training data set are also examined for System 2. Figures 9.6 and 9.7 typify two sets of training data for System 2 for the cases of (i) an inrush current, and (ii) a three-phase short circuit on HV side. From these figures it is apparent that there are differences in the features between the internal fault and the inrush current, which are similar in comparison to those presented for System 1.
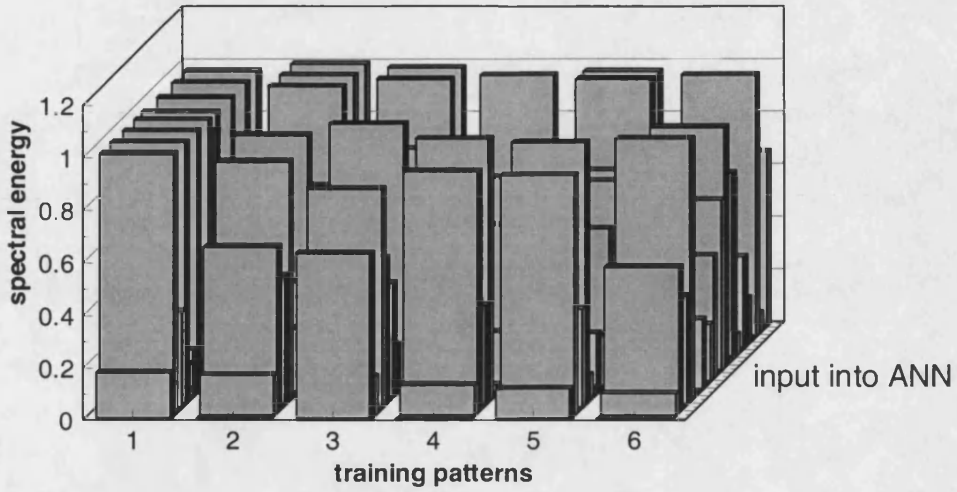
Figure 9.6 A typical training data set under an inrush current for System 2
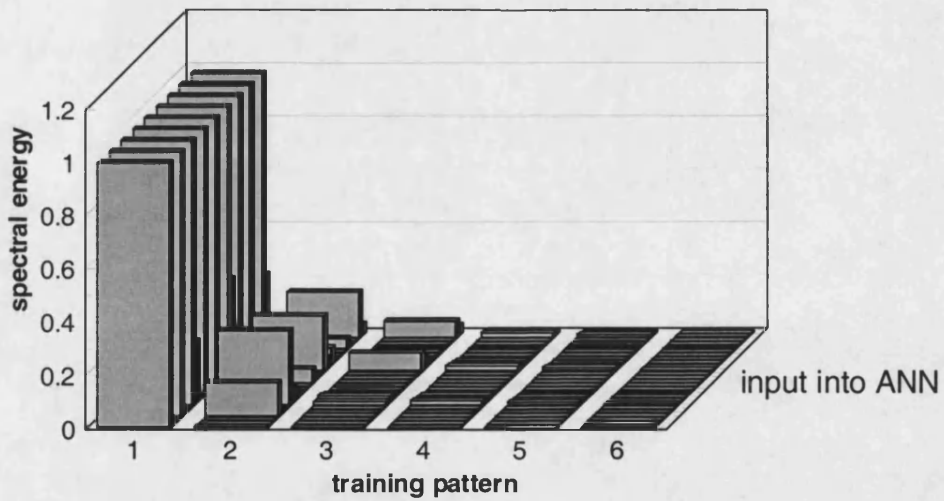
**Figure 9.7 A typical training data set under a three-phase short circuit on HV
side for System 2**

9.4.2 ANN Architecture

As described in Chapter 6, a three-layer network has been again employed herein. With the 27 input samples, the target output of the ANN is set in such a way that a value of unity represents an internal fault; and a value of zero represents an inrush current or an external fault. Through a series of tests and modifications, 6 hidden neurons produced a satisfactory performance. Moreover, the common sigmoid function was employed herein. Figure 9.8 shows the ANN architecture chosen in this work.
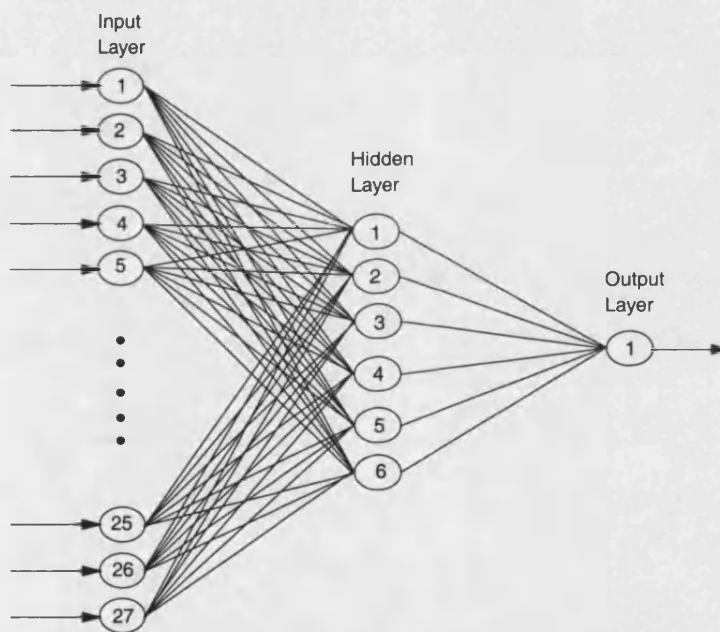
Figure 9.8 ANN architecture for combined WT and ANN based approach

9.4.3 ANN Training

The data employed herein for training and testing the ANN is the same as that shown in Table 6.1 of Chapter 6. A total of 245 cases relating to System 1 were firstly simulated to train and evaluate the performance of the ANN. As discussed

previously, the training methodology adopted was: roughly, 60 % of these cases were used for the ANN training, and the other 40% were used for the subsequent testing. The training process was repeated until the root mean square (RMS) error between the actual output and the desired output reached an acceptable value of 0.01 (RMS error criteria). The learning performance is shown in Figure 9.9. Comparing Figure 9.9 with Figure 6.6 presented in Chapter 6, it is evident that the ANN based on inputs comprising of spectral energy components reaches the requisite RMS of 0.01 in approximately 3000 learning iterations, rather than a relatively very large number 55000 learning iterations when the inputs into ANN are directly based on differential current signals. This clearly demonstrates the far superior performance of the combined WT and ANN based approach over the traditional ANN-based approach both in the accuracy and training speed.
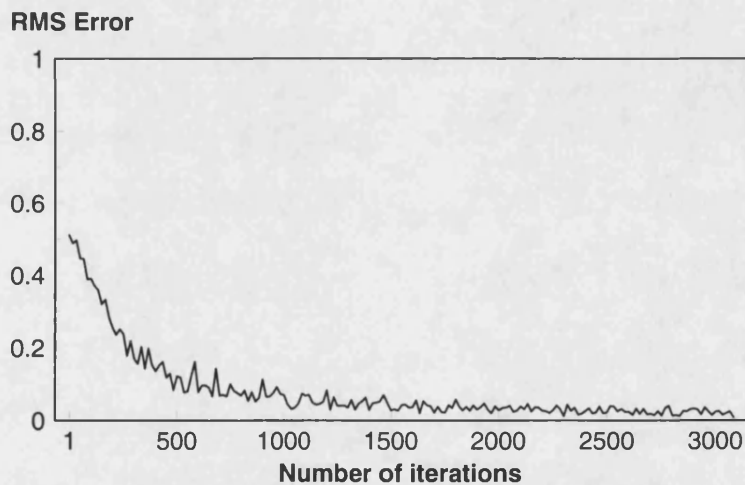
Figure 9.9 Performance of ANN training

Importantly, it should be stressed that during the training process, the convergence performance of the ANN is no longer affected by those low-level faults, which adversely affected the performance of the ANN when employed in a traditional ANN-based approach, this can be directly attributed to a near optimal feature extraction methodology coupled with more effective selection of the ANN inputs.

9.5 Performance of Relay for System 1

In order to examine the effectiveness of the combined WT and ANN based approach, the data used for testing is different and 'unseen' from that used for training; the data used is the same as shown in Table 6.1 of Chapter 6. Figures 9.10-9.13 depict the responses of the ANN for some typical cases. Note that in each figure, (a) represents the differential currents through CT secondary side, and (b) represents the response of the ANN. It is clearly evident from the results that although the ANN gives a high accuracy, there are small fluctuations in the actual ANN outputs around '1' and '0'; since in practice this cannot be avoided, a target tolerance of 0.15 was used in order to minimise the degree of uncertainty; this effectively means that the relay is set to issue a trip signal when the ANN output is ≥ 0.85, and block when the ANN output is ≤ 0.15.

Figure 9.10 gives the response of the ANN for an inrush current. It is apparent that the ANN produces the correct classification result by virtue of its output being less than 0.15.

(a)

(b)
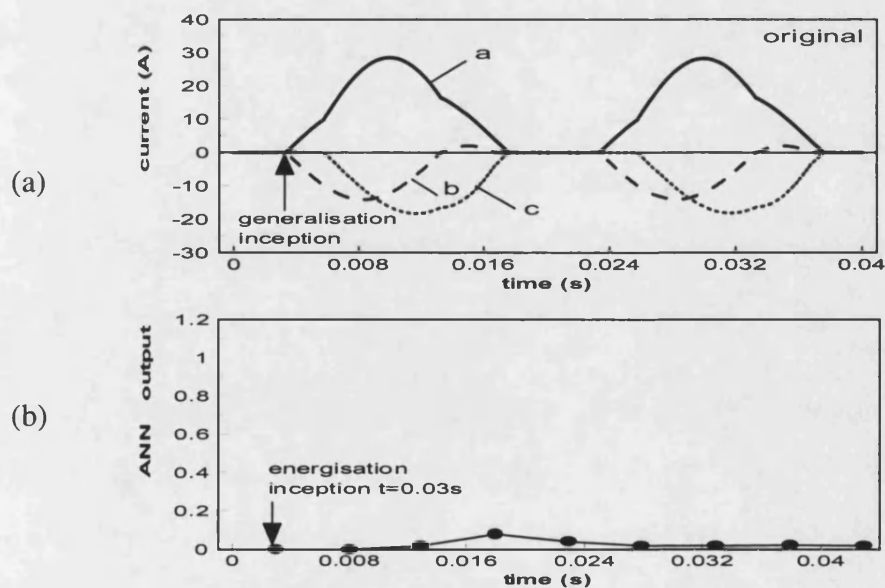
Figure 9.10 Response of ANN for an inrush current in System 1

Figures 9.11-9.12 illustrate the responses of the ANN for the cases of (i) an ab-phase to earth fault on HV side (Figure 9.11); (ii) a three-phase to earth fault on HV side together with a-phase CT saturation on LV side (Figure 9.12).
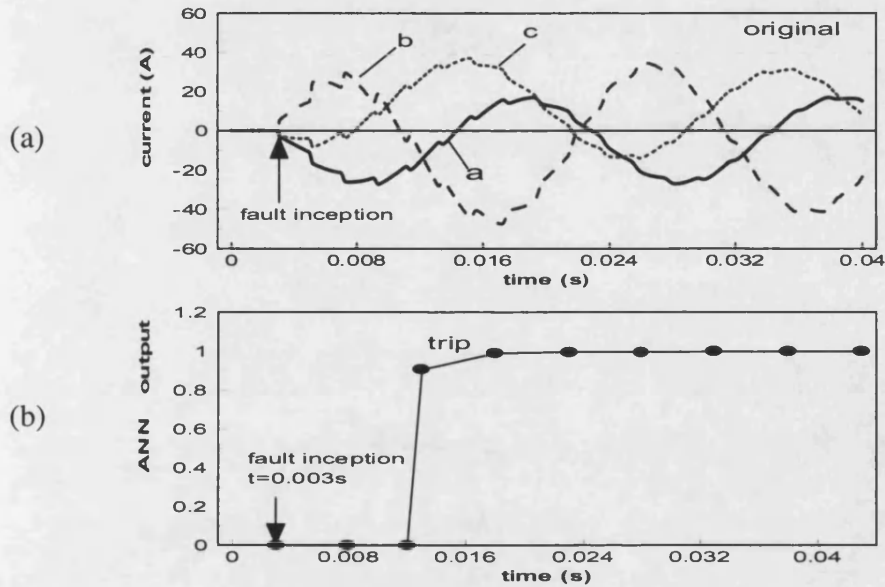
Figure 9.11 Response of ANN for an ab-phase to earth fault on HV side in System 1
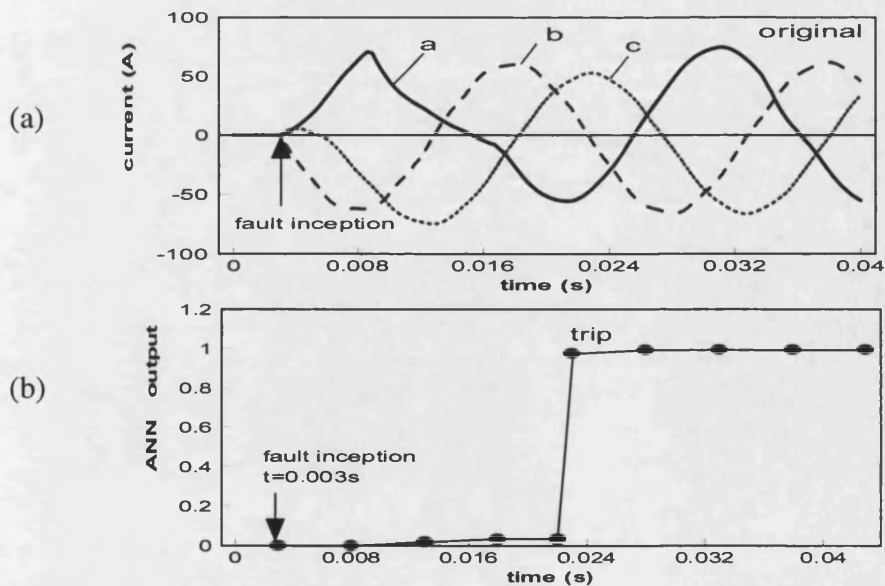
Figure 9.12 Response of ANN for an internal three-phase to earth fault on HV side together with a-phase CT saturation on LV side in System 1

It is apparent from the results that the ANN produces correct classification by virtue of its output being greater than 0.85, and in practice, the relay would issue a trip signal in both the cases. It is interesting to note that the response speed of the ANN in case (ii) becomes slower and this can be attributed due to the presence of CT saturation.

Figure 9.13 gives the response of the ANN for an a-phase 5% turn-to-turn fault at mid-point of the winding on LV side (low-level fault). Here again, as expected the ANN produces the correct classification result by virtue of its output being greater than 0.85.

(a)

(b)
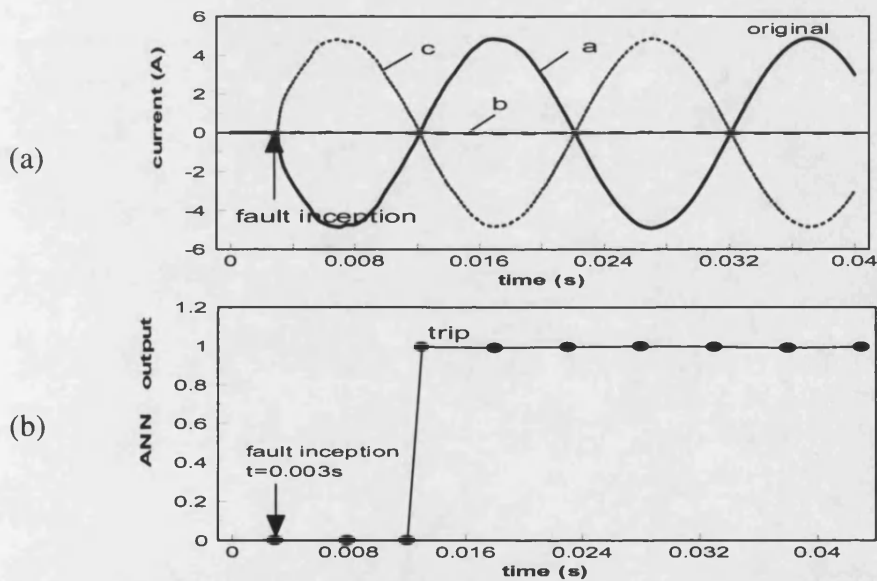
Figure 9.13 Response of ANN for an a-phase 5% turn-to-turn fault at mid-point of winding on LV side in System 1

An extensive series of the test results have indicated that the combined WT and ANN based approach is able to distinguish between internal faults and inrush currents/external faults with a very high classification rate. Importantly, the approach gives correct classification for all low-level faults, which posed certain difficulties

for the traditional ANN-based approach. This is so by virtue of the good separation of classes provided by the feature extraction methodology, coupled with the good selection of the ANN input, i.e., employment of spectral energies of signal components.

In the real world, the information dealt with is likely to be noisy or incomplete. In order to examine and verify if the designed relay can still give the correct classification results under such input conditions, a series of tests were carried out under conditions that in some ANN input patterns, the parts of data were manually taken out from original input patterns to simulate the situations that the parts of measured data are missing; in practice, this constitutes the presence of the noise.

Figure 9.14 shows the response of the ANN for an inrush current with the missing data. The area marked with a circle in Figure 9.14 (a) means that the sharp spikes appearing at this area, which was implemented by DWT and described in detail in section 7.3.1 of Chapter 7, was assumed to be zero value instead of the sharp spikes.
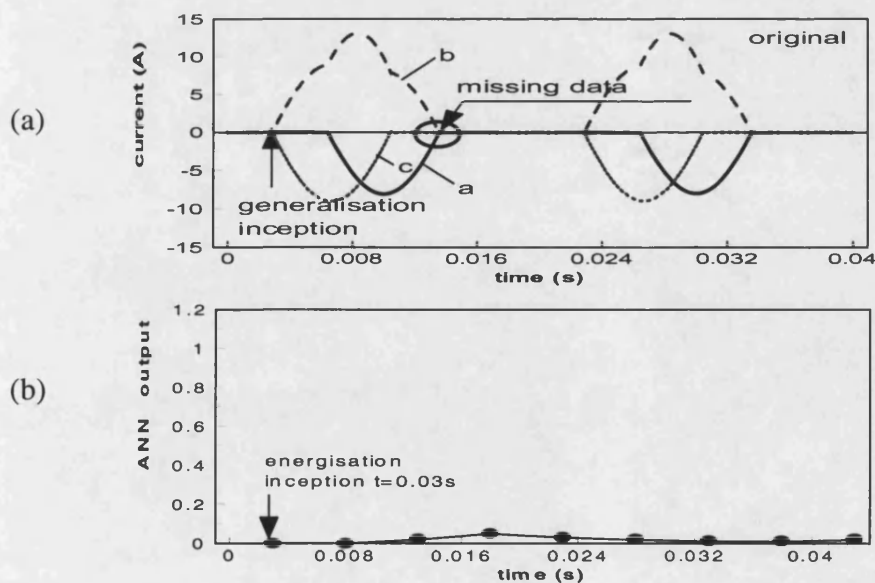
Figure 9.14 Response of ANN for an inrush current with the missing data

The studied results indicated that the designed relay still successfully gives the correct classification results. This can be directly attributed to the fact that the ANN can deal with incomplete or noisy input data, and has an ability to be fault tolerant.

It should be mentioned that the previously described WT-based approach might produce an unstable response under the foregoing situation that the parts of measured data are missing. This effectively means that the combined WT and ANN approach thus has the attribute of dealing with the presence of extraneous noise in signals than the technique solely based on the WT.

9.6 Performance of Relay for System 2

The ANN trained for System 1 was also directly tested by data generated from System 2, without actually training the ANN. The objective of this test was to examine the robustness and generalisation of the ANN, particularly its ability to deal with the different power transformer systems comprising of different transformer design and specification. The cases employed for testing for System 2 are the same as those shown in Table 6.1 of Chapter 6; there are 120 test cases generated from System 2 and these were employed for assessing the performance of the proposed approach.

For all 120 cases studied, the results clearly indicate that the combined WT and ANN based approach is also very effective in distinguishing between internal faults and inrush currents through very high classification rate. This is so by virtue of the fact that the feature extraction methodology adopted in the approach herein is representative of a feature space wide enough to cope with a different transformer system; it therefore overcomes the problem of robustness, which posed difficulties for the traditional ANN-based approach (as discussed in Chapter 6).

Figure 9.15 and Figure 9.16 typify the responses of the ANN for the cases of (i) an inrush current, and (ii) an ab-phase short circuit fault on HV side. Again, in each

figure, (a) represents the differential currents through CT secondary side; (b) represents the response of the ANN. From the figures it can be seen that the relay gives the correct classification results by virtue of its output being less than 0.15 for the inrush current, and greater than 0.85 for the internal fault.
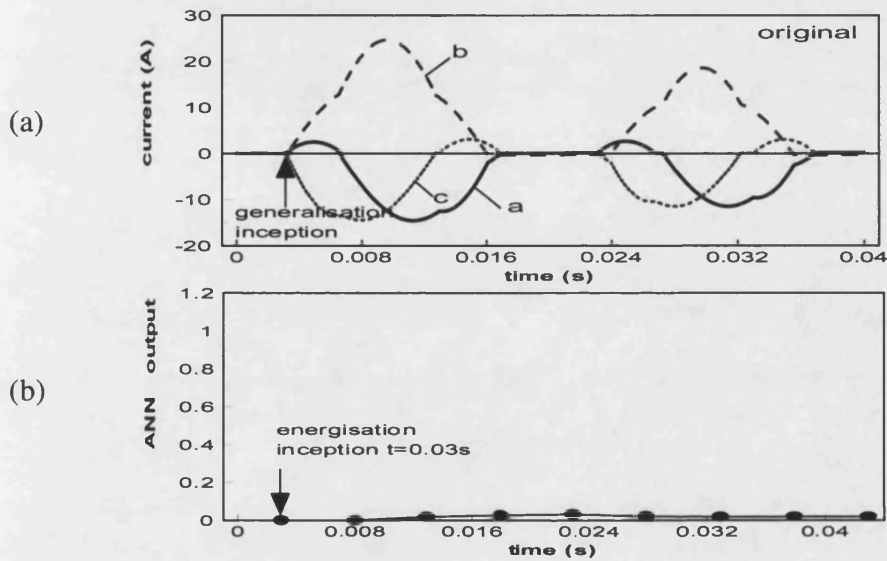
Figure 9.15 Response of ANN for an inrush current in System 2
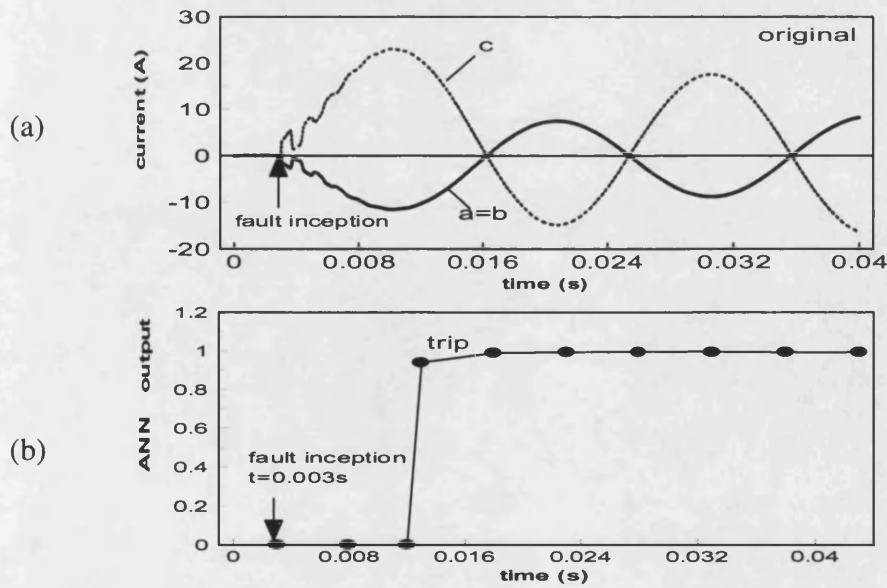
Figure 9.16 Response of ANN for an ab-phase short circuit on HV side in System 2

9.7 Response Evaluation

A total of 365 various system and fault cases relating to Systems 1 and 2 were tested. The results illustrates the misclassification rate of the relay is only 0.5 % within the tested 365 cases (i.e. correct classification rate ≥ 99.5%). More importantly, the results clearly demonstrate the robustness and generalisation of the combined WT and ANN based approach in its ability to deal satisfactorily with two different power transformer systems (Systems 1 and 2).

9.8 A Performance Comparison among Three Different Approaches

In this thesis, three different approaches for power transformer fault diagnosis (shown in Figure 9.17) have been described; these are respectively described and their performances discussed in Chapters 6, 8 and this Chapter.

```
┌─────────────────────────────────────────┐
│ Power Transformer Fault Diagnosis        │
│ Approaches Particularly for Distinguishing│
│ between Internal Faults and Inrush Currents│
└─────────────────────────────────────────┘
```

| Fault Diagnosis by Traditional ANN Based Approach | Fault Diagnosis by WT Based Direct Decision Making Approach | Fault Diagnosis by Combined WT and ANN Approach |
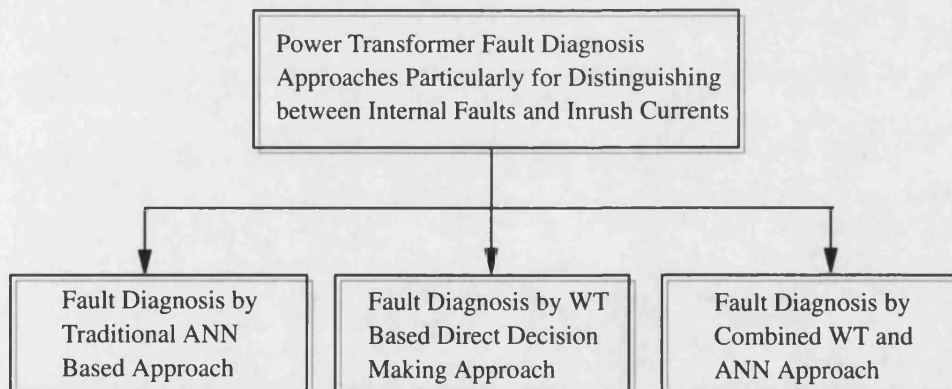
Figure 9.17 Three approaches for power transformer fault diagnosis

To clearly understand the advantages and disadvantages of each approach, a performance comparison amongst the three approaches was carried out. The comparison results are summarised in Table 9.1. From this table, it can be clearly seen that the WT based direct decision making approach and the combined WT and ANN based approach have a significant improvement over the traditional ANN based approach, as they give higher correct classification rates; in particular, they are robust to the different power transformer systems. It is apparent from performance evaluation that the approach based combined WT and ANN gives the most satisfactory performance.

Table 9.1: A performance comparison among three different approaches

Performance Comparison	Fault diagnosis approaches		
	Traditional ANN based approach	**WT based direct decision making approach**	**Combined WT and ANN based approach**
Input signal	Three-phase differential currents	Wavelet signal at detail 1	Spectral energies at details 1-3
Window length	20 ms	10ms	10ms
Training requirement	Required	Not required	Required
Convergence performance	Convergence in 55000 iterations	_	Convergence in 3000 iterations
Requisite RMS	0.05	_	0.01
Correct classification rate	$\geq 95\%$	$\geq 98.6\%$	$\geq 99.5\%$
Tripping time	$\leq 40ms$	$\leq 20\ ms$	$\leq 20\ ms$
Generalisation	Only for a particular power transformer system	For different power transformer systems	For different power transformer systems
Ability against input signal noise	Strong	Weak	Strong

9.9 Summary

This Chapter has described a novel approach for the power transformer fault diagnosis, particularly for distinguishing between internal faults and inrush currents/external faults based on combined WT and ANN technique. The proposed approach is robust to different power transformer systems; this is a significant advantage and can be directly attributed to the fact that WT technique effectively extracts the very crucial time-frequency features from different power transformer system transient waveform, common to all large practical transformers. Case studies presented indicate that the combined WT and ANN approach is able to give a very high accuracy in the classification rate of the transients. A performance comparison amongst traditional ANN based and the other two approaches, viz. WT-based and combined WT and ANN based, developed in this work clearly shows that the latter two approaches are very effective in overcoming the disadvantages and improving the accuracy over the traditional ANN based approach, and they can thus be used as attractive and effective alternatives to the protection schemes of power transformers.

Chapter 10

Conclusions and Future Work

10.1 Introduction

A power transformer forms a vital link between generation, transmission and distribution in any electric power supply network. However, improved and more efficient designs of modern power transformers coupled with increasing complexity of modern power systems is posing difficulty for conventional protection, in particular in accurately distinguishing between the magnetising inrush current phenomenon for which the protection should block operation of circuit breakers, and transformer internal faults for which the protection should isolate the transformer from the rest of the power system. There has thus been an upsurge in investigating new improved protection techniques for modern power transformers by a number of researches. This thesis is devoted to the research and development of alternative power transformer fault diagnosis techniques for accurately discriminating internal faults from inrush currents/external faults. In this thesis, two novel fault diagnosis classification approaches, one based on the WT and another employing a combined WT and an ANN, are proposed, and performance evaluation clearly show that the proposed approaches are very effective in overcoming the disadvantages and improving the accuracy over traditional approaches, including those solely based on ANNs developed more recently by a number of researchers. This chapter briefly reviews the previous work in the field of power transformer fault diagnosis, outlines major achievements and contributions in this research project and discusses further directions.

10.2 Previous Work

A number of approaches have been proposed and the methodologies published in the open literature to distinguish between internal faults and magnetising inrush currents in a power transformer. Some of these are based on advanced numerical methods and a few on AI, and all the techniques developed hitherto have advantages and disadvantages.

10.2.1 Advanced Numerical Methods

Differential Power Method. This relaying principle uses differential active power to discriminate between internal faults and inrush currents. It can discriminate an internal fault from an inrush current independent of the harmonics in differential current. However, the approach cannot deal successfully with a condition involving CT saturation. In practise, the CT saturation cannot be avoided under certain system and fault conditions and therefore must be considered in the power transformer protection [6].

Multisetting Overcurrent Principle. This relay principle classifies the differential current level into four classes, namely A, B, C, D, and three thresholds associated with the differential current level are set. The approach improves the dependability of the conventional differential relay by speeding up the operation. However, for such an approach, there are no recommended criteria for setting various internal parameters of a relay; in particular, there is no definite approach on how to co-ordinate relay parameters for different current settings; these problems thus need to be investigated further [2].

Inrush Current Detection. The inrush current detector is based on the detection of the inrush current waveform feature; it assumes that a gap or zero value period in the inrush current waveform exists, so that the gaps can be employed to detect inrush currents from internal faults. However, under certain conditions (such as CT

saturation) the gaps may be non-existent; thus, the effectiveness of the inrush current detector becomes questionable [15].

10.2.2 Artificial Intelligence

Fuzzy Logic Applications. In the fuzzy logic based approach, the criteria signals (such as amplitude, harmonic contents, etc.) and thresholds associated with the criteria signals are fuzzified and represented by fuzzy numbers. The fuzzy signals (i.e., the fuzzified criteria signals) are then compared with fuzzy settings. Several relaying criteria are used in parallel; the tripping decision is made based on the results of the criteria aggregation. However, here again for such an approach, there are no recommended criteria for setting various internal threshold parameters of a relay [17].

ANN Applications. Since ANN can provide excellent pattern recognition, they are proposed by many researchers for the power transformer fault diagnosis. Due to highly non-linear nature of power transformer systems, different types of solution may be required. In this respect, ANNs have shown an encouraging prospect to discriminate between internal faults and inrush currents; this is so by virtue of its ability in dealing with non-linearity and parallelism in processing information [7,8,18,19]. However, the ANNs in these existing studies are specific to particular transformer systems, and would have to be retrained again for other systems.

10.3 Major Achievements in This Research Project

On the basis of some previous investigations into power transformer fault diagnosis, the work described in this thesis represents three years research in the development of novel approaches to improve upon the performance of existing power transformer fault diagnosis techniques relating to three important aspects, viz. dependability, security and robustness. The following sections give an outline of the major achievements.

10.3.1 Integrated Modelling and Simulation in Power Transformer Systems

As a starting point, an integrated modelling approach for simulating the transient phenomena in power transformer systems, and followed by the development of the novel protection techniques are presented. Based on a rudimentary model of the power transformer provided within the EMTP software, the model developed herein is a significantly modified form of the basic model, capable of not only simulating internal terminal faults, but also internal winding faults. Importantly, the modelling approach developed integrates the power transformer model with the associated CT model which takes into account CT saturation thereby allowing the effect of the latter on transformer protection performance to be studied. In addition, the power transformer model developed is also capable of simulating the highly complex and non-linear inrush current phenomenon.

Based on the integrated models developed, the fault and inrush current transient behaviours of power transformer systems were thoroughly studied and simulated in two different (but practical) power transformer systems.

10.3.2 Study of the Traditional ANN-Based Approach

A study of the traditional ANN-based approach for the power transformer fault diagnosis is a necessary precursor to improving on the performance through alternative approaches. In this work, a traditional ANN-based fault diagnosis technique as applied to a power transformer was firstly investigated; and in particular, its advantages and disadvantages were examined and discussed. The performance obtained showed that an ANN can be very effective in the field of power transformer fault diagnosis; the trained ANN can give a correct classification rate of over 95%. However, if the trained ANN is then directly applied to a different power transformer system without actually retraining it, the ANN-based technique will give a very poor classification rate. This is so because the feature extraction methodology adopted is not representative of a feature space wide enough to cope

with a different transformer system. This understanding and the drawback then led to an investigation and development of a new feature extraction methodology as well as a novel fault diagnosis technique (the subject of this work) to improve the performance of the existing power transformer protection techniques.

10.3.3 Feature Extraction Methodology Based on WT

In the course of this work, an investigation and study of the traditional ANN-based approach have shown that an effective feature extraction methodology is crucial for accurate power transformer fault diagnosis. A new method to analyse and identify power transformer transient phenomena was thus investigated and effected using the WT technique. In this respect, case studies carried out on two different transformers have clearly shown that realisation of the signals through the WT gives features which show very distinct (almost unique) differences between internal faults and the inrush current phenomenon. Extraction of such unique features combined with a decision logic methodology then formed the basis of an alternative approach in this work for distinguishing between internal faults and the magnetising inrush current phenomenon.

10.3.4 WT-Based Direct Decision Making Approach

Based on the developed feature extraction methodology, a new WT-based direct decision making approach for distinguishing internal faults from inrush currents was investigated and effected. In this approach, the WT technique is firstly applied to decompose the differential current signals into a series of wavelet components; then by processing the selected wavelet components, a decision for distinguishing an internal fault from an inrush current is directly made based on pre-defined decision making logic criterion. The results presented show that the proposed approach can more accurately discriminate between an internal fault and an inrush current; in particular, the approach is able to give a correct classification result for low-level

fault cases and is robust to different power transformer systems, in comparison to the traditional ANN-based approach presented in Chapter 6.

10.3.5 Combined WT and ANN Based Approach

A novel approach based on integrating a WT with ANN for distinguishing between internal faults and inrush currents is then proposed in this work to further improve the accuracy of power transformer fault diagnosis. As expected, the results presented show that the combined WT and ANN approach is able to give a very high accuracy in the classification of the transients and is robust to different power transformer systems in comparison to the traditional ANN-based approach. This is a significant advantage and this is largely so by virtue of the fact that WT technique effectively extracts the very crucial time-frequency features from different power transformer systems, common to all large practical transformers. Importantly, the combined WT and ANN approach shows greater immunity to input signal noise compared to the previous technique based on WT-based approach alone. Furthermore, the approach is also able to give correct classification result for low-level fault cases.

10.3.6 Performance Evaluation

A performance comparison amongst the traditional ANN based and the two approaches developed were given in the performance criteria presented in the table, the following inferences can be explicitly drawn:

- The performances of the proposed approaches under a whole variety of practically encountered system and fault conditions have the correct classification rate of 98.6 % for WT based direct decision making approach, and 99.5% for the combined WT and ANN based approach. This clearly shows that the proposed approaches have effectively improved the accuracy of power transformer fault diagnosis over traditional ANN based approach, which has the correct classification rate 95%.

- It is also shown that the proposed approaches are robust to different power transformer systems compared with the traditional ANN-based approach.

- It is clearly shown that the proposed approaches are able to give correct classification results for the low-level faults that poses difficulties for the traditional ANN-based approach.

It is clearly evident that the proposed approaches are very effective in overcoming the disadvantages and improving the accuracy over the traditional ANN based approach, and they can thus be used as attractive and effective approaches for alternative protection schemes for power transformers.

It is also worth pointing out that although the approaches developed in this work are based on the Computer Aided Design (CAD), they take into account the practical limitations associated with hardware errors such as anti-aliasing filters and A/D converters so that the performance attained is close to that which would be expected from a hardware model under service conditions.

10.4 Future Work

Power transformer fault diagnosis is a very broad subject. The work presented in this thesis deals mainly with the modelling and simulation of power transformer systems as well as the study and development of new alternative techniques for power transformer fault diagnosis particularly for distinguishing between internal faults and inrush currents. This work could be further expanded and improved in the following aspects:

10.4.1 Testing Proposed Approaches with Data from Real Systems

As emphasised in the thesis, the proposed approaches have been tested off-line to evaluate their accuracy under a whole variety of practically encountered system and

fault conditions. As a next logical step, the approaches should be tested with real input data captured from practical power transformer systems. This is important in view of the fact that although the approaches developed take into account the practical limitations associated with hardware errors such as anti-aliasing filters and A/D converters and it is expected that it should retain the high degree of accuracy in power transformer fault diagnosis, in practice there is always some environmental noise present in the measured signals and this can have some detrimental effect on the performance achievable in practice. Furthermore, testing a techique with real data or under serious conditions and attaining a performance close to that obtained with simulated data gives confidence in the CAD of the technique. It also highlights any refinements that need to be carried out on the algorithm and /or hardware design in order to maintain its expected performance under practical conditions.

10.4.2 Performance Evaluation under Other Inrush Conditions

As mentioned in section 5.2 of Chapter 5, inrush conditions occur not only when switching a transformer on, which are considered as the basis of case studies in this work, but also when clearing a close-up external fault and energising one of two parallel transformers. Although their severity and frequency of occurrences are less common, the performance of the internal fault/inrush discriminator presented herein under such conditions should also be considered as part of the further work.

10.4.3 Application of the Techniques under More Complex System Conditions

Although the proposed approaches have been tested on two different power transformer systems, in which a 750MVA power transformer is connected between a 25kV source at the sending end and a single 400kV transmission line connected to an infinite bus power system at the receiving end (System 1), and a 35MVA power transformer is connected between an 11kV source and a single 110kV transmission line connected to a load (System 2), the performances of the approaches under more

complex system conditions still need to be investigated. These include the power transformer linked with

- double circuit lines: Because of the mutual inductive and capacitive coupling between the two lines, when calculating the equivalent series impedance and shunt admittance matrices for the lines, these couplings should not be neglected. If the power transformer is connected into such double circuit lines, its transient behaviour may be affected by the contribution of the mutual coupling of the double circuit lines; the performance of the proposed approaches for such systems should therefore be investigated as part of the future work.

- three-terminal line circuits (teed circuits): The three-terminal line circuit is attractive both from environmental and economical points of view. However, the system configuration is significantly different with that studied in this work in that, the power transformer transients may be affected by the intermediate in-feed from the third terminal and therefore require special attention. The performance of the proposed approaches for such multi-ended systems warrants further investigation.

- series-compensated lines: Series capacitor compensation in long distance EHV transmission lines is a widely accepted method to solve the problem of stability, increase power transmission capabilities, improve voltage control, etc [68]. The capacitors connected in series with the transmission line result in the reduction of the total equivalent line impedance by virtue of their associated impedance being negative; moreover, an additional transient could be introduced due to the capacitor being taken out of the system by its own overvoltage protection. The transient behaviours of the power transformer linked with such a system configuration may be affected. Thus, the application of the proposed approaches for such a system configuration should also be investigated as part of the future work.

Bibliography

[1] Stanley H. Horowitz, Arun G. Phadke, "Power System Relaying (Second edition)", Research Studies Press Ltd, Taunton, Somerset, England, 1995

[2] Bogdan Kasztenny, Mladen Kezunovic, "Digital Relays Improve Protection of Large Transformers", IEEE Computer Applications in Power, October 1998, pp. 39-45

[3] Walter A. Elmore , "Protective Relaying Theory and Applications", ABB Power T&D Company Inc, Relay Division, Coral Springs, Florida, 1994.

[4] M. A. Rahman and B. Jeyasurya, "A State-of-the-Art Review of Transformer Protection Algorithms", IEEE Trans. on Power Delivery, Vol.3, No.2, 1988, pp.534-544.

[5] P. Liu, O. P. Malik, D. Chen, G. S. Hope, and Y. Guo "Improved Operation of Differential Protection of Power Transformers for Internal Faults", IEEE Trans. on Power Delivery, Vol. 7, No.4, 1992, pp.1912-1919.

[6] Kuniaki Yabe, "Power Differential Method for Discrimination between Fault and Magnetizing Inrush Current in Transformers", IEEE Trans. on Power Delivery, Vol.12, No.3, July 1997, pp.1109-1118.

[7] L. G. Perez, A. J. Flechsig, J. L. Meador and Z. Obradovic, "Training an Artificial Neural Network to Discriminate Between Magnetizing Inrush and Internal Fault", IEEE Trans. on Power Delivery, Vol. 9, No. 1, January 1994, pp.434-441

[8] M. R. Zaman, M. A. Rahman, "Experimental Testing of the Artificial Neural Network Based Protection of Power Transformers", IEEE Trans. on Power Delivery, Vol. 13, No. 2, April 1998, pp.510-517

[9] T. S. Sidhu, M. S. Sachdev, "On-Line Identification of Magnetising Inrush and Internal Faults in Three-phase Transformers", IEEE Trans. on Power Delivery, Vol. 7, No. 4, October 1992, pp. 1885-1891

[10] Y. G. Paithankar, "Transmission Network Protection – Theory and Practice", Marcel Dekker, Inc. 1998.

[11] GEC Alsthom, "Protective Relays Application Guide", Third Edition, GEC Alsthom Measurements Ltd. 1987.

[12] T. S. Sidhu, M. S. Sachdev, H. C. Wood, and M. Nagpal, "Design, Implementation and Testing of A Micorprocessor-Based High-Speed Relay for Detecting Transformer Winding Faults", IEEE Trans. on Power Delivery, Vol. 7, No.1, January 1992, pp.108-117.

[13] A. Wright, C. Christopoulos, "Electrical Power System Protection", Chapman & Hall, 2-6 Boundary Row, London, 1993

[14] A. T. Johns, S. K. Salman, " Digital Protection for Power System", Peter Peregrinus Ltd., The Institution of Electrical Engineers, Michael Faraday House, United Kingdom, 1995

[15] ALSTOM T&D, "Protective Relays for Power Systems", ALSTOM T&D Protection & Control Ltd, Stafford, England, 1998, pp. 502-507

[16] Andrzej Wiszniewski, Bogdan Kasztenny, "A Multi-Criteria Differential Transformer Relay Based on Fuzzy Logic", IEEE Trans. on Power Delivery, Vol. 10, No. 4, October 1995, pp.1786-1792

[17] B. Kasztenny, E. Rosolowski, M. M. Saha, B. Hillstrom, "A Self-Organizing Fuzzy Logic Based Protective Relay - An Application to Power Transformer Protection", IEEE Trans. on Power Delivery, Vol. 12, No. 3, July 1997, pp.1119-1127

[18] P. Bastard, M. Meunier and H. Regal, "Neural Network-Based Algorithm for Power Transformer Differential Relays", IEE Proc. - Generation, Transmission and Distribution, Vol. 142, No. 4, July 1995, pp. 386-392

[19] J. Pihler, B. Grcar and D. Dolinar, "Improved Operation of Power Transformer Protection Using Artificial Neural Network", IEEE Trans. on Power Delivery, Vol. 12, No. 3, July 1997, pp.1128-1136

[20] EMTP Rule Book, Bonneville Power Administration, P.O. Box 36212, Portland, Ore. 97208, USA.

[21] Electromagnetic Transients Program (EMTP) Volume 1: Work Book, Electric Power Research Institute, 3412 Hillview Avenue, Palo Alto, California 94304

[22] Electromagnetic Transients Program (EMTP) Volume 3: Work Book, Electric Power Research Institute, 3412 Hillview Avenue, Palo Alto, California 94304

[23] G. Emperur, "Transformer Modelling-Basic Theory and Examples", LEC EMTP Summer Course, Katholieke Universiteit Leuven, Belgium, Leuven, July 1991.

[24] Patrick Bastard, Pierre Bertrand and Michel Meunier, "A Transformer Model for Winding Fault Studies" , IEEE Trans. on Power Delivery, Vol. 9, No.2, April 1994, pp.690-699

[25] F. A. Fouad, T. W. Nehl and N. A. Demerdash, "Saturated transformer inductances determined by energy perturbation techniques", IEEE Trans. on Power Apparatus and Systems, Vol. PAS-101, No.11, Nov.1982, pp.4185-4193.

[26] V. Brandwajn, H. W. Dommel, and I. I. Dommel, "Matrix Representation of Three-Phase N-Winding Transformers for Stead-State and Transient Studies", IEEE Trans. on Power Apparatus and System, Vol. PAS-101, No.6, June 1982, pp.1369-1378

[27] H. L. Nakra, T. H. Barton, "Three Phase Transformer Transients", IEEE Trans. on Power Apparatus and Systems, Vol. PAS-93, 1974, pp. 1810-1819

[28] M. A. Rahman, A. Gangopadhyay, "Digital Simulation of Magnetising Inrush Currents in Three-Phase Transformers", IEEE Trans. on Power Delivery, Vol. PWRD-1, No. 4, October 1986, pp. 235-242.

[29] R. Yacamini and A. Abu. Nasser, "The Calculation of Inrush Current in Three-Phase Transformers", IEE Proceedings, Vol.133, Pt. B, No.1, January 1986, pp. 31-40

[30] C. E. Lin, C. L. Cheng, C. L. Huang, J. C. Yeh, "Investigation of Magnetizing Inrush Current in Transformers. Part I - Numerical simulation", IEEE Trans. on Power Delivery, Vol. 8, No. 1, Jan. 1993, pp. 246-254

[31] C. E. Lin, C. L. Cheng, C. L. Huang, J. C. Yeh, "Investigation of Magnetizing Inrush Current in Transformers. Part II -Harmonic Analysis", IEEE Trans. on Power Delivery, Vol. 8, No. 1, Jan. 1993, pp. 255-263

[32] J. C. Yeh, C. E. Lin, C. L. Huang, C. L. Cheng, "Calculation and Harmonic Analysis of Transient Inrush Currents in Three-Phase Transformers", Electric Power Systems Research , Vol. 30, No. 2, July-Aug 1994, pp. 93-102

[33] Working Group of the Relay Input Sources Subcommittee of the Power System Relaying Committee, "Transient Response of Current Transformers", IEEE Trans. on Power Apparatus and Systems, Vol. PAS-96, No.6, November/December 1977, pp. 1809-1814

[34] M. Poljak; N. Kolibas, "Computation of Current Transformer Transient Performance", IEEE Trans. on Power Delivery, Vol. 3, No. 4, October 1988, pp. 1816-1822

[35] J. R. Lucas, P. G. McLaren, W. W. L. Keerthipala, R. P. Jayasinghe, "Improved Simulation Models for Current and Voltage Transformers in Relay Studies", IEEE Trans. on Power Delivery, Vol. 7, No. 1, January 1992, pp. 152-159

[36] Y. C. Kang, J. K. Park, S. H. Kang, A. T. Johns, R. K. Aggarwal, "An Algorithm for Compensating Secondary Currents of Current Transformers", IEEE Trans. on Power Delivery, Vol. 12, No. 1, January 1997, pp. 116-124.

[37] J. R. Marti, L. R. Linares, H. W. Dommel, "Current Transformers and Coupling-Capacitor Voltage Transformers in Real-Time Simulations", IEEE Trans. on Power Delivery, Vol. 12, No. 1, January 1997, pp. 164-168.

[38] PSRC Working Group Members, "C37.110 Guide for the Application of Current Transformers Used for Protective Relaying Purposes", IEEE Trans. on Power Delivery, Vol. 14, No. 1, January 1999, pp. 94-97

[39] M. Kezunovic; C. W. Fromen; F. Phillips, "Experimental Evaluation of EMTP-Based Current Transformer Models for Protective Relay Transient Study", IEEE Trans. on Power Delivery, Vol.9, No.1, January 1994, pp.405-413

[40] R. K. Aggarwal, Y. H. Song, "Tutorial: Artificial Neural Networks in Power System ", Power Engineering Journal June 1997

[41] Stamatios V. Kartalopoulos, " Understanding Neural Network and Fuzzy Logic: Basic Concepts and Applications", The Institute of Electrical and Electronics Engineers, Inc., New York, 1996

[42] Kevin Warwick, Arthur Ekwue, Raj Aggarwal, "Artificial Intelligence Techniques in Power Systems", The Institution of Electrical Engineers, London, United Kingdom, 1997

[43] Carl G. Looney, "Pattern Recognition Using Neural Networks: Theory and Algorithms for Engineers and Scientists", New York, Oxford University Press, 1997

[44] Shigeo Abe, "Neural Networks and Fuzzy Systems: Theory and Applications", Kluwer Academic Publishers, Boston/London/Dordrecht, 1997

[45] Richard P. Lippmann, "An Introduction to Computing with Neural Nets", IEEE ASSP Magazine, April 1987, pp.4-22

[46] Y. Zhang, X. Ding, Y. Liu, P. J Griffin, "An Artificial Neural Network Approach to Transformer Fault Diagnosis", IEEE Trans. on Power Delivery, Vol. 11, No. 4, October 1996, pp. 1836-1841

[47] B. Kasztenny, M. Lukowicz, E. Rosolowski, "Selecting Type of a Neural Network, Pre- and Post-processing Algorithms for Power Transformer Relaying" 32th University Power Engineering Conference. Sept. 1997, pp. 708-712.

[48] Thomas Dalstein, Bernd Kulicke, "Neural Network Approach to Fault Classification for High Speed Protective Relaying", IEEE Trans. on Power Delivery Vol. 10, No. 2, April 1995, pp. 1002-1011

[49] Atish K. Ghosh, David L. Lubkeman, "The Classification of Power System Disturbance Waveforms Using A Neural Network Approach", IEEE Trans. on Power Delivery, Vol. 10, No. 1, January 1995, pp. 109-115

[50] Mladen Kezunovic, Igor Rikalo, "Detect and Classify Faults Using Neural Nets", IEEE Computer Applications in Power, October,1996, pp.42-47

[51] A. I. Megahed, O. P. Malik, "An Artificial Neural Network Based Digital Differential Protection Scheme for Synchronous Generator Stator Winding Protection", IEEE Trans. on Power Delivery, Vol. 14, No. 1, January 1999, pp. 86-93

[52] A. I. Taalab, H. A. Darwish, T. A. Kawady, "ANN-Based Novel Fault Detector for Generator Windings Protection", IEEE Trans. on Power Delivery, Vol. 14, No. 3, July 1999, pp. 824-830

[53] NeuralWare, Inc., "Neural Works Professional II/Plus and Neural Works Explore", 1993

[54] O. Rioul and M. Vetterli, "Wavelets and Signal Processing", IEEE SP Magazine, October 1991, pp.14-38

[55] Randy K. Young, "Wavelet Theory and Its Applications" Kluwer Academic Publishers, Boston/London/Dordrecht, 1993

[56] C. K. Chui, "Wavelets: A Tutorial in Theory and Applications", Academic Press, Inc., 1992.

[57] M. Misiti, Y. Misiti, G. Oppenheim, J. Poggi, "Wavelet Toolbox User's Guide", MathWorks, Inc., Natick, Mass, 1996

[58] A. W. Galli, G. T. Heydt, P. F. Ribeiro, "Exploring the Power of Wavelet Analysis", IEEE Computer Applications in Power, October,1996, pp.37-41

[59] V. M. Reddy, S. S. Rao, F. J. Mercede, "On The Use of Wavelets for the Detection and Analysis of Power system Transients", Proceeding of 1999 IEEE Winter Power Meeting, pp. 1293-1299.

[60] W. A. Wilkinson and M. D. Cox, "Discrete Wavelet Analysis of Power System Transients", IEEE Trans. on Power System, Vol.11, No.4, November 1996, pp. 2038-2044.

[61] Antony C. Parsons, W. Mack Grady, Edward J. Powers, "A Wavelet-Based Procedure for Automatically Determining the Beginning and End of Transmission System Voltage Sags", Proceeding of 1999 IEEE Winter Power Meeting, pp.1310-1315.

[62] David C. Robertson, Octavia I. Camps, Jeffrey S. Mayer, William B. Gish, "Wavelets and Electromagnetic Power System Transients", IEEE Trans. on Power Delivery, Vol. 11, No. 2, April 1996, pp. 1050-1058

[63] G. T. Heydt and A. W. Galli, "Transient Power Quality Problems Analyzed Using Wavelets", IEEE Trans. on Power Delivery, Vol.12, No.2, April 1997, pp. 908-915.

[64] L. Angrisani, P. Daponte, M. D'Apuzzo, A. Testa, "A Measurement Method Based on the Wavelet Transform for Power Quality Analysis", IEEE Trans. on Power Delivery, Vol. 13, No. 4, October 1998, pp. 990-997

[65] Stantosh Kumar Pandey and L.Satish, "Multiresolution Signal Decomposition: A New Tool for Fault Detection in Power Transformers During Impulse Tests", IEEE Trans. on Power Delivery, Vol.13, No.4, October 1998, pp.1194-1200.

[66] John D Martin, "Signals & Processes: A Foundation Course", Printed and bound in Great Britain, 1991

[67] Leland B. Jackson "Digital Filters and Signal Processing (Third Edition)", Kluwer Academic Publishers, Boston Dordrecht London, 1996

[68] J. A. S. B. Jayasinghe, R. K. Aggarwal, "A Novel Non-unit Protection for Series Compensated EHV Transmission Lines Based on Fault Generated High Frequency Voltage Signals", IEEE Trans. on Power Delivery, Vol. 13, No. 2, April 1998, pp. 405-413

[69] Andrzej Wiszniewski, "Digital Algorithms for Differential Protection of Power Transformers", Ninth Power Systems Computation Conference, Cascais, Portugal, 30 August to 4 September 1987, pp. 725-731.

[70] M. Habib and M. A. Marin, "A Comparative Analysis of Digital Relaying Algorithms for the Differential Protection of Three Phase Transformers", IEEE Trans. on Power System, Vol.3, No.3, 1988, pp.1378-1384.

[71] T. S. Sidhu, M. S. Sachdev, H. C. Wood, "Microprocessor-Based Relay for Protecting Power Transformers", IEE Proceedings, Vol. 137, Pt. C, No. 6, November 1990, pp. 436-444

[72] Bodgan Kasztenny, Eugeniusz Rosolowski, "Two New Measuring Algorithms for Generator and Transformer Relaying", IEEE Trans. on Power Delivery, Vol. 13, No. 4, October 1998, pp. 1053-1059

[73] T. S. Sidhu, H. S. Gill, M. S. Sachdev, "A Power Transformer Protection Technique with Stability During Current Transformer Saturation and Ratio-Mismatch Conditions", IEEE Trans. on Power Delivery, Vol. 14, No. 3, July 1999, pp. 798-804

Appendix

Power Transformer System Parameters

This Appendix gives the parameters of the two power transformer systems, which were employed in the research and development of the novel fault diagnosis techniques described herein.

A.1 Power Transformer System Parameters Employed in System 1

A.1.1 [R] and [L] Matrices

System 1 is *a three-phase and two-winding 750 MVA, 27kV/420kV, Dy11-connected, five-leg, core-type* power transformer in a double-end-fed power system network. The transformer neutral terminal on HV side is grounded. The power transformer basic parameters are obtained from reference [23], which are provided by the transformer manufacturer, and are shown in Tables A.1.1, A.1.2 and A.1.3.

Table A.1.1 Power and voltage ratings in System 1

Rated Power (MVA)	750	
Rated Voltage (kV) (line-line value)	27 (low-voltage side)	420 (high-voltage side)

Table A.1.2 Short circuit test data in System 1

Test Type \\ Value	Positive Sequence Short Circuit Test	Zero Sequence Short Circuit Test
Short-circuit losses (kW)	1425	158.3
Short-circuit current (A)	1031	343.7
Short-circuit voltage (kV)	68.46	13.205

Table A.1.3 Excitation test data in System 1

Test Type \\ Value	Positive Sequence Excitation Test	Zero Sequence Excitation Test
Excitation losses (kW)	311	311
Excitation current (A)	21.16	21.16
Excitation voltage (kV)	27	-

Based on the parameters given in Tables A.1.1, A.1.2 and A.1.3, the supporting routine BCTRAN in the EMTP is used to derive [R] and [L] representation for the transformer, they are shown as follows:

$$[R] = \begin{bmatrix} R_1 & 0 & 0 & 0 & 0 & 0 \\ 0 & R_2 & 0 & 0 & 0 & 0 \\ 0 & 0 & R_3 & 0 & 0 & 0 \\ 0 & 0 & 0 & R_4 & 0 & 0 \\ 0 & 0 & 0 & 0 & R_5 & 0 \\ 0 & 0 & 0 & 0 & 0 & R_6 \end{bmatrix}$$

$$= \begin{bmatrix} .22346375 & & & & & \\ 0.0 & .0027702 & & & & \\ 0.0 & 0.0 & .22346375 & & & \\ 0.0 & 0.0 & 0.0 & .0027702 & & \\ 0.0 & 0.0 & 0.0 & 0.0 & .22346375 & \\ 0.0 & 0.0 & 0.0 & 0.0 & 0.0 & .0027702 \end{bmatrix}$$

$$[L] = \begin{bmatrix} L_1 & M_{12} & M_{13} & M_{14} & M_{15} & M_{16} \\ M_{21} & L_2 & M_{23} & M_{24} & M_{25} & M_{26} \\ M_{31} & M_{32} & L_3 & M_{34} & M_{35} & M_{36} \\ M_{41} & M_{42} & M_{43} & L_4 & M_{45} & M_{46} \\ M_{51} & M_{52} & M_{53} & M_{54} & L_5 & M_{56} \\ M_{61} & M_{62} & M_{63} & M_{64} & M_{65} & L_6 \end{bmatrix}$$

$$= \begin{bmatrix} 187741.18742585 \\ 20898.873837545 & 2326.8849221184 \\ 0.0 & 0.0 & 187741.18742585 \\ 0.0 & 0.0 & 20898.873837545 & 2326.8849221184 \\ 0.0 & 0.0 & 0.0 & 0.0 & 187741.18742585 \\ 0.0 & 0.0 & 0.0 & 0.0 & 20898.873837545 & 2326.8849221184 \end{bmatrix}$$

Note that as the [R] and [L] matrices are symmetric, the elements below the diagonal are only specified.

A.1.2 Flux-Current Curve ($\phi - i$) for Inrush Current Simulation

When the core saturation is taken into consideration in the power transformer simulation, a flux-current curve ($\phi - i$ curve) of the power transformer core must be supplied. Although it is generally not directly available, it can be calculated from the data (V_{RMS} versus I_{RMS}) given by manufactures.

Table A.1.4 shows V_{RMS} - I_{RMS} data obtained from the reference [23], which is provided by manufacture. Based on the parameters given in Table A.1.4, the auxiliary program CONVERT in the EMTP is used to derive $\phi - i$ data, which is shown in Table A.1.5.

Table A.1.4 V$_{RMS}$ - I$_{RMS}$ data of power transformer core in System 1

V$_{RMS}$ (pu)	I$_{RMS}$ (pu)
0.8430	0.3942 E-3
0.8996	0.6113 E-3
0.9496	0.8888 E-3
1.000	1.253 E-3
1.019	1.480 E-3
1.054	1.920 E-3
1.078	2.333 E-3
1.204	5.011 E-3

Table A.1.5 $\phi - i$ data of power transformer core in System 1

i (A)	ϕ (Vs)
5.16	102.46
12.34	109.34
17.51	115.42
24.80	121.54
31.63	123.79
38.88	128.16
50.24	131.00
97.02	146.30
68097.02	316.00

A.1.3 CTs Parameters

The CT data chosen are shown in Table A.1.6

Table A.1.6 CT data in System 1

CTs	CT1*	CT2 *
Ratio	18000/5	2000/5
Accuracy Class	C800	C800
Burden (VA)	200	200
Burden (Ω)	8	8
Power factor	0.5	0.5

    *   CT1 and CT2 refer to the CTs on LV and HV sides of the power

       transformer, respectively.

In order to simulate the effects of CT saturation on the relay performance, the V-I curve of CT core has to be taken into consideration. However this data that should be provided by manufactures, in practice, is not often available. In this work, the V-I curve for CTs was obtained from reference [39]. According to the V-I curve, the EMTP auxiliary program HYSDAT generates λ-i hysteresis loop, which is then embedded into the basic system model using the EMTP software to implement the simulation of the power transformer coupled with the CTs.

A.2 Power Transformer System Parameters Employed in System 2

A.2.1 [R] and [L] Matrices

System 2 is *a three-phase and two-winding 35MVA, 11kV/132kV, Yy0-connected, three-leg, core-type* power transformer in a single-end-fed power system. The transformer neutral terminal on both LV and HV side is grounded. The power transformer basic parameters are provided from EMTP Rule Book [20], which were

obtained by standard measurements on this transformer (at 50 Hz). The parameters are shown in Table A.2.1, A.2.2 and A.2.3.

Table A.2.1 Power and voltage ratings in System 2

Rated Power (MVA)	35	
Rated Voltage (kV) (line-line value)	11 (low-voltage side)	132 (high-voltage side)

Table A.2.2 Short circuit test data in System 2

Test Type Value	Positive Sequence Short Circuit Test	Zero Sequence Short Circuit Test
Short-circuit losses (kW)	192.53	8.825
Short-circuit current (A)	153.1	70
Short-circuit voltage (kV)	35.213	2.86

Table A.2.3 Excitation test data in System 2

Test Type Value	Positive Sequence Excitation Test	Zero Sequence Excitation Test
Excitation losses (kW)	18.112	115.325
Excitation current (A)	2.39	500
Excitation voltage (kV)	11.01	1.183

Here again, based on the parameters given in Tables A.2.1, A.2.2 and A.2.3, the supporting routine BCTRAN is used to derive a [R]-[L] representation for the transformer, they are shown as follows.

$$
[R] = \begin{bmatrix} R_1 & 0 & 0 & 0 & 0 & 0 \\ 0 & R_2 & 0 & 0 & 0 & 0 \\ 0 & 0 & R_3 & 0 & 0 & 0 \\ 0 & 0 & 0 & R_4 & 0 & 0 \\ 0 & 0 & 0 & 0 & R_5 & 0 \\ 0 & 0 & 0 & 0 & 0 & R_6 \end{bmatrix}
$$

$$
= \begin{bmatrix} .00959610 & & & & & \\ 0.0 & 1.36923346 & & & & \\ 0.0 & 0.0 & .00959610 & & & \\ 0.0 & 0.0 & 0.0 & 1.36923346 & & \\ 0.0 & 0.0 & 0.0 & 0.0 & .00959610 & \\ 0.0 & 0.0 & 0.0 & 0.0 & 0.0 & 1.36923346 \end{bmatrix}
$$

$$
[L] = \begin{bmatrix} L_1 & M_{12} & M_{13} & M_{14} & M_{15} & M_{16} \\ M_{21} & L_2 & M_{23} & M_{24} & M_{25} & M_{26} \\ M_{31} & M_{32} & L_3 & M_{34} & M_{35} & M_{36} \\ M_{41} & M_{42} & M_{43} & L_4 & M_{45} & M_{46} \\ M_{51} & M_{52} & M_{53} & M_{54} & L_5 & M_{56} \\ M_{61} & M_{62} & M_{63} & M_{64} & M_{65} & L_6 \end{bmatrix}
$$

$$
= \begin{bmatrix} 1936.00837538 & & & & & \\ 23125.89314854 & 276371.46702413 & & & & \\ -964.38735758 & -11519.74302843 & 1936.00837538 & & & \\ -11519.74302843 & -137608.3908058 & 23125.89314854 & 276371.46702413 & & \\ -964.38735758 & -11519.74302843 & -964.38735758 & -11519.74302843 & 1936.00837538 & \\ -11519.74302843 & -137608.3908058 & -11519.74302843 & -137608.3908058 & 23125.89314854 & 276371.46702413 \end{bmatrix}
$$

A.2.2 Flux-Current Curve ($\phi - i$) for Inrush Current Simulation

The $\phi - i$ data of the power transformer in System 2 are not available, instead, only a steady state working point is provided in the EMTP Rule Book [20], which is I = 3.37A, ϕ = 28.6Vs. The $\phi - i$ curve was therefore expanded based on available data information and the experience, as shown in Table A.2.4:

Table A.2.4 $\phi - i$ data of power transformer core in System 2

i (A)	ϕ (Vs)
0.34	1.8
0.67	7.15
1.01	10.73
3.37	**28.6**
4.04	30.38
4.72	32.18
5.39	33.96
6.06	35.75
218	37.53

A.2.3 CTs Parameters

The CT data chosen in System 2 are shown in Table A.2.5

Table A.2.5 CT data in System 2

CTs	CT1*	CT2*
Ratio	2000/5	200/5
Accuracy Class	C800	C400
Burden (VA)	200	100
Burden (Ω)	8	4
Power factor	0.5	0.5

* CT1 and CT2 refer to the CTs on LV and HV sides of the power transformer, respectively.

The V-I curve for CT in System 2 was obtained from the reference [39]. According to the V-I curve, the EMTP auxiliary program HYSDAT generates λ-i hysteresis loop, which is then embedded into the basic system model using the EMTP software to implement the simulation of the power transformer system coupled with the CTs.

Related Publications

[1] R. K. Aggarwal, P. L. Mao, "Digital Simulation of the Transient Phenomena in High Voltage Power Transformers with Particular Reference to Accurate Fault Detection", Proceeding of International Conference on Simulation, pp: 390-397, 1998, IEE Conf. Publ. No. 457, IEE, London, United Kingdom.

[2] P. L. Mao, R. K. Aggarwal, Z. Q. Bo "A Novel Technique to Distinguish between Magnetic Inrush and Fault Transients in Power Transformers Using Artificial Neural Network", Proceedings of 33rd University Power Engineering Conference (UPEC'98), Vol.1, pp: 170-173, Sept. 1998, Napier University, Edinburgh, United Kingdom.

[3] P. L. Mao, R. K. Aggarwal, Z. Q. Bo "An ANN Based Electromagnetic Transients Identification Technique for Power Transformer Systems", Proceeding of 3rd International Conference on Power System Transient (IPST'99), pp: 207-212, June 1999, Technical University of Budapest, Budapest, Hungary.

[4] P. L. Mao, R. K. Aggarwal, "Analysis of Transient Phenomena in Power Transformers Using Wavelet Transforms", Proceedings of 34th University Power Engineering Conference (UPEC'99), Vol.2, pp: 471-474, Sept. 1999, Leicester University, Leicester, United Kingdom.

[5] P. L. Mao, R. K. Aggarwal, "A Wavelet Transform Based Decision Making Logic Method for Discrimination between Internal Faults and Inrush Currents in Power Transformers", Accepted for Publication by International Journal of Electrical Power & Energy System.

[6] P. L. Mao, R. K. Aggarwal, "A Novel Approach to the Classification of the Transient Phenomena in Power Transformers Using Combined Wavelet Transform and Neural Network", Submitted to IEEE Transactions on Power Delivery.

[7] P. L. Mao, R. K. Aggarwal, "An Alternative Approach to Digital Simulation of the Transient Phenomena in Power Transformers Utilising EMTP Functions", Submitted to Electric Power Systems Research.

Digital simulation of the transient phenomena in high voltage power transformers with particular reference to accurate fault detection

R. K Aggarwal PhD FIEE,   P Mao BSc

Department of Electronic and Electrical Engineering,
University of Bath, Bath BA2 7AY

Abstract: This paper presents a technique developed to accurately model a power transformer for the purposes of simulating its transient phenomena both under faults and due to magnetising inrush, under a whole variety of different system and fault conditions. The transient characteristics of magnetising inrush currents and internal faults, including symmetrical and asymmetrical faults as well as the winding turn-to-turn and turn-to-ground faults of the power transformer are studied in details. The simulation also includes a model of a current transformer(CT) used for measuring current flowing through the power transformer under faults; in the latter case, the effect of CT saturation on the measured current is also modelled. The purpose of the simulation is to develop alternative techniques for satisfactorily protecting the power transformer under a whole variety of practically encountered faults and at the same time being able to distinguish internal faults from magnetising inrush current.

Keywords: Power transformer, current transformer, transient fault simulation, transformer protection, magnetising inrush current

Introduction

Power transformers are essential and important elements of electrical power systems; in particular, they form a vital link between power generation and transmission lines. However, they do suffer from internal winding faults principally due to insulation failure; these faults must be quickly and accurately detected and the appropriate action taken to isolate the faulty transformer from the rest of the power system, essentially to minimise damage and expedite repairs to damaged equipment thereby keeping both outage times and maintenance costs down. The importance of the latter has increased significantly due to the privatisation and deregulation of the electricity supply industry world-wide.

Conventional transformer protection based on current differential principles offers an adequate means of detecting internal winding faults. However, when transformers are energised, a large magnetising inrush current flows in the transformer windings, setting up a differential current in the protection relays. This is not a fault condition, and therefore does not necessitate the operation of protection, which on the contrary must remain stable during the inrush transient. Since this current has a large second harmonic component in comparison to an internal fault, transformer protection systems are designed to restrain during this inrush transient phenomenon by sensing the large second harmonic.

Due to an increase in demand for electricity, power transmission systems are steadily becoming larger both in capacity and voltage levels and transmission lines, which are normally composed of multi-conductors, are becoming longer. A direct consequence of the latter is an increase in line capacitance to ground and a widespread usage of underground cable sections also contributes to an increase in the line capacitance. This inevitably results in an increase in the level of lower harmonics (in particular the second harmonic) present in the transformer windings due to a fault, arising as a result of the interaction of the line inductance with capacitance; in certain cases its magnitude can be close to or greater than that present in the magnetising inrush current. The problem is accentuated by the employment of special iron-cored materials in modern large transformers; their magnetising characteristics have shown that the increased residual flux can lead to transformer saturation on energisation and a reduction in the second harmonic component present in the inrush current, consequently. Conventional protection techniques will thus have difficulty in distinguishing between an internal fault and an inrush transient. Alternative, improved protection techniques have thus to be found, and in order to achieve this, it is vitally important to be able to accurately model a transformer and simulate its transient phenomena.

This paper presents a technique developed to accurately model a power transformer (and CT) for the purposes of simulating its transient phenomena both under faults and due to magnetising inrush, under a whole variety of different system and fault conditions. The developed technique can accurately

simulate the effects of saturation of power transformers and CTs, and simulations were implemented in a typical 11kV/132 kV power transformer connected between an 11kV generator and a 132kV transmission line.

Mathematical Models

The mathematical models presented in this paper are developed based on the electromagnetic transients program (EMTP) functions; these transformer models are then incorporated into a power system model developed using EMTP.

1) Power transformer modelling

The power transformer models are built up based on the mutual coupling concept. By this method, any multi-winding transformer consisting of n coupling coils can be electrically modelled in terms of the terminal voltage V_i, and current i_i, as well as total flux linkage λ_i, of the ith coil as follows[1]:

$$V_i = R_i i_i + \frac{d\lambda_i}{dt} \qquad (1)$$

where $i=1,2,3,...,n$. Such a transformer can be represented schematically. Figure 1. shows an example of a transformer with six windings.
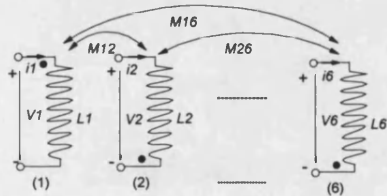
Fig. 1 a schematic representation of a multi-winding transformer

When magnetic saturation is taken into consideration, λ_i becomes a non-linear function of the n-winding currents. That is

$$\lambda_i = \lambda_i(i_1, i_2, \cdots, i_n)$$

For the ith coil, equation (1) can be expanded using the chain rule as follows:

$$V_i = R_i i_i + \frac{\partial \lambda_i}{\partial i_1} \frac{di_1}{dt} + \frac{\partial \lambda_i}{\partial i_2} \frac{di_2}{dt} + \cdots + \frac{\partial \lambda_i}{\partial i_n} \frac{di_n}{dt} \qquad (2)$$

The partial derivatives of the flux linkage λ_i with respect to a winding current i_k $(k=1,2,...,n)$, are the incremental inductance, L_i and M_{ik}, that is

$$L_i = \frac{\partial \lambda_i}{\partial i_i} \qquad (3)$$

$$M_{ik} = \frac{\partial \lambda_i}{\partial i_k} \qquad (i \neq k) \qquad (4)$$

Thus, if the power transformer is a three-phase-two-winding transformer, which consists of the six windings, then the mathematical models for such a transformer can be clearly represented by the following matrix relationship:

$$[V] = [R][i] + [L]\left[\frac{di}{dt}\right] \qquad (5)$$

or

$$\left[\frac{di}{dt}\right] = [L]^{-1}[V] - [L]^{-1}[R][i] \qquad (6)$$

where

$$[R] = \begin{bmatrix} R_1 & 0 & 0 & 0 & 0 & 0 \\ 0 & R_2 & 0 & 0 & 0 & 0 \\ 0 & 0 & R_3 & 0 & 0 & 0 \\ 0 & 0 & 0 & R_4 & 0 & 0 \\ 0 & 0 & 0 & 0 & R_5 & 0 \\ 0 & 0 & 0 & 0 & 0 & R_6 \end{bmatrix} \qquad (7)$$

$$[L] = \begin{bmatrix} L_1 & M_{12} & M_{13} & M_{14} & M_{15} & M_{16} \\ M_{21} & L_2 & M_{23} & M_{24} & M_{25} & M_{26} \\ M_{31} & M_{32} & L_3 & M_{34} & M_{35} & M_{36} \\ M_{41} & M_{42} & M_{43} & L_4 & M_{45} & M_{46} \\ M_{51} & M_{52} & M_{53} & M_{54} & L_5 & M_{56} \\ M_{61} & M_{62} & M_{63} & M_{64} & M_{65} & L_6 \end{bmatrix} \qquad (8)$$

$$[V] = [V_1, V_2, V_3, V_4, V_5, V_6]^T$$

$$[i] = [i_1, i_2, i_3, i_4, i_5, i_6]^T$$

$$\left[\frac{di}{dt}\right] = \left[\frac{di_1}{dt} \quad \frac{di_2}{dt} \quad \frac{di_3}{dt} \quad \frac{di_4}{dt} \quad \frac{di_5}{dt} \quad \frac{di_6}{dt}\right]^T$$

and V_1, V_2, V_3, V_4, V_5 and V_6 are the terminal voltages of the primary and secondary windings respectively; i_1, i_2, i_3, i_4, i_5 and i_6 are the currents of the primary and secondary windings respectively; R_1, R_2, R_3, R_4, R_5 and R_6 are the resistances of the primary and secondary windings respectively; L_1, L_2, L_3, L_4, L_5 and L_6 are the self inductances of the primary and secondary windings respectively; M_{ij} are the mutual indutances between windings i and j respectively $(i=1,2,...,6; j=1,2,...,6; i \neq j)$.

It should be emphasised that since λ_i is a non-linear function of the 6-winding currents, it is related to the nonlinearity of the power transformer core, which in turn is decided by the non-linear magnetising curve of the power transformer core. In a practical simulation, when saturation effects of the power transformer core are taken into account, the transient characteristic of the power transformer

can be simulated equivalently using the mutual coupling models, in which the matrix *[L]* is linear, together with a non-linear magnetising branch added to the winding closest to the core through the *EMTP* software.

2) Modelling of an internal winding fault

The principle used to model a fault between a coil turn and earth or between turn and turn is to divide the faulty coil[4], as shown in Figures 2(a) and 2(b) respectively.

(a)   (b)
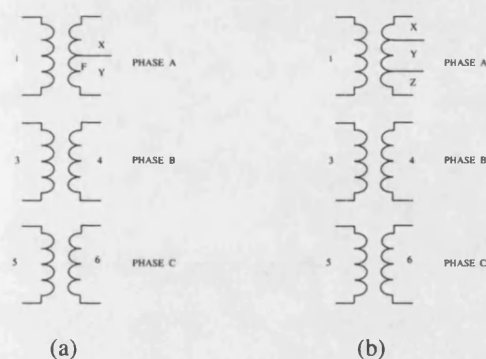
Fig. 2 Internal fault Modelling in a power transformer (a) turn-to-earth fault(b) turn-to-turn fault

When the power transformer is without an internal winding fault, matrices [R] and [L] for a three phase transformer with two windings are of 6 order. When a turn-to-earth fault occurs, the transformer can be described with two *7x7* matrices *[R]₇ₓ₇* and *[L]₇ₓ₇*. Similarly, two *8x8* matrices are required to describe the turn-to-turn fault. For example, when a turn-to-earth fault occurs at point *F* of the secondary winding 2, the *7x7* matrices *[R]₇ₓ₇* and *[L]₇ₓ₇* will be determined as follows:

$$[R]_{7x7} = \begin{bmatrix} R_1 & 0 & 0 & 0 & 0 & 0 & 0 \\ 0 & R_X & 0 & 0 & 0 & 0 & 0 \\ 0 & 0 & R_Y & 0 & 0 & 0 & 0 \\ 0 & 0 & 0 & R_3 & 0 & 0 & 0 \\ 0 & 0 & 0 & 0 & R_4 & 0 & 0 \\ 0 & 0 & 0 & 0 & 0 & R_5 & 0 \\ 0 & 0 & 0 & 0 & 0 & 0 & R_6 \end{bmatrix}$$

$$[L]_{7x7} = \begin{bmatrix} L_1 & M_{1X} & M_{1Y} & M_{13} & M_{14} & M_{15} & M_{16} \\ M_{X1} & L_X & M_{XY} & M_{X3} & M_{X4} & M_{X5} & M_{X6} \\ M_{Y1} & M_{YX} & L_Y & M_{Y3} & M_{Y4} & M_{Y5} & M_{Y6} \\ M_{31} & M_{3X} & M_{3Y} & L_3 & M_{34} & M_{35} & M_{36} \\ M_{41} & M_{4X} & M_{4Y} & M_{43} & L_4 & M_{45} & M_{46} \\ M_{51} & M_{5X} & M_{5Y} & M_{53} & M_{54} & L_5 & M_{56} \\ M_{61} & M_{6X} & M_{6Y} & M_{63} & M_{64} & M_{65} & L_6 \end{bmatrix}$$

The position of the fault point is expressed by

n_X = number of turns of "sub-coil" x

n_Y = number of turns of "sub-coil" y

and the parameters in the above matrices [R] and [L] are defined by the following equations:

$$R_X = \frac{n_X}{n_2} R_2 \; ; \qquad R_Y = \frac{n_Y}{n_2} R_2 \; ; \qquad K = \frac{n_X}{n_Y} \; ;$$

where K is the voltage ratio between coils X and Y, and

$$L_X = \frac{L_2}{(1/K^2) + (2\sqrt{1-\sigma_{XY}}/K) + 1}$$

$$L_Y = \frac{L_2}{K^2 + 2K\sqrt{1-\sigma_{XY}} + 1}$$

$$M_{XY} = \frac{L_2\sqrt{1-\sigma_{XY}}}{K + 1/K + 2\sqrt{1-\sigma_{XY}}}$$

$$M_{Xi} = (K/(K+1))M_{2i} \; ; \qquad M_{Yi} = (1/(1+K))M_{2i} \; ;$$

L_2 and M_{2i} are given by the original *6x6* matrix. For turn-to-turn faults shown in Fig.2(b), the *8x8* matrices *[R]₈ₓ₈* and *[L]₈ₓ₈* will be required, and the calculation method is given in reference [4] .

The method used for simulating the internal winding faults is based on the *BCTRAN* routine of EMTP. Basic steps are as follows:

Step 1: use the *BCTRAN* routine to obtain the linear matrices *[R]* and *[L]* of the power transformer, which is without considering the internal winding faults.

Step 2: modify the above matrices *[R]* and *[L]* according to the internal winding fault type and obtain the new internal winding fault matrices *[R]** and *[L]**;

Step 3: carry out the internal winding fault simulation using the modified internal winding fault matrices *[R]** and *[L]*** by the *EMTP* software

3) CT modelling

CT models developed are based on those outlined in reference [5]. This model comprises of an equivalent circuit built around an ideal transformer as shown in Fig.3. The magnetising branch is represented as a non-linear inductor: it is presented by λ-i hysteresis loop.
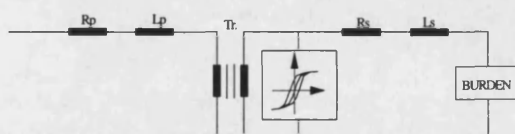
Fig.3 EMTP-based CT Models (Rp- primary winding resistance; Lp- primary winding leakage inductance; Rs- secondary winding resistance; Ls- secondary winding leakage inductance; Tr- ideal transformer)

A Description of the Simulated System

The power transformer transient phenomenon is simulated in a system comprising of a typical 11kV/132kV power transformer connected between an 11kV generator and a 132kV transmission line, as shown in Figure 4.
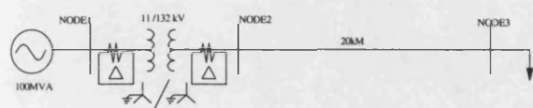
Fig.4 System configuration simulated for Case Studies

In order to fully investigate the effects of fault transients and inrush currents, on say, the differential protection of a power transformer, the various power transformer inrushes and internal faults are simulated using the foregoing transformer models based on *EMTP* functions, which are capable of representing transformers, transmission lines, various types of switches, electrical machines, and control system dynamics, etc.

Since the variation of winding connections in the power transformer will influence the transient performances of faults and inrush currents, and will make a difference to the protection scheme chosen, the transient performances of various power transformer connections, including the Y-Δ, Δ-Y, and Y_0-Y_0 connections, are also simulated in this paper. For simplicity, Figure 5 only shows a connection of the differential protection for a Y_0-Y_0 connected power transformer.
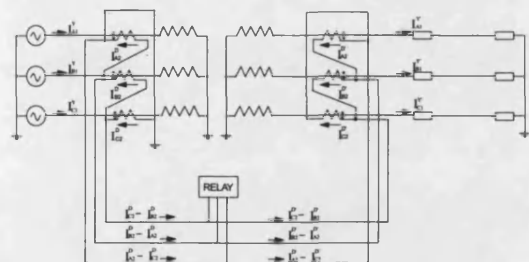
Fig. 5 A typical power transformer differential protection scheme

Moreover, since the transient performance of power transformers are related to a power system load demands, the variation in load demands has been taken into consideration in simulation for each power transformer connection.

Case Studies and Simulation Results

In order to demonstrate the effectiveness of the developed power transformer and CT models as fully as possible, some typical simulation results are given in this section.

(1) Simulation of power transformer under internal faults

Figs 6-9 typify transient response results of the power transformer for *(i)* three phase short-circuit fault on secondary side *(Fig 6)* , *(ii)* A-phase 5% winding fault on secondary side *(Fig 7)*, *(iii)* A-phase to ground fault on mid-point of winding at secondary side *(Fig 8)*, and *(iv)* Energisation with A-phase to ground fault on secondary side of the power transformer *(Fig 9)*. It is apparent from these results that there is a wide variation in the fault current waveforms depending upon the type of fault and its location. Importantly, any new protection technique must be capable of satisfactorily dealing with such diversity of fault data.

(a) primary current of transformer

(b) secondary current of transformer

(c) differential current of transformer
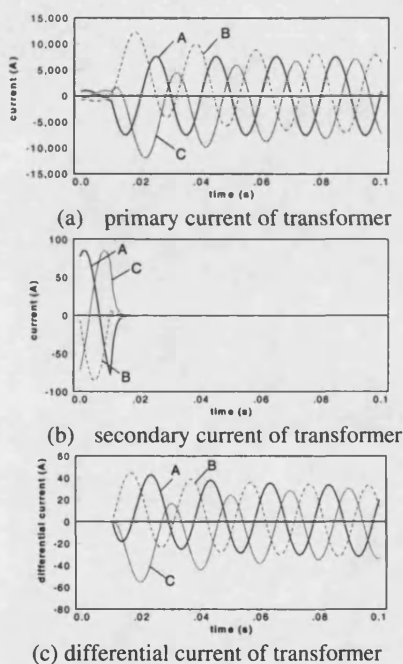
Fig.6 Three phase short-circuit fault on transformer's secondary side

(a) primary current of transformer

205

(b) secondary current of transformer

(c) current in the turn-to-turn short-circuited loop

(d) differential current of transformer
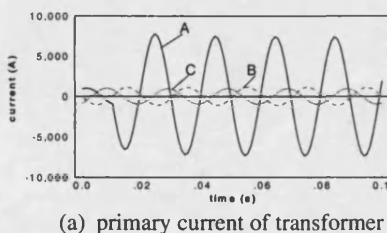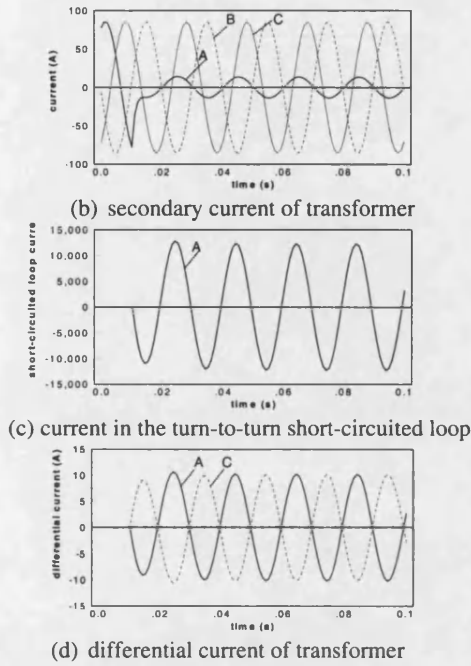
Fig.7 A-phase 5% winding fault on transformer's secondary side

(a) primary current of transformer

(b) secondary current of transformer

(c) differential current of transformer
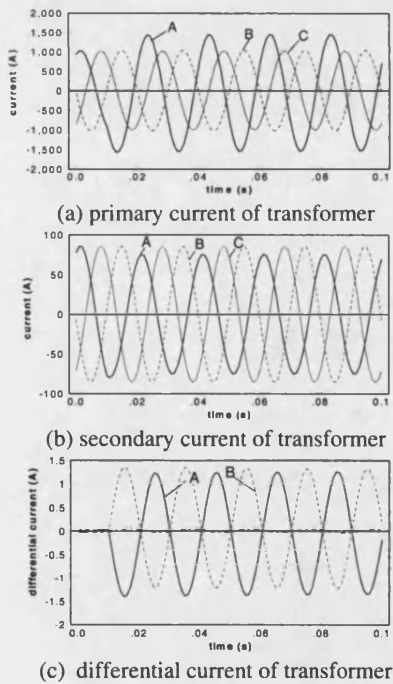
Fig.8 A-phase to ground fault on mid-point of winding on transformer's secondary side

(a) primary current of transformer

(b) differential current of transformer
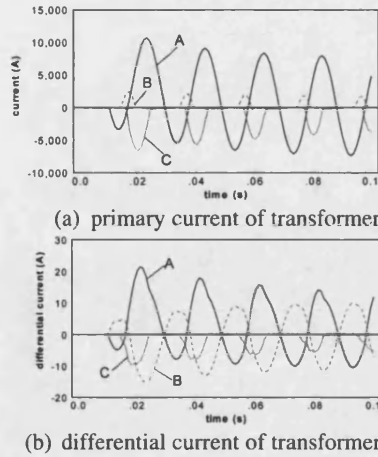
Fig.9 Energisation with A-phase to ground fault on transformer's secondary side

(2) Simulation of power transformer internal faults with CT effects included

The effects of CT saturation on internal fault transient characteristics of the power transformer are simulated under such conditions as: *(i)* different fault inception angles, *(ii)* different levels of CT remnant fluxes and *(iii)* different type of CT secondary burdens.

(i) Effect of fault inception angle on measured CT currents

Since the D.C. component of the fault current is the dominant factor in causing CT saturation and it is influenced by the fault inception angle, two case studies involving an 'A'-earth fault on the secondary side of the power transformer near V $_{A}0^0$ and V $_{A}90^0$, respectively were simulated; the results are depicted in Fig.10. From Fig.10 (b) we can see that for the fault inception angle near voltage zero, the D.C. component is very large and as a consequence, the CT core flux exceeds the saturation point value of the 4.0 Wb as evident from Fig10(a); this manifests itself into distorting the measured current signal through the CT secondary as apparent from Fig10(b). In sharp contrast, when a fault occurs near voltage maximum, there is little D.C. offset, as expected, the CT core flux stays below the saturation level and the measured CT secondary current is faithfully reproduced, as evident from Figs. 10(c)-10(d).

(a) flux with 70% remnant flux for V $_A0^0$ fault

(b) A-phase differential current for V $_A0^0$ fault

(c) flux with 70% remnant flux for V $_A90^0$ fault

(d) A-phase differential current for V $_A90^0$ fault
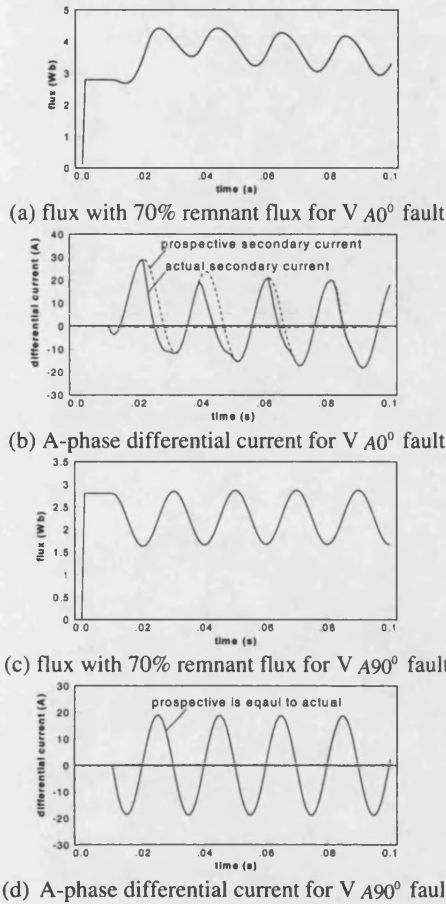
Fig.10 Simulation with different fault inception angles

(ii) Effect on CT output due to remnant flux

In practice, there are many conditions (such as line auto-reclosure after a transient fault clearance) that may leave remnant flux on the core of the CT; this can have a significant bearing on the CT secondary current measured. Comparing Figs 10(a)-(b) with Fig 11(which are for the same fault condition except that in the case of the former there is a 70% remnant flux on the CT core right at the outset), it is apparent that in the absence of remnant flux, the CT core remain devoid of saturation inspite of D.C. offset and hence the measured CT fault current is faithfully reproduced as evident from the waveforms shown in Fig 11.
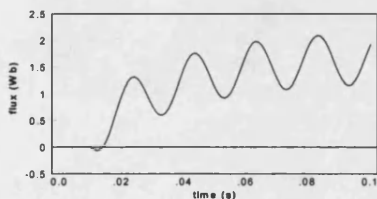
(a) flux without remnant flux for V $_0$ fault
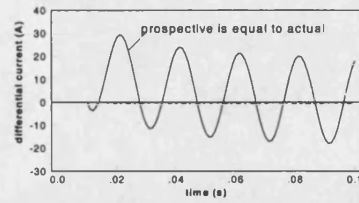
(b) A-phase differential current for V $_A0^0$ fault

Fig.11 Effect of remnant flux on CT core

(iii) CT Simulation with different secondary burdens

It is well known that a purely resistive burden can cause more saturation than a resistive inductive burden or a purely inductive burden. In order to investigate the effect of the CT's secondary burden on CT saturation, two cases were simulated, and their results are shown in Fig.12. As shown in Fig.12(b), the CT is driven into saturation much earlier on, i.e. in the first half-cycle compared to Fig.12(a); as a consequence, a distortion in the secondary current of the CT occurs.

(a) A-phase differential current with resistive inductive burden

(b) A-phase differential current with purely resistive burden
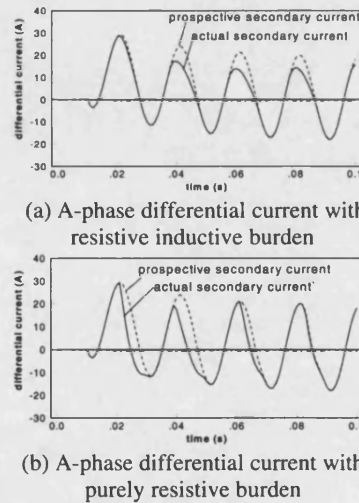
Fig.12 Simulation with different CT secondary burdens

(3) Simulation of magnetising inrush currents

The magnetising inrush currents of the power transformer were simulated in detail under (*i*)different energisation angles, (*ii*)different remnant fluxes on the iron-core of the power transformer, and (*iii*)different three-phase winding connections of the power transformer.

(i) effects of different transformer energisation angles

When a power transformer is energised with secondary open circuited at different points-on-wave from an open-circuited position, the inrush current waveforms with respect to zero remnant flux are depicted in Fig.13. First of all considering the switch-on at voltage maximum-point-on wave with respect to the 'A'-phase, Fig.13(a) typifies the value of the inrush current waveforms; their magnitudes are relatively small (which gradually die down due to losses) and the inrush current is virtually non-existent in the 'A'-phase. This is expected by virtual of the fact that the flux change in the transformer core is small. However, when the transformer is energised near voltage zero, the magnitudes of the inrush current increase and this current now also appears on the 'A'-phase as evident from Fig 13(b). Again, this is expected due to the fact that for this switch-on condition the change in core flux is nearly twice that in the previous case of energisation near voltage maximum.

(a) primary current of transformer under V $_{A90^0}$

(b) primary current of transformer under V $_{A0^0}$
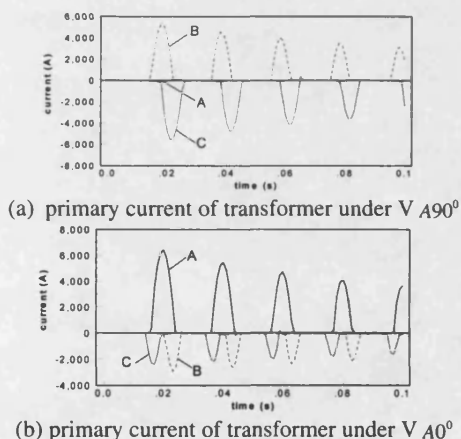
Fig.13 Effect of transformer energisation angles on inrush current

(ii) effects of remnant flux on inrush current

The presence of remnant (or residual) flux in the core can further increase the magnetising inrush current. This is evident from a comparison of Fig 14 and Fig 13(b), the former being the inrush current when there is a initial remnant flux of 30% on the transformer core. As can be seen, the presence of the residual flux very significantly increases the magnitudes of the magnetising inrush current on all the three phase. In practice, this phenomenon can further accentuate the problems of instability with transformer protection systems.

primary current of transformer with 30% remnant flux
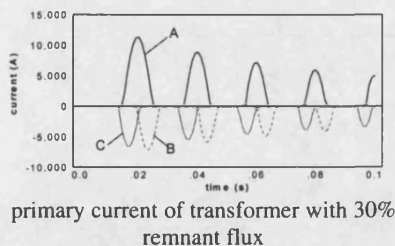
Fig.14 magnetising inrush current with initial remnant flux on core

(iii) effect of different winding connections on inrush current

The electrical connections of a transformer has an affect on the inrush current flowing in the phases. In order to ascertain the effect of different electrical connections of a transformer on inrush current, two cases were simulated, and their results are shown in Fig.15. In Fig.15(a), the transformer is energised from its Y-side with no-load condition, i.e. the terminals of Δ-connected secondary are disconnected. In this case, the Δ winding acts as a trap for some of the harmonics associated with the inrush current when the transformer is energised. In Fig.15(b), when the transformer is energised from its Δ-connected primary side, the inrush current phenomena is simpler in comparison to the Y-Δ case, as there is no auxiliary source present in Δ-Y connection. Again, the Δ winding acts as a trap for the inrush current thereby lowering its magnitude. In conclusion, the inrush current under Y-Δ connection is much greater than when energised under Δ-Y connection by virtual of the Δ winding acting as a trap for the inrush current.

(a) primary current of transformer with Y-Δ connection

(b) primary current of transformer with Δ-Y connection
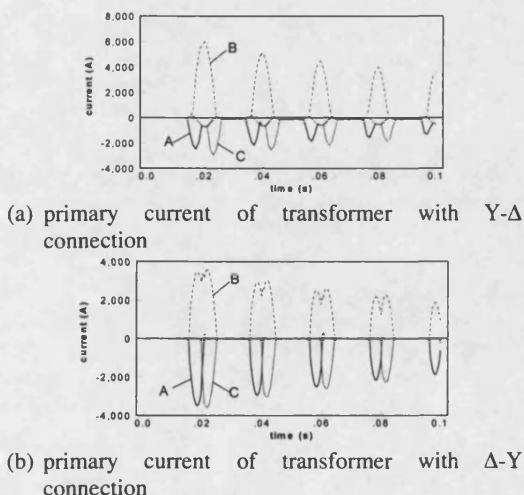
Fig.15 magnetising inrush current with different transformer winding connections

(4) Simulation of power transformer external faults with CT effects included

It is well known that when fault currents are large for certain external faults, it is possible for the CTs to saturate. In order to investigate the effect of the CT saturation on the differential protection under an external fault condition, two cases were simulated, and their results are shown in Fig.16 and Fig.17, respectively. As shown in Fig.16, the resulting current waveforms of the CT secondary winding on both sides of the transformer distort to a different degree; the differential current is the difference between the two saturated current waveforms. In Fig.17, the differential current is the difference between the unsaturated current waveform and the saturated current waveform. In this case, the differential current is larger than in Fig.16. In conclusion, when the CT's saturation characteristics of the primary side of the transformer are not in agreement with the secondary side of the transformer, the transient imbalance current is sufficiently large, and this can lead to the mal-operation of the differential protection.
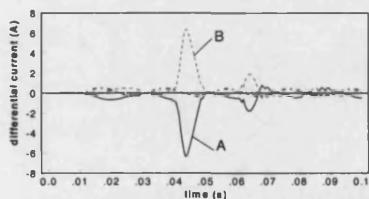
differential current of transformer

Fig.16 three-phase short-circuit with saturation of both CTs on low and high voltage sides of transformer
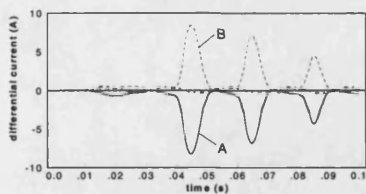
differential current of transformer

Fig.17 three-phase short-circuit with saturation of only CT on low voltage side of transformer

Conclusions

In this paper, a model and methodology for accurately simulating the transient behaviour of three phase power transformers and the CTs have been presented. The transient behaviour of a power transformer under magnetising inrush currents and internal faults, including symmetrical and asymmetrical faults as well as the winding turn-to-turn and turn-to-ground faults under various system conditions have been simulated and examined in detail. CT saturation and its effects on the differential currents in various situations have also been studied in detail. Results clearly indicate that the power transformer magnetising inrush current phenomenon, and particularly the effects of CT saturation, can lead to the mal-operation of conventional differential protection of power transformers. It is now hoped that this technique of accurately modelling the transient phenomenon in transformers has laid the basis for developing new improved protection systems for power transformers.

References

[1] F.A.Fouad, T.W.Nell and N.A. Demerdash, "Saturated transformer inductances determined by energy perturbation techniques", IEEE Trans. Power Apparatus and Systems, Vol. PAS-101, No.11, Nov 1982, pp.4185~4193

[2] Inagaki, Keizo; Higaki, Masaru; Matsui, Yoshiaki and Kurita, Kentaro, "Digital Protection method for Power Transformers Based on an Equivalent Circuit Composed of Inverse Inductance", IEEE Trans. on Power Delivery, Vol.3, No.4, October 1988, pp:1501~1510

[3] P.Liu, O.P.Malik, C.Chen, G.S.Hope, and Y.Guo "Improved Operation of Differential Protection of Power Transformers for Internal Faults", IEEE Trans on Power Delivery, Vol. 7, No.4, pp:1912~11919, 1992

[4] Patrick Bastard, Pierre Bertrand and Michel Meunier, "A Transformer Model for Winding Fault Studies", IEEE Trans. on Power Delivery, Vol. 9, No.2, April 1994.pp:690~699

[5] M.Kezunovic; C.W.Fromen; F.Phillips "Experimental Evaluation of EMTP-Based Current Transformer Models for Protective Relay Transient Study", IEEE Trans. on Power Delivery, Vol.9, No.1, pp:405~413, January 1994

[6] Kang, Y.C.; Park, J. K.; Kang, S.H.; Johns, A.T.; Aggarwal, R.K., "An Algorithm for Compensating Secondary Currents of Current Transformers", IEEE Transactions on Power Delivery, Vol 12, No 1, January 1997, pp: 116~124.

[7] Lin, C. E.; Cheng, C. L.; Huang, C. L.; Yeh, J. C. "Investigation of magnetizing inrush current in transformers. Part I - Numerical simulation". IEEE Transactions on Power Delivery Vol 8, No 1, Jan 1993, pp: 246-254

[8] V Brandwajn, H.W. Dommel, and I. I. Dommel, "Matrix Representation of Three-Phase N-Winding Transformers for Stead-State and Transient Studies", IEEE Trans. on Power Apparatus and System, Vol. PAS-101, No.6, June 1982, pp:1369~1378

A NOVEL TECHNIQUE TO DISTINGUISH BETWEEN MAGNETIC INRUSH AND FAULT TRANSIENTS IN POWER TRANSFORMER USING ARTIFICIAL NEURAL NETWORK

P L Mao, R K Aggarwal, Z Q Bo

University of Bath, UK

ABSTRACT

This paper presents a novel technique for discrimination between magnetising inrush and internal fault currents based on the detection of switching operations and faults generated high frequency transients using the neural network. The detector, tuned to a band of high frequencies, is connected to the power transformer through current transformers(CTs) which is used to capture the high frequency transient current signals. The captured signals are then employed to train a neural network. Simulation results presented clearly show that the proposed neural network based technique is able to accurately distinguish a magnetising inrush from an internal fault current and therefore can be used as an alternative and effective method to discriminate between the magnetising inrush and internal faults in power transformer protections, thereby enhancing protection performance.

I. INTRODUCTION

Accurate discrimination between magnetising inrush and internal fault currents is of importance to the correct operation of the differential protection of the power transformer. However, under the magnetising inrush condition, a very large differential current that is in fact not an internal fault current, will be produced in the differential protection; this can lead to protection relay maloperation. To avoid undesired tripping due to inrush currents, the conventional methods hinge upon either implementation of delays in the protection devices or restraining the relay operation according to the second harmonic content of the measured current. The latter is based on the assumption that the second harmonic component of the magnetising inrush is considerably larger than an internal fault current.

However, it has been found that in certain cases, particularly when the power transmission systems are longer and composed of multi-conductors, there will be an increase in the capacitance from line to line and from line to ground. This inevitably results in an increase in the level of lower harmonics (in particular the second harmonic) presented in the transformer windings due to a fault, and the second harmonic component of the internal fault can be close to or greater than that present in the magnetising inrush current. On the other hand, the second harmonic component in magnetising inrush currents is comparatively smaller in power transformers with new built-in transformer cores which operate at higher magnetic field density. This effectively means that the relays can no longer be relied upon for protecting power transformers.

Thus, it becomes increasingly difficult to perform an accurate discrimination between magnetising inrush and internal fault currents.

Successful applications of neural networks in the area of power engineering have demonstrated that they can be employed as an alternative method for solving certain long standing problems, where conventional techniques have experienced difficulties. In the context of protection, neural networks have been applied to the power transformer protection to discriminate the magnetising inrush from the internal faults[1,2,3], transient identification and directional discrimination for protection for EHV transmission lines, etc.

The method presented in the paper is different from conventional schemes, which are based on using the power frequency or second harmonic signals; it detects the high frequency components in a current transient signal to classify the patterns in the waveforms, thereby discriminating between the two disturbances. Particular emphasis is placed on the design of a neural network. Simulation results presented clearly show that the proposed neural network has the potential to accurately distinguish the magnetising inrush from internal faults.

II. DIGITAL SIMULATION OF POWER TRANSFORMER TRANSIENTS

The digital simulations of the power transformer magnetising inrush and faults are implemented in a typical 11kV/132kV power transformer connected between an 11kV generator and a 132kV transmission line using the electromagnetic

transients program (EMTP). The CT model and its saturation effect to differential currents have also been taken into consideration. To evaluate the high frequency behaviour of the transformer, particularly under fault conditions, the shunt capacitances were added to the transformer model[4]. The simulated power transformer system is shown in Figure 1.
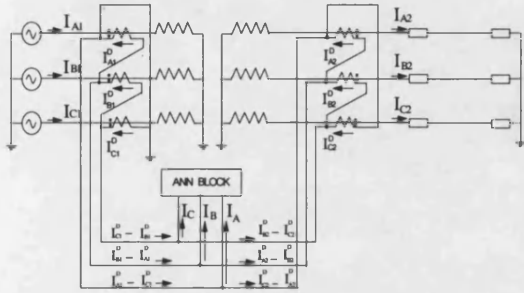
Figure 1 The studied power transformer system

A. Simulation of internal fault

Figures 2 and 3 show two typical results of simulations of *(i)*a three-phase-to-ground internal fault occurring on the high voltage side of the power transformer, and *(ii)*a-phase 5% winding fault on the high voltage side of the power transformer. For each fault case, three phase differential currents are given in each Figure.
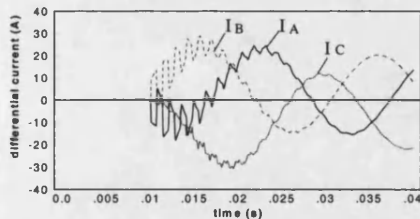
Figure 2 Three-phase-to-ground fault on high voltage side
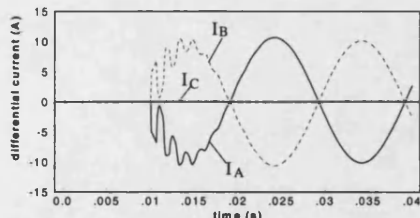
Figure 3 A-phase 5% winding fault on high voltage side

It is apparent that fault generated high frequency components current are presented in the current signals. This is as a direct consequence of the effects of the coupled winding inductance and capacitance of the power transformer, together with the distributed inductance and capacitance of the

transmission line, that is, when a fault occurs, the current is interrupted, and the energy originally stored in the inductance is transferred back and forth between the inductance and the capacitance until the stored energy is finally dissipated by the system resistance.

B. Simulation of magnetising inrush

The various magnetising inrush current conditions have been simulated, including the effects of different transformer energisation angles. Figure 4 typifies a simulation result of the magnetising inrush currents of the power transformer.
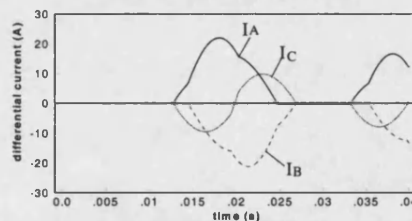
Figure 4 three-phase differential current waveshapes under the magnetising inrush condition

III. DETECTION OF FAULT GENERATED HIGH FREQUENCY CURRENT TRANSIENT

In general, when a fault occurs on a power transformer, DC offset, fundamental frequency and non-fundamental frequency components are produced. It has been shown that non-fundamental frequency components change as the power transformer operating conditions, such as various magnetising inrush and fault conditions change. This can be clearly seen by the spectrum analysis of the differential current signals.

A. Behaviour of high frequency electromagnetic transients

Figure 5 presents the spectra of the differential currents corresponding to Fig.3 and Fig.4.
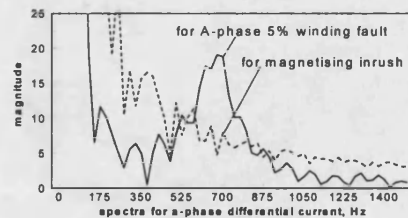
Figure 5 Spectra of differential currents

It is important to note that there is a much larger non-fundamental frequency that is around approximate 700 Hz for the internal fault case than the magnetising inrush case, but decays more rapidly than the magnetising inrush case. This

demonstrates the fact that the high frequency signal features between the magnetising inrush and internal fault currents are different and these can be used as the basis to distinguish the magnetising inrush from internal fault currents through pattern recognition techniques such as neural network.

B. Detection of high frequency current signals
The switching operations and fault generated high frequency current signals are captured through a specially designed relay hardware/software, which is utilised to distinguish the magnetising inrush from internal faults to the protected transformer by the artificial neural network. Fig.6 shows the basic arrangement of this technique.
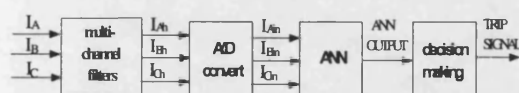
Figure 6 ANN block diagram of the protection scheme
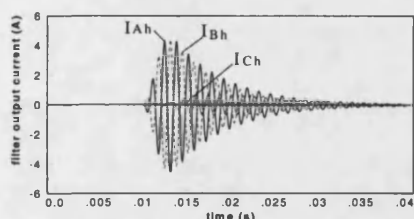
(a) high frequency differential currents
for three phase short-circuit fault
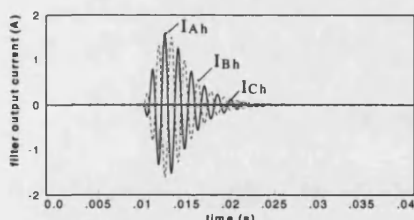
(b) high frequency differential currents
for 5% winding fault
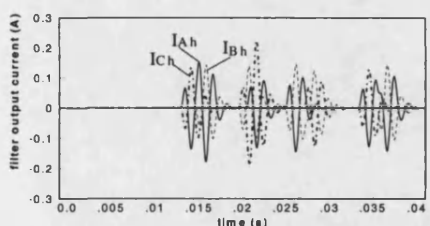
(c) high frequency differential currents
for magnetising inrush current

Figure 7 high frequency differential currents under internal faults and a magnetising inrush current

As shown in Fig 6, the differential current signals I_A, I_B and I_C are captured from each end of the CTs. The multi-channel filter unit which consists of the main part of the relay is then used to extract high frequency differential current signals I_{Ah}, I_{Bh}, and I_{Ch} (700Hz centre frequency). Fig.7 shows the filter outputs corresponding to Fig.2, Fig.3 and Fig.4.

IV. ARTIFICIAL NEURAL NETWORK BASED PROTECTION SCHEME

A. Input selection of the neural network
Since an ANN has multi-input parallel processing ability, the moving data window length is a major factor which needs to be considered carefully. Theoretically, a long data window can produce more selective frequency response characteristics, but in general, a fast trip signal is needed, and it follows that a short data window which reduces the size of the ANN is required. The appropriate data window length must meet both of these requirements. In this study, the high frequency differential signals are extracted by the moving data window process to form the ANN training/testing data set where the length of a moving window of the waveform is 1.43ms, and there are 6 samples in one window (this corresponds to 4.2 kHz sampling frequency). Thus, the three-phase differential currents comprising of 18 samples are used as the input signals to ANN, and each moving window takes three new samples in.

The training and test patterns are generated by sampling the simulation data attained from the EMTP. In order to cover the typical scenario of interest, various power transformer system operating conditions are simulated, which include the effects of variations in source parameters, fault location, fault inception angle, fault resistance, and fault types such as symmetrical and asymmetrical faults as well as winding turn-to-turn faults. Some of the generated sampling patterns are used for training and some for testing and performance evaluation.

B. Network structure and training
A total of 18 sampled high frequency differential current signals are employed as inputs to the neural network. The target output of the ANN was built in such way that the network was trained to produce a *0* output when the presented signals were the magnetising inrush or/and an external fault; and an *1* output for the internal faults.

The selection of the number of hidden layers and hidden neurons in ANN is quite important. As known, there are open issues and have to be consequently determined by experimentation

involving training and testing various network configurations. The process is terminated when a suitable network with a satisfactory performance is established. In this study, one hidden layer with 14 neurons produced an acceptable performance; the ANN output converged in a shortest time when a sigmoid function was used. The complete structure of the ANN employed is shown in Figure 8.
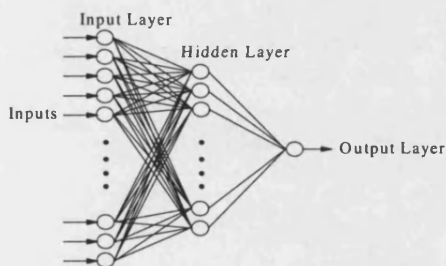
Figure 8 ANN structure

V. PERFORMANCE EVALUATION

The ANN was extensively tested and was then embedded into the power transformer system shown in Fig 1 to evaluate the performance and ability of the decision making. In practice, a target tolerance of 0.1 was used, meaning that the network was trained to produce a response of 0.9 or greater to represent one class and 0.1 or less to represent the other class.

Figures 9(a) to (d) respectively give the responses of the ANN-based protection scheme.
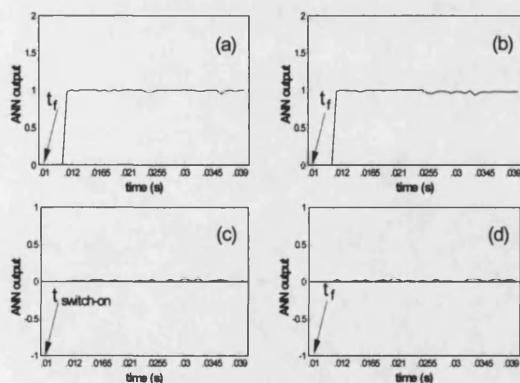
Figure 9 The responses of the ANN based power transformer differential protection. (a) an internal three-phase-to-ground fault occurring on the high voltage side; (b) a-phase 5% internal winding fault occurring on the high voltage side; (c) the transformer is energised when A-phase switch-on angle of a power supply is zero (d) external fault occurring on the high voltage side; t_f=fault inception time; $t_{switch-on}$=transformer energising time.

From these results it can be clearly seen that the ANN- based protection scheme gives correct responses to internal faults, and effectively blocks the protection operation in the cases of the magnetising inrush and external fault.

VI. CONCLUSIONS

This paper presents a novel technique for discrimination between the magnetising inrush and internal faults based on the detection of the switching operations and faults generated high frequency transient current signals using a neural network. Results presented clearly show that the proposed neural network is able to accurately distinguish the magnetising inrush from internal fault currents and therefore can be used as an alternative and effective method to discriminate between magnetising inrush and internal faults in power transformer protection, effectively increasing the reliability and dependability of the power transformer protection system.

VII. REFERENCES

[1]. G Perez, A J Flechsig, J L Meador and Z Obradovic, "Training an artificial neural network to discriminate between magnetizing inrush and internal fault", IEEE Trans. On Power Delivery, Vol. 9, No. 1, pp.434-441, January 1994.

[2]. Pihler, B Grcar and D Dolinar, "Improved operation of power transformer protection using artificial neural network", IEEE Trans. On Power Delivery, Vol. 12, No. 3, pp.1128-1136, July 1997.

[3]. Bastard, M Meunier and H Regal, "Neural-network-based algorithm for power transformer differential relays", IEE Proc., Gener. Transm. Distrib., Vol. 142, No. 4, pp. 386-392, July 1995.

[4]. Z Q Bo, R K Aggarwal, A T Johns, "A New Measurement Technique for Power Transformer Faults", 30th University Power Engineering Conference, Sept. 1995

[5]. A T Johns, Z Q Bo and R K Aggarwal, "A novel non-unit protection scheme based on fault generated high frequency noise on transmission lines", IEE Pul. No.368 , pp65-68

[6]. Atish K Ghosh and David L Lubkeman, "The classification of power system disturbance waveformes using a neural network approach", IEEE Trans. on Power Delivery., Vol. 10, No. 1, pp.109-115, January 1995.

[7]. P.Liu, O.P.Malik, C.Chen, G.S.Hope, and Y.Guo " Improved Operation of Differential Protection of Power Transformers for Internal Faults", IEEE Trans on Power Delivery, Vol. 7, No.4, pp:1912~11919, 1992

[8]. Patrick Bastard, Pierre Bertrand and Michel Meunier, " A Transformer Model for Winding Fault Studies" , IEEE Trans. on Power Delivery, Vol. 9, No.2, pp:690~699, April 1994.

An ANN Based Electromagnetic Transients Identification Technique for Power Transformer Systems

P L Mao, R K Aggarwal, Z Q Bo

Department of Electronic and Electrical Engineering, University of Bath, Claverton Down, Bath BA2, 7AY

Abstract - **Power transformers are subject to transient overvoltages/overcurrents which invariably accompany any disturbance such as a switching operation, internal/external fault, etc. It is imperative to be able to accurately distinguish the various types of disturbances both for correct transformer design (in terms of insulation level specification) and the associated protection technique design. Conventional techniques based on power frequency signals have limitations in distinguishing correctly the different types of disturbances. This paper addresses the problem through the use of an artificial neural network (ANN), which has the ability to map highly complex non-linear input/output patterns and is capable of very effectively dealing with the high frequency transient phenomena associated with any disturbance. The results presented show that the proposed technique is able to not only capture the high frequency current transient signals inside a transformer, but also fast and accurate identification of the cause and nature of the transients.**

Keywords: Power transformer, High frequency signal, Artificial neural network, Transient identification

I. INTRODUCTION

Power transformers are subject to many types of electromagnetic transient disturbances, which result in abnormal voltages and currents. For example, physical phenomena such as fault and lightning may generate transient overcurrents and/or overvoltages. On the other hand, normal operating procedures, such as breaker closing and switching of equipment cause electromagnetic transients. Overcurrents may damage the power transformer due to excessive heat dissipation and the high dynamic mechanical stress. Overvoltages may result in flashovers or insulation deterioration, and eventual breakdown of the power transformer.

Electromagnetic transient analysis of the power transformer plays an important role in the design and operation of the power transformer. It is widely accepted that measurement of transient-induced quantities and determination of the nature of transients would be invaluable. It would not only provide useful information in terms of optimal design and functionality of the power transformer, but also provide information for designing new protection schemes. The signals generated by switching are high frequency transients in nature, a genuine fault on the transformer will also generate high frequency noise signals. They cannot be detected by conventional techniques, which are mainly based on the measurement at power frequency signals. In this respect, recent developments in transient detection and identification techniques[1] make it possible the on-line measurement of switching transients and fault transients. However, distinguishing between the signals generated by the two events cannot be accomplished using the more traditional techniques. In this respect, the advent of ANNs, with their ability to map complex and highly non-linear input/output patterns, provides an attractive solution to the problem of transient identification in the power transformer system.

In recent years, a few studies which investigate the feasibility of using ANNs for transformer protection have been reported[2,3,4]. The work reported in this paper is concerned with designing a novel technique for transient identification in the power transformer system using neural networks. A specially designed transient detector unit is firstly applied to capture the various transient signals. The spectral energies of these captured signals are extracted, and then used to train a neural network in order to determine the source and nature of the transient in terms of the changes in spectral energies. The neural network takes into consideration the various transient events. The results presented demonstrate the feasibility of the new technique. It can be an attractive alternative for distinguishing the magnetising inrush from internal faults in the field of power transformer protection.

II. ELECTROMAGNETIC TRANSIENTS SIMULATION IN POWER TRANSFORMER

2.1 Studied System

Transient simulations in a power transformer are implemented using the electromagnetic transients program *(EMTP)* in a typical 11 kV/132 kV three-phase power transformer connected between an 11kV generator and a 132kV transmission line, which is shown in Figure 1. The current transformer (CT) model and its saturation have also been taken into consideration in the simulations. To evaluate the high frequency transient behaviour of the transformer, particularly under switching operation and internal fault conditions, the winding shunt capacitances were added to the transformer model[5].
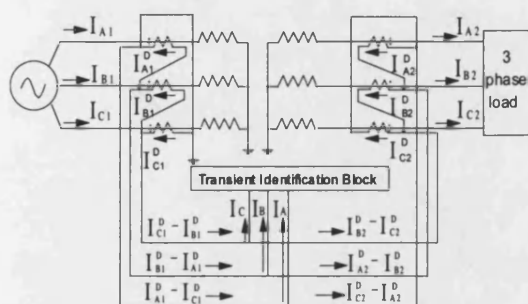
Figure 1: The studied power transformer system

2.2 Simulated Transient Event Types

In this paper, the following electromagnetic transient events of the power transformer have been taken into consideration

(a) internal fault transients, these include:
   (i) terminal three-phase faults without CT saturation and with CT saturation, respectively;
   (ii) terminal two-phase short-circuits without CT saturation and with CT saturation, respectively;
   (iii) terminal single-phase-to-earth faults without CT saturation and with CT saturation, respectively;
   (iv) internal winding turn-to-earth faults without CT saturation and with CT saturation, respectively;
   (v) internal winding turn-to-turn faults without CT saturation and with CT saturation, respectively.
(b) switch operating transients, such as when the transformer is energised at no-load condition.
(c) external faults with extreme CT saturation.

All the above transient events are simulated via electromagnetic transients program (EMTP). Some typical results of the simulation are given in detail here.

2.3 Transient Simulations of Internal Faults

Figure 2, Figure 3 and Figure 4 respectively show some typical simulation results under different fault conditions. They are *(i)* terminal two-phase (b and c phase) short-circuit occurring on the high voltage side of the transformer as shown in Figure 2; *(ii)*'a'-phase turn-to-earth fault occurring at mid-point of winding on the high voltage side of the transformer as shown in Figure 3; and *(iii)* an 'a'-phase 5% turn-to-turn fault occurring on the high voltage side of the transformer at 50% of voltage winding from the neutral point as shown in Figure 4. For each fault case, the primary currents in CTs on the high voltage side of the transformer as well as the three phase differential currents are given respectively in each figure.
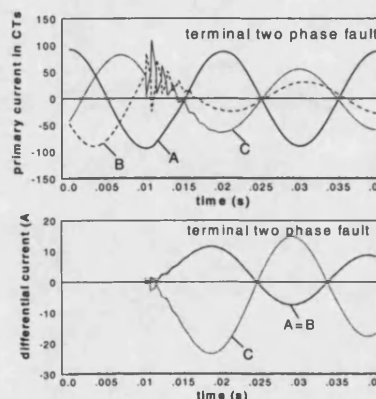
Figure 2: terminal two-phase (b and c) short-circuit fault on the high voltage side of the transformer
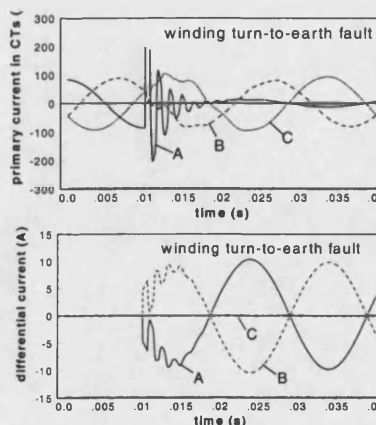
Figure 3: 'a'-phase turn-to-earth fault at mid-point of winding on the high voltage side of the transformer
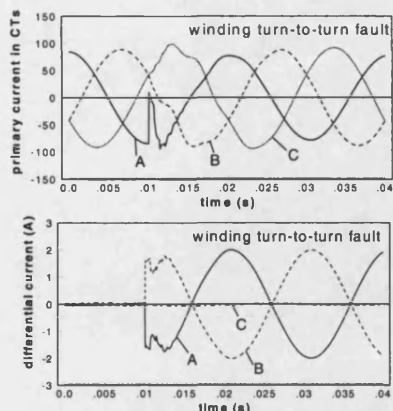
Figure 4: 'a'-phase 5% turn-to-turn fault on the high voltage side of the transformer at 50% of voltage winding from the neutral point

From the above figures it can be clearly seen that the fault generated high frequency current is present in the period at the start of the fault in the current signals. It is a direct result of the interaction between the coupled winding inductance and capacitance of the power transformer and the distributed inductance and capacitance of the transmission line.

2.4 Transient Simulations of Switching Operations

The various types of switching operation transients were also simulated. Figure 5 illustrates a typical simulation result of the switching operation condition (magnetising inrush case). It is observed that under such a condition, a large differential current is produced.
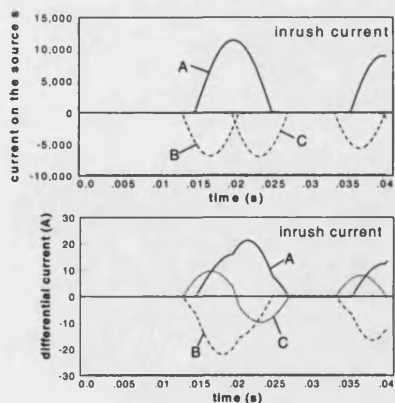
Figure 5: magnetising inrush current in the transformer

2.5 Transient Simulations Under CT Saturation

Figure 6 shows the differential currents for an 'a'-phase to earth fault occurring on the high voltage side of the power transformer with CT

saturation. For clarity, this figure has presented the secondary currents in CTs on the high and low voltage sides in the transformer as well as the differential currents. It is apparent that the differential currents are severely distorted due to CT saturation. In practice, this may cause mal-operation of the conventional differential protection which is based on second harmonic restraint. This is so because a large second harmonic also exists in the internal fault current, and not just in the magnetising inrush current. A spectral analysis of this differential current has shown that there is around 25% second harmonic component present in the fault current under CT saturation.

Figure 7 shows the differential currents for an external three-phase fault occurring on the high voltage busbar connected to the high voltage side of the power transformer under CT saturation. In this case, the transient unbalance currents are very large due to the saturation on one side CTs of the power transformer.

It can be seen from Fig.6 and Fig.7 that the high frequency current transients are also present in the current signals.
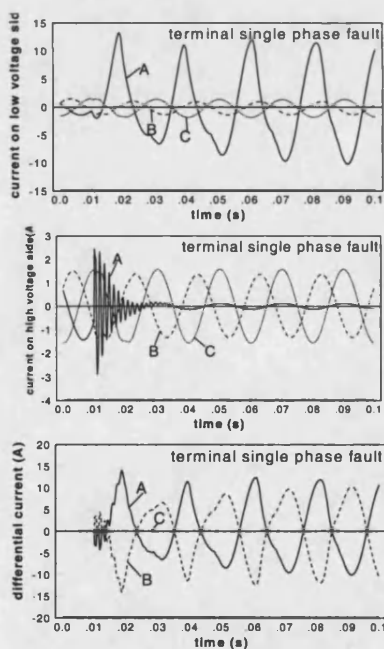
Figure 6: 'a'-phase to earth fault under CT saturation
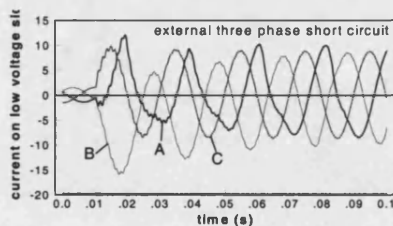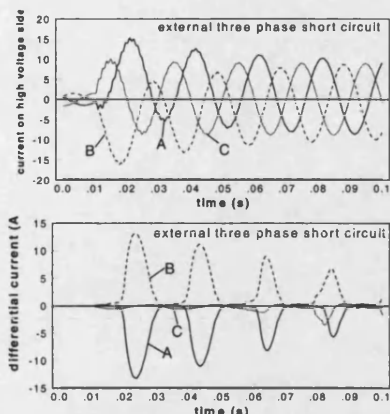
Figur7: external three-phase short circuit with CT saturation on low voltage side only

III. DETECTION OF HIGH FREQUENCY CURRENT TRANSIENT SIGNALS

When a fault occurs on a power transformer, DC offset, fundamental frequency and non-fundamental frequency components are produced. The non-fundamental frequency components change according to the power transformer operating conditions, such as variations in the internal faults and switching operation conditions. This can be clearly seen through the spectrum analyses of their differential current signals.

3.1 Behaviour of High Frequency Signals

In order to confirm the existence of the high frequency current transients in the differential currents, figure 8 presents the frequency spectra for the differential currents under the internal fault case shown in Figure 3 and switching operation (magnetising inrush) case shown in Figure 5, over a small range of frequencies. It is important to note that in Figure 8, non-fundamental frequency components exist under both internal fault and magnetising inrush condition. In this paper, the high frequency current transients with a centre frequency around 1kHz has been captured and employed to implement the transient identification.
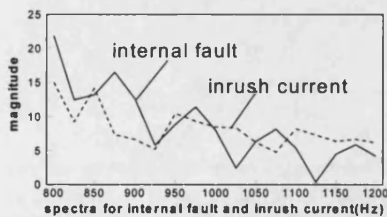
Figure 8: Spectra of differential currents

3.2 Detection and Feature Extraction of High Frequency Current Transient Signals

The high frequency current signals generated under both switching operations and internal faults are captured through a specially designed relay hardware/software. The spectral energies of the captured signals are extracted and then utilised to identify fault transients and switching operations by using the artificial neural network. The diagram of transient identification logic block is shown in Figure 9. A differential current threshold is set and a starting instruction will be issued to enable transient identifications when the differential current exceeds this threshold.

As shown in Figure 9, three phase differential current signals I_A, I_B and I_C are first converted into one modal signal I_{mode} by the modal mixing circuit using the following transformation:

$$I_{mode} = I_A + 2I_B - I_C \qquad (1)$$
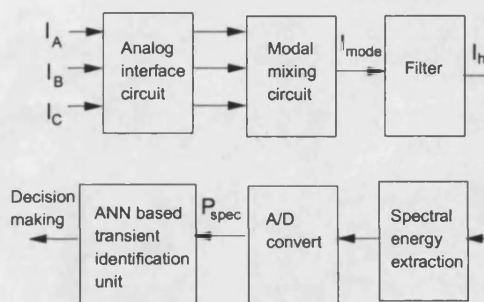
Figure 9: Transient identification block

A 4th order Butterworth band-pass filter is then applied to the modal signal I_{mode} to extract the high frequency current transient signal I_h, which is around a centre frequency of 1kHz, the sampling frequency is 10kHz. Figures 10-15 show the filter outputs corresponding to the typical signal waves shown in Figures 2-7.

From these figures it is worth noting that the features of the high frequency current transient signals between the internal faults and switching operations are significantly different. In the two cases, for example, in the internal fault case (Fig10-12) the high frequency components generated on fault inception rapidly ring down to a near zero value due to losses. However, in the case of magnetising inrush current (Fig 13, resulting from a switching operation) there are burst of high frequency signals (these are as a direct consequence of the transformer core and/or CT saturation). These thus produce the different spectral energy features between internal faults and switching operations, and can be used as the main signature to identify the transients between the

217

internal faults and switching operations via a neural network.

The spectral energies of the high frequency transient current I_h in each sampled window are extracted by the following equation

$$P_{spec} = \sum_{k=1}^{N} I_h^2(k)\Delta t \qquad (2)$$

where Δt= time step length; N = No. of samples in the window.
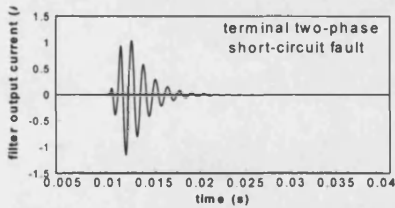
Figure 10: filter output current for two phase short circuit fault
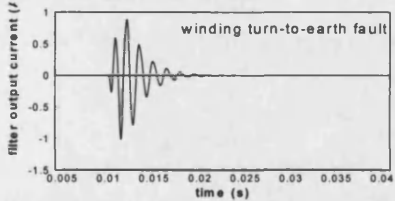
Figure 11: filter output current for winding turn-to-earth fault
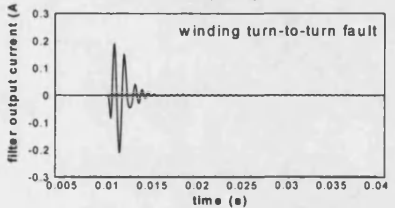
Figure 12: filter output current for winding turn-to-turn fault
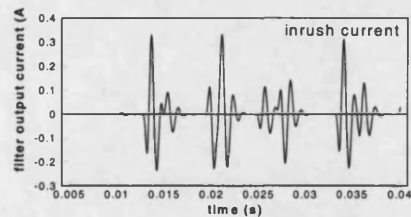
Figure 13: filter output current for inrush current
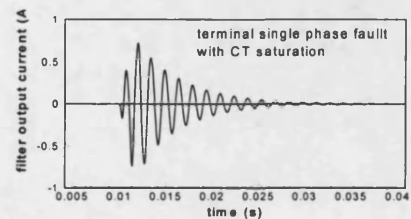
Figure 14: filter output current for internal fault with CT saturation
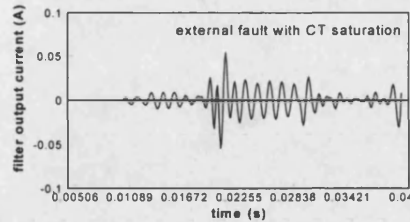
Figure 15: filter output current for external fault with CT saturation

IV. ARTIFICIAL NEURAL NETWORK BASED TRANSIENT IDENTIFICATION

One of the most difficult tasks in applying ANN technique to a particular power system protection is to formulate the problem that needs to be solved. The most important step to formulate the problem is to select the best input and output features that must correctly represent the problem. The vast majority of studies carried out hitherto involving ANN based power transformer protection have been based on the fundamental power frequency signals, which have been sampled over a window length of one power frequency cycle[2,3,4]. Furthermore, some of them have used the moving window principle to sample the signal over a period of several cycles. Both these approaches suffer from drawbacks; the first approach leads to prolonged fault detection times, the second approach can result in very long training times. And also, for certain fault conditions, the ANN may not converge to the required RMS error.

The work presented herein is based on employing the spectral energies of the high frequency current transient signals for the implementation of the transient identification through using the ANN for the power transformer. By detecting the changes of the spectral energies of the high frequency signals in a given observation window, the transient identifications are achieved. The diagram of transient identification logic block has been shown in Figure 9.

4.1 Input selection to the neural network

As shown above, the high frequency transient signals generated by a fault and switching operations mainly exist within a short period of time following a fault or a switching operation; this means that the decision about the nature of transient must be made within this period. Therefore, in this paper, the observation window of the high frequency current transient signals associated with each transient event has been

constrained to a time window length of ½ cycle, which in turn is divided into 10 equal time periods, as shown in Figure 16.

main window
(ten high frequency cycles, 10 ms)

subwindow
(one high frequency cycle,1 ms)

Pspec,1 Pspec,2 Pspec,3   Pspec,9 Pspec,10

ANN input
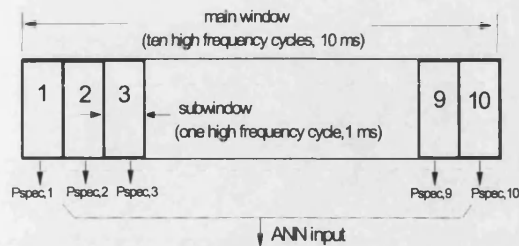
Figure16: Representation of feature extraction

The waveform associated with each subwindow is effectively sampled into ten samples (this is at 10kHz sampling frequency), and the spectral energy of the signal in each subwindow is then calculated by equation (2). Thus, the ten subwindows produce the 10 integrated spectral energies, which represent the main features of the signals for each given case; they are then used as input data to the ANN.

4.2 Network structure and training

A total of 10 sampled signals are employed as inputs to the ANN. The target output of the ANN was built in such way that the value [1, 0] represents the transient caused by an internal fault; the value [0, 1] represents the transient caused by the switching operation; and the value [0, 0] represents the transients caused by the external fault.

The selection of the number of hidden layers and the number of neurons required in each hidden layer is determined by experimentation involving training and testing various network configurations. The process is terminated when a suitable network with a satisfactory performance is established. In this work, it was found that one hidden layer with 6 hidden neurons gave a satisfactory performance.

The training and testing date sets of the ANN consist of 120 cases, comprising of various internal faults and switching operation transients, with and without taking CT saturation into consideration, as well as the external fault transients again with and without CT saturation.

V. RESPONSE EVALUATION

The ANN was extensively tested and was then embedded into the structure shown in Fig 1 to evaluate the performance and ability of the

transient identification. The value of 0.1 is set as the tolerate RMS error of the ANN output. Table 1 shows the performance obtained from the trained ANN when it is subjected to 'unseen' fault/switching operation data. It is apparent from the results presented that the ANN-based technique gives the correct results for all the test cases presented to it.

Table 1: Performance of the ANN based transient identification technique

Type*		Desired output		Actual output	
Internal fault	①	1	0	1.007	0.065
	②	1	0	0.978	-0.005
	③	1	0	1.006	0.003
	④	1	0	0.996	-0.010
	⑤	1	0	1.005	0.025
	⑥	1	0	0.901	-0.031
	⑦	1	0	1.008	0.010
	⑧	1	0	1.004	-0.058
inrush	①	0	1	-0.042	0.932
	②	0	1	0.009	1.007
external fault	①	0	0	0.021	0.002
	②	0	0	0.026	-0.004

type*
Internal fault:
①'b'-phase turn-to-earth faults occuring on the low voltage side of the transformer at mid-point of winding winding.
②'a'-phase turn-to-turn faults occuring on the high voltage side of the transformer at 20% of voltage winding from the neutral point.
③terminal two-phase(a and b) fault on the high voltage side of the transformer.
④terminal two-phase(a and b) fault on the low voltage side of the transformer.
⑤terminal two-phase(a and c) fault on the low voltage side of the transformer.
⑥terminal 'a'-phase to earth fault on the low voltage side of the transformer.
⑦terminal 'b'-phase to earth fault on the low voltage side of the transformer.
⑧terminal 'c'-phase to earth fault on the low voltage side
of the transformer.
Inrush:
①: inrush when a fault inception time is at 13ms.
②: inrush when a fault inception time is at 15ms.
External fault:
①an external three phase fault occuring on the high voltage busbar connected to the load.
②an external two phase fault occuring on the high voltage busbar connected to the high voltage side of transformers.

VI. CONCLUSIONS

This paper presents a novel technique for transient identification based on the detection of changes of spectral energies of high frequency current transient signals in the power transformer using the artificial neural network. The various transient events have been taken into consideration. The results show that the proposed technique is able not only to capture the high frequency current transient signals inside a transformer, but also accurately identify the cause and nature of a transient. It is an attractive alternative method to distinguish the magnetising inrush from internal faults in the power transformer protection, compared to the more traditional methods.

VII. REFERENCES

[1]. Z Q Bo, R K Aggarwal, A T Johns, "A New Measurement Technique for Power Transformer Faults", the 30th University Power Engineering Conference, University of Greenwich, 5-7 Sept. 1995

[2]. G Perez, A J Flechsig, J L Meador and Z Obradovic, "Training an Artificial Neural Network to Discriminate Between Magnetizing Inrush and Internal Fault", IEEE Tran. on Power Delivery, Vol. 9, No. 1, January 1994, pp.434~441

[3]. J Pihler, B Grcar and D Dolinar, "Improved Operation of Power Transformer Protection Using Artificial Neural Network", IEEE Trans. On Power Delivery, Vol. 12, No. 3, July 1997, pp.1128~1136, pp.510-517.

[4]. B.Kasztenny, M.Lukowicz, E.Rosolowski, "Selecting Type of a Neural Network, Pre- and Post-processing AAlgorithms for Power Transformer Relaying" 32th University Power Engineering Conference, Vol.2, pp.708-712. Sept. 1997, UMIST, UK.

[5]. Walter A. Elmore , "Protective Relaying Theory and Application", ABB Power T&D Company Inc, Relay Division, Coral Springs, Florida, 1995

ANALYSIS OF TRANSIENT PHENOMENA IN POWER TRANSFORMERS USING WAVELET TRANSFORMS

P. L. Mao, R. K. Aggarwal

University of Bath, UK

ABSTRACT

Discrimination between an internal fault and a magnetising inrush current has long been recognised as a very challenging protection problem in power transformers. In this paper, we have proposed a new and powerful method capable of analysing the internal fault and the inrush current. The approach is based on a wavelet transform to decompose a given faulted current signal or inrush current signal into a series of wavelet components, each of which is a time-domain signal that covers a specific frequency band. Simulated results presented show that particular wavelet components can be used as the features to distinguish the internal fault from the inrush current.

I. INTRODUCTION

Electromagnetic transient signal analysis of a power transformer plays a crucial role in the design and operation of a large modern power transformer. It is well known that most of the signals in a power system, such as current and voltage signals, are time-domain signals commonly known as a time-amplitude representation of the signal; however, this is not always the best representation of the signals. In many cases, the most significant information is hidden in the frequency content of the signal.

Fourier Transform (FT) is the most widely employed transform technique being used in Electrical Engineering. FT gives what frequency components (spectral components) exist in the signal, but it does not tell us when in time these frequency components exist. However, the latter is an important characteristic for analysing transient signals, such as those present in the fault and inrush currents in a power transformer. Thus, FT is not the best technique to analyse a non-stationary signal.

Compared with FT, the Short Term Fourier Transform (STFT) overcomes the time location problem. It treats a non-stationary signal as a stationary signal by means of dividing the signal into small segments into small windows, and these segments are then assumed to be stationary. However, STFT can only give a fixed resolution at all times; furthermore, wide windows may disobey the condition of being assumed stationary. In this respect, Wavelet Transform (WT) provides a multiple resolution of the transient signal both in time and frequency [1]. Unlike FT which uses one basis function (sine waves or cosine waves), Wavelet Transform relies on wavelets of a rather wide functional form. The basis wavelet is termed as a mother wavelet. Wavelet transform decomposes a given signal into a series of wavelet components, each of which is a time-domain signal that covers a specific frequency band and it allows the detection of the time of occurrence of abrupt disturbances, such as fault transient in power transformer systems. Thus the

Wavelet Transform is more suitable to the study of the signal, which has low frequency components with discontinuities and sharp spikes.

The potential benefits of applying wavelet transform for analysing the power system transients have been well recognised in recent years. Several relevant papers have been presented for power system analyses using the wavelets transforms [2-5]. These application studies cover the detection and analysis of power system transient signals [2-3] and the transient power quality problem [4] as well as the fault detection of power transformers during impulse test [5], etc.

In this paper another useful application of the wavelet transform is presented for analysing the transient phenomena in a power transformer under conditions of faults and magnetising inrush currents. A *750MVA 27/420 kV* power transformer system is first modelled by the EMTP and simulated under various typical faults and magnetising inrush currents. Wavelet transform approach is then employed to decompose these fault and magnetising inrush current signals into a series of wavelet components, which represent an approximate and detailed version of the original signal. Simulated results presented clearly show that certain wavelet components can be used as the features to discriminate between the internal fault and the magnetising inrush current. In addition, this attribute can be used in fault classification, which is under investigation.

II. WAVELET TRANSFORM AND ITS IMPLEMENTION

Similar to the relationship between a continuous FT and a discrete FT, there is a continuous wavelet transform and a discrete wavelet transform.

Mathematically, the Continuous Wavelet Transform (CWT) of a given function $x(t)$, with respect to a mother wavelet $g(t)$, is defined as [1]

$$CWT(a,b) = \frac{1}{\sqrt{a}} \int_{-\infty}^{+\infty} x(t)g(\frac{t-b}{a})dt \qquad (1)$$

where a is a scale parameter, b is the translation parameter, and $g(t)$ is the mother wavelet function. It is apparent from eqn. (1) that the original one dimensional time-domain signal $x(t)$ is mapped to a new two-dimensional function space across scale a and translation b by the wavelet transform. A wavelet transform coefficient, $CWT(a, b)$, at a particular scale and translation represents how well the original signal $x(t)$, and scaled and translated mother wavelet match. Thus, the set of all wavelet coefficients, $CWT(a, b)$, are the wavelet representation of the original signal $x(t)$ with respect to the mother wavelet $g(t)$.

There are many types of mother wavelets [1], such as Harr, Daubichies, Coiflet and Symmlet wavelets. The choice of mother wavelet plays a significant role in detecting and localising different types of fault transients. In addition to this, the choice also depends on a particular application. In this study, we are particularly interested in detecting and analysing low amplitude, short duration, fast decaying and oscillating type of high frequency current signals. One of the most popular mother wavelets suitable for a wide range of application used is Daubichies's wavelet. In this paper, D4 wavelet is used, as shown in Fig.1.
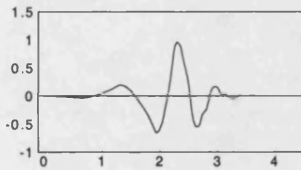
Figure 1 D4 mother wavelet

Analogous to the relationship between Continuous Fourier Transform and Discrete Fourier Transform, the wavelet transform has a digitally implementable counterpart Discrete Wavelet Transform (DWT). The CWT is not employed as often as the DWT. The continuous transform is primarily employed to derive properties, whereas the discrete forms are necessary for most computer implementations. The DWT is defined as [1]:

$$DWT(m, n) = \frac{1}{\sqrt{a_0^m}} \sum_k x(k) g\left(\frac{n - ka_0^m}{a_0^m}\right) \tag{2}$$

where $g(n)$ is the mother wavelet; the scaling and translation parameters a and b of eqn. (1) are replaced by a_0^m and ka_0^m, and k and m are integer parameters.

Fig.2 illustrates the implementation procedure of the DWT, in which x[n] is the original signal, h[n] and g[n] are low-pass and high-pass filters, respectively. At the first stage, an original signal is divided into two halves of the frequency bandwidth, and sent to both high-pass filter and low-pass filter. Then the output of low-pass filter is further cut in half of the frequency bandwidth, and sent to the second stage. The same procedure is performed until the signal is decomposed to a pre-defined certain level. Finally we obtain a

bunch of signals, which actually represent the same original signal, but all corresponding to different frequency bands.
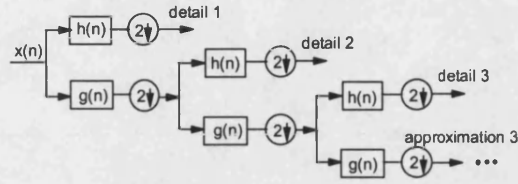
Figure 2 Implementation of DWT

It is worth pointing out that the frequency band of each detail of the DWT is directly related to the sampling rate of the original signal. As indicated in Figure 3, if the original signal is being sampled at F_s Hz, the highest frequency that the signal could contain, from Nyquist's theorem, would be $F_s/2$ Hz. This frequency would be seen at the output of the high frequency filter, which is the first detail. Thus the band of frequencies between $F_s/2$ and $F_s/4$ would be captured in detail 1; similarly, the band of frequencies between Fs/4 and Fs/8 would be captured in detail 2, and so on.
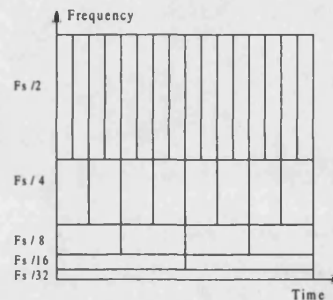
Figure 3 Time-Frequency relationship of DWT

III. WAVELET ANALYSIS OF TRANSIENT PHENOMENA IN POWER TRANSFORMERS

A. Power Transformer System

In this paper the power transformer transient phenomenon is simulated in a system comprising a typical *27/420kV, 750MVA* large power transformer connected between a *1GVA* generator at the sending end and a *300kM 400kV* transmission line connected to an infinite bus power system at the receiving end, as shown in Fig.4.
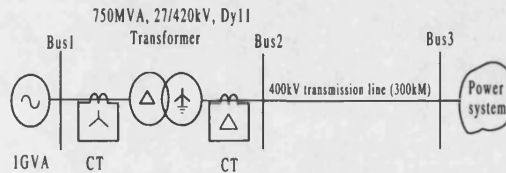
Figure 4: Simulated system configuration

In order to investigate the effectiveness of the wavelet transforms to detect and analysis the power transformer transients, particularly fault and inrush

current transients, various internal faults and inrush currents are simulated using *EMTP* software; the corresponding differential current signals are evaluated and realised using wavelet transform technique. D4 wavelet is used in DWT in the following studies.

B. Wavelet Analysis of Inrush Current

When the power transformer is energised on the primary side with the secondary side open-circuited, a transient magnetising inrush current flows in the primary side. This current may reach instantaneous peaks of 6-8 times full-load current because of the extreme saturation of the iron-core in power transformer. Fig.5(a) shows typical magnetising inrush current waveforms, which correspond to a, b and c three phase differential currents through the CT secondary sides. As can been seen, the current waveforms are distorted quite significantly; gaps appear over the times of the inrush currents. At the edges of the gaps, the current magnitude changes from near zero to a significant value or from a significant value to near zero; this would be expected by virtue of the fact that sudden changes from one state to other different states produce little ripples, which very often are not visible from the fundamental frequency signals as apparent Fig.5(a). However, this can be discerned and clearly demonstrated by wavelet transform. For brevity, only the DWT of the a-phase differential current is shown herein.

In implementing the DWT, the original inrush current signal has been sampled at 25kHz and passed through a discrete wavelet transform, with the structure of Fig.2. The frequency space is divided as indicated in Fig.3. Thus, 5-detailed signals that contain a frequency band of 12.5kH ~ 6.25kH at detail 1, 6.25kH ~ 3.125kH at detail 2, 3.125kH ~ 1.562kH at detail 3, 1.562kH ~ 781Hz at detail 4 and 781Hz ~ 390 Hz at detail 5 as well as one approximate signal in the frequency band 390Hz ~ DC level), are shown in Figure 5(b)-(g). From these Figures we can clearly see that there are very useful features in the decomposed magnetising inrush signals. A certain high frequency component can be located better in time than a low frequency component. In contrast, a low frequency component can be located better in the frequency domain than the high frequency component; and this effectively means that all of the features for a particular signal are obtained. In this study, we are interested in those components that are located better in time, so that, detail 1 and detail 2 are taken for the feature analysis.

From Figure 5(b)-(c), which correspond to detail 1 and detail 2, it can be seen that there are eight sharp spikes during the shown period of the inrush current transient. From the foregoing analysis, the four sharp spikes exist at edges of gaps at which the inrush current suddenly changes from one state to other different states. Another four sharp spikes are produced because the primary windings of the power transformer are connected as delta, so that the a-phase differential current is in fact the difference between

the a-phase magnetising inrush current and c-phase magnetising inrush current. This gives rise to the non-smooth points in the current waveforms, which in turn cause sharp spikes appear in the DWT of the current waveforms.
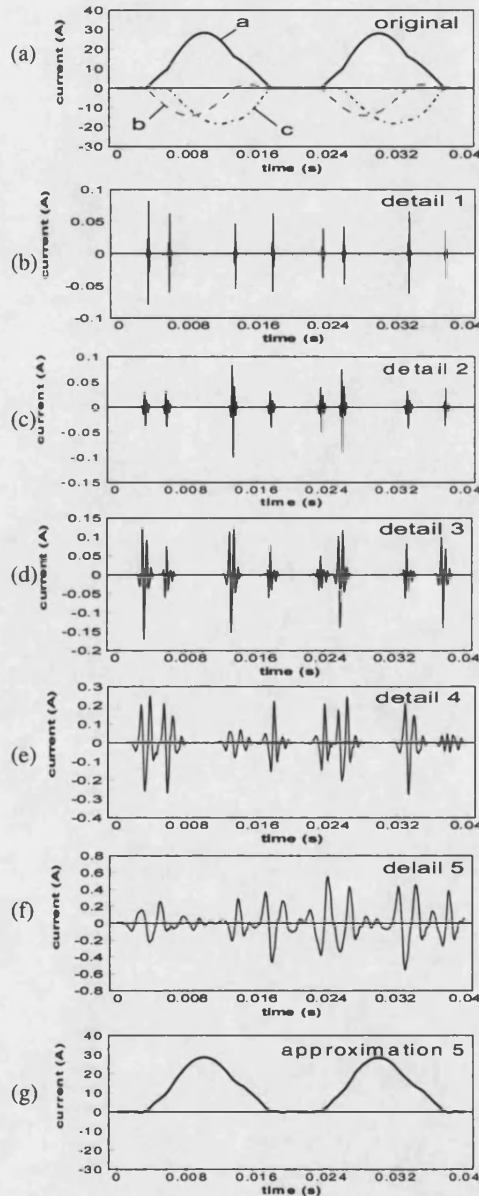
Figure 5: 5-successive details and approximation for inrush current

C. Wavelet Analysis of Internal Fault Current

Fig.6(a) shows an internal fault current, which corresponds to a, b and c three phase differential currents through the CT secondary sides, under an a-b earth fault on the high voltage side of the power transformer. It is apparent from Fig.6(a) that there is a high frequency distortion in the current waveforms. This is as a direct consequence of the effects of the distributed inductance and capacitance of the

transmission line. This can lead to a significant second harmonic in the internal fault[6], thereby posing difficulty in an accurate discrimination between magnetising inrush and internal fault currents by the conventional protection method.

(a)

(b)

(c)

(d)

(e)

(f)

(g)
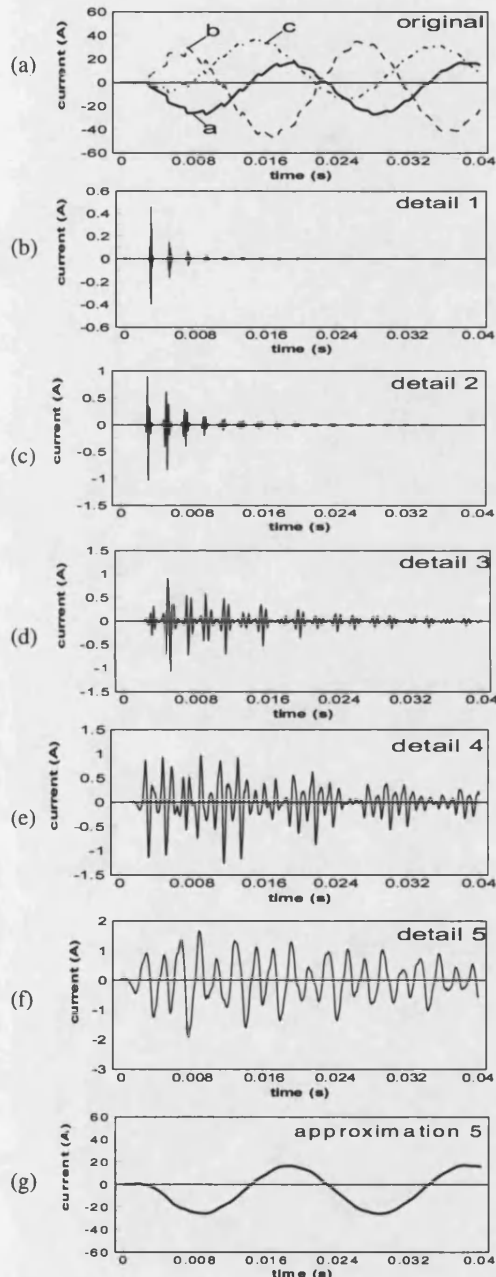
Figure 6: 5-successive details and approximation for A-B two-phase to earth fault on high voltage side

For brevity, only the DWT of the a-phase differential current is presented here as shown in Figure 6(b)-(g). From Figure 6(b)-(c), which correspond to the detail 1 and detail 2 of the DWT, we can see that there are

several sharp spikes appearing from the inception time of the internal fault. However, in marked contrast to the inrush current case, these sharp spikes rapidly decay to near zero within one cycle, whereas those sharp spikes under inrush current case suffer from little attenuation during the entire inrush transient period, which can last from perhaps 10 cycle for small transformers to 1 min for large units [7]. It is apparent that this difference can be effectively used as one of the key features to distinguish the internal fault from the inrush current.

IV. CONCLUSION

The wavelet transform is a powerful method capable of analysing the internal fault and the inrush current in power transformers. It offers important advantages over Fourier transform. Simulated results presented show that particular wavelet components can be used as the features to distinguish the internal fault from the inrush current. It can also be used in the design of novel protection techniques of power transformer. Furthermore, this attribute is expected to be able to be used in fault classification in transforms and this investigation is underway.

V. REFERENCE

[1]   Randy K. Young, Wavelet theory and its application, Kluwer Academic Publishers, 1993.

[2]   V.M.Reddy, S.S.Rao, F.J.Mercede, "On The Use of Wavelets for the Detection and Analysis of Power system Transients", Proceeding of 1999 IEEE Winter Power Meeting, pp:1293-1299.

[3]   W.A.Wilkinson and M.D. Cox, "Discrete Wavelet Analysis of Power System Transients", IEEE Trans. On Power System, Vol.11, No.4, November 1996, pp:2038-2044.

[4]   G. T. Heydt and A. W. Galli, "Transient Power Quality Problems Analyzed Using Wavelets", IEEE Trans. On Power Delivery, Vol.12, No.2, April 1997, pp:908-915.

[5]   Stantosh   Kumar   Pandey   and   L.Satish, "Multiresolution Signal Decomposition: A New Tool for Fault Detection in Power Transformers During Impulse Tests", IEEE Trans. On Power Delivery, Vol.13, No.4, October 1998, pp:1194-1200.

[6]   P.Liu, O.P.Malik, C.Chen, G.S.Hope, and Y.Guo "Improved Operation of Differential Protection of Power Transformers for Internal Faults", IEEE Trans on Power Delivery, Vol. 7, No.4, 1992, pp.1912-1919.

[7]   Walter A. Elmore , "Protective Relaying Theory and Application", ABB Power T&D Company Inc, Relay Division, Coral Springs, Florida, 1995

A Wavelet Transform Based Decision Making Logic Method for Discrimination between Internal Faults and Inrush Currents in Power transformers

P L Mao, R K Aggarwal

Department of Electronic and Electrical Engineering,
University of Bath, Bath BA2, 7AY, England

Abstract-This paper describes a decision making logic method for discrimination between internal faults and inrush currents in power transformers using wavelet transform based feature extraction technique. It is shown that the features extracted by wavelet transform have a more distinctive property than those extracted by fast Fourier transform due to the good time and frequency localisation characteristics of wavelet transform. As a result, by quantifying the extracted features, the decision for distinguishing an internal fault from an inrush current in different power transformer systems can be accurately made. The extensive simulation studies have verified that the proposed method is more reliable and simpler, and is suitable for different power transformer systems.

Keywords: Power transformer, Fault detection, Internal fault, Inrush current, Wavelet transform, Decision logic

1 Introduction

The power transformer protection is of critical importance in power systems. Any power transformer protective scheme has to take into account the effect of magnetising inrush currents. This is because the magnetising inrush current, which occurs during the energisation of the transformer, sometimes results in 10 times full load currents and therefore can cause mal-operation of the relays. Accurately discriminating magnetising inrush currents from internal faults has long been recognised as a very challenging problem to power transformer protection engineers.

There are many existing schemes proposed to cope with this problem. Among them, the second harmonic restraint principle based schemes is one of the methods, which restrains or blocks the relay operation under the inrush current conditions based on the level of second harmonic content of the measured current [1,2,3]. However, it has been reported that in certain cases, the internal fault current might contain considerable amount of second harmonic [4]. On the other hand, it has been also reported that the second harmonic content in magnetising inrush currents tends to be relatively small in modern power transformers because of improvements in the power transformer core material [5]. Considering these facts, it is necessary to develop new algorithms or schemes for accurately and efficiently discriminating between internal faults and inrush currents.

Recently, several new protective schemes have been proposed to deal with the foregoing problem in power transformer protection. Most of them have mainly focused on the applications of neural networks and fuzzy logic techniques. In one approach, neural network techniques have been applied to distinguish internal faults from the magnetising inrush currents[6,7,8,9,10]. However, the ANNs in such approach might need re-training for use in other power transformer systems if the transformer, for example, is changed in capacity and voltage ratings as well as iron-core constructions and winding connections. In the another approach, multi-criteria aggregation technique based on fuzzy logic has been employed [11,12]. However, for such an approach, there are no recommended criteria for setting the internal parameters of a relay. Moreover, since fuzzy logic is still rule-based, the technique is not robust to cater for many commonly encountered transient conditions.

This paper introduces a simple decision making logic scheme based on the wavelet transform for distinguishing internal faults from inrush currents. The wavelet transform technique is firstly applied to decompose the differential current signals through the CTs secondary side into a series of wavelet components, each of which is a time-domain signal that covers a specific frequency band. Thus, more distinctive signal features that respectively represent internal faults and inrush currents are extracted. As a result, by quantifying the extracted features, a decision for distinguishing an internal fault from an inrush current in different power transformer systems can be accurately made in terms of the differences in the quantified features. The extensive simulation results presented show that the proposed technique needs very simple input signals (differential currents), but can accurately discriminate between an internal fault

and an inrush current in different power transformer systems.

2 Wavelet Analysis of Transient Phenomena in Power Transformer Systems

2.1 Power Transformer Systems

To demonstrate the effectiveness of the proposed scheme, two different power transformer systems, namely system 1 and system 2, are studied. System 1 is a three-phase and two-winding *750MVA, 27kV/420kV, Dy11-connected, five-leg core type* power transformer in a double-end-fed power system network; System 2 is three-phase and two-winding *35MVA, 11kV/132kV, Yy0-connected, three-leg core type* power transformer in a single-end-fed power system. Their connections are shown in Figure 2 (a) and (b), respectively.

The simulations of these two power transformer systems have been carried out using the well known EMTP software. In each simulation of the system, the power transformer faults and system parameters are varied, including the fault types, fault positions, fault inception angles, remnant fluxes in power transformer core. The CT saturation has been taken into consideration. The CT models developed herein are essentially based on those outlined in reference [13]. This model comprises of an equivalent circuit built around an ideal transformer. The magnetising branch is represented as a non-linear inductor, and is represented by a λ-i hysteresis loop.

27/420kV, 750 MVA, Dy11

(a) System 1

11/132kV, 35MVA, Yy0
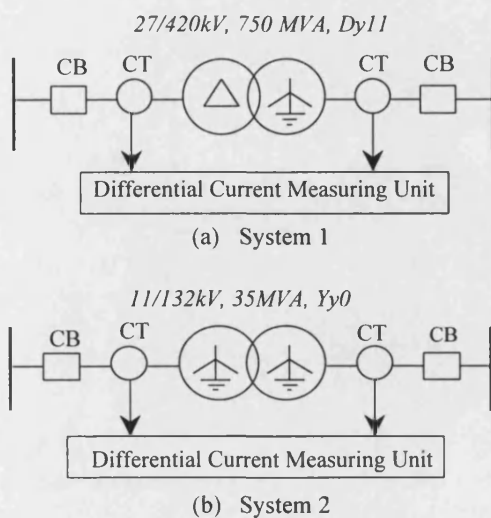
(b) System 2

Figure 1: Simulated power transformer systems

2.2 Implementation of Wavelet Transform

In this study, the original differential current signal has been sampled at 25kHz and passed through a discrete wavelet transform (DWT), with the structure of Fig.2, in which x[n] is the original signal, h[n] and g[n] are low-pass and high-pass filters, respectively. At the first stage, an original signal is divided into two halves of the frequency bandwidth, and sent to both high-pass filter and low-pass filter. Then the output of low-pass filter is further cut in half of the frequency bandwidth, and sent to the second stage. The same procedure is performed until the signal is decomposed to a pre-defined certain level. Finally we obtain a bunch of signals, which actually represent the same original signal, but all corresponding to different frequency bands. Thus, 5-detailed signals that contain a frequency band of 12.5kH ~ 6.25kH at detail 1, 6.25kH ~ 3.125kH at detail 2, 3.125kH ~ 1.562kH at detail 3, 1.562kH ~ 781Hz at detail 4 and 781Hz ~ 390 Hz at detail 5 as well as one approximate signal in the frequency band 390Hz ~ DC level), are obtained.

It should be mentioned that the technique presented is based on employing the high frequency phenomenon associated with transformer transients. It is therefore necessary to use the high sampling rate of 25 kHz. Furthermore, in practice this high sampling rate should not pose much difficulty in the hardware implementation of the technique in view of the fact that modern digital processors are well equipped to cater for very high sampling rates in excess of 200 kHz.

Figure 2 Implementation of DWT

2.3 Wavelet Transform and Feature Analysis of Transformer Transient Signals

As mentioned before, the feature analysis and comparisons between inrush currents and internal faults using wavelet transform have been studied in two different power transformer systems.

2.3.1 Inrush currents

Fig.3(a) shows typical magnetising inrush current waveforms (i.e., the EMTP output signal), which correspond to *a, b* and *c* three phase differential currents through the CT secondary sides in the system 1. As can be seen, the current

waveforms are distorted quite significantly; gaps appear over the times of the inrush currents. At the edges of the gaps, the current magnitude changes from near zero to a significant value or from a significant value to near zero; this would be expected by virtue of the fact that sudden changes from one state to other different states produce little ripples, which very often are not visible from the fundamental frequency signals as apparent in Fig.3(a). However, this can be discerned and clearly demonstrated by wavelet transform. Since in this study, we are interested in the component that is located better in time, thus, the detail 1 signals of the DWT of the *a, b* and *c* three phase differential currents are considered for the feature extractions shown in Figure 3(b)-(d).
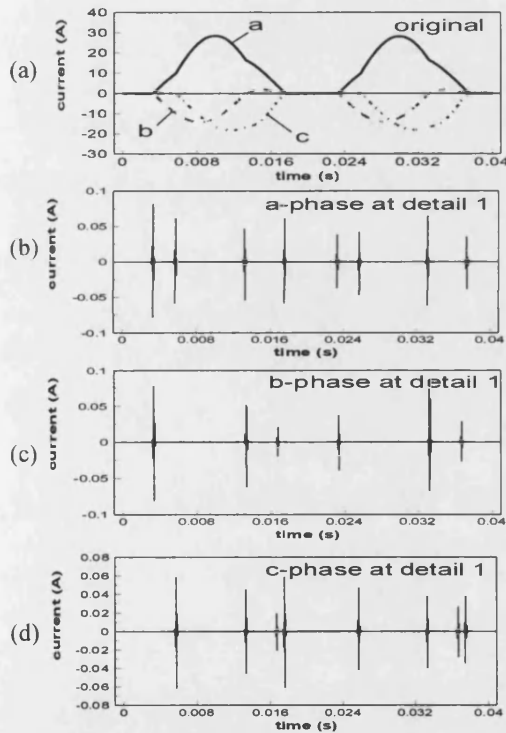
Figure 3: Magnetising inrush currents in system 1: (a)original a,b and c three phase differential currents; (b) a-phase DWT at detail 1;(c) b-phase DWT at detail 1;(d)c-phase DWT at detail 1

From Figure 3(b)-(d), which correspond to a, b and c three phase wavelet signals at detail 1, it can be seen that there are spikes during the shown period of the inrush current transient in phase *a, b and c* respectively. From the foregoing analysis, in Fig.3(b), the four sharp spikes exist at edges of gaps at which the inrush current suddenly changes from one state to other different states. Another four sharp spikes are produced because the primary windings of the power transformer are connected in

delta; for example the a-phase differential current is in fact the difference between the a-phase magnetising inrush current and c-phase magnetising inrush current. This gives rise to the non-smooth points in the current waveforms, which in turn cause sharp spikes to appear in the DWT of the current waveforms.

In Fig.4(a)-(d), the magnetising inrush currents in system 2 are presented. It has been found that wavelet signals between system 1 and system 2 have analogous features. For brevity, those analyses have been omitted here.
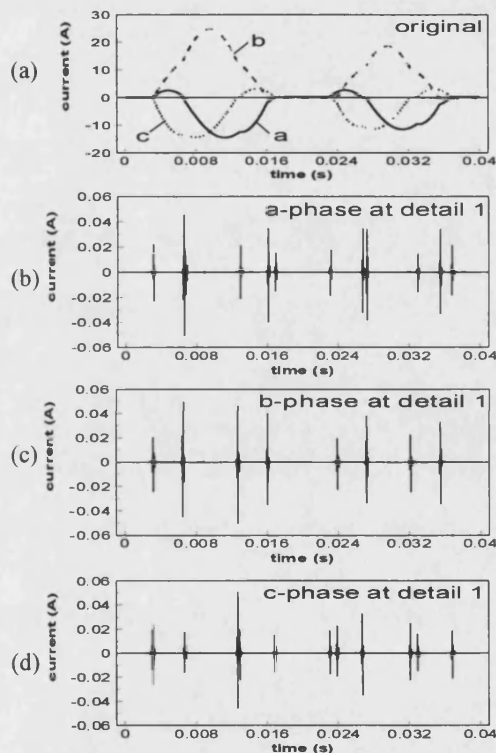
Figure 4: Magnetising inrush currents in system 2: (a)original a,b and c three phase differential currents; (b) a-phase DWT at detail 1;(c) b-phase DWT at detail 1;(d)c-phase DWT at detail 1

2.3.2 Internal Faults

Fig.5(a) shows an internal fault current, which corresponds to *a, b* and *c* three phase differential currents through the CT secondary sides, under an *a-b* to earth fault on the high voltage side of the power transformer in the system 1. It is apparent from Fig.5(a) that there is a high frequency distortion in the current waveforms. This is as a direct consequence of the effects of the distributed inductance and capacitance of the transmission line. This can lead to a significant second harmonic in the internal fault [4], thereby posing difficulty in an accurate discrimination between magnetising

inrush and internal fault currents by the conventional protection method.

As before, detail 1 is taken as the feature extraction shown in Figures 5(b)-(d). From Figures 5(b)-(d), we can see that there are several sharp spikes appearing from the inception time of the internal fault. The maximum value of the sharp spike appears at the beginning of the fault. It is worth pointing out that this phenomenon exists at least in one of all three phases for whatever the fault type it is. Here again, the internal fault currents in system 2 are shown in Fig.6(a)-(d), and analogous features with the system 1 can be found.
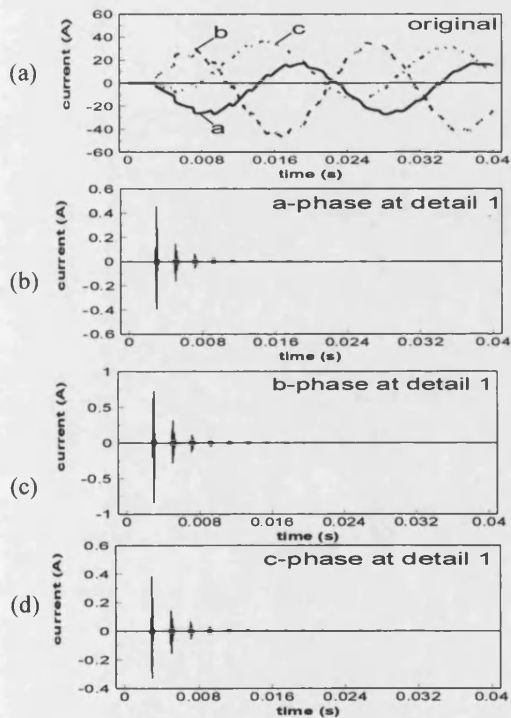
Figure 5: Internal fault currents in system 1: (a)original a,b and c three phase differential currents; (b) a-phase DWT at detail 1; (c) b-phase DWT at detail 1; (d) c-phase DWT at detail 1
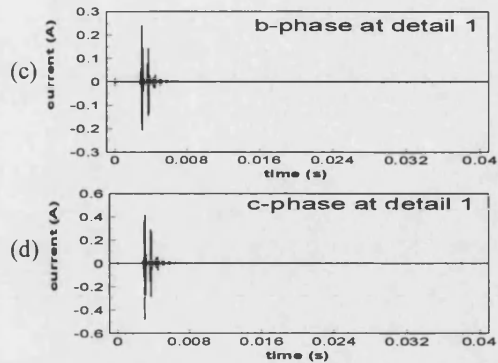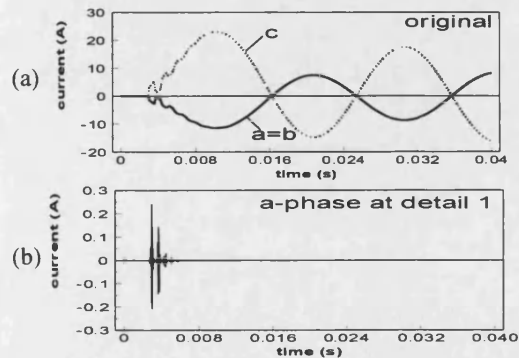
Figure 6: Internal fault currents in system 2: (a)original a,b and c three phase differential currents; (b) a-phase DWT at detail 1;(c)b-phase DWT at detail 1;(d) c-phase DWT at detail 1

Although not shown here, it should be mentioned that a short circuit of a few turns of the winding will give rise to heavy fault current in the short circuited loop, but the terminal currents both on HV and LV sides are quite small; this in turn results in the differential currents generated being much smaller compared to those caused by other types of faults, such as the fault shown in Fig.5 (a). However, this is of little consequence for the DWT which, for such low-level faults, gives features similar to those caused by severe faults.

2.4 Feature Comparisons between Internal Faults and Inrush Currents

Extensive simulation studies have shown that the wavelet transforms of magnetising inrush currents and internal fault currents have the following different features. For internal fault cases shown in Fig.5 and 6, we can clearly see that there are several sharp spikes appearing from the inception time of the internal fault. The maximum value of the sharp spike appears at the beginning of the fault. However, in marked contrast to the inrush current cases shown in Fig.3 and 4, these sharp spikes rapidly decay to near zero within one cycle, whereas those sharp spikes under inrush current cases suffer from little attenuation during the entire inrush transient period, which can last from perhaps 10 cycle for small transformers to 1 min for large units [3]. It is apparent that this difference can be used as the key feature to effectively distinguish internal faults from inrush currents.

3 Wavelet Transform based Decision Making Logic Method

3.1 Quantification of extracted features

The decision for discriminating between internal faults and inrush currents are made based on the extracted features that are quantified by a ratio in a certain wavelet component, which is given by following equations.

$$I_{a-ratio} = \frac{I^k_{a-d1,\max}}{I_{a-d1,\max}} \qquad (1)$$

$$I_{b-ratio} = \frac{I^k_{b-d1,\max}}{I_{b-d1,\max}} \qquad (2)$$

$$I_{c-ratio} = \frac{I^k_{c-d1,\max}}{I_{c-d1,\max}} \qquad (3)$$

where, $I_{a-d1,\max}$, $I_{b-d1,\max}$, $I_{c-d1,\max}$, respectively, represent the maximum peak values of a-phase, b-phase, c-phase wavelet at detail 1 in the first window; $I^k_{a-d1,\max}$, $I^k_{b-d1,\max}$, $I^k_{c-d1,\max}$, respectively, represent the maximum peak values of a-phase, b-phase, c-phase wavelet at detail 1 in the kth subsequent moving windows after the first window.

Note that $I_{a-ratio}$, $I_{b-ratio}$ and $I_{c-ratio}$ represent the ratios of the maximum peak value between the first window and the kth subsequent moving window. The window length in this study is ½ cycle (10 ms in 50Hz), the step length of moving window is ¼ cycle (5ms in 50Hz).

3.2 Decision Making Logic

The decision for distinguishing between internal faults and inrush currents is made in terms of the ratio change in $I_{a-ratio}$, $I_{b-ratio}$ and $I_{c-ratio}$ in each moving window, which is given as follows:

if ($I_{a-ratio} > \varepsilon$ *or* $I_{b-ratio} > \varepsilon$ *or* $I_{c-ratio} > \varepsilon$)
then
　　　"This is an inrush"
else
　　　"This is an internal fault"
endif

where, ε represents the predefined threshold ($\varepsilon=0.4$ in this paper).

Extensive simulation and analysis have indicated that in inrush current cases, at least one of $I_{a-ratio}$, $I_{b-ratio}$ and $I_{c-ratio}$ will be greater than a predefined threshold ε, while in internal fault causes, all these values will be less than ε.

3.3 Relay Architecture

A simplified flow chart of the decision making logic is showed in Figure 7; block (1) implements the calculation of the three-phase differential currents and restraint currents; the restraining currents are only used at the stage of block (1) and (2) to prevent false tripping due to the CT mismatch, CT error between LV and HV side and error caused by tap changer; block (2) signifies that the relay is activated if any one of three phase differential currents is over a setting of the differential protection; block (3) implements the wavelet transform to the windowed differential currents; block (4) carries out the calculation of equations (1)-(3); finally the decision is made by block (5) to distinguish internal faults from inrush currents and external fault currents with CTs saturation. If an internal fault is detected, the relay will issue a tripping signal; otherwise, the relay will be restrained and go on to the next moving window signal.
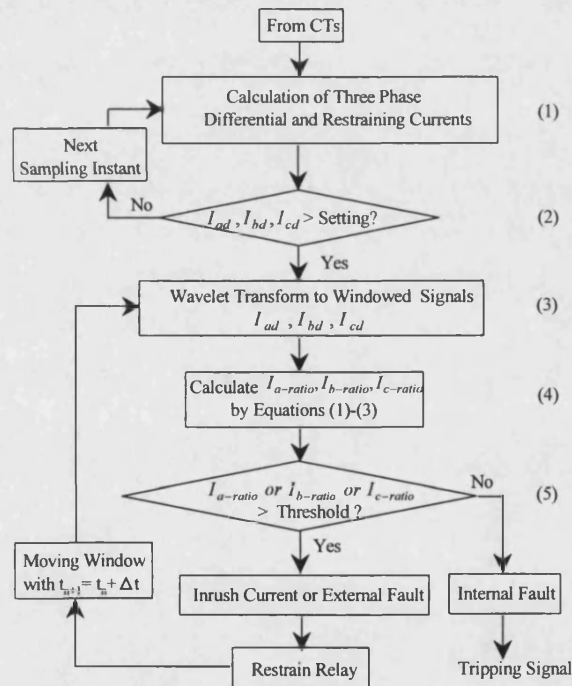
Figure 7: Flow chart of based decision making logic

4 Response Evaluation

In order to evaluate the accuracy of the proposed protection scheme, 220 different power transformer transient events have been generated in two different power transformer systems using the well known EMTP. These cases cover: (a)internal faults, including terminal three-phase short-circuit, terminal two-phase-to-earth fault, terminal phase-to-phase fault, terminal single-phase-to-earth fault,

internal winding turn-to-earth and turn-to-turn faults; (b)various magnetising inrush currents with different energising angles and different remnant fluxes in core of the power transformer; such as the inrush currents are simulated without the remnant flux in a, b and c three-phase transformer core and with the remnant flux under the condition that there are a remnant flux of 70% rated flux in a-phase core, -35% rated flux in both b-phase and c-phase core; (c)external faults with extreme CT saturation. The diversity of transient events both in the system 1 and system 2 is distributed as shown in Table 1.

Table 1: The distribution of different transient events

No	Specification	Number of Cases
1	Internal terminal faults	120
2	Internal winding faults	24
3	Inrush currents	72
4	External faults with CT saturation	4
	Total Cases	220

Fig.8(b)-9(b) present typical responses of the relay to inrush current cases in the system 1 and system 2 respectively, while Fig.8(a)-9(a) present corresponding a-phase DWT of inrush currents at detail 1. For brevity, b-phase and c-phase DWT are not shown herein. Fig.10(b)-11(b) present typical responses of the relay to internal faults in the system 1 and system 2 respectively, while Fig.10(a)-11(a) present corresponding a-phase DWT of internal fault currents at detail 1. Here again, b-phase and c-phase DWT are not shown. From these figures we can see that the proposed scheme can correctly discriminate internal faults from inrush currents.
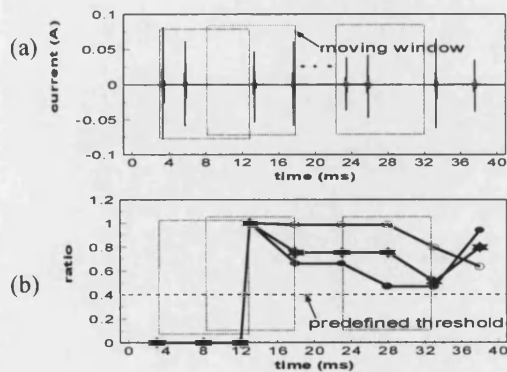
Figure 8 Relay Response under inrush current in system 1(a) a-phase DWT at detail 1 (b) restraint signal under inrush current
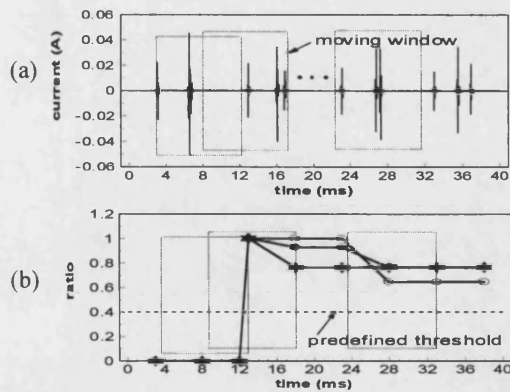
Figure 9 Relay Response under inrush current in system 2(a) a-phase DWT at detail 1(b) restraint signal under inrush current
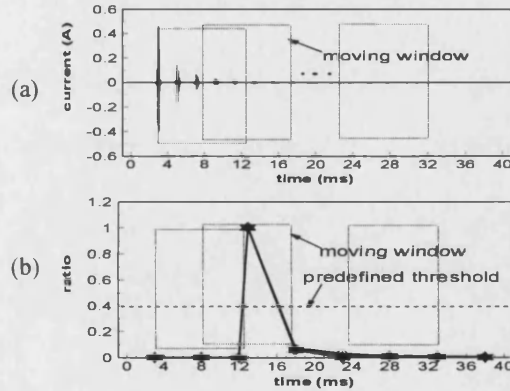
Figure 10 Relay Response under internal fault in system 1(a) a-phase DWT at detail 1 (b) tripping signal under internal fault
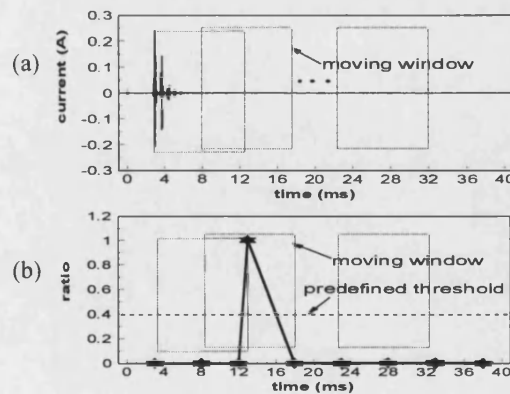
Figure 11 Relay Response under inrush current in system 2(a) a-phase DWT at detail 1 (b) tripping signal under internal fault

Table 2 presents the results of the relay responses to all case studies. From this table we can see the misclassification rate is zero within the given 220 cases.

Table 2: Statistical testing results by decision making logic

Case number	Correct classification	Incorrect classification	Correct (%)
220	220	0	100

As the decision is made from the second moving window, the time for making decision is at least $t_{decision} = t_2 - t_1$, where t_2 = time instant at the end of the second moving window and t_1 = the time instant of the relay activation. Hence, the time for making decision in the proposed scheme is within 20 ms.

5 Conclusions

A new decision making logic scheme based on the wavelet transform has been proposed to distinguish internal faults from magnetising inrush transients. The case studies have been implemented in two different power transformer systems. The results indicate that the proposed scheme can not only accurately distinguish internal faults from inrush currents (correct%=100% within studied 220 cases), but is also suitable for different power transformer systems. Extensive simulation studies have verified the suitability and effectiveness of the proposed method. It can be therefore used as an attractive and effective protection scheme in power transformers.

6 References

[1] M. A. Rahman and B. Jeyasurya, "A State-of-the-Art Review of Transformer Protection Algorithms", IEEE Trans. On Power Delivery, Vol.3, No.2, 1988, pp.534-544.

[2] Stanley H. Horowitz, Arun G. Phadke, "Power System Relaying (Second edition, book)", Research Studies Press Ltd, Taunton, Somerset, England, 1995

[3] Walter A. Elmore , "Protective Relaying Theory and Application", ABB Power T&D Company Inc, Relay Division, Coral Springs, Florida, 1995

[4] P.Liu, O.P.Malik, C.Chen, G.S.Hope, and Y.Guo "Improved Operation of Differential Protection of Power Transformers for Internal Faults", IEEE Trans on Power Delivery, Vol. 7, No.4, pp:1912~11919, 1992

[5] Sidhu, T. S., Sachdev, M. S., wood, H. C. and Nagpal, M., "Design, Implementation and Testing of A Micor-processor-based High-speed Relay for Detecting Transformer Winding Faults", IEEE Trans on Power Delivery, Vol. 7, No.1, 1992, pp.108-117.

[6] G Perez, A J Flechsig, J L Meador and Z Obradovic, "Training an Artificial Neural Network to Discriminate Between Magnetizing Inrush and Internal Fault", IEEE Trans. On Power Delivery, Vol. 9, No. 1, pp.434-441, January 1994.

[7] P Bastard, M Meunier and H Regal, "Neural-Network-Based Algorithm for Power Transformer Differential Relays", IEE Proc., Generation, Transmission and Distribution, Vol. 142, No. 4, pp. 386-392, July 1995.

[8] Pihler, B Grcar and D Dolinar, "Improved Operation of Power Transformer Protection Using Artificial Neural Network", IEEE Trans. On Power Delivery, Vol. 12, No. 3, pp.1128-1136, July 1997.

[9] B.Kasztenny, M.Lukowicz, E.Rosolowski, "Selecting Type of a Neural Network, Pre- and Post-processing Algorithms for Power Transformer Relaying" 32th University Power Engineering Conference. pp. 708-712. Sept. 1997

[10] M.R.Zaman, M.A. Rahman, "Experimental Testing of the Artificial Neural Network Based Protection of Power Transformers", IEEE Trans. On Power Delivery, Vol. 13, No. 2, pp.510-517, April 1998.

[11] A. Wiszniewski and B.Kasztenny, " A Multi-Criteria Differential Transformer Relay Based on Fuzzy Logic", IEEE Trans. On Power Delivery, Vol. 10, No. 4, pp.1786-1792, October 1995.

[12] B.Kasztenny, E.Rosolowski, M.M.Saha, B.Hillstrom, " A Self-Organizing Fuzzy Logic Based Protective Relay-An Application to Power Transformer Protection" , IEEE Trans. On Power Delivery, Vol. 12, No. 3, pp.1119-1127, July 1997.

[13] M. Kezunovic, C. W. Fromen, F. Phillips "Experimental Evaluation of EMTP-Based Current Transformer Models for Protective Relay Transient Study", IEEE Trans. on Power Delivery, Vol.9, No.1, January 1994, pp.405-413

[14] P L Mao, R K Aggarwal, Z Q Bo, "Analysis of Transient Phenomena in Power Transformers using Wavelet Transforms", the 34th University Power Engineering Conference, *United Kingdom*, 8-10 Sept. 1999

A Novel Approach to the Classification of the Transient Phenomena in Power Transformers Using Combined Wavelet Transform and Neural Network

P L Mao,   R K Aggarwal (FIEE, Sen. MIEEE)

Department of Electronic and Electrical Engineering,
University of Bath, Bath BA2, 7AY, England

Abstract - The wavelet transform is a powerful tool in the analysis of the power transformer transient phenomena because of its ability to extract information from the transient signals simultaneously in both the time and frequency domain. This paper presents a novel technique for accurate discrimination between an internal fault and a magnetising inrush current in the power transformer by combining wavelet transforms with neural networks. The wavelet transform is firstly applied to decompose the differential current signals of the power transformer into a series of detailed wavelet components. The spectral energies of the wavelet components are calculated and then employed to train a neural network to discriminate an internal fault from the magnetising inrush current. The simulated results presented clearly show that the proposed technique can accurately discriminate between an internal fault and a magnetising inrush current in power transformer protection.

Keywords: Power transformer, Fault detection, Magnetising inrush current, Wavelet transform, Artificial neural network,

I. INTRODUCTION

Large power transformers are a class of very expensive and vital components of electric power systems. Since it is very important to minimise the frequency and duration of unwanted outages, these is a high demand imposed on power transformer protective relays; this includes the requirements of dependability associated with no mal-operations, security associated with no false tripping, and operating speed associated with short fault clearing time. Protection of large power transformers is a very challenging problem in power system relaying [1].

Discrimination between an internal fault and a magnetising inrush current has long been recognised as a challenging power transformer protection problem. Since a magnetising inrush current generally contains a large second harmonic component in comparison to an internal fault, conventional transformer protection systems are designed to restrain during inrush transient phenomenon by sensing this large second harmonic

[2]. However, the second harmonic component may also be generated during internal faults in the power transformer. This may be due to CT saturation or the presence of a shunt capacitor or the distributive capacitance in a long EHV transmission line to which the transformer may be connected [3]. In certain cases, the magnitude of the second harmonic in an internal fault current can be close to or greater than that present in the magnetising inrush current. Moreover, the second harmonic components in the magnetising inrush currents tend to be relatively small in modern large power transformers because of improvements in the power transformer core material [4]. Consequently, the commonly employed conventional differential protection technique based on the second harmonic restraint, will thus have difficulty in distinguishing between an internal fault and an inrush current thereby threatening transformer stability. Alternative, improved protection techniques for accurately and efficiently discriminating between internal faults and inrush currents have thus to be found.

Recently, Artificial Neural Network (ANN) techniques have been applied to power transformer protection to distinguish internal faults from magnetising inrush currents [5-8]. The main advantage of the ANN method over the conventional method is the non-algorithmic parallel distributed architecture for information processing. In references [5] and [6], neural network based schemes for protection of a one-phase power transformer have been investigated, while applications of the neural network for a three-phase power transformer protection have been reported in references [7] and [8]. However, the ANNs in these existing studies are specific to particular transformer systems, and would have to be retrained again for other systems. Moreover, the employed feature extraction techniques are based on either time or frequency domain signals, and not both time and frequency features of the signal; this is very important for accurately distinguishing between an internal fault and inrush current.

The wavelet transform is a relatively new and powerful tool in the analysis of the power transformer transient phenomenon because of its ability to extract information from the transient

signals simultaneously in both the time and frequency domain, rather than conventional Fourier Transform which can only give the information in the frequency domain. Recently, the wavelet transforms have been applied to analyse the power system transients[9], power quality[10], as well as fault location and detection problems[11]. In reference [12], the wavelet transform for analysing the transient phenomena in a power transformer under conditions of faults and magnetising inrush currents was presented, and simulated results have shown that it is possible to use certain wavelet components to discriminate between internal faults and magnetising inrush currents.

This paper presents a technique to discriminate between an internal fault and a magnetising inrush current by combining the wavelet transform with the neural network. The wavelet transform technique is firstly applied to decompose differential current signals of power transformer systems into a series of detailed wavelet components, each of which is a time-domain signal that covers a specific frequency band. Thus, the time and frequency domain features of the transient signals are extracted. The spectral energies of the wavelet components are calculated and then employed to train a neural network to discriminate internal faults from magnetising inrush currents. The effectiveness and robustness of the technique is demonstrated by firstly training and testing a *750MVA, 27/420 kV* transformer connected to a power system, and secondly, by testing its performance for a *35MVA, 11/132 kV* transformer system. The simulated results presented clearly show that the proposed technique can accurately discriminate between an internal fault and a magnetising inrush current in different power transform systems.

II. SIMULATION OF POWER TRANSFORMER TRANSIENTS

An extensive series of simulation studies have been carried out to obtain various power transformer transient signals for subsequent analysis. Two different power transformer systems, i.e., system 1 and system 2, are considered in this study. In system 1, a typical *750MVA, 27/420 kV, Dy11* power transformer is connected between a *25 kV* source at the sending end and a *400kV* transmission line connected to an infinite bus power system at the receiving end. The system 1 configuration and its three-phase connection diagrams are shown in Figures 1 (a) and (b), respectively. In Fig.1(b), I_{ad}, I_{bd}, I_{cd} refer to a, b and c three phase differential currents through the CT secondary sides; n_1 and n_2 are the number of turns on the low voltage (LV) and high voltage (HV) sides, respectively. System 2 is the second

system considered, comprising of a *35MVA, 11/132 kV, Yy0* power transformer.

The simulations of these two power transformer systems have been carried out using the well known EMTP software. In each simulation of the system, the power transformer faults and system parameters are varied, including the fault types, fault positions, fault inception angles, remnant fluxes in power transformer core. The effect of CT saturation is also studied.
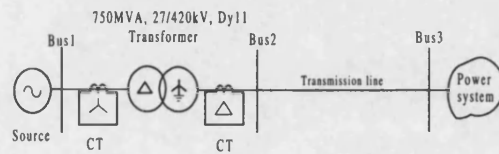
(a) system configuration
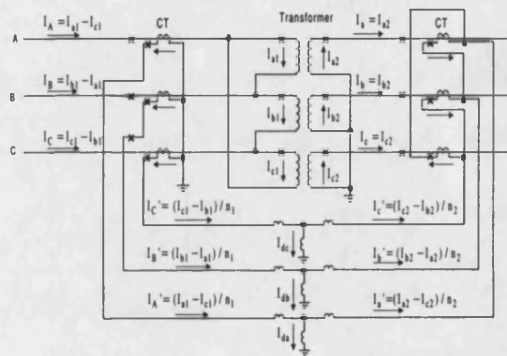
(b) three-phase connection

Figure 1: Simulated power transformer system

III. WAVELET ANALYSIS OF TRANSIENT PHENOMENA

A. Implementation of Wavelet Transform

There are many types of mother wavelets, such as Harr, Daubichies, Coiflet and Symmlet wavelets. The choice of mother wavelet plays a significant role in detecting and localising different types of fault transients. In addition to this, the choice also depends on a particular application. In this study, we are particularly interested in detecting and analysing low amplitude, short duration, fast decaying and oscillating type of high frequency current signals. One of the most popular mother wavelets suitable for a wide range of applications used is Daubichies's wavelet. In this paper, D4 wavelet is used.

Figure 2 illustrates the implementation procedure of a Discrete Wavelet Transform (DWT), in which x[n] is the original signal, h[n] and g[n] are low-pass and high-pass filters, respectively. At the first stage, an original signal is divided into two halves of the frequency

bandwidth, and sent to both high-pass filter and low-pass filter. Then the output of low-pass filter is further cut in half of the frequency bandwidth, and sent to the second stage; this procedure is repeated until the signal is decomposed to a pre-defined certain level. The set of signals thus attained represent the same original signal, but all corresponding to different frequency bands.

It is worth pointing out that the frequency band of each detail of the DWT is directly related to the sampling rate of the original signal. If the original signal is being sampled at F_s Hz, the highest frequency that the signal could contain, from Nyquist's theorem, would be $F_s/2$ Hz. This frequency would be seen at the output of the high frequency filter, which is the first detail. Thus the band of frequencies between $F_s/2$ and $F_s/4$ would be captured in detail 1; similarly, the band of frequencies between Fs/4 and Fs/8 would be captured in detail 2, and so on.
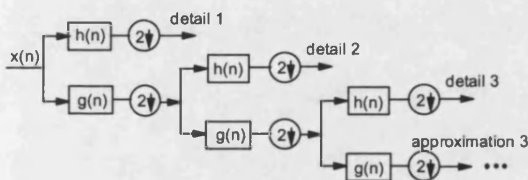
Figure 2 Implementation of DWT

B. Wavelet Transform of Magnetising Inrush Current

When the power transformer is energised on the primary side with the secondary side open-circuited, a transient magnetising inrush current flows in the primary side. This current may reach instantaneous peaks of 6-8 times full-load current because of the extreme saturation of the iron-core in the power transformer. Figure 3 (a) typifies the magnetising inrush current waveforms, which correspond to a, b and c three phase differential currents through the CT secondary sides in the power transformer system 1. As can be seen, the current waveforms are distorted quite significantly; gaps appear over the times of the inrush currents. At the edges of the gaps, the current magnitude changes from near zero to a significant value or from a significant value to near zero; this would be expected by virtue of the fact that sudden changes from one state to other different states produce small ripples, which very often are not visible due to the large fundamental frequency signals as apparent Fig.3 (a). However, these phenomena can be discerned and clearly demonstrated by wavelet transform. For brevity, only the DWT of the a-phase differential current is shown herein.
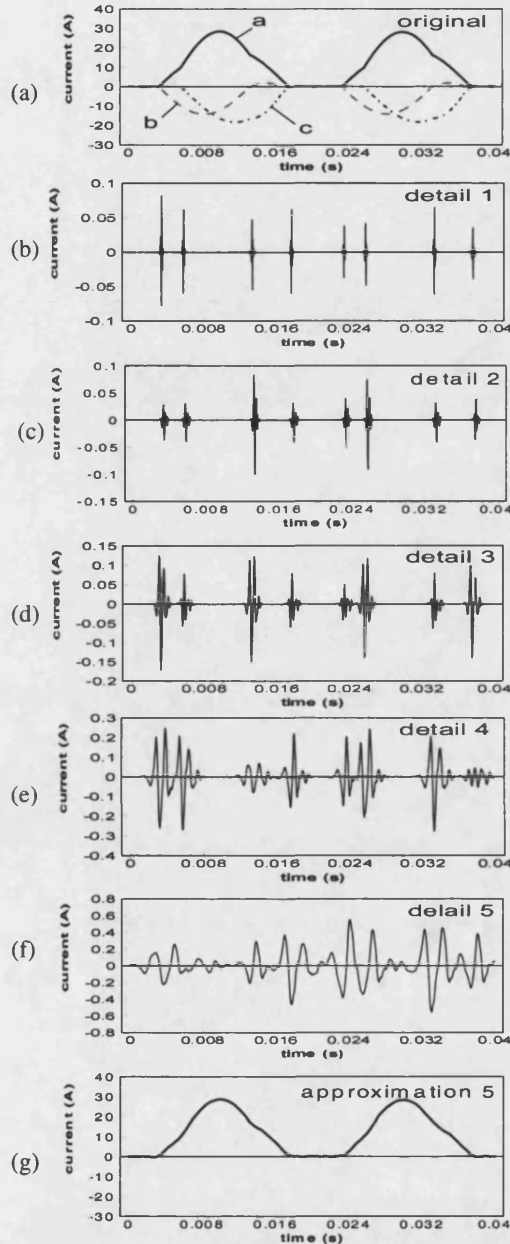
Figure 3: 5-successive details and approximation for inrush current

It should point out that in implementing the DWT, the original inrush current signal has been sampled at 25kHz and passed through a DWT, based on the structure shown in Figure 2. Based on the foregoing, 5-detailed signals that contain a frequency band of 12.5kH ~ 6.25kH at detail 1, 6.25kH ~ 3.125kH at detail 2, 3.125kH ~ 1.562kH at detail 3, 1.562kH ~ 781Hz at detail 4 and 781Hz ~ 390 Hz at detail 5 as well as one approximate signal in the frequency band 390Hz ~ DC level), are shown in Figures 3(b)-(g). From these Figures, it can be clearly seen that there are very useful

features in the decomposed magnetising inrush signals. A certain high frequency component can be located better in time than a low frequency component. In contrast, a low frequency component can be located better in the frequency domain than the high frequency component; this effectively means that all the features for a particular signal are obtained. In this study, since we are interested in those components that are located better in time, details 1-3 are the ones employed in the analysis and feature extraction.

From Figures 3(b)-(d), which correspond to details 1-3, it can be seen that there are a number of sharp spikes during the period of the inrush current transient. From the foregoing analysis, a number of these arise at edges of gaps at which the inrush current suddenly changes from one state to other different states; others are produced because the primary windings of the power transformer are connected as delta, so that the a-phase differential current is in fact the difference between the a-phase magnetising inrush current and c-phase magnetising inrush current. This results in the non-smooth points in the current waveforms, which in turn cause sharp spikes to appear in the DWT of the current waveforms.

C. Wavelet Transform of Internal Fault Current

Fig.4(a) typifies current signals for an internal fault, and corresponds to a, b and c three phase differential currents through the CT secondary sides, under an a-b earth fault on the high voltage side of the power transformer. It is apparent from Fig.4(a) that there is a high frequency distortion in the current waveforms. This is as a direct consequence of the effects of the distributed inductance and capacitance of the transmission line. This can lead to a significant second harmonic in the internal fault[3], thereby posing difficulty in an accurate discrimination between magnetising inrush and internal fault currents by the conventional protection method.

For brevity, only the DWT of the a-phase differential current is presented here as shown in Figures 4(b)-(g); these correspond to the details 1-3 of the DWT and it can be seen that there are several sharp spikes appearing immediately following the fault inception time. However, in marked contrast to the inrush current case, these sharp spikes rapidly decay to near zero within one cycle, whereas those sharp spikes associated with the inrush current suffer from little attenuation during the entire inrush transient period, which can last from perhaps 10 cycles for small transformers to 1 min for large units [13]. It is apparent that this difference can be effectively used as the key feature to distinguish the internal fault from the inrush current.
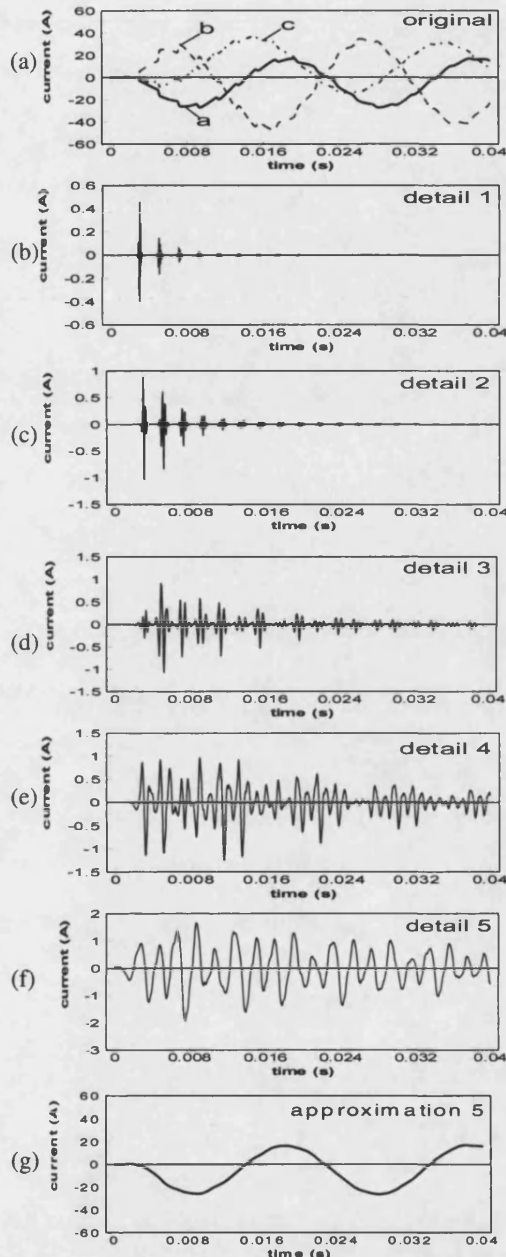
Figure 4: 5-successive details and approximation for a-b two-phase to earth fault on high voltage side

D. Wavelet Transform of External Fault Current with CT Saturation

A differential current is designed to restraint under normal load flows and for external faults. However, external short circuits can in fact result in very large differential currents, if the CTs saturate. It is thus crucial to be able to ascertain CT saturation effects on the measured currents under external faults. The severity of CT saturation is accentuated by the presence of remnant flux in the CT core. Fig.5(a) shows the simulated differential

current waveforms (through the CT secondary sides) for an external three-phase short circuit, which occurs on the Bus 2 (see Fig.1(a)) under the condition that there is an initial remnant flux (65% rated flux) in the a-phase CT core on the low voltage side, and a zero remnant flux in a-phase CT core on the high voltage side. From Fig.5(a), it can be seen that, as expected, there is a significant imbalance current appearing in a-phase differential current.
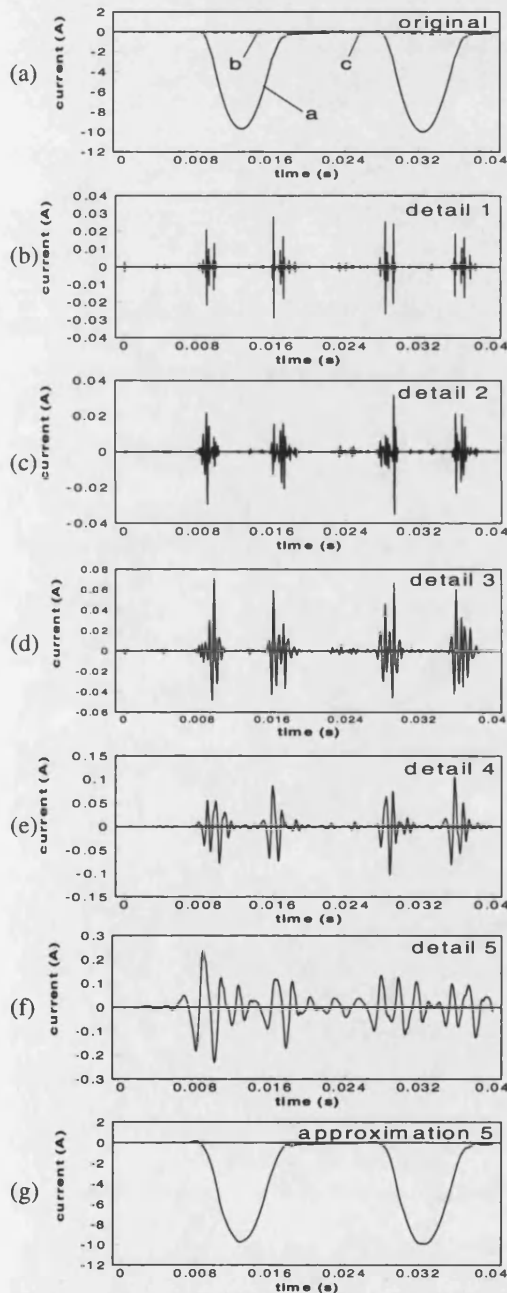
Figure 5: 5-successive details and approximation for external fault under CT saturation condition

From Figs 5(b)-(d), which correspond to the details 1-3 of the DWT, it can be seen that there are several sharp spikes that last during the entire period of the saturation transient, which depends on the D.C component and the remnant flux of CT core. However, unlike the case for inrush current, these bursts comprise of a number of spikes clustered very close to each other. Here again, It is the apparent unique features that can be used to distinguish between an internal fault and an external fault under CT saturation.

IV. NEURAL NETWORK ARCHITECTURE

A. Input Selection of Neural Network

The input data set for the neural network is organised in the form of a moving data window with a fixed window length of a half cycle (10 ms at 50Hz frequency). It is not practical to directly use the windowed wavelet signals as the input to ANN, because this will result in a large number of inputs to ANN, i.e. a large size ANN, thereby causing difficulty in ANN convergence. The usage of the signal spectral energy overcomes this drawback. Essentially, in this approach, spectral energy of the wavelet signal is calculated within the time length Δt; this not only reduces ANN size, but also retains important features of the wavelet signals. In this study, the data window is divided into 3 equal time periods to calculate the spectral energy, and hence, 9 samples are obtained from details 1-3 for each phase. Thus, for a, b and c phase, there are total 27 samples that are fed into the ANN.

The step length of the moving window is ¼ cycle (5ms at 50 Hz frequency). Sliding motion is to put ¼ cycle of the new spectral energies at the front of the window, and discard ¼ cycle of the spectral energies from the end of the previous window.

B. Neural Network Structure and Training

Neural networks have been developed in a wide variety of configurations, where each of them has its individual characteristics, advantages and disadvantages. In this study, a multi-layer feedforward network has been employed.

With the 27 inputs, the target output of the ANN was built in such way that the value 1 represents an internal fault; the value -1 represents a magnetising inrush current or an external fault current.

One of the most critical problems in constructing the ANN is the choice of the number of hidden layers and the number of neurons for each layer. Using too few neurons in the hidden layer may prevent the training process to converge, while using too many neurons would produce long training time, and/or result in the ANN to lose its generalisation attribute. In this study, a number of

tests were performed varying with the one or two hidden layers as well as varying the number of neurons in each hidden layer. Table 1 shows the architectures tested for this purpose. From the table it can be seen that the combination of 5 neurons in the first hidden layer and 4 neurons in the second hidden layer shows the best performance, and this is the architecture adopted in this paper.

The neural network employs the back-propagation algorithm, and the hyperbolic tangent activation function with the cumulative delta rule was used.

V. COMBINED WAVELET TRANSFORM AND NEURAL NETWORK PROTECTION TECHNIQUE

The proposed relay logic for distinguishing an internal fault from a magnetising inrush current by combining the wavelet transform with neural network is shown in Figure 6.
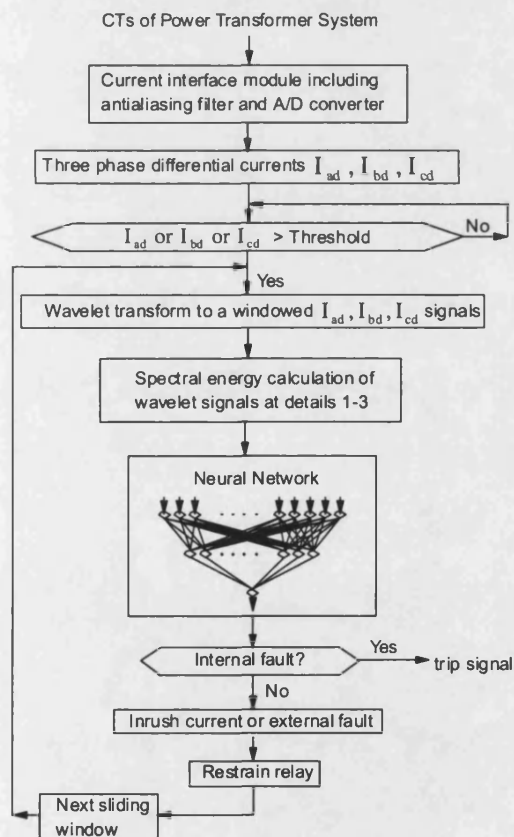
Figure 6: Relay logic based on wavelet transform and neural network

In Fig.6, the relay is activated if any one of the three-phase differential currents (through the secondary side of CTs) I_{ad}, I_{bd}, I_{cd} exceeds the predefined thresholds. The wavelet transforms are

applied to the windowed differential currents I_{ad}, I_{bd}, I_{cd} (the method of wavelet transforms is summarised in section IV). Thus, the a, b and c three phase wavelet signals, i.e., $I_{a-detail,1}, I_{a-detail,2}, I_{a-detail,3}$ at details 1-3 for a phase, $I_{b-detail,1}, I_{b-detail,2}, I_{b-detail,3}$ at details 1-3 for b phase and $I_{c-detail,1}, I_{c-detail,2}, I_{c-detail,3}$ at details 1-3 for c phase, are obtained. Then, the spectral energies of the wavelet signals are calculated by the following equations:

$$P_{a-detail,i} = \sum_{k=1}^{n} I_{a-detail,i}^2(k)\Delta t \quad ; (i=1,2,3) \qquad (1)$$

$$P_{b-detail,i} = \sum_{k=1}^{n} I_{b-detail,i}^2(k)\Delta t \quad ; (i=1,2,3) \qquad (2)$$

$$P_{c-detail,i} = \sum_{k=1}^{n} I_{c-detail,i}^2(k)\Delta t \quad ; (i=1,2,3) \qquad (3)$$

where $P_{a-detail,i}, P_{b-detail,i}, P_{c-detail,i}$ respectively represent the spectral energies of wavelet signals in a, b and c three-phase; i respectively represents wavelet detail 1, 2 and 3 (i=1,2,3); Δt= time step length; n = No. of samples in a window.

The obtained spectral energies of the wavelet signals are then inputted to the ANN to carry on the discrimination between an internal fault and inrush current. If the internal fault is detected, a tripping signal will be issued, otherwise, the relay will be restrained.

VI. RESPONSE EVALUATION

A total of 200 cases were simulated using the EMTP software under internal faults and magnetising inrush currents as well an external faults for both system 1 and system 2 (150 cases from the system 1 and another 50 cases from the system 2). About 80% of the cases were used for training and the rest 20% were used for testing. Broadly, the following electromagnetic transient events of the power transformer were taken into consideration in the design/testing of the ANN:
(a) Internal faults including: (i)terminal three-phase fault; (ii)terminal two-phase to earth fault; (iii) terminal two-phase fault; (iv)terminal single-phase to earth fault; (v)internal winding turn-to-earth fault; (vi) internal winding turn-to-turn fault;
(b) various magnetising inrush currents, such as inrush currents with different energising angles and different remnant fluxes in core of the power transformer
(a) external faults with extreme CT saturation.

Figure 7 graphically illustrates the typical responses of the protection scheme for an internal single-phase fault and a three-phase-to-earth fault,

while Figure 8 shows a typical response of the technique under magnetising inrush current. Figure 9 shows a typical response of the relay to an external fault with a-phase CT saturation on LV side. From these results, it can be seen that 10-15 ms after the occurrence of a fault, the protection technique developed correctly identifies the nature of the transient events, i.e. whether it is an internal fault, in which case it will issue a trip signal or whether it is an external fault or a inrush current situation(in which case the protection will restrain).

(a) a-phase to earth on LV side

(b)abc-phase to earth on LV side with a-phase CT saturation
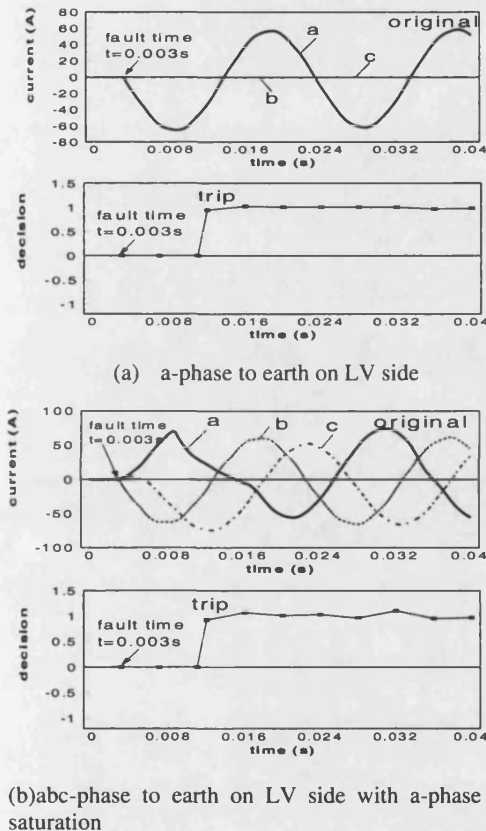
Figure 7: Response of relay to internal faults
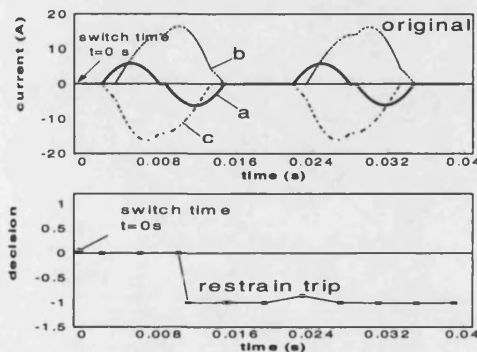
Figure 8: Response of relay to inrush current
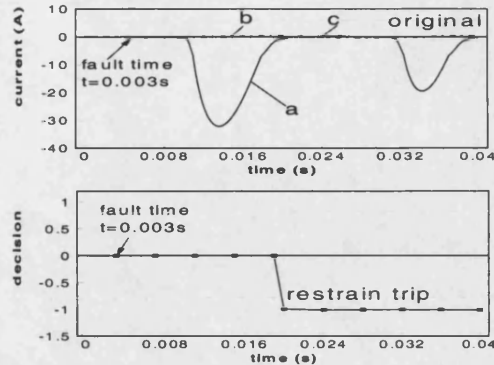
Figure 9: Response of relay for an external fault with a-phase CT saturation on LV side

An extensive series of studies involving many practically encountered different system and fault conditions have shown that the protection technique based on a combined WT and ANN is very effective in accurately discriminating between internal and external faults (including under CT saturation); equally importantly, the technique developed is stable in the presence of the magnetising inrush current. The performance for different ANN architectures is summarised in Table 1. It is apparent that an ANN with 5 neurons in the first hidden layer and 4 in the second, when combined with a DWT, gives the best performance.

Table 1 Summary of neural network performances

ANN Size	Perfor-mances	Correct Patterns	Incorrect Patterns	Classifica -tion rate
27/20/10/1	diverge	-	-	-
27/9/4/1	Converge	97	3	97 %
27/5/4/1	Converge	99	1	99 %
27/20/1	diverge	-	-	-
27/9/1	Converge	96	4	96 %
27/5/1	Converge	95	5	95 %

Note: Classification rate %=100 × (Total patterns– Incorrect patterns) / Total patterns

VII. CONCLUSIONS

This paper presents a novel technique for distinguishing between internal faults and inrush currents in power transformer systems by combining wavelet transform and neural network techniques. The proposed technique is robust to different power transformer systems; this is a significant advantage and this is largely so by virtue of the fact that the wavelet transform technique effectively extracts the very crucial time-frequency features from different power transformer systems, common to all large practical transformers. The performance shown demonstrates that the proposed technique gives a very high accuracy in the classification of the transients ($\approx 99\%$). The proposed technique can be used as an attractive and effective approach for

alternative protection schemes for large power transformers.

VIII. REFERENCES

[1] Bogdan Kasztenny, Mladen Kezunovic, "Digital Relays Improve Protection of Large Transformers", IEEE Computer Application in Power, October 1998, pp:39-45

[2] M. A. Rahman and B. Jeyasurya, "A State-of-the-Art Review of Transformer Protection Algorithms", IEEE Trans. On Power Delivery, Vol.3, No.2, 1988, pp.534-544.

[3] P.Liu, O.P.Malik, C.Chen, G.S.Hope, and Y.Guo "Improved Operation of Differential Protection of Power Transformers for Internal Faults", IEEE Trans on Power Delivery, Vol. 7, No.4, 1992, pp.1912-1919.

[4] Sidhu, T. S., Sachdev, M. S., wood, H. C. and Nagpal, M., "Design, Implementation and Testing of A Micorprocessor-based High-speed Relay for Detecting Transformer Winding Faults", IEEE Trans on Power Delivery, Vol. 7, No.1, 1992, pp.108-117.

[5] P Bastard, M Meunier and H Regal, "Neural-Network-Based Algorithm for Power Transformer Differential Relays", IEE Proc., Generation, Transmission and Distribution, Vol. 142, No. 4, pp. 386-392, July 1995.

[6] G Perez, A J Flechsig, J L Meador and Z Obradovic, "Training an Artificial Neural Network to Discriminate Between Magnetizing Inrush and Internal Fault", IEEE Trans. On Power Delivery, Vol. 9, No. 1, pp.434-441, January 1994.

[7] Pihler, B Grcar and D Dolinar, "Improved Operation of Power Transformer Protection Using Artificial Neural Network", IEEE Trans. On Power Delivery, Vol. 12, No. 3, pp.1128-1136, July 1997.

[8] M.R.Zaman, M.A. Rahman, "Experimental Testing of the Artificial Neural Network Based Protection of Power Transformers", IEEE Trans. On Power Delivery, Vol. 13, No. 2, pp.510-517, April 1998.

[9] W.A.Wilkinson and M.D. Cox, "Discrete Wavelet Analysis of Power System Transients", IEEE Trans. On Power System, Vol.11, No.4, November 1996, pp:2038-2044.

[10] G. T. Heydt and A. W. Galli, "Transient Power Quality Problems Analyzed Using Wavelets", IEEE Trans. On Power Delivery, Vol.12, No.2, April 1997, pp:908-915.

[11] Stantosh Kumar Pandey and L .Satish, "Multiresolution Signal Decomposition: A New Tool for Fault Detection in Power Transformers During Impulse Tests", IEEE Trans. On Power Delivery, Vol.13, No.4, October 1998, pp:1194-1200.

[12] P L Mao, R K Aggarwal, Z Q Bo, "Analysis of Transient Phenomena in Power Transformers using Wavelet Transforms", the 34th University Power Engineering Conference, *United Kingdom*, 8-10 Sept. 1999

[13] Walter A. Elmore , "Protective Relaying Theory and Application", ABB Power T&D Company Inc, Relay Division, Coral Springs, Florida, 1995

[14] M. Habib and M. A. Marin, "A comparative analysis of digital relaying algorithms for the differential protection of three phase transformers", IEEE Trans. On Power System, Vol.3, No.3, 1988, pp.1378-1384.

[15] Stanley H. Horowitz, Arun G. Phadke, "Power System Relaying (Second edition, book)", Research Studies Press Ltd, Taunton, Somerset, England, 1995.

[16] G Perez, A J Flechsig, J L Meador and Z Obradovic, "Training an Artificial Neural Network to Discriminate Between Magnetizing Inrush and Internal Fault", IEEE Trans. On Power Delivery, Vol. 9, No. 1, pp.434-441, January 1994.

[17] M.R.Zaman, M.A. Rahman, "Experimental Testing of the Artificial Neural Network Based Protection of Power Transformers", IEEE Trans. On Power Delivery, Vol. 13, No. 2, pp.510-517, April 1998.

[18] Kasztenny, M.Lukowicz, E.Rosolowski, "Selecting Type of a Neural Network, Pre- and Post-processing Algorithms for Power Transformer Relaying" 32th University Power Engineering Conference. pp. 708-712. Sept. 1997

[19] Charles K. Chui, An Introduction to Wavelets, Academic Press, Inc, 1992

[20] Randy K. Young, *Wavelet theory and its application*, Kluwer Academic Publishers, 1993.

[21] David C. Robertson, Octavia I. Camps, Jeffrey S. Mayer and William B. Gish, "Wavelets and Electromagnetic Power System Transients", IEEE Trans. On Power Delivery, Vol.11, No.2, April 1996, pp:1050-1058.

[22] L. Angrisani, P. Daponte, M.D.Apuzzo and A.Testa, "A Measurement method Based on the Wavelet transform for Power Quality Analysis", IEEE Trans. On Power Delivery, Vol.13, No.4, October 1998, pp:990-998.

[23] S. Stantoso, E. J. Powers and W. M. Grady, "Power Quality Disturbance Data Compression using Wavelet Transform Methods", IEEE Trans. On Power Delivery, Vol.12, No.3, July 1997, pp:1250-1256.

[24] Fernando H. Magnago and Ali Abur, "Fault Location Using Wavelets", IEEE Trans. On Power Delivery, Vol.13, No.4, October 1998, pp:1475-1480.

BIOGRAPHIES

Peilin Mao is a PhD student in the Power and Energy System Group at the University of Bath, England. Her current research interests are the electromagnetic transient simulation of power systems and application of artificial intelligence techniques to power system protection. She is an Associate Member of the IEE (U.K.). Her email address is eeppm@bath.ac.uk

Raj K Aggarwal (SM'91) received the B.Eng and Ph.D degrees from the University of Liverpool, England. in 1970 and 1973, respectively. He joined the Power and Energy System Group at the University of Bath, England, where he is now a Professor. His main areas of research interests are power system modelling and application of digital technology and artificial intelligence to protection and control. He has published over 200 technical papers and co-authored three text books. Prof. Aggarwal is a fellow of the IEE (U.K.).

An alternative approach to digital simulation of the transient phenomena in power transformers utilising EMTP functions

P. L. Mao   R. K. Aggarwal

Department of Electronic and Electrical Engineering,
University of Bath, Bath BA2 7AY

Abstract: An accurate digital simulation of a power transformer system provides a good supplementary tool to new relay design and relay performance evaluation. This paper presents a technique for accurately modelling a large power transformer for the purposes of simulating its transient phenomena under both fault and magnetising inrush current conditions. The simulation also includes a model of a current transformer (CT) used for providing correct operating currents to a protective relay system; in the latter case, the effect of CT saturation on the protective devices is also modelled. The purpose of the simulation is to develop alternative techniques for satisfactorily protecting a power transformer under a whole variety of practically encountered faults concomitant with their ability to distinguish internal faults from magnetising inrush currents.

Keywords: Power transformer, fault transient simulation, magnetising inrush current, transformer protection, current transducers

1 INTRODUCTION

Power transformers are essential and important elements of electrical power systems; in particular, they form a vital link between power generation and transmission lines and/or between transmission lines and loads. Thus, the power transformer protection is of crucial importance. A conventional transformer protection based on current differential principles offers an adequate means of detecting internal winding faults of a power transformer. However, when transformers are energised, a large magnetising inrush current flows in the transformer windings, setting up a differential current in the protection relays. This is not a fault condition, and therefore does not necessitate the operation of protection, which on the contrary must remain stable during the inrush transient phenomenon.

Since a magnetising inrush current generally contains a large second harmonic component in comparison to an internal fault, transformer protection systems are designed to restrain this inrush transient phenomenon by sensing the large second harmonic [1,2,3,4]. However, the second harmonic component may also be generated during internal faults in the power transformer. These may be due to CT saturation or the

presence of a parallel capacitor or the distributed capacitances in a long EHV transmission line to which the transformer may be connected [5]. In certain cases, the magnitude of the second harmonic in an internal fault can be close to or greater than that present in the magnetising inrush current. Moreover, the second harmonic components in the magnetising inrush currents tend to be relatively small in modern large power transformers because of improvements in the power transformer core material [6]. Consequently, the commonly employed conventional differential protection technique, based on the second harmonic restraint, will thus have difficulty in distinguishing between an internal fault and an inrush current thereby threatening transformer stability. Alternative, improved protection techniques have thus to be found. In order to achieve this, it is vitally important to be able to accurately model a transformer with its associated transient phenomena.

An accurate digital simulation of the power transformer system provides a good supplementary tool to new relay design and/or performance evaluation of existing protection techniques. It can, not only simulate and analyse the complex fault transient phenomena of a power transformer system, but also can be used as a valuable preliminary step for overall relay system designs and performance testing. This paper presents a technique for accurately modelling a power transformer and measurement CTs for the purposes of simulating the transient phenomena in a power transformer system under a whole variety of practically encountered faults and system conditions, such as under external faults and internal winding faults, magnetising inrush currents, and with/without CT saturation. The simulated waveforms are illustrated with respect to a typical *750MVA, 27/420kV* power transformer connected between a *25kV* source and a *400kV* transmission line.

2 MATHEMATICAL MODELS

Realistic modelling of power transformers under various conditions in particular transient is never an easy task. The widely used Electromagnetic Transient Programs (EMTP) provides several possibilities for simulating the main characteristics of a power transformer. This involves several subprograms such as XFORMER, TRELEG and BCTRAN. The XFORMER is based on data relating to resistances,

inductances and the winding ratio for the simplest transformers. BCTRAN is based excitation and short-circuit tests in both positive and zero sequence networks for the more complex transformers. TRELEG has been replaced by BCTRAN because of ill-conditioning problems. However, all these programs do not have ability to model winding faults. However, as mentioned before, it is vitally important to be able to accurately model the fault transient phenomena in a transformer, for example, for the purposes of designing a protection technique. It was against this background that the technique presented here was developed, and is an extension of that presented in reference [7].

2.1 Modelling of power transformers

A power transformer model is built up based on the mutual coupling concept. With this approach, any multi-winding transformer consisting of n coupling coils can be electrically modelled in terms of the terminal voltage V_i, and current i_i, as well as total flux linkage λ_i, of the ith coil as follows [8,9]:

$$V_i = R_i i_i + \frac{d\lambda_i}{dt} \qquad (1)$$

where $i=1,2,3,...,n$. Such a transformer can be represented schematically, and Figure 1 shows an example of a transformer with six windings. When magnetic saturation is taken into consideration, λ_i becomes a non-linear function of the n-winding currents, that is:

$$\lambda_i = \lambda_i(i_1,i_2,\cdots,i_n) \qquad (2)$$

Thus, for the ith coil, eqn. 1 can be expanded using the chain rule as follows:

$$V_i = R_i i_i + \frac{\partial \lambda_i}{\partial i_1}\frac{di_1}{dt} + \frac{\partial \lambda_i}{\partial i_2}\frac{di_2}{dt} + \cdots + \frac{\partial \lambda_i}{\partial i_n}\frac{di_n}{dt} \qquad (3)$$

The partial derivatives of the flux linkage λ_i with respect to a winding current i_k $(k=1,2,...,n)$, are the incremental inductances, L_i and M_{ik}, given as:

$$L_i = \frac{\partial \lambda_i}{\partial i_i} \qquad (4)$$

$$M_{ik} = \frac{\partial \lambda_i}{\partial i_k} \qquad (i \neq k) \qquad (5)$$

Thus, if the power transformer is a three-phase two-winding transformer comprising of six windings, then the mathematical model for such a transformer can be represented by the following matrix relationship:

$$[V] = [R][i] + [L]\left[\frac{di}{dt}\right] \qquad (6)$$

or

$$\left[\frac{di}{dt}\right] = [L]^{-1}[V] - [L]^{-1}[R][i] \qquad (7)$$

where

$$[R] = \begin{bmatrix} R_1 & 0 & 0 & 0 & 0 & 0 \\ 0 & R_2 & 0 & 0 & 0 & 0 \\ 0 & 0 & R_3 & 0 & 0 & 0 \\ 0 & 0 & 0 & R_4 & 0 & 0 \\ 0 & 0 & 0 & 0 & R_5 & 0 \\ 0 & 0 & 0 & 0 & 0 & R_6 \end{bmatrix} \qquad (8)$$

$$[L] = \begin{bmatrix} L_1 & M_{12} & M_{13} & M_{14} & M_{15} & M_{16} \\ M_{21} & L_2 & M_{23} & M_{24} & M_{25} & M_{26} \\ M_{31} & M_{32} & L_3 & M_{34} & M_{35} & M_{36} \\ M_{41} & M_{42} & M_{43} & L_4 & M_{45} & M_{46} \\ M_{51} & M_{52} & M_{53} & M_{54} & L_5 & M_{56} \\ M_{61} & M_{62} & M_{63} & M_{64} & M_{65} & L_6 \end{bmatrix} \qquad (9)$$

$$[V] = [V_1,V_2,V_3,V_4,V_5,V_6]^T \qquad (10)$$

$$[i] = [i_1,i_2,i_3,i_4,i_5,i_6]^T \qquad (11)$$

$$\left[\frac{di}{dt}\right] = \left[\frac{di_1}{dt} \quad \frac{di_2}{dt} \quad \frac{di_3}{dt} \quad \frac{di_4}{dt} \quad \frac{di_5}{dt} \quad \frac{di_6}{dt}\right]^T \qquad (12)$$

and $V_1 - V_6$ are the terminal voltages of the primary and secondary windings respectively; $i_1 - i_6$ are the currents of the primary and secondary windings respectively; $R_1 - R_6$ are the resistances of the primary and secondary windings respectively; $L_1 - L_6$ are the self inductances of the primary and secondary windings respectively; M_{ij} are the mutual indutances between windings i and j respectively $(i=1,2,...,6; j=1,2,...,6; i \neq j)$. The foregoing transformer model is than embedded into the basic transmission network model using the EMTP software.

2.2 Modelling of internal winding faults

The principle used to model a fault between a coil turn and earth or between turn and turn hinges upon dividing the faulted coil, as shown in Figure 2. When the power transformer winding has no fault, matrix [R] and [L] for a three-phase two-winding transformer are of order 6 as given in eqn.8. and eqn.9. When a turn-to-earth fault occurs as shown in Figure 2, the transformer can be described by two 7×7 matrices, $[R]_{7 \times 7}$ and $[L]_{7 \times 7}$ respectively. These are described by:

$$[R]_{7x7} = \begin{bmatrix} R_1 & 0 & 0 & 0 & 0 & 0 & 0 \\ 0 & R_X & 0 & 0 & 0 & 0 & 0 \\ 0 & 0 & R_Y & 0 & 0 & 0 & 0 \\ 0 & 0 & 0 & R_3 & 0 & 0 & 0 \\ 0 & 0 & 0 & 0 & R_4 & 0 & 0 \\ 0 & 0 & 0 & 0 & 0 & R_5 & 0 \\ 0 & 0 & 0 & 0 & 0 & 0 & R_6 \end{bmatrix} \quad (13)$$

$$[L]_{7x7} = \begin{bmatrix} L_1 & M_{1X} & M_{1Y} & M_{13} & M_{14} & M_{15} & M_{16} \\ M_{X1} & L_X & M_{XY} & M_{X3} & M_{X4} & M_{X5} & M_{X6} \\ M_{Y1} & M_{YX} & L_Y & M_{Y3} & M_{Y4} & M_{Y5} & M_{Y6} \\ M_{31} & M_{3X} & M_{3Y} & L_3 & M_{34} & M_{35} & M_{36} \\ M_{41} & M_{4X} & M_{4Y} & M_{43} & L_4 & M_{45} & M_{46} \\ M_{51} & M_{5X} & M_{5Y} & M_{53} & M_{54} & L_5 & M_{56} \\ M_{61} & M_{6X} & M_{6Y} & M_{63} & M_{64} & M_{65} & L_6 \end{bmatrix} \quad (14)$$

The position of the fault point is expressed by n_X and n_Y where:

n_X = number of turns of "sub-coil" x

n_Y = number of turns of "sub-coil" y

and the additional elements in the matrix $[R]_{7x7}$ in eqn. 13 are defined by:

$$R_X = \frac{n_X}{n_2} R_2 \; ; \qquad R_Y = \frac{n_Y}{n_2} R_2 \quad (15)$$

where R_2 is given by the original 6×6 matrix $[R]$ given in eqn. 8. The additional elements in the matrix $[L]_{7x7}$ in eqn. 14 are given by:

$$L_X = \frac{L_2}{(1/K^2)+(2\sqrt{1-\sigma_{XY}}/K)+1} \quad (16)$$

$$L_Y = \frac{L_2}{K^2 + 2K\sqrt{1-\sigma_{XY}}+1} \quad (17)$$

$$M_{XY} = \frac{L_2\sqrt{1-\sigma_{XY}}}{K+1/K+2\sqrt{1-\sigma_{XY}}} \quad (18)$$

$$M_{Xi} = (K/(K+1))M_{2i} \quad (19)$$

$$M_{Yi} = (1/(1+K))M_{2i} \quad (20)$$

$$K = \frac{n_X}{n_Y} \quad (21)$$

where K is the voltage ratio between sub-coils x and y; σ_{XY} is a leakage factor. A very simple method is proposed to evaluate the leakage factor [9] (herein, $\sigma_{XY} = 0.016$); L_2 and M_{2i} are given by the original 6×6 matrices given by eqn. 9. For a turn-to-turn fault (as shown in figure 2), the dimensions of the aforementioned $[R]$ and $[L]$ matrices are increased to 8×8. A mathematical method representing such a fault can be similarly described.

2.3 Modelling of inrush currents

When a power transformer is energised on the primary side with the secondary open-circuited, a transient magnetising inrush current may flow in the primary side of the power transformer, and this current may reach 10 times the full-load current because of the extreme saturation of the transformer iron-core. It is thus apparent that modelling inrush current must take into account the core saturation.

It should be noticed, in eqn.4 and eqn.5, that since λ_i is a non-linear function of the n-winding currents, it is related to the non-linearity of the power transformer core, which in turn is dictated by the non-linear magnetising curve of the core. This problem of simulating non-linearity is overcome here by adding equivalently a non-linear element ($\phi - i$ curve) to the liner matrix $[L]$ shown in eqn.9.

2.4 CT modelling

A CT is the interface component between the protective devices and the practical power transformer system, and is used for providing the correct operating current to the protective relay system. Accurate modelling and simulating the transient behaviour of the CT, particularly its saturation characteristics, is vitally important for relay studies. CT models developed herein are essentially based on those outlined in reference [10,11]. This model comprises of an equivalent circuit built around an ideal transformer as shown in Figure 3. The magnetising branch is represented as a non-linear inductor, and it is represented by a λ-i hysteresis loop.

3 THE SIMULATED SYSTEM STUDIED

The power transformer transient phenomenon is simulated in a system comprising a typical *750MVA 27/420kV*, power transformer connected between a *25kV* source at the sending end and a *400kV* transmission line connected to an infinite bus power system at the receiving end. Generally, there are typically four types of connections (star-delta, delta-star, star-star, and delta-delta) used for a three-phase two-winding transformer. The most common connection for stepping up the generator voltage for transmission purposes is the delta-star, with the high voltage neutral (star secondary) solidly grounded, and this is one chosen for the simulated power transformer system herein, as shown in Figure 4. In order to fully investigate the effects of fault transients and inrush currents, on say, the differential current (which is the main variable of the commonly employed Current Differential Protection in transformer protection), the various internal fault and inrush currents are simulated using the foregoing power transformer and CT models based on EMTP functions.

Unlike a three-phase generator, where the input and output currents are in phase as well as equal in magnitude under normal steady state operation, in a transformer, these currents are different. Figure 5 shows the connections of power transformer windings and CT, the latter being connected not only to

transduce the primary system currents, but also compensate phase shift between input and output currents.

4 CASE STUDIES AND SIMULATION RESULTS

In order to fully demonstrate the effectiveness of the power transformer and CT models developed herein, a number of power transformer fault transient and magnetising inrush current waveforms were simulated, these are described in this section.

4.1 Typical internal fault waveforms

Figures 6-9 respectively depict the transient response results of the power transformer system for some typical internal faults. Hereafter, the nomenclature of subscripts is such that *ap, bp, cp* refer to a, b and c three phases on primary side of the power transformer (low voltage side), *as, bs, cs* refer to a, b and c three phases on secondary side of the power transformer (high voltage side), *ad, bd, cd* refer to a, b and c three phases differential signals through the CT secondary sides.

First of all considering an a-b earth fault on the high voltage side of the transformer, it is apparent from Figs 6(a) and 6(b) that there is more high frequency (HF) distortion in the current waveforms on the high voltage (HV) side compared to that experienced on the low voltage (LV) side. This would be somewhat expected by virtue of the fact that the magnitudes of currents are significantly higher on the LV side and predominantly power frequency which swamps over any high frequency distortion. Moreover, the HV side is directly connected to the transmission line and the travelling wave effect generated on the transmission line also has some bearing on the distortion observed on the HV side.

Fault transient phenomenon similar to the foregoing (particularly in terms of waveform distortion) is observed for a b-phase earth fault on the LV side of the transformer (Fig.7). Here of course, a and c phase currents on the LV are very small compared to faulted b-phase and this is also the case when observing the differential currents through the CT secondary.

A c-phase 5% turn-to-turn fault at mid-point of winding on the HV side of the transformer is shown in Fig.8. A short circuit of a few turns of the winding will give rise to heavy fault current in the short-circuited loop, but the terminal currents both on the HV and LV sides are quite small. It is evident from Fig.8 (a)-(c) that the currents on either the HV side or LV side during the period of the turn-to-turn fault are only slightly different from the normal load current and as a direct consequence of this, the differential

currents generated are much smaller compared to those caused by other types of fault.

Fig. 9 shows the transformer currents for an a-phase earth fault at the mid-point of the winding on the LV side. The fault current magnitude for such a delta-connected winding may be no more than the rated current, or even less [12], and here again the terminal currents are little different from the normal load currents. From Fig.9, it can be seen that the differential currents are again very small.

It is thus apparent from the foregoing that there is a wide variation both in the magnitude and distortion in the fault current waveforms, depending upon the type of fault and its location. Importantly, any new protection technique must be capable of dealing with this wide diversity of fault data.

4.2 Simulation results for internal faults with CT saturation effects included

It is well known CT saturation can cause a severe distortion in CT secondary currents thereby rendering them to totally different from the CT primary waveforms. This in turn can lead to a large second harmonic to be generated during internal faults; this can result in the conventional differential protection, based on the second harmonic restraint, to block the operation of the protection under certain internal faults. It is thus vitally important to be able to simulate CT saturation under internal faults; this has been accomplished herein by (i) variation in the fault inception angles, (ii) through different levels of CT remnant flux.

Since the D.C. component in the fault current is the dominant factor in causing CT saturation and it is influenced by the fault inception angle (α), two typical case studies involving the three-phase short circuit on the HV side of the power transformer at voltage $V_a(\alpha=0°)$ and $V_a(\alpha=90°)$, respectively are presented, and the results are depicted in Fig.10. From Fig.10 (a), corresponding to voltage V_a ($\alpha=0°$), it can be seen that for a fault inception angle near voltage zero, the D.C. component is large in the initial period following a fault, and as a consequence, the CT saturates, resulting in a marked difference between the CT primary current (referred to secondary) and the CT secondary current. In sharp contrast, when a fault occurs at maximum voltage point of the a-phase voltage, there is no D.C. offset, and therefore as expected, the a-phase current is faithfully reproduced, as evident from Fig.10 (b).

In practice, there are many conditions (such as line auto-reclosure after a transient fault clearance) that may leave a remnant flux in the core of the CT; this can have a significant bearing on the CT secondary current. Comparing Fig.10 (a) and Fig.10 (c), which

are for the same fault inception angle, except that there is a higher remnant flux in the case shown in Fig.10(c), it is apparent that the remnant flux level has a significant influence on the CT secondary current in that there is more severe distortion in the CT secondary as evident from comparing Fig.10 (c) and Fig.10 (a).

4.3 Simulation results associated with magnetising inrush currents

When a power transformer is energised on the primary side with the secondary open-circuited, the current drawn by the primary is the magnetising current, which, in steady state, is about 5% (or even less) of the full-load current. This current, however, in the first a few cycles (called inrush current) can be very large, hence called as magnetising inrush current. Herein, the magnetising inrush currents of the power transformer are simulated in detail under (i) different remnant fluxes in the iron-core of the power transformer; (ii) different point-on-wave energisation.

It is well established that the best operating efficiency of a transformer under normal conditions is achieved when the working flux is close to flux saturation value. This effectively means that when a transformer is energised near voltage zero, it will result in a doubling of the flux in the iron-core; a direct consequence of this is that the transformer becomes severely saturated and finally generates a large inrush current. These inrush current waveforms for a transformer with no remnant flux are shown as I_{am}, I_{bm} and I_{mc} in Fig.11(a). From Fig.11(a), it can be seen that the inrush currents decay slowly by virtue of the fact that the transformer is near the generator, and the resistance of the generator-transformer loop is therefore very small.

If a transformer has undergone the process of energisation previously, there is a high probability that upon de-energisation, some flux would have been left in the iron; this can be positive or negative, which may either add to or subtract from the total flux upon re-energisation, thereby increasing or decreasing the inrush current. To demonstrate this scenario, it has been assumed that there is a remnant flux of +72.9Wb (70% rated flux) in a-phase core, -36.5Wb (-35% rated flux) in both b-phase and c-phase, respectively. The magnetising inrush currents with respect to these initial remnant flux conditions are depicted in Fig. 11(b). As can be seen, the presence of the remnant flux significantly increases the magnitude of the magnetising inrush current. This is evident from a comparison between Figs. 11(a) and (b). Corresponding to the same initial remnant flux conditions as in Fig.11 (b), Fig.11 (c) shows the variations of the three phase core fluxes (F_a, F_b and F_c). Fig.11 (d) importantly shows that the magnetising

inrush current gives rise to significant differential currents I_{ad}, I_{bd} and I_{cd}. This is not a fault condition and any new protection technique must be able to discern this clearly from a genuine internal fault condition.

However, a transformer may not always be energised near voltage zero, which causes the maximum inrush currents. If a transformer is energised near voltage maximum, there will be negligible or no transient inrush current flowing. To demonstrate the effect of the different energising conditions on the inrush currents, Fig.12 illustrates the changes in the a-phase differential current I_{ad} ($I_{ad} = I_{am} - I_{cm}$) corresponding to energisation angles $\phi=0°$, $120°$, $240°$, $270°$, $360°$, respectively.

4.4 Simulation results for external faults with CT effects included

A differential current is designed to restraint under normal load flows and for external faults. However, external short circuits can in fact result in very large differential currents, if the CTs saturate. It is thus crucial to be able to ascertain CT saturation effects on the measured currents under external faults. Figure 13 shows the simulated waveforms for an external three-phase short circuit, which occurs on the Bus 2 (see Fig.4) under the condition that there is an initial remnant flux (50% rated flux) in CT cores on the LV side, and a zero remnant flux in CT cores on the HV side. From Fig13(a) it can be seen that, as expected, there is some distortion in the a-phase CT secondary current on the LV side. The CT secondary current waveforms on the HV side are, on the other hand, distortion free as shown by Fig.13 (b). This imbalance (due to distortion on the LV side) manifests itself into significantly distorting the differential current (particularly in increasing its magnitude) as evident from Fig. 13 (c) and this can lead to relay instability in the conventional current differential protection.

Generally, the degree of the CT saturation is dependent on the DC components in the primary current and the CT parameters. Fig. 14 therefore shows the effects on the a-phase differential current with different levels of CT initial remnant flux for an external three-phase short circuit occurring on Bus2. From Fig 14 it is apparent that as CT initial remnant flux progressively increases from 0% to 35%, 50%, 60% rated flux respectively, the magnitude of the differential current also gradually increases and under certain conditions can exceed the setting of the differential current protection thereby resulting in mal-operation of the power transformer protection.

5. CONCLUSIONS

An accurate digital simulation of the power transformer system provides a good supplementary tool for the protective relay performance evaluation or

new relay design. In this paper, a modelling technique and methodology for accurately simulating the transient behaviour of a large three-phase two-winding power transformer and the associated CTs has been presented. The transient behaviour of a power transformer under magnetising inrush currents and commonly encountered internal faults (including some external fault) and various system conditions have been simulated and examined in detail. CT saturation and its effects on the measured fault current waveforms (including under a variety of system conditions) have also been studied in detail. The results clearly indicate that there is a wide variation in the nature of the current waveforms measured both under internal faults and magnetising inrush current phenomenon. The problems is accentuated by the onset of saturation in measurement CTs and this diversity can have a detrimental effect on conventional transformer protection, particular of the commonly employed current differential protection. It is now hoped that this technique of accurately modelling the transient phenomenon in transformers has laid the basis for developing new improved protection systems for power transformers, capable of satisfactorily dealing with the aforementioned problems.

6. REFERENCES

[1] M. A. Rahman and B. Jeyasurya, "A State-of-the-Art Review of Transformer Protection Algorithms", IEEE Trans. On Power Delivery, Vol.3, No.2, 1988, pp.534-544.

[2] M. Habib and M. A. Marin, "A comparative analysis of digital relaying algorithms for the differential protection of three phase transformers", IEEE Trans. On Power System, Vol.3, No.3, 1988, pp.1378-1384.

[3] Stanley H. Horowitz, Arun G. Phadke, "Power System Relaying (Second edition, book)", Research Studies Press Ltd, Taunton, Somerset, England, 1995.

[4] J. Lewis Blackburn "Protective Relaying: Principles and Applications", Second Edition, ABB Power T&D Company Inc, Cary, North Carolina, 1997.

[5] P. Liu, O. P. Malik, C. Chen, G. S. Hope, and Y. Guo "Improved Operation of Differential Protection of Power Transformers for Internal Faults", IEEE Trans on Power Delivery, Vol. 7, No.4, 1992, pp.1912-1919.

[6] Sidhu, T. S., Sachdev, M. S., wood, H. C. and Nagpal, M., "Design, Implementation and Testing of A Micorprocessor-based High-speed Relay for Detecting Transformer Winding Faults", IEEE Trans on Power Delivery, Vol. 7, No.1, 1992, pp.108-117.

[7] Patrick Bastard, Pierre Bertrand and Michel Meunier, "A Transformer Model for Winding Fault Studies", IEEE Trans. on Power Delivery, Vol. 9, No.2, April 1994.pp.690-699.

[8] F. A. Fouad, T. W. Nell and N. A. Demerdash, "Saturated transformer inductances determined by energy perturbation techniques", IEEE Trans. Power Apparatus and Systems, Vol. PAS-101, No.11, Nov 1982, pp.4185-4193.

[9] F. A. Fouad, T. W. Nell and N. A. Demerdash, "Saturated transformer inductances determined by energy perturbation techniques", IEEE Trans. Power Apparatus and Systems, Vol. PAS-101, No.11, Nov 1982, pp.4185-4193.

[10] V. Brandwajn, H. W. Dommel, and I. I. Dommel, "Matrix Representation of Three-Phase N-Winding Transformers for Stead-State and Transient Studies", IEEE Trans. on Power Apparatus and System, Vol. PAS-101, No.6, June 1982, pp:1369-1378.

[11] M. Kezunovic; C. W. Fromen; F. Phillips "Experimental Evaluation of EMTP-Based Current Transformer Models for Protcctive Relay Transient Study", IEEE Trans. on Power Delivery, Vol.9, No.1, January 1994, pp.405-413.

[12] Kang, Y.C.; Park, J. K.; Kang, S.H.; Johns, A.T.; Aggarwal, R.K., "An Algorithm for Compensating Secondary Currents of Current Transformers", IEEE Transactions on Power Delivery, Vol 12, No 1, January 1997, pp.116-124.

[13] "Protective Relay Application Guide", Third Edition, GEC Alsthom Measurements Ltd.
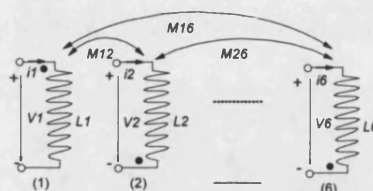
Figure 1 a schematic representation of a six-winding transformer
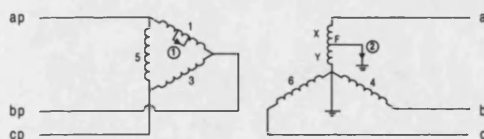
Figure 2 Internal winding fault modelling in a power transformer ①turn-to-turn fault ②turn-to-earth fault
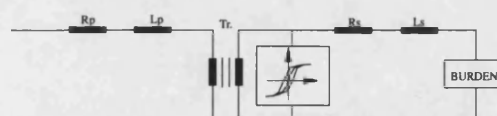
Figure 3 EMTP-based CT Models Rp- primary winding resistance; Lp- primary winding leakage inductance; Rs- secondary winding resistance; Ls- secondary winding leakage inductance; Tr- ideal transformer)
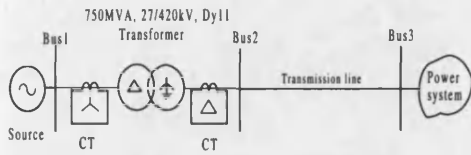
Figure 4 System configuration simulated for case studies
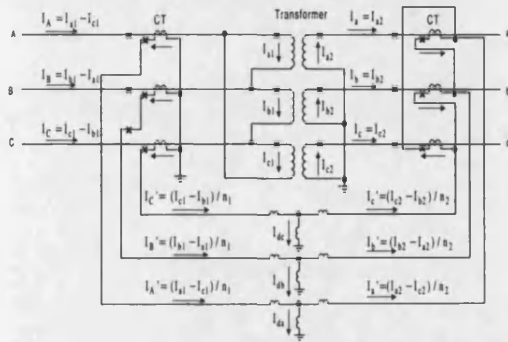
Figure 5 Connections for delta-star (Dy 11) power transformer and corresponding CTs connections
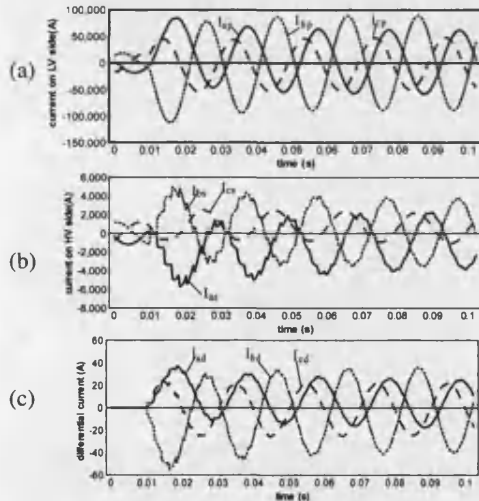
Figure 6 a-b two phase to earth terminal fault on high voltage side: (a)currents on LV side;(b) currents on HV side; (c) differential currents
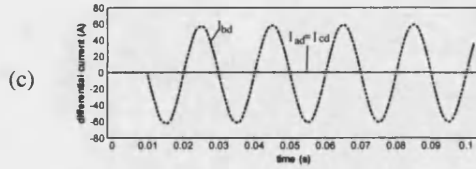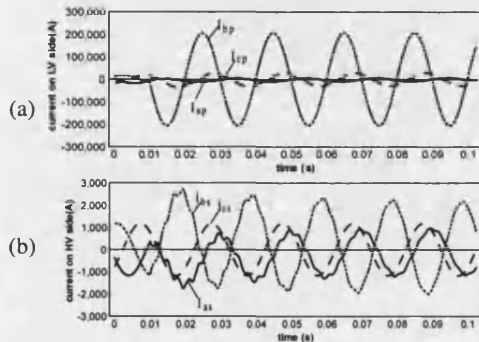
Figure 7 b-phase to earth terminal fault on low voltage side: (a) currents on LV side; (b) currents on HV side; (c) differential currents
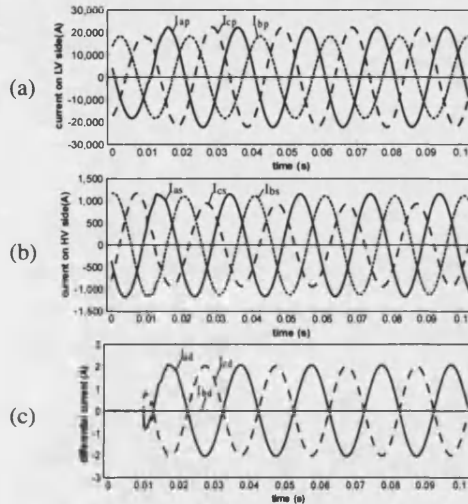
Figure 8 c-phase 5% turn-to-turn fault at mid-point of winding on HV side: (a) currents on LV side; (b) currents on HV side; (c) differential currents
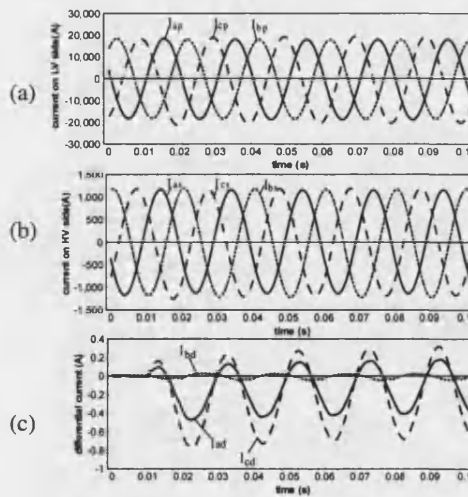
Figure 9 a-phase turn-to-earth fault at mid-point of winding on LV side: (a) currents on LV side; (b) currents on HV side; (c) differential currents

Figure 12 Magnetising inrush currents under different energisation angle φ: (1) φ=0°;(2) φ=120°;(3) φ=240°; (4) φ=270°; (5) φ=360°

Figure 10 Simulation of internal faults with CT saturation ①CT primary current (referred to secondary) ② CT secondary current: (a) currents for fault inception angle α=0°; (b) currents for fault inception angle α=90°;(c) currents under 20% more remnant flux than case (a)
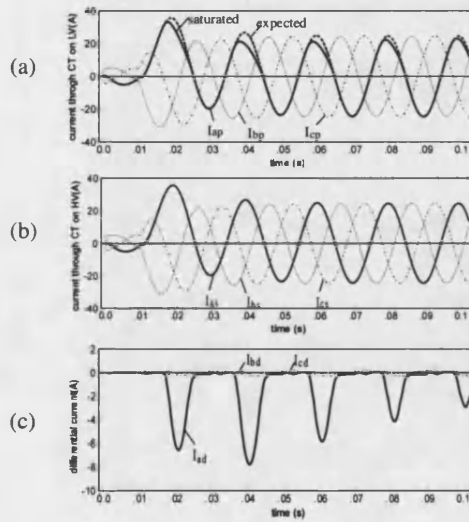
Figure 13 Simulation of an external fault with CT saturation: (a) CTs secondary currents on LV side; (b) CTs secondary currents on HV side; (c)differential currents

Figure 11 Simulation of magnetising inrush currents: (a) inrush currents with no remnant flux; (b) inrush currents with remnant flux; (c) winding fluxes; (d) differential currents
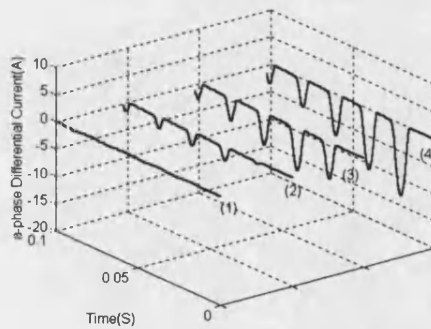
Figure 14 Differential currents of various CTs remnant flux in CT on an external fault: (1) 0% rated flux of remnant flux; (2) 35% rated flux of remnant flux; (3) 50% rated flux of remnant flux; (4) 60% rated flux of remnant flux